CARBON NANOTUBE AND NANOFIBER REINFORCEMENT FOR IMPROVING THE FLEXURAL STRENGTH AND FRACTURE TOUGHNESS OF PORTLAND CEMENT PASTE

A Thesis

by

BRYAN MICHAEL TYSON

Submitted to the Office of Graduate Studies of
Texas A&M University
in partial fulfillment of the requirements for the degree of

MASTER OF SCIENCE

May 2010

Major Subject: Civil Engineering

CARBON NANOTUBE AND NANOFIBER REINFORCEMENT FOR IMPROVING THE FLEXURAL STRENGTH AND FRACTURE TOUGHNESS OF PORTLAND CEMENT PASTE

A Thesis

by

BRYAN MICHAEL TYSON

Submitted to the Office of Graduate Studies of
Texas A&M University
in partial fulfillment of the requirements for the degree of

MASTER OF SCIENCE

Approved by:

Chair of Committee,	Rashid Abu Al-Rub
Committee Members,	Zachary Grasley
	Eyad Masad
	Jaime Grunlan
Head of Department,	John Niedzwecki

May 2010

Major Subject: Civil Engineering

ABSTRACT

Carbon Nanotube and Nanofiber Reinforcement for Improving the Flexural Strength and Fracture Toughness of Portland Cement Paste. (May 2010)

Bryan Michael Tyson, B.S., Texas A&M University

Chair of Advisory Committee: Dr. Rashid Abu Al-Rub

The focus of the proposed research will be on exploring the use of nanotechnology-based nano-filaments, such as carbon nanotubes (CNTs) and nanofibers (CNFs), as reinforcement in improving the mechanical properties of portland cement paste as a construction material. Due to their ultra-high strength and very high aspect ratios, CNTs and CNFs have been used as excellent reinforcements in enhancing the physical and mechanical properties of polymer, metallic, and ceramic composites. Very little attention has been devoted on exploring the use of nano-filaments in the transportation industry. Therefore, this study aims to bridge the gap between nano-filaments and transportation materials.

This will be achieved by testing the integration of CNTs and CNFs in ordinary portland cement paste through state-of-the-art techniques. Different mixes in fixed proportions (e.g. water-to-cement ratio, air content, admixtures) along with varying concentrations of CNTs or CNFs will be prepared. Different techniques commonly used for other materials (like polymers) will be used in achieving uniform dispersion of nano-filaments in the cement paste matrix and strong nano-filaments/cement bonding. Small-scale specimens will be prepared for mechanical testing in order to measure the modified mechanical properties as a function of nano-filaments concentration, type, and distribution. With 0.1% CNFs, the ultimate strain capacity increased by 142%, the flexural strength increased by 79%, and the fracture toughness increased by 242%.

Furthermore, a scanning electron microscope (SEM) is used to discern the difference between crack bridging and fiber pullout. Test results show that the strength, ductility, and fracture toughness can be improved with the addition of low concentrations of either CNTs or CNFs.

DEDICATION

To my family and friends who have always been supportive.
My gratitude extends beyond words.

ACKNOWLEDGEMENTS

I would like to acknowledge the support and guidance of my advisor, Dr. Abu Al-Rub. Along with Dr. Abu Al-Rub, I would like to recognize my committee members, Dr. Grasley, Dr. Masad, and Dr. Grunlan, and fellow researcher Ardavan Yazdanbakhsh for their gracious help. This study was mainly sponsored by the Southwest University Transportation Center (SWUTC) through the US Department of Transportation and also by the US Federal Highway Administration through the cooperative agreement DTFH61-08-H-00004. I also wish to thank David Burton from Applied Science, Inc. for providing the Pyrograph carbon nanofibers used in this research. Thanks to Ara Jeknavorian from W.R. Grace for providing the superplasticizers and related technical information. Finally, the FE-SEM acquisition was supported in part by the NSF grant DBI-0116835, the VP for Research Office, and the Texas Engineering Experiment Station.

NOMENCLATURE

A	Agglomeration percentage
CNF	Carbon nanofiber
CNT	Carbon nanotube
D	Dispersion percentage
FRC	Fiber reinforced cement
MWCNT	Multi walled carbon nanotube
P	Pressure
PDF	Probability density function
RC	Reinforced cement
SEM	Scanning electron microscope
SWCNT	Single walled carbon nanotube
TEM	Transmission electron microscope
μ	Mean of the associated normal distribution
σ	Standard deviation of the associated normal distribution

TABLE OF CONTENTS

Page

LIST OF FIGURES

Page

Page

Page

Page

Page

LIST OF TABLES

Page

1 INTRODUCTION

1.1 Problem Statement

Concrete is the second most used material on earth (after water), and is the most common and widely used construction material in the world. However, cementitious materials in general are very brittle and characterized by a very low tensile strength and a very low strain to failure. Macroscopic steel reinforcing bars have been added to concrete since the late 1850's to provide tensile strength and ductility. Within the last few decades, researchers started testing discrete meso and micro fibers as a means to control crack growth in cementitious materials (e.g. cement paste, cement grout, concrete) [1-7]. The idea behind this transition to fiber reinforced cement (FRC) is that the tensile strength is developed from many individual fibers rather than a few pieces of steel [1]. Therefore, the use of discrete fibers results in a more uniform distribution of stress within cementitious materials. Recently, exceptional types of carbon nano-filaments have raised the interest of some concrete researchers due to their remarkable mechanical, chemical, electrical, and thermal properties, and excellent performance in reinforcing polymer-based materials [8-10]. Micro-fibers may delay the nucleation and growth of cracks at the micro-scale; however, nano reinforcements can further delay the nucleation and growth of cracks at the nano-scale. If cracks are successfully controlled at the nano scale, their propagation to the micro level can be prevented. These nano-filaments, both carbon nanotubes (CNTs) and carbon nanofibers (CNFs), may prove to be superior alternatives or compliments to traditional fibers, and promising candidates for the next-generation of high-performance and multi-functional cement-based materials and structures.

To successfully utilize CNTs and CNFs as reinforcement within the cement matrix, four key requirements must be met. These include good dispersion, uniform alignment, large aspect ratios, and optimal bond strength [8]. CNTs and CNFs attract each other due to van der Waals

---

This thesis follows the style of *Cement & Concrete Composites.*

forces. This results in the formation of agglomerations (bundles) in the form of entangled ropes and clumps which are very difficult to disentangle. These agglomerations form large voids within the cement matrix, and are unable to transfer stresses across the bundles. A well dispersed matrix of nanotubes/nanofibers helps insure that every nano-filament is uniformly coated with cement. This will allow the stresses to transfer uniformly from the cementitious matrix to the nano-filaments. In return, this reduces stress concentrations caused by uneven dispersion of nano-filaments.

The second requirement is the alignment of nano-filaments. Alignment will help produce a uniform stress transfer when under axial loads. The idea behind aligning the nano-filaments is that the nano-filaments perpendicular to the primary stresses cannot transfer stresses along its axis efficiently. However, if the nano-filaments are aligned parallel to the primary stress direction, they can be fully utilized. This type of uniform alignment is not always beneficial. The main drawback is that the nanocomposite matrix will be very anisotropic, which can weaken out of plane mechanical properties.

The next requirement is to have a large aspect ratio. To optimize the bond between cement and nano-filaments, the surface area should be maximized. For example, high aspect ratio single walled carbon nanotubes (SWCNTs) can have a surface area as high as 790 m^2/g [11]. However, too large of an aspect ratio can cause problems with dispersing the nano-filaments.

The last requirement is to obtain an optimal bond between cement and nano-filaments. Bonding between the cement matrix and filaments is very weak which causes them to slide out of the cement matrix under a load much lower than the strength of the individual nanotubes. Due to the graphitic nature of the CNTs and CNFs, a proper adhesion with cementitious matrix is very difficult to achieve; therefore, the nano-filaments can be pulled out of the matrix very

easily. Also, due to the very smooth surfaces of the CNTs and CNFs, even upon debonding from the cement matrix frictional forces are very small to delay complete pullout. This sliding becomes more pronounced within the bundles if the nano-filaments lack proper dispersion. In order to utilize as much of the nanotube's mechanical properties as possible, the interfacial bonding and frictional properties need to be optimized.

1.2 Portland Cement

Portland cement was first created in the early 1800's by a British bricklayer named Joseph Aspdin. Modern day production of portland cement involves blending and subsequent heating of raw materials in a rotating kiln. The kiln causes calcium carbonate to react with silica-bearing minerals to form a mixture of calcium silicates. Calcium silicates are the hydration products responsible for developing the strength of hydrated portland cement paste [12].

1.3 Carbon Nanofibers and Nanotubes

In the early 1990's, Sumio Iijima reported, for the first time, the formation of tubular structures comprised almost exclusively out of carbon atoms [13]. These hollow tubes consisted of carbon – carbon bonds, and the thickness equivalent to the diameter of a single carbon atom. These carbon nanotubes (CNTs) are described as ultrathin filaments of carbon formed by layering carbon atoms bonded in a hexagonal pattern to form a tubular structure. The tubes have nanometer-size diameters and micrometer-size lengths which can be classified as either single walled carbon nanotubes (SWCNT) consisting of a single tube layer (Fig. 1a), or multi walled carbon nanotubes (MWCNT) which are multiple layers of evenly spaced concentric tubes (Fig. 1b). Today, most MWCNTs can have anywhere from 2 to 20 concentric layers. The orientation of the hexagonal structure of the nanotubes can be described by their chiral vector, $\vec{C} = m\vec{a_1} + n\vec{a_2}$, where *m* and *n* are integer numbers along unit vectors $\vec{a_1}$ and $\vec{a_2}$ as shown in

Fig. 2a [14]. A tube can be (*m*,0) which is described as a zig-zag structure (Fig. 2b), or an armchair structure when *m*=*n* (Fig. 2c).

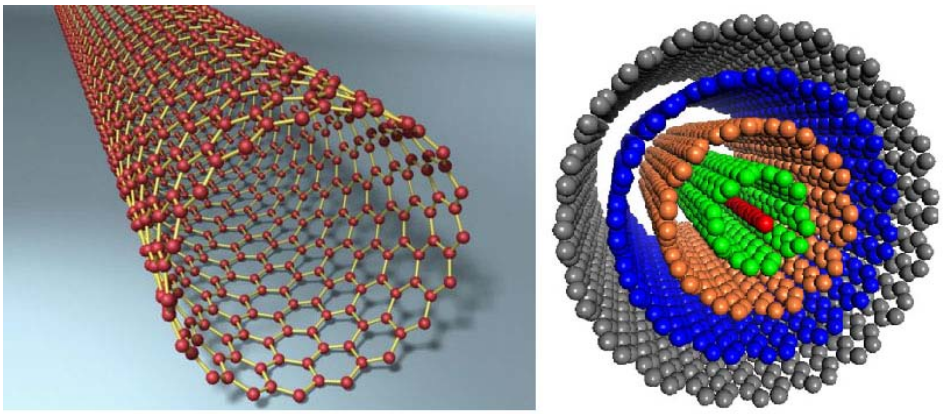

Fig. 1. (a) Schematic of a SWCNT consisting of a single layer of carbon atoms bonded in a hexagonal pattern [15], and (b) MWCNT which are comprised of many layers of individual SWCNTs [16].

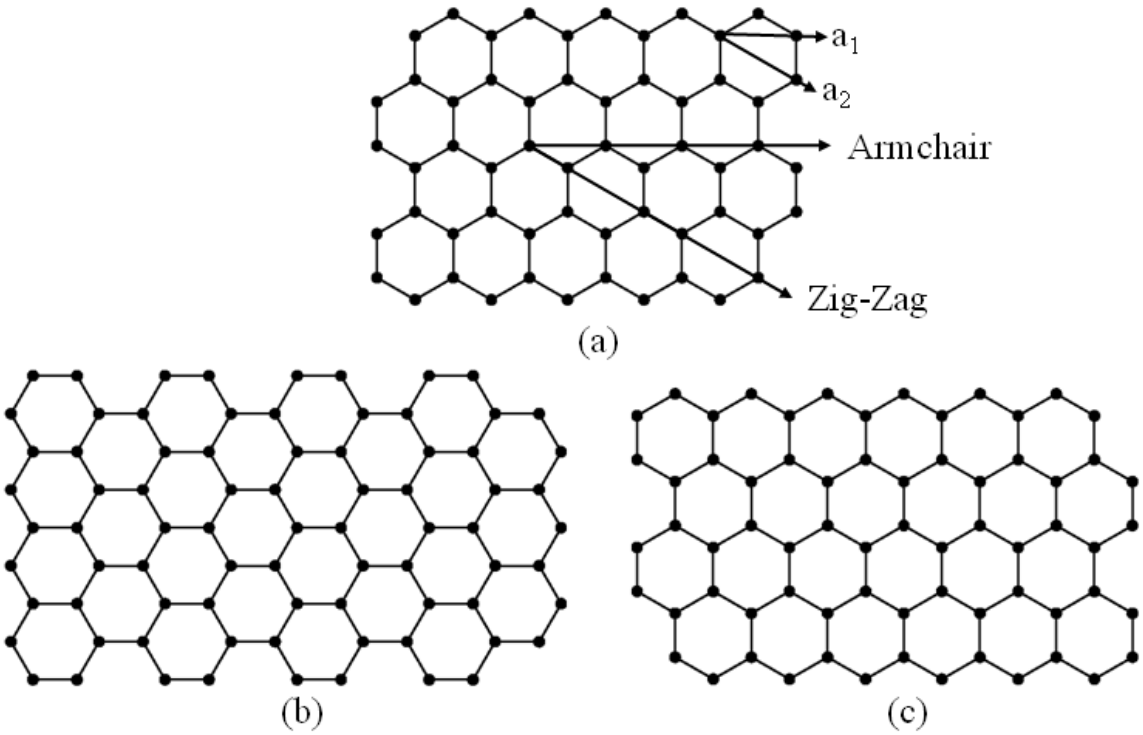

Fig. 2. CNT hexagonal structures, (a) unit vectors a_1 and a_2, (b) zig-zag structure, (c) armchair structure.

1.3.1 Manufacturing

According to Mamalis et al. [17], today there are three primary approaches taken to produce CNTs. The first process is electric arc-discharge, where an electrical arch is passed through an inert gas such as argon or helium between two carbon electrodes. The high temperatures caused by the arc (upwards of 3000^{o}C) cause the carbon to sublimate and re-solidify into the highly organized CNT structure [18]. Electric arc-discharge produces CNT with purity around 30 % by wt and can produce both SWNT and MWCNT.

The second method, called chemical vapor deposition (CVD), uses a carbon based gas (such as acetylene, ethanol, or methane) along with a metal catalyst to initiate the growth of the CNT. CVD is the most widely used method to produce CNTs on an industrial scale due to its low cost/unit ratio. However, CVD also contain higher amounts of defects when compared to other production methods. The sizes and lengths can be changed depending on the size of the

metal catalyst and the atmosphere within the reaction chamber. CVD can be used to produce large quantities of CNTs with minimum cost and high purity.

The final method is the laser ablation (LA) process. This method uses a pulsing laser to vaporize a piece of graphite within an inert gas within a furnace at temperature around 1200^{o}C. The vaporized graphite solidifies onto the cooler walls of the reaction chamber and forms the CNT. This method produces purity around 70 % by wt of mostly SWCNT with a diameter controlled by the temperature of the chamber [19]. CNTs produced by LA are very pure and highly uniform; however, it is very expensive to produce due to the cost of the laser.

1.3.2 Properties

CNTs are quickly becoming one of the most promising nano-materials due to their unique mechanical properties. Experimental tests on CNFs have shown them to have a Young's Modulus as high as 400 GPa, with a tensile strength of 7 GPa [20]. Alternatively, CNTs have an average Young's modulus around 1 TPa, an average tensile strength of 60 GPa, and an average ultimate strain of 12% [21]. When compared to the strongest steel, CNTs have a modulus of elasticity of approximately 5 times higher, a tensile strength 100 times larger, and can reach elastic strain capacities 60 times greater than steel, and yet a specific gravity one sixth that of steel.

CNTs differ from diamonds in that a diamond is formed by a three-dimensional lattice where a carbon atom is attached to four other carbon atoms, which gives diamonds their exceptional strength as shown in Fig. 3a. On the other hand, CNTs form two-dimensional lattice structures where the carbon atom is attached to three other carbon atoms as shown in Fig. 3b. One of the C-C bonds consists of a double bond. This creation of a two-dimensional hexagonal structure gives CNTs stronger bonds than a diamond along the plane, and relatively weak

interplanar bonds. This allows the different tubes within MWCNTs to slide relative to one another.

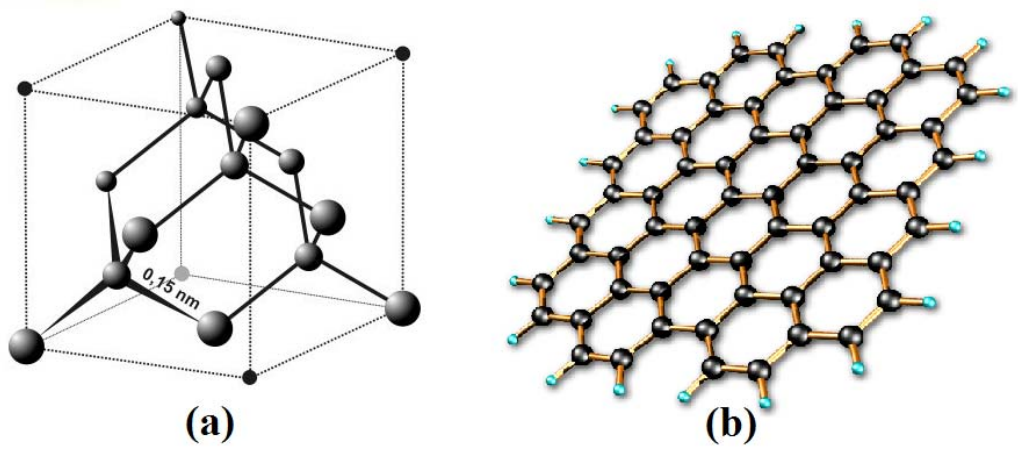

Fig. 3. Comparison between (a) diamond structure [22], and (b) graphene sheet [23]. The diamond structure consists of a carbon atom bonded to four other carbon atoms is a tetrahedral geometry. The graphene sheets consist of hexagonally bonded carbon atoms.

1.4 Literature Review

While considerable research on CNTs/CNFs has been focused around their incorporation within polymers, very little attention has been focused on combining CNTs/CNFs with cement. Therefore, the research on integration of CNTs/CNFs in cementitious materials is at a relatively novel stage; currently, very limited research regarding their effectiveness in enhancing the tensile strength or toughness of concrete has been conducted. Within the area of dispersion techniques applicable to cementitious materials, Makar and Beaudoin [24] have shown promising results in the dispersion of carbon nanotubes in cement by mixing 1.6 wt% by weight of cement of nanotubes first with ethanol and sonicating for 2 hours, then adding cement powder to the mixture and further sonicating for 5 hours. After the sonication was completed, the ethanol was allowed to evaporate leaving behind unhydrated cement with nanotubes dispersed throughout. This dried

mixture was then ground with a mortar and pestle and viewed under a scanning electron microscope (SEM). These images showed evidence of cement powder coated with CNTs.

Later, Makar et al. [25] made cement paste using 2 wt% of SWCNT-coated cement produced with a similar method. Through SEM imaging of the fractured surface of dry paste, they found that the distribution of the CNTs in the hydrated samples is not the same as seen on the non-hydrated cement grains. CNT bundles were smaller in apparent diameter and more widely distributed in the hydrated matrix. The smallest bundles imaged had diameters less than 5 nm, suggesting that they were composed of only a few 1.4 nm diameter SWCNTs. Moreover, the SEM images of the broken samples showed evidence of crack bridging across cracks approximately 500 nm wide, while the surface of the samples broken completely apart have shown the nanotubes experienced fiber pull-out rather than remaining attached to both sides. The Vickers hardness test showed a definite increase in the hardness at early stages of hydration; however as the hydration neared completion, the hardness of the carbon nanotube composites were about the same as the plain cement samples. However, Makar and Beaudoin [24] and Makar et al. [25] have not reported any mechanical testing.

Saez de Ibarra et al. [26] used an extremely fine cement which they hypothesized would be the best for the inclusion of nanotubes. They used both single- as well as multi-walled nanotubes dispersed with either plain distilled water or water with gum Arabic to increase the Young's modulus, and hardness. The amount of carbon nanotubes used in each sample varied from 0.05 % to 0.20 % by weight of cement. The mixes were poured into 10 mm x 10 mm x 160 mm prism shaped moulds, and allowed to cure for 28 days. The mechanical properties of each sample were measured using an atomic force microscope and a nano-indentation unit. Overall, the samples without gum Arabic have worse mechanical properties than the plain cement sample due to the difficulties in dispersing the nanotubes. They also noted that the single-walled

nanotubes are worse than the multi-walled nanotubes because the single-walled nanotubes are straighter, more defect free, and more difficult to disperse. As for the samples with the gum Arabic, the Young's modulus increased for both the multi-walled as well as the single-walled nanotubes. However, the hardness decreased with respect to the plain cement sample.

Li et al. [27] experimented with the functionalization (i.e. surface treatment) of multi-walled carbon nanotubes using both sulfuric (H_2SO_4) and nitric (HNO_3) acid with a ratio of 3:1. One hundred grams of the nanotubes were mixed with one thousand milliliters of the acid solution and then sonicated for 3 hours at ambient temperature. After the sonication, the mixture was diluted with distilled water five times, then the mixture was filtered and washed with water until no residual acid was present. Three types of samples were made. First was a cement mortar containing a ratio of water/cement/sand of 0.45:1:1.5. The second was the same ratio of cement mortar with the addition of 0.5 % of carbon fibers by weight of cement. The third sample is the same mortar with the addition of 0.5 % of carbon nanotubes by weight of cement. The samples were poured into oiled molds with a dimension of 160 mm x 40 mm x 40 mm for flexural tests, and 10 mm x 10 mm x 10 mm molds for compression. An electric vibrator was used to ensure good compaction. All samples cured for 28 days before testing. After curing, the flexural strength of the cement with carbon nanotubes increased by 25.1 %, and the compressive strength increased by 18.9 %.

In another study, Li et al. [28] used both untreated and treated (functionalized) multi-walled carbon nanotubes as the reinforcement in cementitious materials to understand the pressure-sensitive properties. In this study, Li et al. used 0.40 water/cement ratio with 0.5 wt% carbon nanotubes for all tests. They first mixed the nanotubes and water, and then used an ultrasonic mixer to disperse the nanotubes along with superplasticizer and a defoamer. The cement was then combined with the aqueous solution and poured into 40 mm x 40 mm x 160 mm

oiled molds and vibrated to ensure a sufficient compaction and allowed to cure for 28 days. The cement paste samples were tested for both compressive and flexural strength. The compressive strength of the treated nanotubes was 2.7 MPa higher than the untreated nanotubes, and the flexural strength of the treated nanotubes was 0.4 MPa higher than the untreated nanotubes. The experiments however did not test the strength of the carbon nanotube reinforced cementitious samples against the unreinforced samples.

Cwirzen et al. [29] mixed both functionalized as well as non-functionalized MWCNT's that ranged from 0.045 – 0.15 wt% into solutions of either poly(acrylic acid), or poly(acrylic acid) and gum Arabic. The tests were conducted with a water/cement ratio of 0.25 and 0.3 along with the nanotubes were mixed in a vacuum mixer and cast into 10 mm x 10 mm x 60 mm molds made from Teflon to avoid contaminations from the release oil. As for the workability, the samples with non-functionalized nanotubes along with the poly(acrylic acid) showed similar workability as the pure cement. However, the functionalized nanotubes caused poorer workability. In the case of the 0.25 water/cement ratio, the mixture was unable to wet. As for the hydration, neither the nanotubes nor the poly(acrylic acid) showed any delay in the hydration process; however, the addition of 0.8 wt% gum Arabic delayed the hydration by 3 days. Although the gum Arabic delayed the hydration, there were no significant losses in either compressive or flexural strength. They were able to increase the compressive strength of the cement by 50% with only 0.045% wt of the nanotubes to the dry cement weight. This was mostly due to the PAA acting as a superplasticizer. However, the overall performance of the samples did not show any significant gains in either compressive or flexural strength. This is mainly due to the challenges of bonding the cement matrix to the carbon nanotubes.

Nasibulin et al. [30] have recently developed a method to grow CNTs directly on the surface of cement particles. The CNTs were grown directly on the cement particles using a

modified chemical vapor deposition (CVD) chamber designed with a rotary screw to feed cement through at a constant rate. The cement was poured into 10 mm x 10 mm x 60 mm Teflon molds. They showed that the tubes were homogeneously dispersed in the paste made with the produced cement and intermingled with the products during the hydration process. Using this cement resulted in more than 100 % increase in the compressive strength of hardened paste.

Shah et al. [31] successfully dispersed untreated 0.02 to 0.33 wt% of MWCNTs in water with surfactants through applying an optimum ultrasonic energy and then mixing with cement using 0.3 and 0.5 water/cement ratios. Improved mechanical (15 to 55 % increase in Young's modulus, 8 to 40 % increase in flexural strength) and durability (30 to 40 % reduction in autogenous shrinkage) properties have been reported. They have concluded that small amounts of MWCNTs of 0.03 to about 0.10 wt% give the best gains in mechanical properties of cementitious nanocomposites.

Konsta-Gdoutos et al. [32] have reported on the comparison between long and short MWCNTs when incorporated within cement. Low concentrations between 0.025 and 0.1 wt% of short MWCNTs and 0.025 to 0.08 wt% of long MWCNTs were used. In general, Konsta-Gdoutos et al. concluded that optimum concentrations of MWCNTs depend on their aspect ratios. Short MWCNTs can use a higher concentration of 0.08 wt%, while long MWCNTs should be used in concentrations lower than 0.048 wt%.

Chaipanich et al. [33] combined 0.5 and 1 wt% CNTs with fly ash cement. The CNTs were added to cement containing 20 % fly ash with a water/cement/sand ratio of 0.5:1:3 and poured into 2 cm x 2 cm x 2 cm cubes. After casting, the cubes were cured in water prior to testing at 7, 28, and 60 days. The cement with CNTs showed slight improvements in the compressive strength(around 10%) when compared to cement with only fly ash. However, the compressive strengths of the CNT samples were lower than that of plain cement.

As far as the integration of CNFs in cementitious materials, very few studies have been conducted as compared to that of CNTs. Recently, Sanchez et al. [34-35] have studied the effect of CNFs on the mechanical properties of hybrid CNF/silica fume (SF) cement composites. SF nanoparticles were used in facilitating dispersion of CNFs and improving the interfacial interaction between the CNFs and the cement paste. However, in this study, the addition of CNFs and SF did not show improvement in the compressive or flexural strengths of the cement composite due to CNF and SF agglomerations and bundling. Therefore, despite the efforts made to date in integrating CNTs/CNFs in cementitious materials, only marginal success has been realized and the objective of this study is to address this issue.

1.5 Scope and Objectives

The objective of the proposed research is to investigate the potential use of nano-filaments such as CNTs and CNFs as nano-reinforcement to improve the tensile and flexural strength, as well as the fracture toughness of portland cement paste. CNTs and CNFs are carbon fibers which have a combination of desirable properties such as ultra-high strength, stiffness, and elongation at ultimate capacity. These nano-filaments will be added to the cement paste to act as bridges across micro- and nano-cracks to form the reinforcing mechanism in shear and tensile zones. Due to their high surface area and aspect ratio, they can act as excellent reinforcements in carrying internal stresses.

To investigate the potential use of CNTs and CNFs as nano-reinforcement in cement paste, two main obstacles have to be overcome. The first obstacle lies in the difficulty to disperse the nano-filaments into the cement matrix. CNTs and CNFs tend to adhere together due to van der Waals forces. The second obstacle lies in creating a sufficient bond between the nano-filaments and the cement matrix. Bonding between either the CNTs, or CNFs, and the cement paste matrix

experiences a very low pullout force, therefore, unable to utilize the full strength of the nano-filaments. The main tasks can be broken down into four major areas in interest:

- Dispersion of nano-filaments into the cement matrix,
- Bonding between the CNT/CNF – and the cement matrix,
- Macro mechanical testing, and
- Micromechanical characterization of the nanocomposite cement microstructure.

The following sections are broken down into the following areas of interest. Section 2 discusses the challenges involved in obtaining a uniform dispersion through the use of both surfactants and surface functionalization. Section 3 discusses a novel method to quantify the dispersion of nano-filaments in both aqueous as well as hydrated cement samples. Section 4 describes the methods involved in combining the nano-filaments with cement. Section 5 details the macro mechanical testing of small-scale specimens. Furthermore, both experimental results as well as microstructural characterization using an electron microscope are presented. Section 6 summarizes the research main conclusions and discusses possible future research in the field of nano-filament reinforced cementitious materials.

2 DISPERSION AND FUNCTIONALIZATION

2.1 Introduction

For carbon nano-filaments to be fully utilized within materials, they must first be properly dispersed. Dispersion is the process of separating the bundles of either CNTs or CNFs into individual filaments within a matrix. Currently there are two common methods used to disperse nano-filaments. The first method is to mechanically separate the nano-filaments by either ultrasonic or high-shear mixing. However, without the use of chemical surfactants, the van der Waals interactions will pull the nano-filaments back out of suspension and agglomerate (bundle) together again. The second method involves chemically altering the surface of the filaments by the creation of either covalent or noncovalent bonds. Covalent bonding includes functionalizing the surface of either the CNFs or CNTs in one of several methods. The first method functionalizes at the defect sites [36], another method is to functionalize the end caps of the CNTs [37-38], and the final common method is to functionalize the entire surface without the need to create defect sites [39]. Noncovalent bonding methods involve dispersing the nano-filaments with the use of chemical surfactants to maintain long term suspension within a variety of liquid solutions. Fig. 4 shows a basic flow chart for the different types of functionalization methods commonly used on nano-filaments.

Chemical surfactants can be classified as one of three chemicals: anionic, cationic, or nonionic. Surfactants contain both hydrophobic groups and hydrophilic groups [40]. The presence of both these groups allows hydrophobic substances (like CNTs and CNFs) to be stable

in water. The majority of current research on the dispersion of nano-filaments is focused around their incorporation within polymers [10, 40-44]. The most common method to disperse nano-filaments without causing excessive damage to their surface involves combining nano-filaments with surfactants into either water or other solvents. After which, the bundles are separated with the use of an ultrasonic mixer. An ultrasonic mixer (Fig. 5) is a device that uses a high frequency driver to transmit acoustical energy throughout a liquid medium. The energy created within the shock waves is extremely high and significantly accelerates chemical reactions and breaks up the agglomerated particles.

Diverse sets of experiments to disperse both CNTs and CNFs have been used in the past. Some examples of dispersion techniques include methods such as, ultrasonic mixing, surface functionalization, and even growing CNTs/CNFs directly within the matrix [30]. While proper dispersion is very challenging, measuring the degree of dispersion in a quantifiable manner possesses its own challenges. To date, there are no set quantifiable standards to measure the dispersion of CNTs/CNFs within any medium. Section 3 proposes a novel method to address this issue.

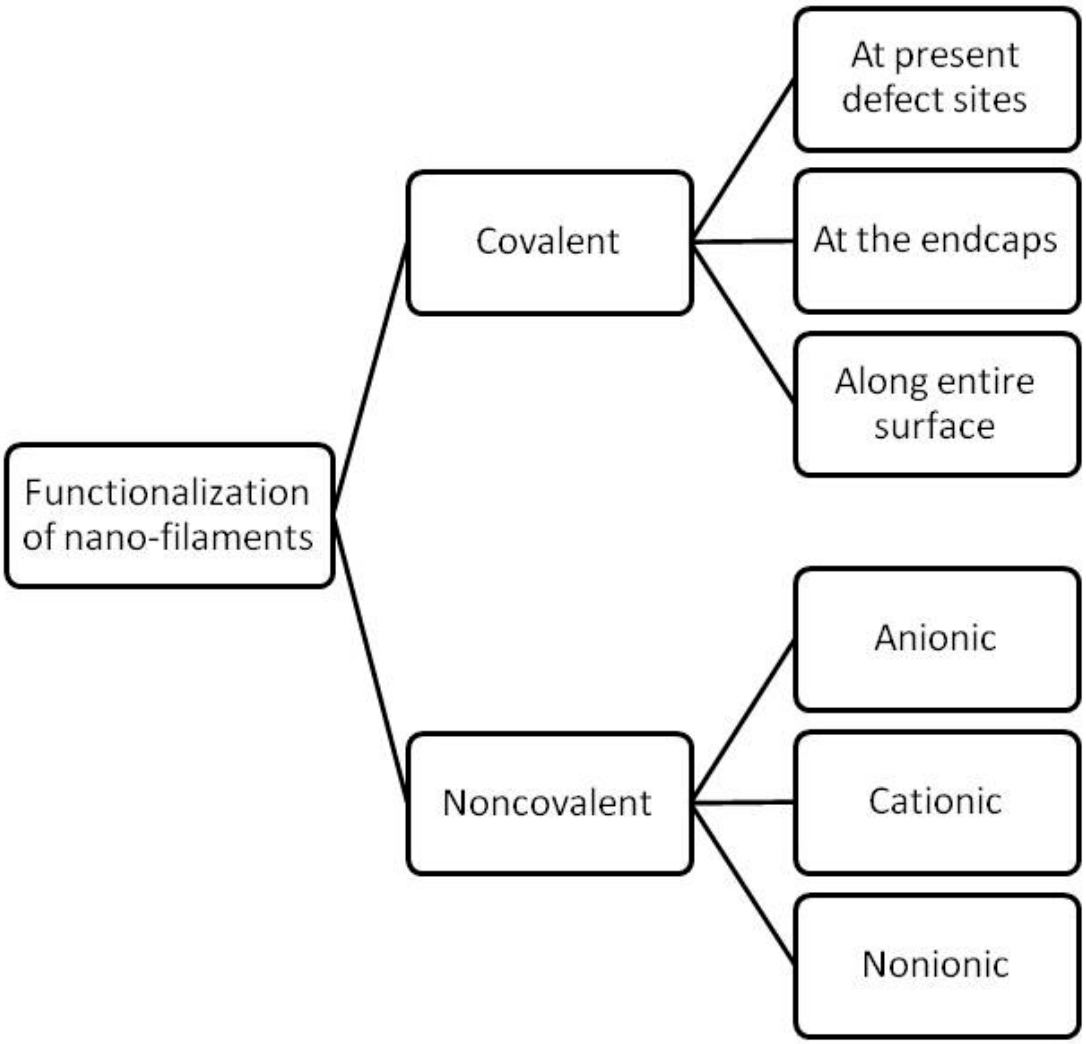

Fig. 4. Flow chart for the functionalization of nano-filaments.

Fig. 5. Sonics & Materials, Inc. ultrasonic mixer is capable of delivering 500 watts of power at 20 kHz.

2.1.1 Noncovalent Functionalization

Noncovalent bonding typically involves the use of various chemical surfactants. Surfactants are wetting agents which are used to lower the surface tension of water to allow easier dispersion of CNTs. Unlike covalent bonding, they do not form strong chemical bonds. Surfactants are known as amphiphilic, meaning they contain both hydrophobic as well as hydrophilic end groups. Therefore, they can combine with other hydrophobic substances like CNTs or CNFs and allow them to be dispersed into water.

Grunlan et al [45-46] has conducted research on the use of poly(acrylic acid) [PAA] as well as poly(allylamine hydrochloride) [PAH] as a means to control the dispersion of non-functionalized CNTs by adjusting the pH of the solution. The PAA solution when first added to water creates an acidic solution with a pH of 2.9. In their 2006 paper, they adjusted the pH from 2.9 to 9.2 and used an SEM to view the dried samples at different pH levels. The SEM images showed evidence of the dispersion increasing as a function of increasing pH. They initially believed this to occur due to the increase in negative charges on the PAA forced the nanotubes to disperse further apart. However, in 2008, this hypothesis was rejected because instead of drying

the samples before viewing them with the SEM, they froze the samples inside the TEM at a temperature of 93 K. This showed that the samples had a lower dispersion at a high pH of 9.2 than at a low pH of 2.9. They now believe the dispersion of nanotubes is not a function of negative charge buildup, but rather a function of how coiled the polymer is. At low pH, the PAA is tightly coiled, and can fit between nanotubes and push them apart; whereas at a higher pH, the PAA becomes straighter and cannot push the nanotubes apart as effectively.

Islam et al [47] was able to achieve high weight fractions of dispersed CNTs with the use of powerful surfactants such as sodium dodecylbenzene sulfonate (NaDDBS), sodium dodecyl sulfate (SDS), and Triton X-100. However, dispersing CNTs within cementitious composites poses major challenges that limit their usefulness. For example, most of these surfactants will delay or even prevent hydration of the cement [29], entrap a lot of air in the paste, or react with other chemical admixtures resulting in reagglomeration [48].

Grafting of polymers to the nanotubes is successfully demonstrated by Zhao et al [49]. These solutions are capable of reaching aqueous concentrations as high as 5 mg/ml. To achieve such a high concentration, poly(aminobenzene sulfonic acid) (PABS) and polyethylene glycol (PEG) were grafted to single-walled nanotubes. The first test combines 500 mg of nanotubes with 5 g of PABS in 500 ml of dimethylformamide (DMF), and the other test consisted of 1.5 g of nanotubes with 15 g of PEG in 800 ml of DMF.

Previous work by the author [48] has shown that a commercial superplasticizer, which is a high range polycarboxylate-based water reducing admixture named ADVA Cast 575, works well to disperse the CNTs without affecting the hydration of the cement paste. This study focused on proper techniques involved in dispersing CNTs into an aqueous solution that would not adversely affect the cured cement. For example, the use of NaDDBS, which is an effective anionic surfactant, caused the cement paste to entrap 5 times more air than is typical in plain

cement paste. The paste also did not reach initial set until after 24 hours. Current methods to disperse CNTs without adversely affecting the cementitious composites involve mixing 0.5 % CNTs by weight of water with 0.4 % ADVA Cast 575 by weight of water in an ultrasonic mixer for 20 minutes.

2.1.2 Covalent Functionalization

Currently, covalent functionalization has significantly expanded the utility of nano-filaments by allowing an otherwise insoluble material to become soluble. This has since led to major breakthroughs in the nanocomposite world. There are three common methods to functionalize nano-filaments through covalent bonding, as shown in Fig. 4. The first method is to use defect sites on the surface of the nano-filaments. This process is typically done with a mixture of sulfuric and nitric acid. Varying the concentration of the sulfuric/nitric acid ratio will control the degree of functionalization [39, 50-53]. Higher sulfuric acid concentration will produce more defect sites allowing the nitric acid to functionalize the newly created defect sites. Another common method is to functionalize only the end caps of the nano-filaments [37-38]. This method is similar to defect site functionalization with the exclusion of sulfuric acid. By removing the sulfuric acid, the oxidizing agent will only oxidize preexisting defects sites. If the nano-filaments are defect free (which is typical for certain SWCNTs), then only the end caps will be oxidized. The final method is to functionalize along the entire surface of the nano-filaments. Sidewall functionalization differs from defect site functionalization in that no strong acids are needed to perform the functionalization. This method is used primarily to form very specific functional groups, and is not always necessary for use in the functionalizing of nano-filaments used in nanocomposite cementitious materials. Dyke et al. [54] gives an excellent summary of different ways to functionalize the sidewalls. These can include methods such as fluorination with fluorine gas [55], using benzenediazonium salts [54], or oleum [56].

In the general context, functionalization is the process of adding functional groups to the surface of a material. These functional groups can be broken down into three main categories: hydrocarbyl groups (which include alkyl and alkenyl), halogen groups (like fluoro and chloro), and oxygen groups (which include hydroxyl, carbonyl, carboxyl, and ester). Out of these groups, oxygen groups are most often used in functionalization at the defect sites.

Previous work by Wang et al. [57] on the dispersion of carbon nanotubes for use in cement has shown that with the use of a microwave along with both nitric and sulfuric acids, stable aqueous concentrations as high as 10 mg/ml can be obtained. To obtain this rapid functionalization, 10 – 20 mg of single-walled nanotubes were mixed with 20 ml of 1:1 solution of sulfuric and nitric acid. The samples were subjected to microwave radiation at 450 watts for 1 – 20 min at a pressure of 20 psi. After this optimal time, the solution was analyzed by Raman and Fourier transformation infrared (RTIR) spectroscopy. RFIR spectroscopy showed that three minutes is the optimal microwave time. After which, the microwave induced oxidation started to destroy the nanotubes. After vacuum drying the solutions overnight, a scanning electron microscope was used to observe the different samples. The SEM images of the thin films showed SWCNTs being aligned parallel to each other probably due to hydrophobic forces and nanotube-nanotube interactions. The average lengths of the nanotubes were around 1 μm which might indicate that the microwave radiation reduces the length of the nanotubes.

2.1.3 Defect Site Functionalization

Defect site functionalization of the nano-filaments is dependent on four key variables when acid treated. Typical acid treatment is performed using two highly concentrated acids. The first is nitric acid (HNO_3) which oxidizes the surface, and the second is sulfuric acid (H_2SO_4) which “roughens” the surface. Roughening the surface of the nano-filaments is the process in which carbon-carbon bonds are broken, creating the defect sites. This allows the nitric acid to

create functional group on the nano-filaments. Varying the ratio of nitric to sulfuric acid will either increase or decrease the amount of functionalization. However, increasing the degree of functionalization by changing the ratio of nitric to sulfuric acid will hinder the performance of the nano-filaments. By increasing the amount of sulfuric acid, the surface becomes rougher. This roughness is what allows the functional groups to bond; however, the rougher the surface, the weaker the nano-filaments. Another negative side effect of the sulfuric acid is its ability to dissolve through sections of the nano-filaments. This will cut the nano-filaments into smaller lengths, reducing their aspect ratios.

The second key variable is concentration of acid to nano-filaments. If there are too many nano-filaments and not enough acid, then all of the acid will get consumed in the reaction. However, simply using massive amounts of acid will only lead to wasting the acid and takes longer for the acid to reach the designated reaction temperature. A balance has to be obtained in the ratio of nano-filaments to acid.

Third, the temperature of the solution must be maintained at a constant level. If the temperature is too high or too low, the difference in energy levels within the solution will either speed up, or slow down the reaction. This will cause the different batches to have either too much or not enough functionalization.

The last variable to control in acid treating nano-filaments is the amount of time the nano-filaments are in the acid. Just like the previous three variables, altering the length of time in which the nano-filaments are suspended in the acidic solution will alter the amount of functionalization. The key to controlling the time of the reaction is to have a standardized start point for the timer. There are three key start points that can be used for the timer: when the nano-filaments first touch the acid, when the nano-filament/acid solution is first placed in the heated oil bath, or when the nano-filament/acid solution reaches the designated reaction temperature.

2.2 Method

2.2.1 Dispersion

In this research project, the dispersion of CNFs into the water/surfactant solution was accomplished by 5 minutes of ultrasonic mixing. The superplasticizer/water ratio was held constant for all batches at 1.25 wt%. The CNF/water ratio was 0.25 wt% and 0.5 wt%. All weight percentages were by weight of water. These ratios are the same ratios used in the creation of the cement samples discussed in section 4. To image the CNFs, a small drop was placed on a glass slide and covered with a thin slip on top. The dispersion was then observed under a Zeiss Axiophot microscope with a 40x dry objectives lens. On the other hand, CNTs were dispersed by ultrasonication for 20 minutes. The superplasticizer/water ratio and CNT/water ratio were the same as for CNFs. For observing the dispersion of CNTs, an FEI Tecnai F20 transmission electron microscope was used with an attached cryo stage. The cryo stage held the dispersion frozen at liquid nitrogen temperatures (-196^{o}C) throughout the session. For SEM observations, a JEOL JSM-7500F FE-SEM was used at an acceleration voltage of 20kV.

2.2.2 Acid Treatment

The functionalization of the surface of the nano-filaments can be broken down into three crucial steps. First, either the CNTs or CNFs are placed into an acid bath. Second, the nano-filaments are washed repeatedly until a neutral pH is reached. Finally, the nano-filaments are dried in an oven. After successful functionalization of the nano-filaments, they are then stored in air-tight jars until they are ready to be used.

To heat the acid solution, a hot plate and large beaker with cooking oil was heated to the designated temperature of 85^{o}C. While the oil was heating up, the acid was measured out and poured into a flat bottom flask with a special base constructed out of PVC pipe to allow a magnetic stirrer to spin freely in the oil bath to improve oil circulation. Once the oil reached

temperature, the nano-filaments were added to the acid and the solution was quickly placed into the oil bath and a reflux condenser was placed on top of the flask. The acid solution also contained a magnetic stirrer to keep the nano-filaments constantly circulating. For each experiment, a ratio of 2:1 sulfuric to nitric acid was used for both CNTs and CNFs. In both cases, 0.1g of nano-filaments was added for every 100ml of acid. The reaction temperature was held constant at 85^{o}C for 1 hour, and all times were taken from when the nano-filament/acid solution is first placed in the hot oil bath.

After 1 hour, the nano-filaments reached the predetermined reaction time, and the acid was washed off and neutralized as quickly as possible. If the acid surrounding the nano-filaments remains in a concentrated state, the reaction will continue. In order to neutralize the acid, the nano-filament/acid solution was first diluted with deionized water in a water/acid ratio of 10:1. This was done not only to stop the reaction, but also to dilute to acid to a pH level safe enough for the filters to handle.

To filter the nano-filaments from the water and acid, a Nalgene 1,000ml capacity filter is used with a 0.45μm pore size (Fig. 6). These filters utilize a vacuum port to speed up the filtration process. After each filtration, the pH of the acidic solution was measured to determine whether or not the nano-filaments need to be washed again. If the acid is too high (the pH is too low), the nano-filaments are added to 4L of deionized water and them filtered again. This process continues until the pH is greater than 6.5. A pH of 6.5 was chosen due to varying pH levels of the deionized water supply. While checking the pH of the deionized water in the lab, the pH ranges between 6.5 and 7.

Fig. 6. Nalgene 1,000 ml vacuum assisted filter with 0.45μm pore size.

After neutralization of the nano-filaments, the solution was dried to remove the remaining water. In order to dry the nano-filaments quickly without causing any unintentional damage, they were dried in a temperature and humidity controlled chamber. The temperature was set to 60^{o}C with a relative humidity set to approximately 0%. All samples took between 1 to 3 days to dry completely depending on the amount of water left in the solution prior to drying.

Finally, after the nano-filaments were completely dried, an X-ray photoelectron spectroscopic (XPS) analysis was carried out. The XPS is used for the detection of variations in chemical compositions and oxidation states on the surface on different materials. The XPS uses an Al Kα source and can provide exceptional resolution. The XPS was used along with the program XPSPeak calibrated by placing the C1s peak at 284.6 eV.

2.3 Results and Discussion

2.3.1 Dispersion

The effects of ultrasonic mixing on the dispersion of CNTs is shown if Fig. 7. These are images comparing the dispersion of CNTs within water containing ADVA Cast 575 surfactant at

1.25 wt% by weight of water. Fig. 7(a) was stirred by hand for 5 minutes then let sit for 5 minutes. This Fig. shows that almost all the CNTs reagglomerated and settled out of suspension. Fig. 7(b) was shaken by hand for 5 minutes and then let sit for 5 additional minutes. Although not as bad as the stirred sample, the shaken sample still reagglomerated. Fig. 7(c) was mixed with an ultrasonic mixer for 5 minutes. The improved dispersion caused by ultrasonic mixing was evident immediately after mixing. The sample was then allowed to sit for 5 minutes prior to capturing the image. The solution was very dark, and when allowed to sit overnight, no obvious differences in settlement could be observed.

The effect of ultrasonic mixing on the dispersion of CNFs is shown in Fig. 8. These are optical microscopy images of the dispersion within an aqueous solution containing 1.25 wt% of surfactant by weight of water. Fig. 8(a) shows a poor dispersion of CNFs which was shaken by hand for 7 minutes. The dark areas are large agglomerations caused by the lack of energy input that would otherwise be transferred into the solution from ultrasonic mixing. It can be seen in Fig. 8(b) that no large agglomerations are present. Most of the darker spots in Fig. 8(b) are caused by impurities in the solution. The reduction in agglomerations is beneficial to the success of creating a well dispersed solution of CNFs; however, the use of ultrasonic mixing should be controlled and optimized to reduce fiber breakage. Many important mechanical properties such as strain capacity and toughness are related to fiber length. When the fibers are shortened, interfacial properties are significantly reduced.

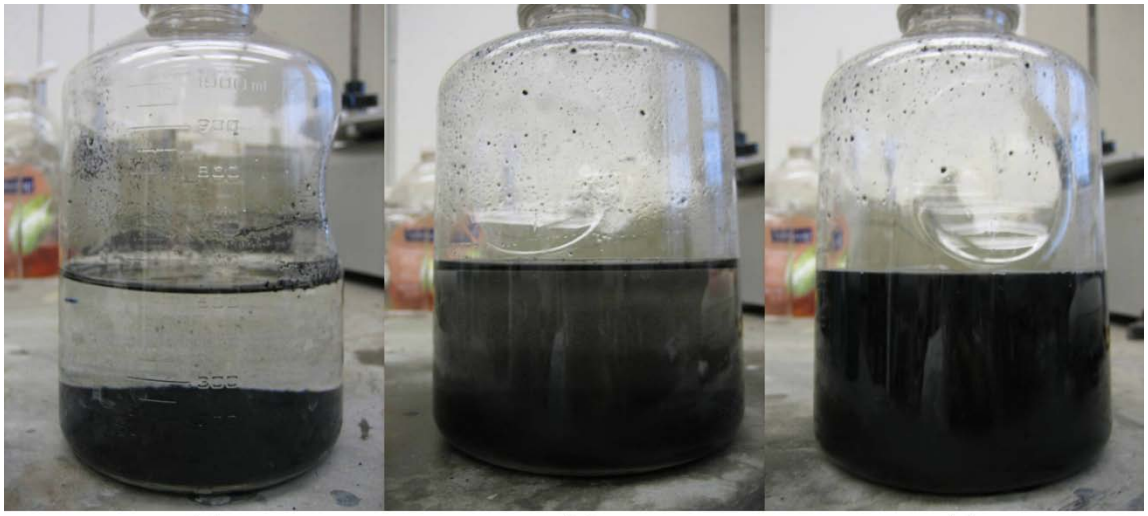

Fig. 7. Effect of CNT dispersion when mixed with water and a surfactant by (a) hand stirring, (b) hand shaking, and (c) ultrasonic mixing.

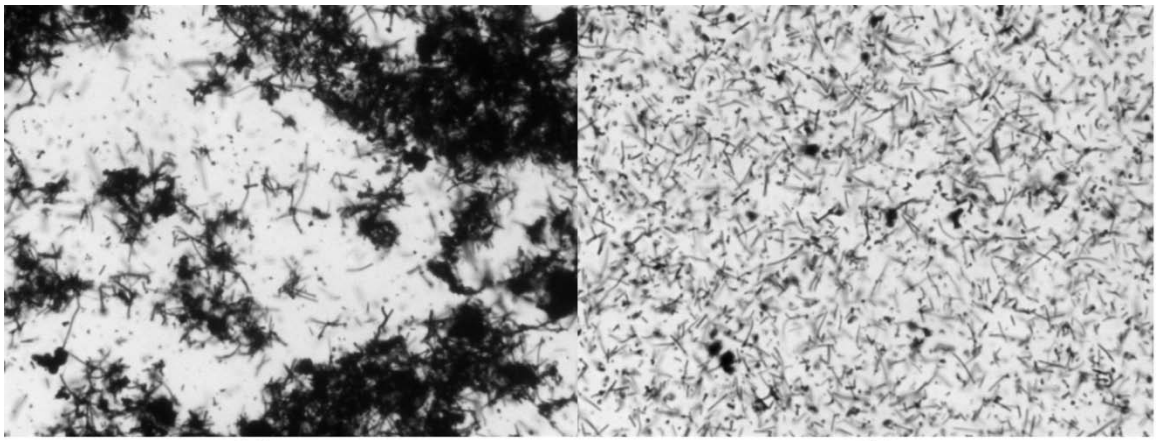

Fig. 8. Effect of ultrasonic mixing on the dispersion of CNFs in an aqueous solution containing a surfactant. Specimen (a) shows a sample shaken by hand, whereas (b) was sonicated for 15 minutes.

Fig. 9 shows a cryo-TEM image of an agglomeration of CNTs in an aqueous solution. In this sample, the CNTs were dispersed in an aqueous solution containing a surfactant and dispersed with an ultrasonic mixer for 5 minutes. The center of the image shows the CNTs bundled together. This group of nanotubes was unable to be fully separated due to the lack of

sufficient ultrasonic mixing. Fig. 10 shows the cryo-TEM image of CNTs dispersed in water and surfactant. The solution was mixed for 20 minutes by ultrasonication prior to cryogenic freezing in liquid nitrogen. Although the solution is not uniform across the entire image, the image lacks bundles of CNTs such as the one in the center of Fig. 9.

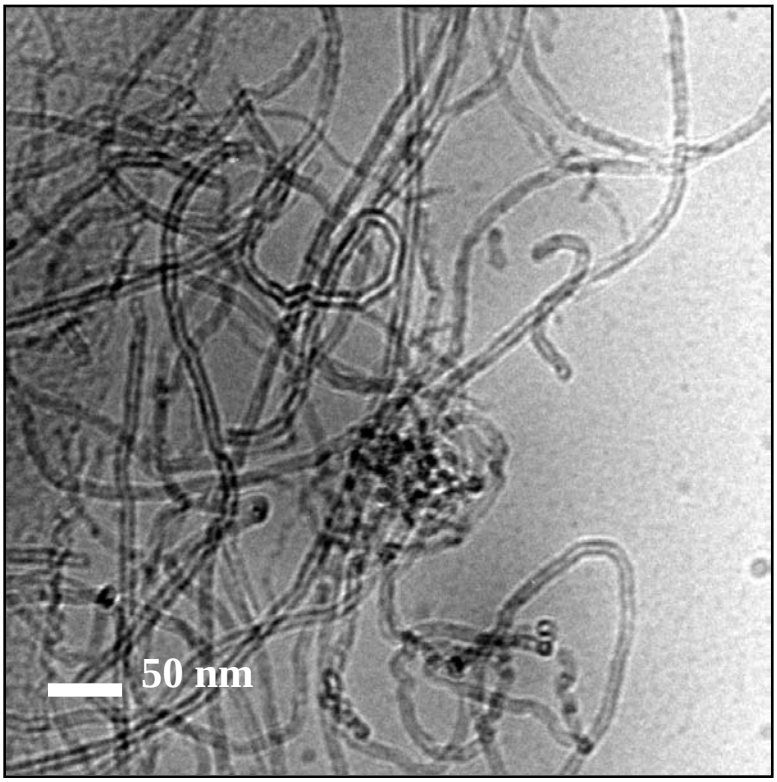

Fig. 9. Cryo-TEM image of CNTs poorly dispersed is an aqueous solution containing a surfactant. The center of the picture contains a large agglomeration of CNTs tangled together.

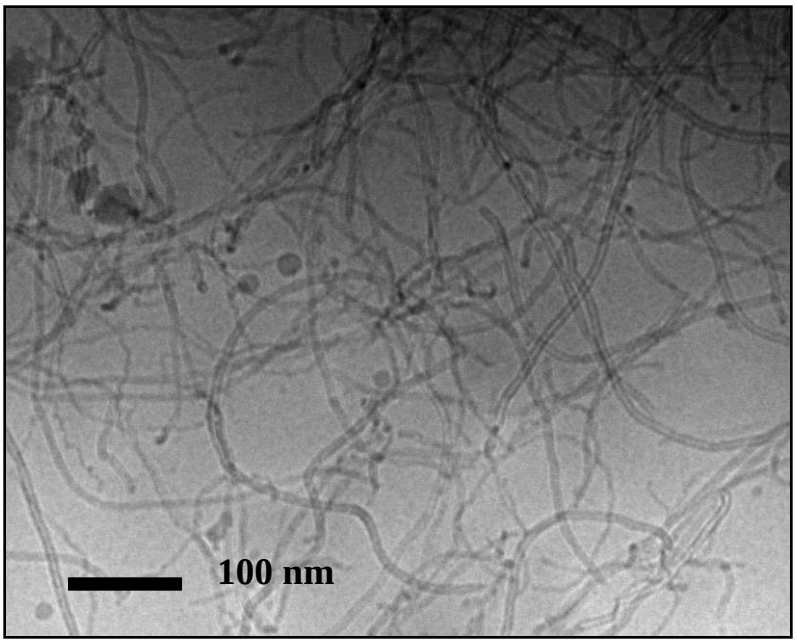

Fig. 10. Cryo-TEM image of CNTs dispersed in an aqueous solution. The small dark circles indicate the presence of impurities within the solution. Many of the CNTs look to be intact indicating ultrasonic mixing did not adversely affect the CNTs.

2.3.2 Acid Treatment

Fig. 11 shows the C1s (Fig. 11a) and O1s (Fig. 11b) spectra of the three samples. These include unaltered CNTs, functionalized CNFs, and functionalized CNTs. Both the CNTs and CNFs were functionalized for 1 hour in a 2:1 solution of N_2SO_4/HNO_3. While the peaks of the different plots can vary based on the relative intensity of the measurements, they are not an indication of functionalization. To properly calculate oxidation induced by acid treatment, the ratio of C1s to O1s was to be calculated. Table 1 shows the atomic mass percentage based on the spectral areas of carbon and oxygen. When treating both CNFs and CNTs for the same time, there is a clear difference in the oxidation of the two nano-filaments. The treated CNTs increased the amount of oxygen atoms by 10 times, whereas the CNFs increased by 16 times. This shows evidence that the CNFs become oxidized at a faster rate than CNTs. This is probably due to an increase in the number of preexisting surface defects when compared to CNTs. However, this

increase in functionalization can have negative effects on the size and strength of the CNFs as discussed earlier.

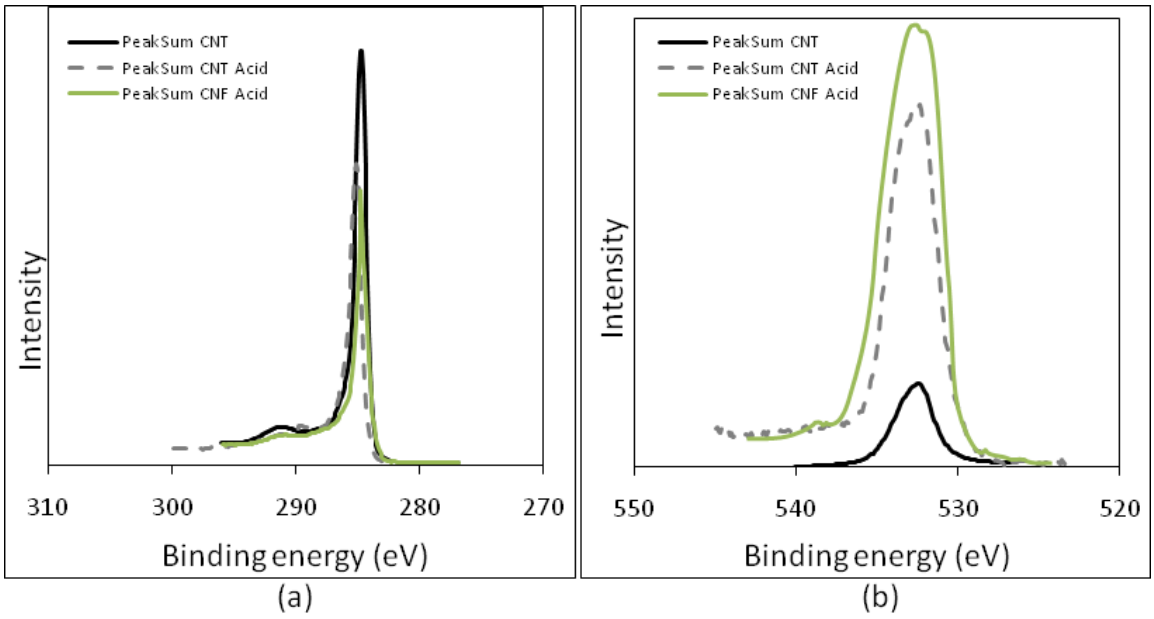

Fig. 11. XPS spectrum of untreated CNTs, acid treated CNTs, and acid treated CNFs showing: (a) C1s peaks, and (b) O1s peaks.

Table 1
The atomic mass percentages of carbon and oxygen at the sample surface.

Sample	Carbon %	Oxygen %
Untreated CNTs	98.78	1.22
Treated CNFs	80.43	19.57
Treated CNTs	87.80	12.20

Fig. 12 compares an untreated CNT (Fig. 12a) to an acid treated CNT (Fig. 12b) under the SEM at a magnification of 50,000x and 80,000x, respectively. In both images, the CNTs appear to be almost identical. This indicates that after treating the CNTs in acid, the structure of the CNT were still intact. Although TEM imaging of the walls will produce higher resolution images to discern the differences between untreated and treated CNTs, the SEM images showed no major defects such as partial cuts, exposed openings, or reduction in cross-sectional area.

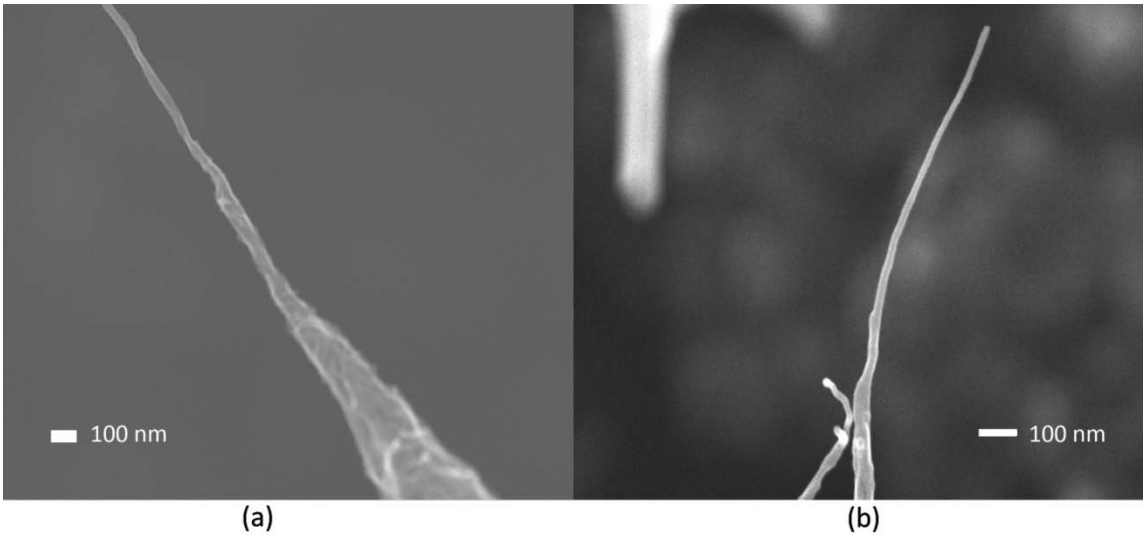

Fig. 12. Compares (a) an untreated CNT and (b) an acid treated CNT. Both CNTs look to be unaltered on the surface, indicating that the acid treatment did not severely alter the CNT structure.

All these findings show that surfactants alone are unlikely to be the sole solution to the problem of producing cementitious composites with uniformly distributed and well-bonded nano-filaments. Surfactants are great for long term dispersion to a certain extent. However, there is a limit to the amount of surfactants that can be used. Less surfactant leads to more ultrasonic mixing; and an increase in ultrasonic mixing damages a greater number of nano-filaments. Approaches such as using specific functional groups which specifically bond with cement grains should be further investigated. Further research is needed to determine an optimal balance between maximizing functionalization while at the same time minimizing damage.

3 QUANTITATIVE DISPERSION MEASUREMENTS

3.1 Introduction

Thus far, research on the dispersion of CNTs and CNFs has revolved around qualitative analysis. There are three common methods to analyze the dispersion of CNTs or CNFs in aqueous solutions. These methods include optical microscopy, electron microscopy (both SEM and TEM), and Fourier transform infrared (FTIR) spectroscopy [40, 57-58]. The most common method used in observing the dispersion of nano-filaments in a composite is by SEM. TEM is used to in order to observe dispersions typically in aqueous solutions, and at much higher magnifications than optical microscopes. Although CNTs are too small to be seen with optical microscopes, poor dispersion can create agglomerations which can be observed. FTIR spectroscopy measures the absorbance of light at specific wavelengths. The idea behind this technique is that the better dispersion, the darker the liquid is and therefore absorbs more light. The down side to these methods is that they all rely on visual observation as to whether or not the sample is well dispersed.

Most work on quantifying the dispersion particles inside nanocomposites revolves around polymer/clay composites. However, that is where the similarities end. Because there is no right or wrong way to quantify dispersion, everyone does it a little differently. Eckel et al. [59] quantified the dispersion of clay particles within a polymer matrix by an array of parallel lines across a TEM image and calculating the number of interceptions. The dispersion was calculated by dividing the total length of the lines by the number of intersections. A smaller line intercept distance indicated a better dispersion. However, this method cannot give a distribution of spacing between particles.

Recently, Xie et al. [60] developed a novel method to calculate dispersion by using two parameters: degree of dispersion (χ) and mean interparticle distance per unit volume of clay (λ_V).

Where χ is the percentage of exfoliated platelets, and λ_V is a measure of spatial separation between particles. A higher χ value indicates better exfoliation, and a lower λ_V number means an increase in the number of clay particles per unit volume, indicating improved exfoliation. This method can show differences between samples, however, the numbers don't provide much meaning as to how "ideal" the dispersion is.

The proposed method developed by the author in this section can place a percentage value to both dispersion and agglomeration. Thus, when analyzing the dispersion of particles, a percentage will give more insight as to how well the dispersion is.

3.2 Proposed Method

Recently, Luo and Koo [61-63] used a method of calculating the statistical distribution of particle spacing through the integration of the probability density function (pdf). First, all spacing data is separated into groups with an interval of Δx. To show the statistical distribution of free-path spacing, a histogram is then created based on the spacing interval and the frequency which the interval occurs as shown in Fig. 13c. Once the histogram is created, either a normal or lognormal distribution curve is fitted to the data, depending on which method gives a better fit. From the superimposed distribution curve (Fig. 13d), $f(x)$ is the probability density function, μ is the mean value, and σ is the standard deviation. It can then be said that the probability of a spacing value (x) being between $a \rightarrow b$ is defined as

$$\int_a^b f(x)dx \tag{1}$$

Usually the free path spacing follows a lognormal distribution which is defined as

$$f(x) = \begin{cases} \dfrac{1}{xn\sqrt{2\pi}} \exp\left[-\dfrac{(\ln x - m^2)}{2n^2} \right] & (x > 0) \\ 0 & (x \le 0) \end{cases} \tag{2}$$

In the above expression, x is the size of the free-path spacing,

$$n = \sqrt{\ln \frac{\mu^2 + \sigma^2}{\mu^2}} \tag{3}$$

and

$$m = \ln \frac{\mu^2}{\sqrt{\mu^2 + \sigma^2}} \tag{4}$$

where μ and σ are the mean and standard deviation, respectively, of the associated normal distribution. The histogram shown in Fig. 13c is normalized so that $\int_0^{+\infty} f(x)dx = 1$. Therefore, it can be said that if one considers the dispersion percentage, *D*, to include all spacing between $x = 0 \to \infty$, then $D = \int_0^{+\infty} f(x)dx = 100\%$. However, the dispersion percentage needs to be defined as a range of spacing. The standard deviation, σ, can be used to measure of the dispersion [64]. Smaller σ indicated a higher dispersion; however, it does not provide reliable bounds for the integral due to the fact that it is not constant from the mean value. Instead, one can say that the dispersion is defined as how many spacing data points are within a certain percentage above and below the mean value, μ.

Therefore, if we assume the dispersion, *D*, to include all spacing between a certain percentage of μ, then

$$D_{0.1} = \int_{0.9\mu}^{1.1\mu} f(x)dx \tag{5}$$

includes all spacing in the range of μ ± 10 % of μ and

$$D_{0.2} = \int_{0.8\mu}^{1.2\mu} f(x)dx \tag{6}$$

includes all spacing in the range of μ ± 20 % of μ as shown by the gray hatched area in Fig. 13d. Similarly, dispersion values can be defined as $D_{0.3}$ for all values ± 30 % of μ, and others can be formulated for higher values as well. Higher *D* values indicate more data within the defined

region around the mean, thus a more uniform spacing between particles. The more uniform the spacing between particles, the higher the degree of dispersion. In theory, the dispersion is defined as 100% if all free path spacing is uniform, although 100% dispersion is impossible to obtain.

The method of only calculating the free space distance between particles works very well when the particles are formed from irregular shapes and sizes. However, when measuring the dispersion of particles such as CNTs or CNFs, the particles can be thought to have a uniform width relative to the free-path spacing. Fig. 14b show an example of when single particles have a uniform free spacing. Fig. 14a shows both single particles as well as a bundle of fibers. According to the current method, the calculated dispersion based exclusively on the free-path spacing between particles will produce identical dispersion percentages. However, visual observations comparing Fig. 14a and Fig. 14b will conclude that Fig. 14a is not as uniformly dispersed as Fig. 14b. A modified method to calculate both the dispersion (free-path spacing) and agglomeration (particle size) should be employed to get a better understanding on the degree of dispersion.

This modified method can easily be adapted to the current method, where MATLAB [65] not only records the lengths of the white pixels used to calculate $D_{x.x}$, (Fig. 14a and b) but also the black pixels for $A_{x.x}$ (Fig. 14c and d). Where $A_{x.x}$ is the same formulas as $D_{x.x}$, but instead of measuring the free path spacing, $A_{x.x}$ measures the particle sizes. MATLAB then plots the distribution of both the free spacing as well as the agglomeration, and lognormal best-fit lines are then used to evaluate the percentage of dispersion and percentage of agglomeration from Eq(1).

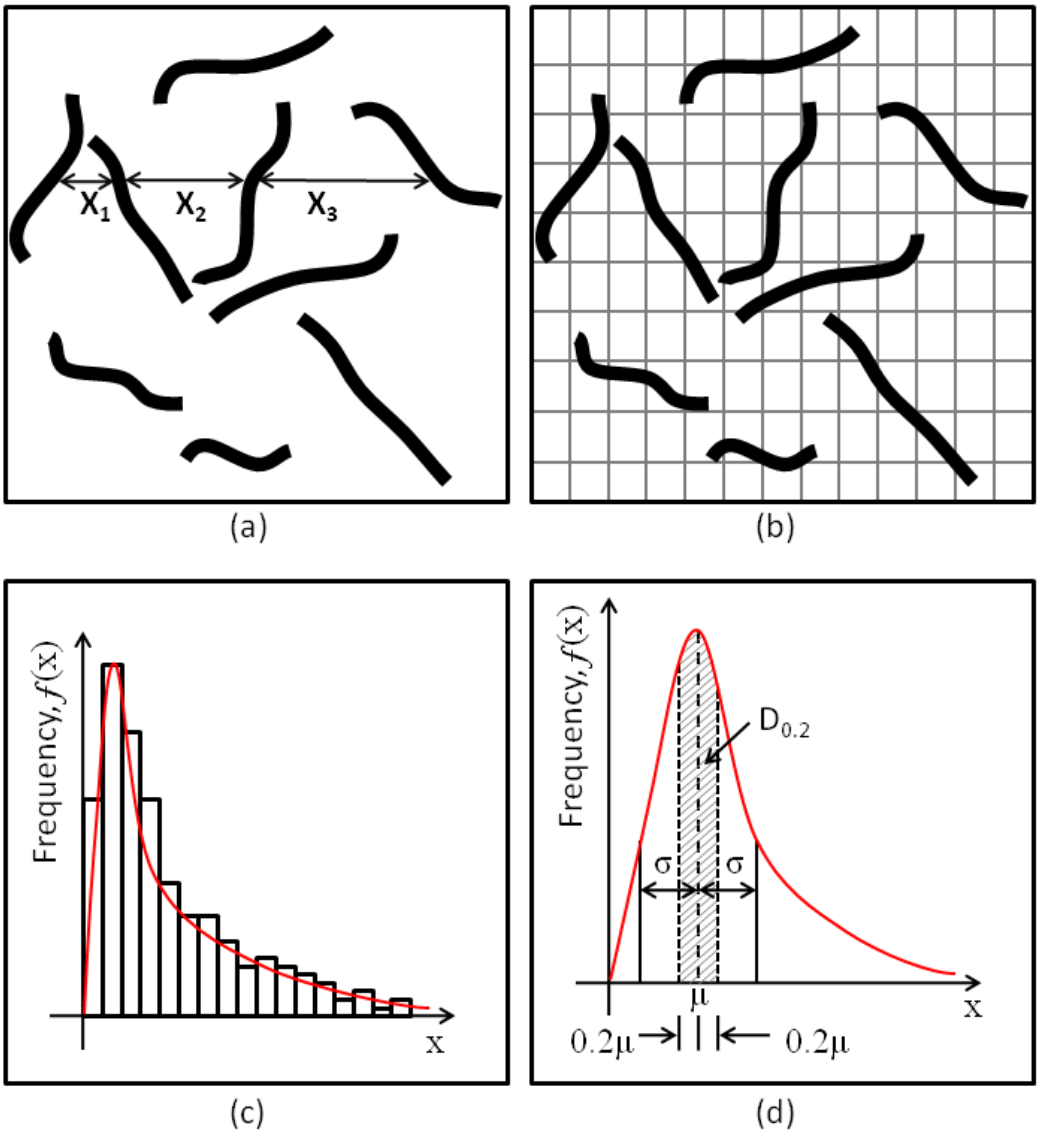

Fig. 13. (a) Free-path spacing of the particles; (b) image with grid lines; (c) construction of histogram; (d) definition of dispersion quantities.

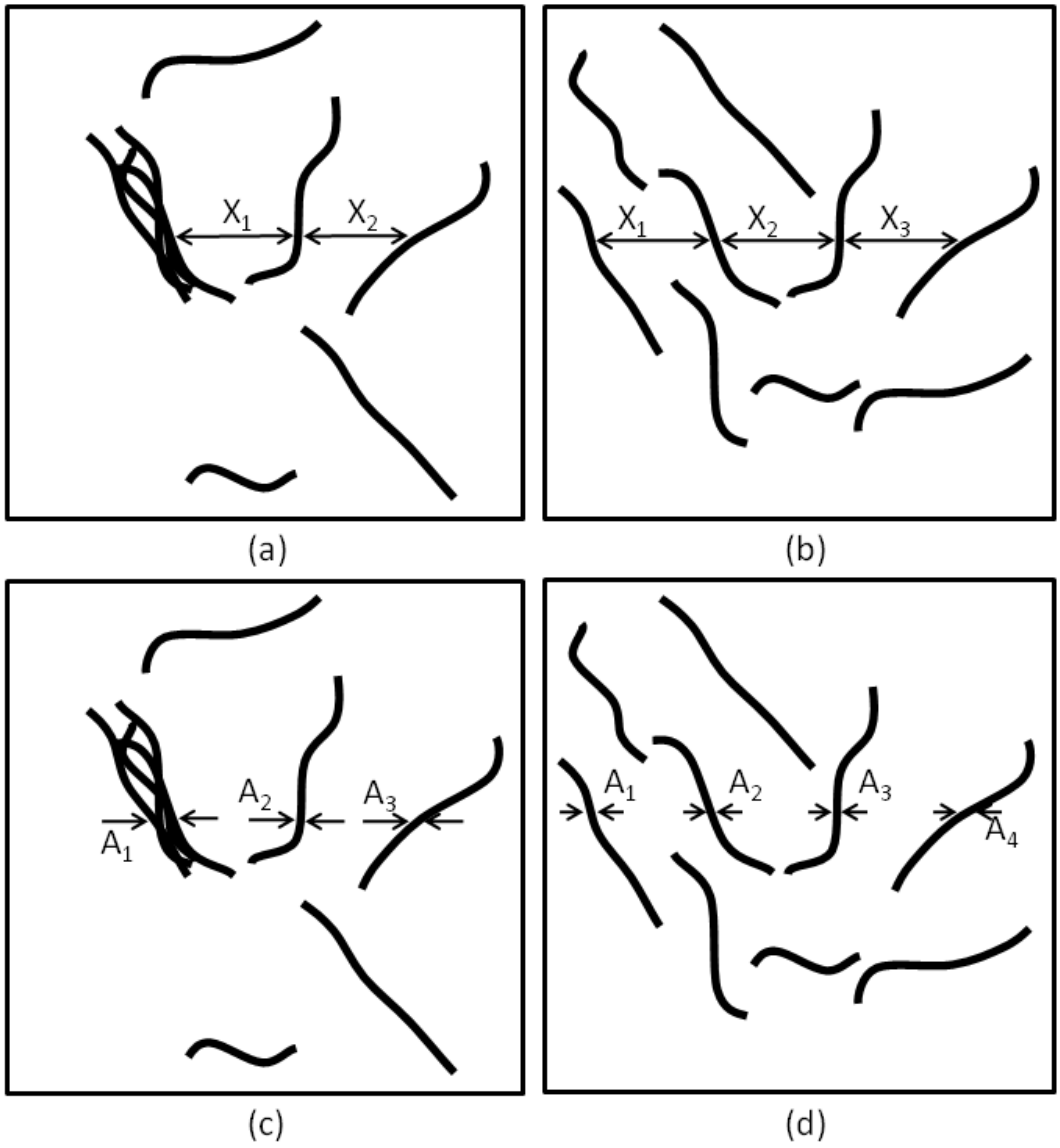

Fig. 14. (a) Uniform free-path spacing with particle agglomeration; (b) uniform free-path spacing and particles; (c) non-uniform particle sizes; (d) uniform particle sizes

3.3 Proof of Concept

To calibrate the program, three major variables are present: number of cross-sectional lines, limits on the upper and lower bounds of the integral used for to calculate the dispersion, and limits on the upper and lower bounds of the integral used to calculate the agglomeration. Fig. 15 was used to calibrate the number of lines using a convergence test as will be shown in section 3.5.

However, these three images could not be used to calculate the limits for the either the dispersion or agglomeration integral. This is due to the images having particles with circular cross-sections, and a nonuniform distribution. To determine the integration limits used to calculate the dispersion and agglomeration percentage, an image with a uniform dispersion and agglomeration needs to be used. Fig. 16a contains equally spaced particles and Fig. 16b had equal spacing with a bundle containing 5 particles in the middle. The equal spacing ensures the integral bounds are set at appropriate values above and below the mean value.

In order to determine how well the program works at calculating particle distribution and agglomeration percentages, a set of images were created that are distinctly different. Fig. 15 contains three sets of images used to simulate a random distribution of particles. Fig. 15a is created to simulate a distribution of circular particles in which no voids are present in the matrix. Fig. 15b has 16 small sized voids scattered throughout the image where there are no particles. These voids simulate air, aggregate, or any other product that may prevent the nano-filaments from properly dispersing throughout the matrix. Fig. 15c has one large void in the center with no particles inside the void. In all three cases, there are an equal number of particles, and all three images are the same size, 1500 x 1500 pixels, and the circular particles have a diameter of 60 pixels across. The dispersion analysis results of Fig. 15 will be shown in section 3.5.

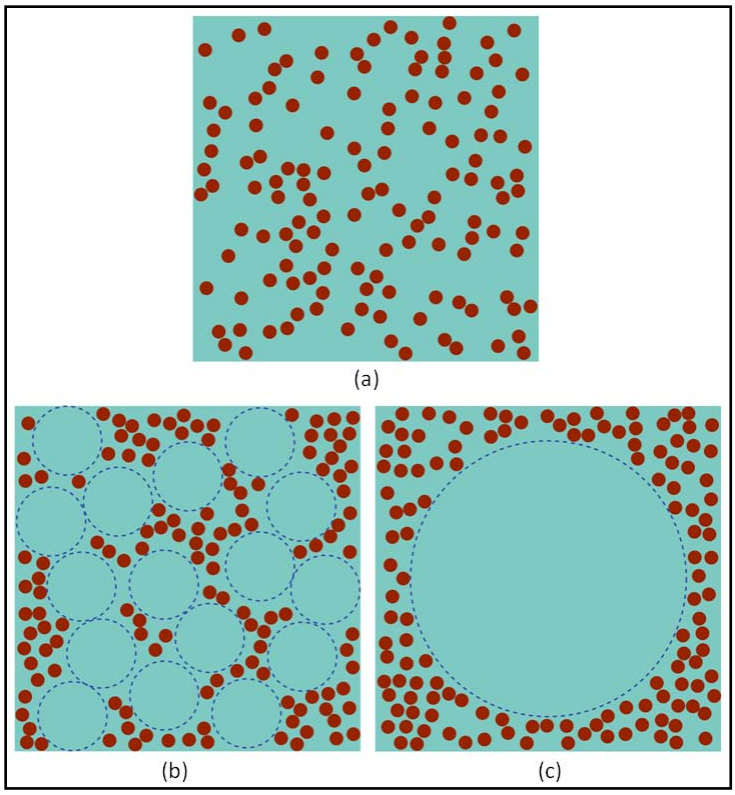

Fig. 15. Randomized circles within a fixed window to simulate particle distribution. Each image contains either: (a) circular particles spread throughout, (b) small 'void' areas with no circular particles, (c) a large void with no circular particles. Each image is 1500 x 1500 pixels.

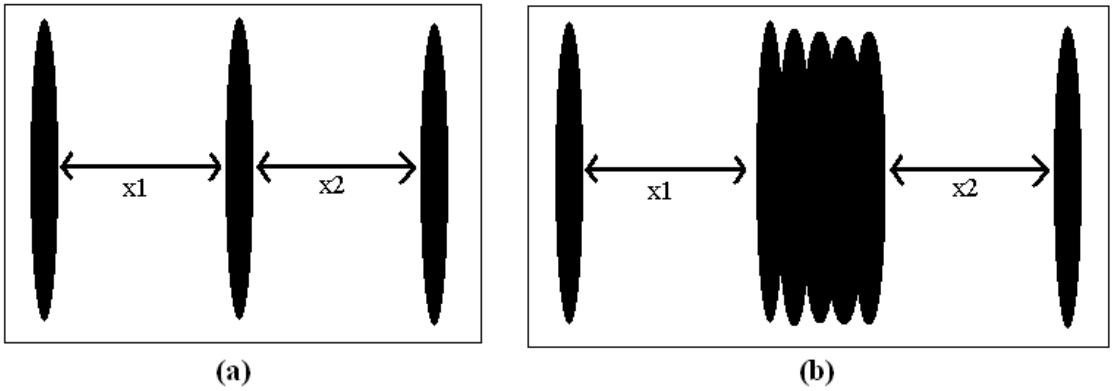

Fig. 16. Two images used to calibrate the bounds for the dispersion and agglomeration integral. Image (a) has three lines equally spaced apart, (b) had equal spacing, and the center is bundled with five particles.

3.4 Microscopy Imaging

Two samples of aqueous solutions containing both CNTs and CNFs were obtained by either TEM or optical microscopy. Fig. 17 is a TEM image of CNTs at a concentration of 0.25 wt% by weight of water. The sample was prepared by ultrasonically mixing the CNTs, surfactant, and water for 20 minutes. After sonication, the solution was placed onto a TEM grid and quickly frozen down to liquid nitrogen temperatures. During the entire imaging session, the holder and TEM grid remained at liquid nitrogen temperature. Fig. 18 shows two optical images of CNFs dispersed within an aqueous solution. Fig. 18a is of CNFs, surfactant, and water which were dispersed by hand shaking the solution for 5 minutes, and Fig. 18b shows CNFs, surfactant and water which were dispersed using an ultrasonic mixer for 5 minutes. A small drop of solution was then placed onto a slide, and covered with a small slip and viewed under a 40x dry objective optical microscope.

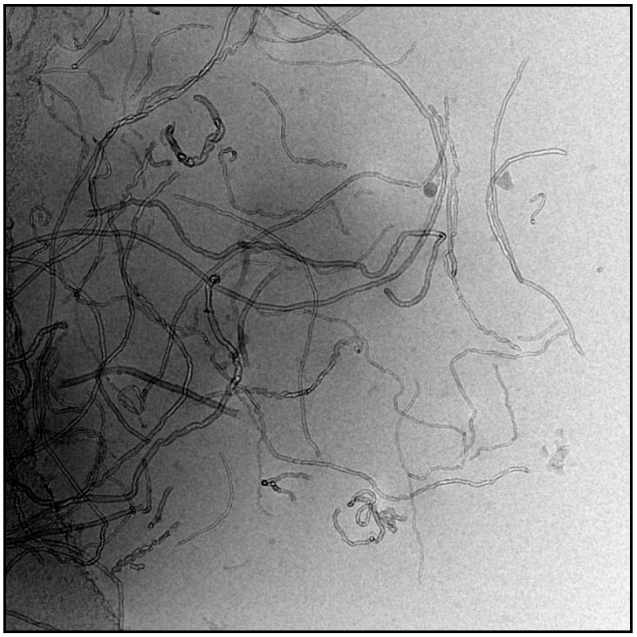

Fig. 17. Unaltered TEM image of CNTs dispersed within an aqueous solution at a concentration of 0.25 % by weight of water.

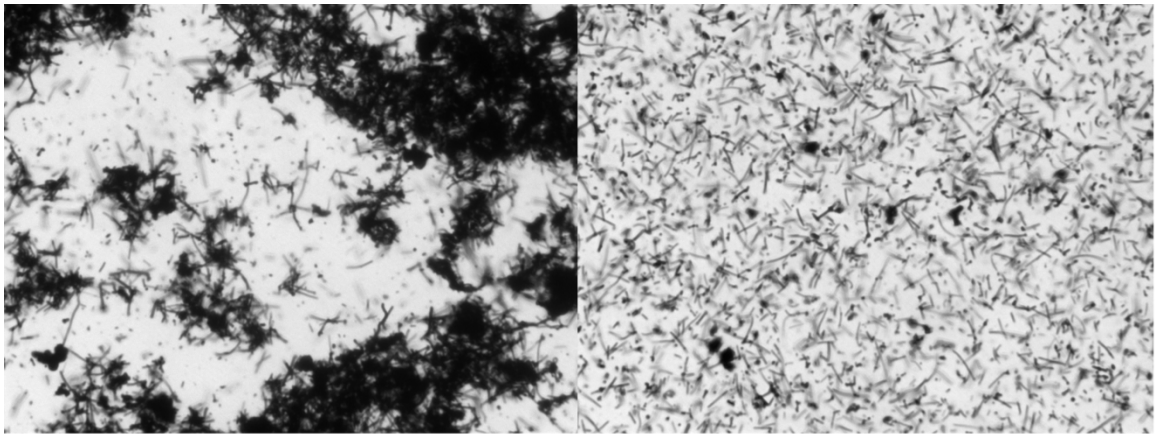

Fig. 18. Unaltered optical image of (a) bundled and (b) dispersed CNFs dispersed within an aqueous solution at a concentration of 0.5 % by weight of water.

3.5 Results and Discussion

To determine how many lines are needed to converge to a reasonable convergence, each image in Fig. 15 was analyzed with the number of vertical and horizontal lines varying from 10 to 400. Fig. 19 shows the results of the convergence test. 100 lines for the horizontal plane, and 100 lines for the vertical plane was chosen as an optimal balance between computation time and relative convergence. The next step was to determine which distribution fit the data better. From the histograms in Figs. 20b, 21b, and 22b, the lognormal distribution (red line) is a better fit when compared to the normal distribution (blue line). Table 2 shows the statistical calculations using a lognormal best fit curve calculated by MATLAB, where μ and σ are the mean and standard deviation, respectively, of the associated normal distribution and $D_{0.2}$ represents the dispersion percentage between 0.8μ and 1.2μ calculated by Eq.(6). These numbers indicate that the best distribution was the image with no circular void space, and the worst dispersion was from the image with the single large void space. Visual inspection of Figs. 20a, 21a, and 22a confirm the calculations. Fig. 20a will have a better dispersion because of the lack of unoccupied void space. Fig. 22a is the worst because of the large area in the middle with no particles.

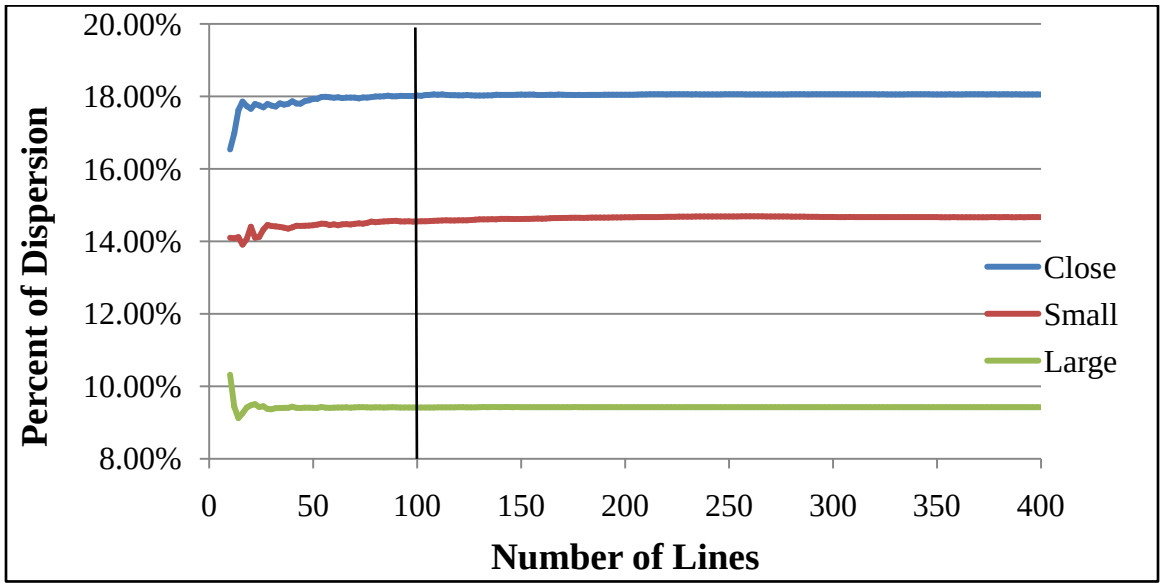

Fig. 19. Convergence test of the three images from Fig. 15. The number of lines is the total for each axis.

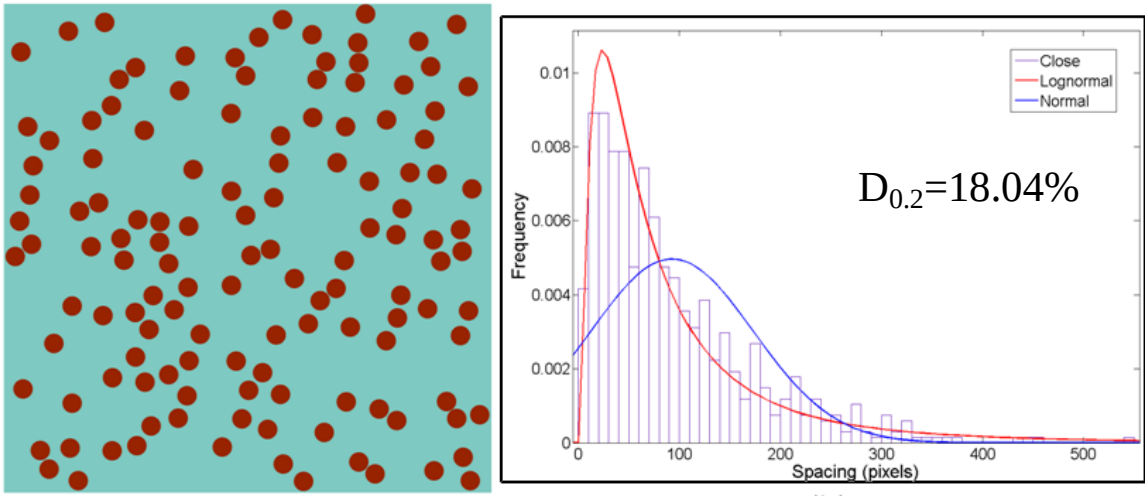

Fig. 20. (a) Artificial image containing circular particles randomly dispersed, (b) normalized histogram containing a lognormal fit (red line) and a normal fit (blue line).

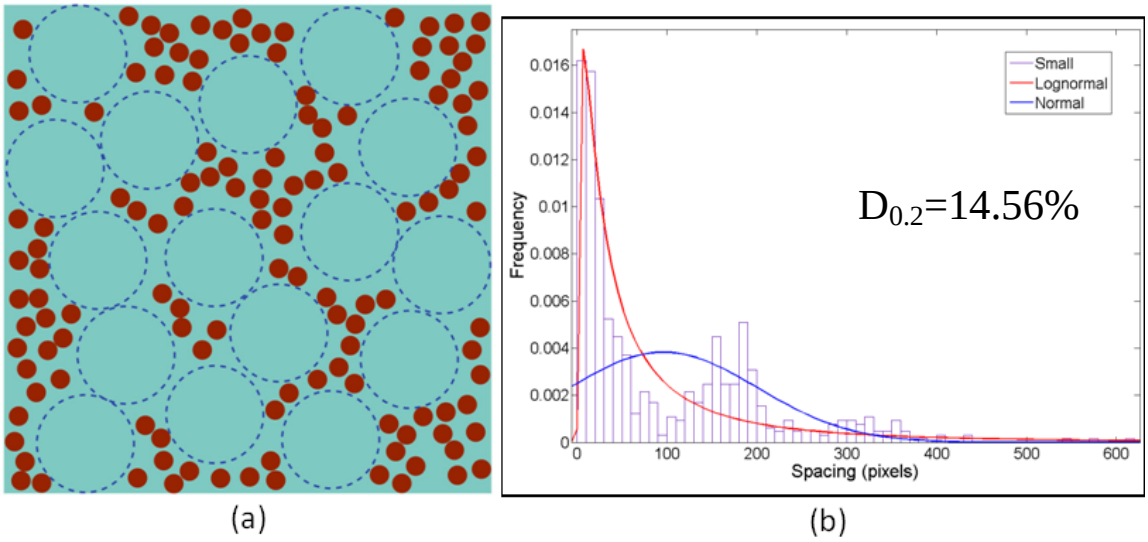

Fig. 21. (a) Artificial image containing circular particles randomly dispersed with small voids containing no particles, (b) normalized histogram containing a lognormal fit (red line) and a normal fit (blue line).

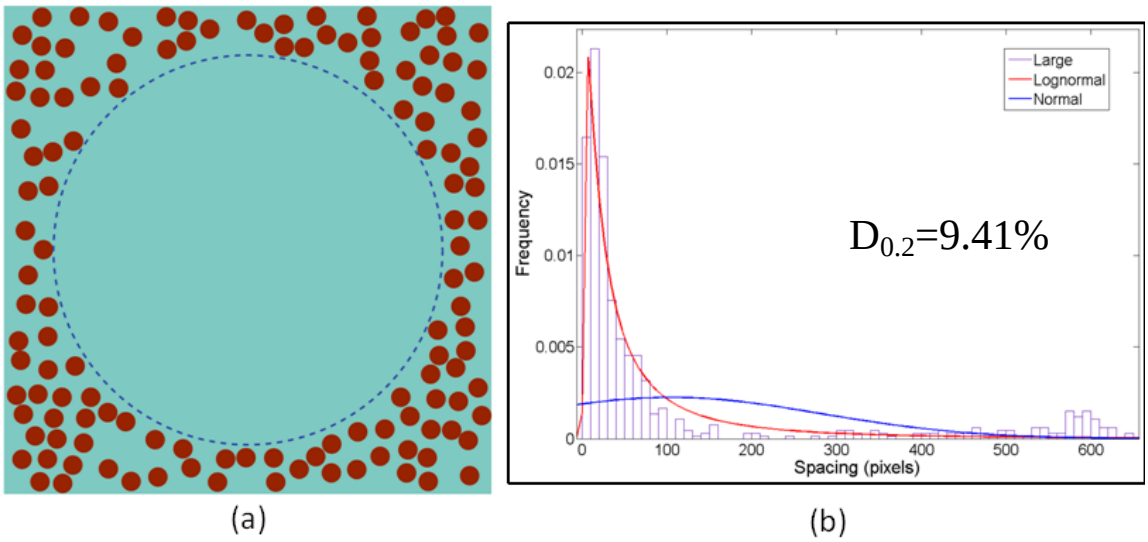

Fig. 22. (a) Artificial image containing circular particles randomly dispersed containing a large void area of no particles, (b) normalized histogram containing a lognormal fit (red line) and a normal fit (blue line).

Table 2
Statistics of the three images simulating random particle distributions.

Image	μ	σ	$D_{0.2}$ (%)
Close (Fig. 20)	100	16293	14.68
Small (Fig. 21)	116	76635	9.33
Large (Fig. 22)	94.2	53705	9.14

The next step was to determine the appropriate bounds for the agglomeration integral. Using Fig. 16a and b, appropriate bounds were determined to be ±30% of μ. Looking at Table 3, dispersion percentage varied by 0.4%, while the agglomeration percentage varied by 12.7%. This is a sharp change in the degree of agglomeration, although, the values are small because the top and bottom of the particles in Fig. 16 have a radius to them which in turn spread out the histogram of the particle sizes.

Table 3
Statistical data for configuring the bounds on the agglomeration integral

Image	μ	σ	$D_{0.2}$ (%)	$A_{0.3}$ (%)
Dispersed (Fig. 16a)	117.5	66.4	99.5	33.4
Bundled (Fig. 16b)	119.5	26.0	99.9	20.7

Fig. 23 shows the TEM image of the CNTs dispersed within an aqueous solution after image processing. The image was converted into a binary image to calculate the free path spacing and particle size. Fig. 24 is the probability density function (PDF) plots for the dispersion (Fig. 24a) and agglomeration (Fig. 24b) for the TEM image. The distribution and agglomeration percentages are 10.19% and 35.5%, respectively. Fig. 25 shows the processed image of the CNFs in a bundled and dispersed state. Fig. 26 shows the PDFs for the CNF image with large bundles. The distribution and agglomeration percentage for Fig. 26 is 10.38% and

26.71%, respectively. Fig. 27 is the PDFs for a well dispersed solution of CNFs. The well dispersed solution has a dispersion and agglomeration percentage of 15.82% and 33.23%, respectively. All the statistical data for the CNTs and CNFs are shown in Table 4.

Fig. 23. TEM image converted to binary black and white pixels of CNTs dispersed in an aqueous solution at 0.25 % by weight of water.

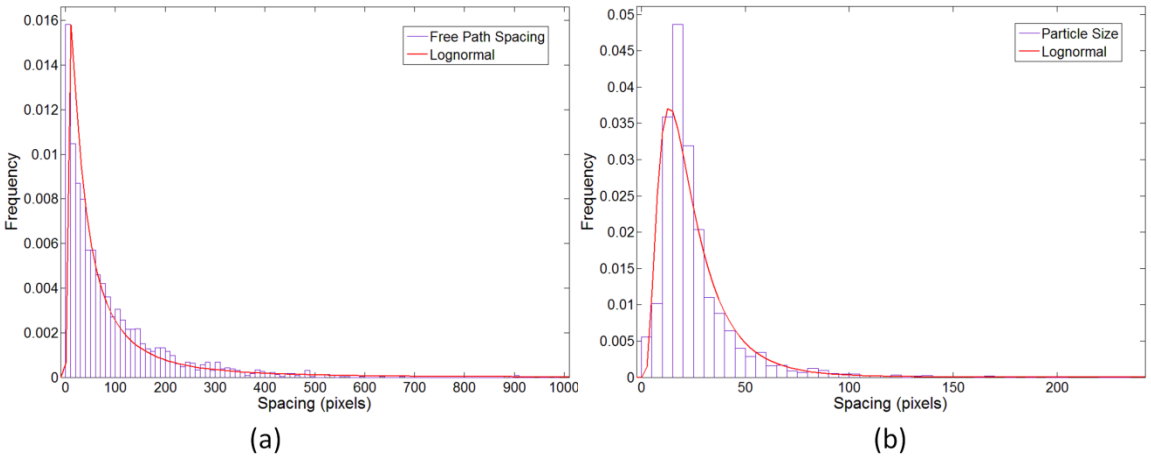

Fig. 24. (a) lognormal PDF of the free path spacing used to calculate the dispersion percentage, (b) lognormal PDF of the particle sizes used to calculate the agglomeration percentage.

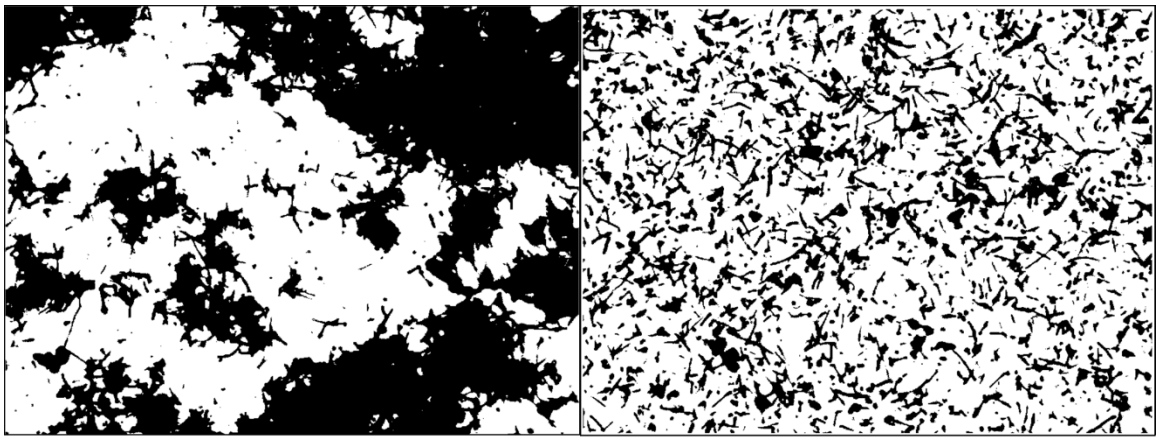

(a) (b)

Fig. 25. (a) CNFs bundled within an aqueous solution, (b) CNFs well dispersed in an aqueous solution.

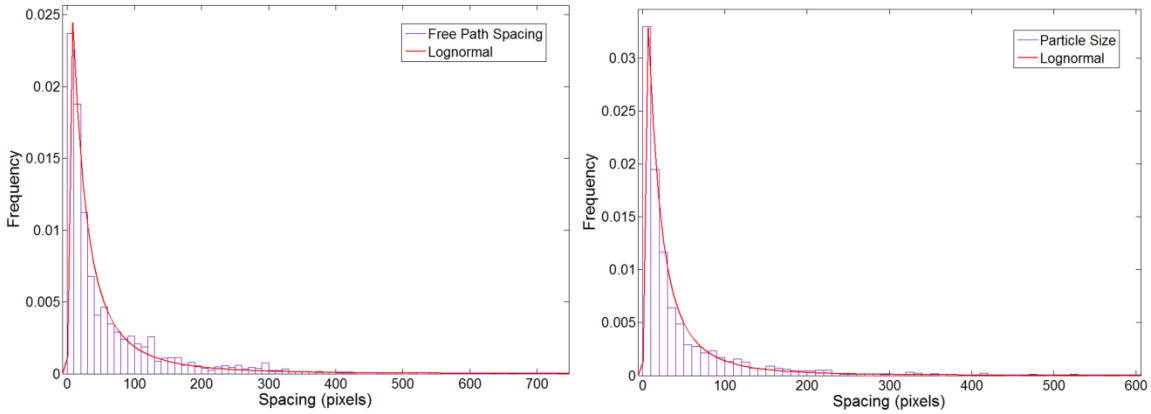

(a) (b)

Fig. 26. PDF plots of the (a) free path spacing and (b) particle sizes from **Fig. 25**a.

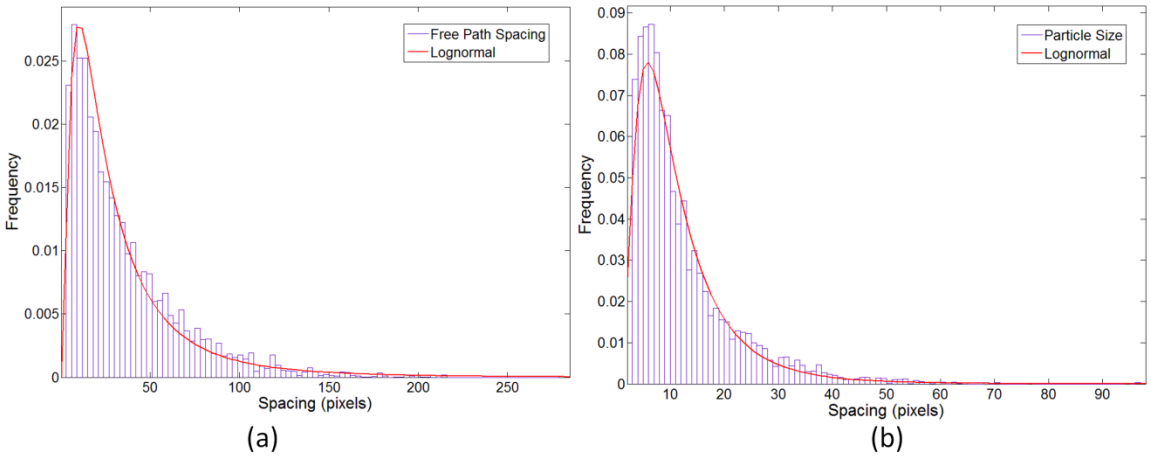

Fig. 27. PDF plots of the (a) free path spacing and (b) particle sizes from Fig. 25b.

Table 4
Statistical data comparing the quantitative dispersion and agglomeration of CNFs and CNTs.

Fig.	μ_D	σ_D	$D_{0.2}$ (%)	μ_A	σ_A	$A_{0.3}$ (%)
CNTs	102.61	46019	10.19	25.17	333.96	35.50
CNFs bundled	62.76	16293	10.38	43.38	6860.20	26.71
CNFs dispersed	36.19	1757.1	15.82	11.90	87.54	33.23

It can be seen from Table 4 that the given method works very well to quantify the dispersion and agglomeration of particles within an image. When comparing dispersed versus bundled CNFs, the presented method was able to show that the dispersion is enhanced by 5.44%, while the bundles were reduced by 6.52%. It important to note that a higher agglomeration percentage indicates fewer bundles are present. A higher number means more sizes are within the integral bounds. This novel method works equally well in optical and electron microscopes. This method can be used to give percentages to different experimental techniques used to disperse nano-filaments within aqueous solutions, and could even be applied to dispersions within hydrated cement as well. However, in the current state, some drawbacks are present. First, the

mean and standard deviation are given in terms of pixels. This should be converted to a length such as μm or nm. Second, the agglomeration is based on a mean value which can change. Therefore, if the bundles have uniform dimensions, then the agglomeration will still be shown as having few bundles. The bounds on the agglomeration integral should not be based on plus or minus a percentage of the statistical mean; rather, the bounds should be plus or minus a percentage of the true diameter of the fiber.

4 COMBINING CEMENT WITH CARBON NANOTUBES AND CARBON NANOFIBERS

4.1 Methods

4.1.1 Nano-filament Preparation

To prepare each mixture, water, surfactant, and either CNTs or CNFs are first measured, and then mixed together using a water jacketed beaker (Fig. 28). The water jacket around the beaker helps to keep the temperature of the dispersion below 45^{o}C during mixing. In order to insure a well dispersed solution, an ultrasonic mixer (Fig. 29) is used from Sonics & Materials, Inc. which can deliver up to 500 watts at 20 kHz through a 13 mm titanium alloy probe. An ultrasonic mixer is a device that uses a high frequency driver to transmit acoustical energy throughout a liquid medium. The energy in the shock waves is extremely high and significantly accelerates chemical reactions and breaks the clumps and agglomerations of particles. To reduce the chances of breaking the nano-filaments, CNFs are mixed for 5 minutes whereas CNTs are mixed for 20 minutes.

Fig. 28. Water jacketed beaker for mixing nano-filaments with the ultrasonic mixer. Continuously flowing water keeps the temperature of the solution below 45^{o}C to prevent excessive evaporation.

Fig. 29. Ultrasonic mixer from Sonics & Materials, Inc. is capable of delivering 500 watts of power at 20 kHz [66].

4.1.2 Incorporation of Cement and Nano-filaments

After ultrasonic mixing, the dispersed solution was added along with the cement powder into a variable speed planetary kitchen blender shown in Fig. 30. Each batch was mixed within the blender for 3 minutes on low, then 4 minutes on high for a total of 7 minutes of blending. This ensures the cement was well dispersed within the water solution. Periodically, the blending was paused and the inside walls of the blender were scraped down with a spatula in order to remove any agglomerations of unhydrated cement which might had been sticking to the walls of the blender.

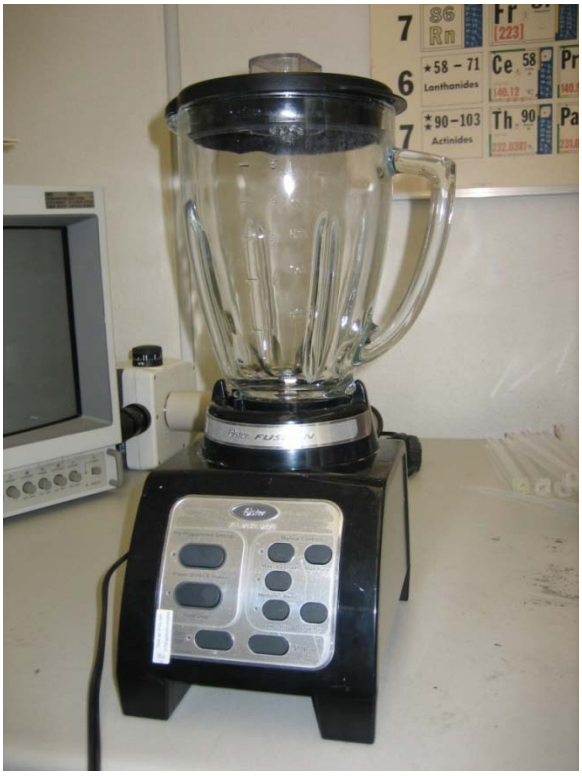

Fig. 30. Mixing blender

4.1.3 Molding

After the 7 minutes of blending are up, the cement paste is transferred into a plastic bottle, and placed into a vacuum chamber for 3 minutes to remove any entrained air caused by the mixing process. Sometimes the vacuuming time will be increased if the cement paste is very thick. Once the vacuuming time has elapsed, an acrylic mold is placed on top of a vibration table shown in Fig. 31, and the cement paste is poured into the molds. The vibrations from the table help to fluidize the cement paste which helps to minimize the formation of large air pockets.

Fig. 31. Vibration table.

Acrylic molds were chosen over other plastics (such as PVC or polyethylene) because acrylic will not absorb water from the samples. Fig. 32 shows the top of the acrylic molds. They were extruded square molds with very tight tolerances and minimal radius at the corners. Another benefit with using extruded acrylic was the smoothness of the surface. No mold release needed to be used. To construct the molds, square acrylic was cut using a bandsaw, and then a piece of flat acrylic was glued to the bottom of the square tube to form a base.

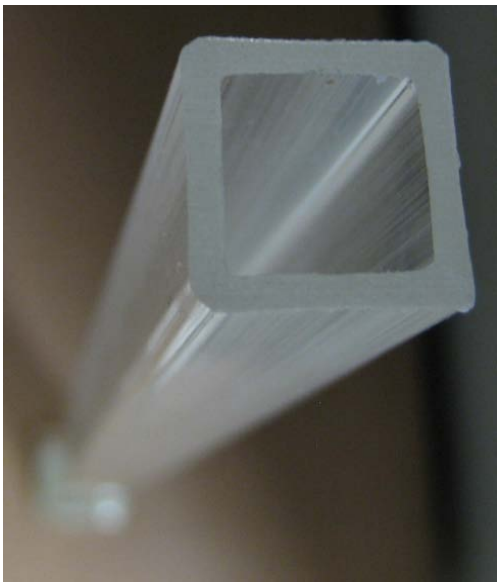

Fig. 32. Top view of acrylic aold.

After pouring the cement into the molds, they were allowed to hydrate for 1 day before demolding. To demold the samples with minimal harm, a soldering iron was used to melt the acrylic. The soldering iron was a 200 watt iron capable of 537^{o}C (1000^{o}F) with a custom made cutting tip made from copper pipe (Fig. 33).

Fig. 33. A 200 soldering iron watt for demolding cement specimens from the acrylic molds. The cutting tip is custom made from copper pipe.

4.2 Results

A total of nine batches of cement specimens were produced. These included a reference sample of plain cement paste, two batches each of cement paste with untreated and treated CNTs at 0.1 wt% and 0.2 wt% by weight of dry cement, two batches each with untreated and treated CNFs at 0.1 wt% and 0.2 wt%. Table 5 summarizes the composition of the nine batches. These batches were labeled to indicate the components and their concentrations. The letter "U" or "T" in the first column indicates whether the samples are untreated or treated, respectively. In the second column, the letter "F" represents CNFs, "T" represents CNTs, and in the third column, "1" and "2" indicate filament dosages of 0.1 wt% and 0.2 wt%, respectively. All five batches had a water/cement ratio of 0.40, and the batches containing either untreated or treated CNTs or CNFs had a surfactant (superplasticizer) to cement ratio of 0.005. No surfactant was used for the plain cement samples. A minimum of four replications (samples) were made for each nanocomposite tested.

Table 5
Mix design of the test specimens.

Test Specimens	Water/cement ratio	Untreated CNFs: % weight of cement	Treated CNFs: % weight of cement	Untreated CNTs: % weight of cement	Treated CNTs: % weight of cement
Reference	0.4	0	0	0	0
UF1	0.4	0.1	0	0	0
TF1	0.4	0	0.1	0	0
UF2	0.4	0.2	0	0	0
TF2	0.4	0	0.2	0	0
UT1	0.4	0	0	0.1	0
TT1	0.4	0	0	0	0.1
UT2	0.4	0	0	0.2	0
TT2	0.4	0	0	0	0.2

5 MECHANICAL TESTING, EXPERIMENTAL RESULTS, AND MICROSTRUCTURAL CHARACTERIZATION

5.1 Test Fixture

The fixture was constructed out of 6061 aluminum, with the individual parts either welded or screwed together. The narrow base was designed to fit within the feet of the AFM, and houses the actuator and load cell. The top half of the fixture expands out to be able to hold the specimens at a distance of 160 cm. The specimen holders were machined with a radius of 1.6 mm (1/16 inch) to reduce stress concentrations caused by sharp corners. In order to minimize initial damage to the specimens before testing, one end of the fixture had a hole all the way through to allow the specimens to slide in without the need to cut the specimens after demolding. Fig. 34 shows detailed dimensions of the specimen holders.

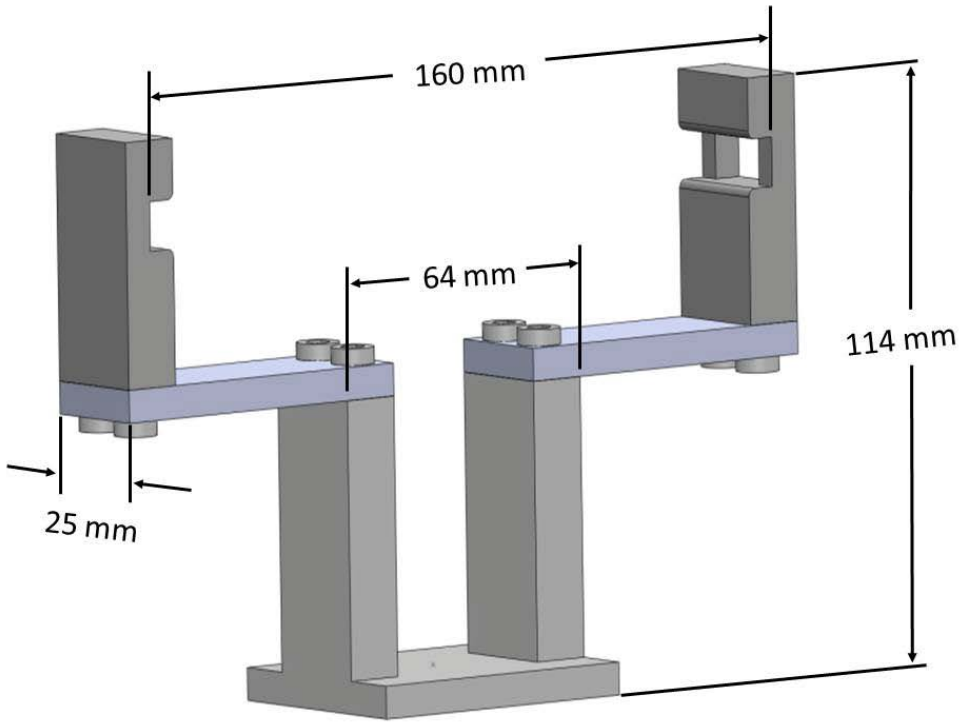

Fig. 34. Load frame dimensions (mm).

5.1.1 Loading

Mechanical testing of the cement specimens was performed with the use of a precision displacement controlled actuator purchased from Newport, Inc. The performance specifications for the actuator are summarized in Table 6. The NSA12 actuator was chosen specifically for the ability to control the speed between 0.001 mm/s to 0.9 mm/s. Having this speed range offers fine control for testing both near static to dynamic loading. Static loading was required to obtain mechanical properties such as Young's modulus, toughness and strengths. High speed loading can obtain properties such as storage and loss modulus. Storage and loss modulus will be investigated in future research.

In order to control the NSA12 actuator, the Newport NSC200 controller was used in conjunction with drivers available for Labview [67]. The NSC200 controller was able to step the NSA200 actuator with 64 micro-steps. With the combination of the NSA200 actuator and the NSC200 controller, the load frame had an incremental motion of 3,072 micro-steps/revolution, or 0.1 μm/micro-step.

Table 6

Newport NSA12 actuator specifications.

Feedback	Open loop, no encoder
Drive Screw Pitch (mm)	0.3048
Travel Range (mm)	11
Minimum Incremental Motion (μm)	0.2
Maximum Speed (mm/s)	0.9
Axial Load Capacity (N)	28

To record the force applied to each beam, a low profile load cell from Strain Measurement Devices (SMD), Inc. was used. The load cell had a capacity of 2.5 kg, and uses a sputtered thin film gauge which created a compact sensor with exceptional resolution. The load cell mounted to a base which sat on top of the actuator. To evenly spread the load across the width of the beam, a

bar was used with a half-circle top, and was attached to the load cell by an adjustable screw. Fig. 35 shows the load cell with the attached base, screw, and loading bar.

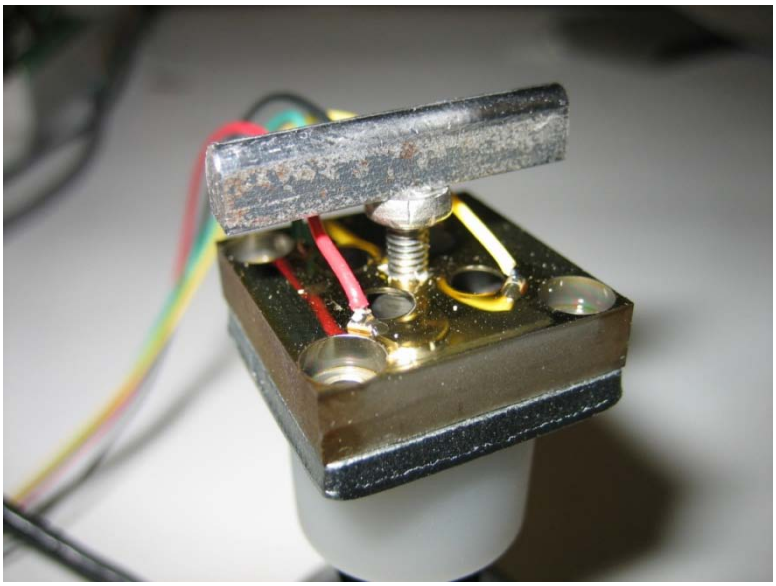

Fig. 35. SMD low profile load cell attached on top of the actuator. The adjustable screw attaches the loading bar to the load cell.

To record the displacement of the beam under load, a linear variable displacement transducer (LVDT) is mounted on top of the frame. Both the LVDT and signal conditioner were purchased from Macro Sensors, Inc. The LVDT had a displacement of 5.0mm and a resolution of 0.002mm. Fig. 36 show the complete set up of the test fixture. The actuator pushes from the bottom with the load cell in between the actuator and specimen. The LVDT mounts on top of the specimen and records the displacement directly from the movement of the specimen.

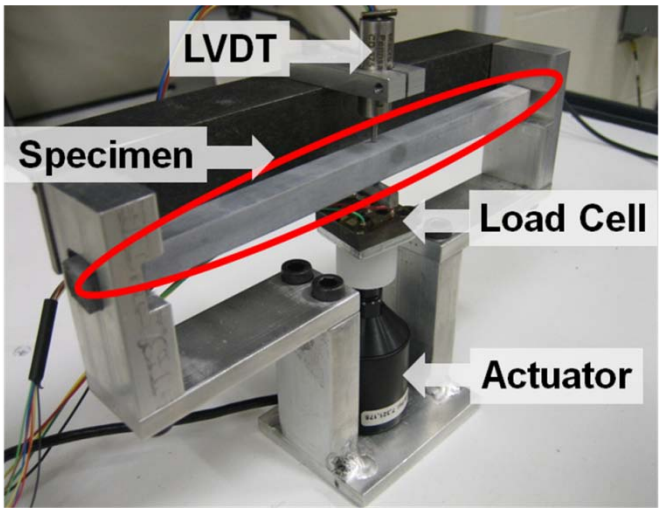

Fig. 36. Complete setup of the test frame with the frame, actuator, load cell, LVDT, and specimen in place.

5.1.2 Data Analysis

The force and displacement from the three-point flexural tests is converted to stress and strain using simple strength of materials relations for a three-point bending beam such that:

$$\sigma = \frac{3PL}{2bd^2} \tag{7}$$

and

$$\varepsilon = \frac{6Dd}{L^2} \tag{8}$$

where P is the force (from the load cell), L is the length (160mm), b and d are the width and depth (6.5mm each), and D is the displacement (from the LVDT).

To statistically compare the results of all batches to the reference batch, the Student's t-test was used. In this test, the null hypothesis tests to determine if the mean of the two normally distributed populations are equal. Note that the statistical analysis cannot prove the batches are similar, instead it provides evidence to support the idea that they might be similar. Due to inherent error in testing the different batches, a confidence interval of 80% was chosen.

5.2 Mechanical Properties

Fig. 37 shows the typical stress versus strain curve for plain cement paste. The material is very brittle and fails after initial crack formation. Fig. 38 shows an example of the nonlinear behavior encountered by the untreated CNFs. The sample had a small load drop once the initial crack opened up, then was able to increase the strength above pre-crack strength. This increase in strength is directly attributed to crack bridging by the CNFs. Post yield softening of the material can also be seen. Neither of these characteristics could be seen on the plain cement paste reference samples. Fig. 39 contains CNTs, and shows similar results as Fig. 38 both in crack bridging and increased ductility. These results are proof that the addition of nano-filaments can lead to a post-crack strength to be higher than the strength at initial crack opening, and an increase in ductility caused by progressive fiber pull-out. All stress-strain diagrams are shown in the appendix.

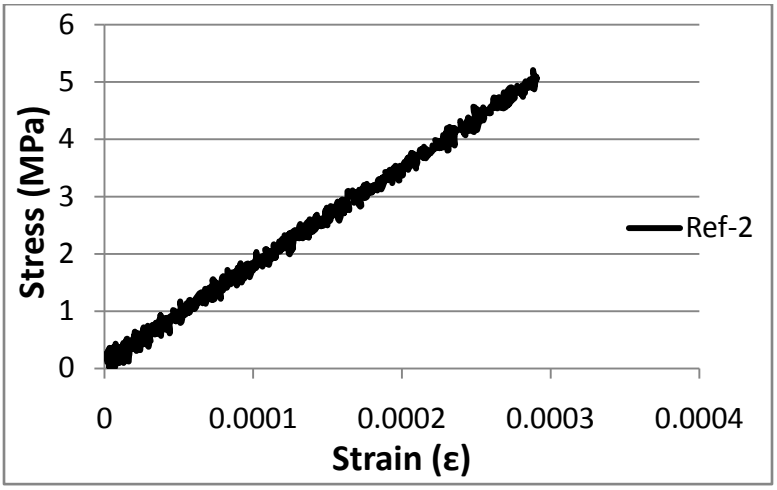

Fig. 37. Typical stress – strain curve for plane cement

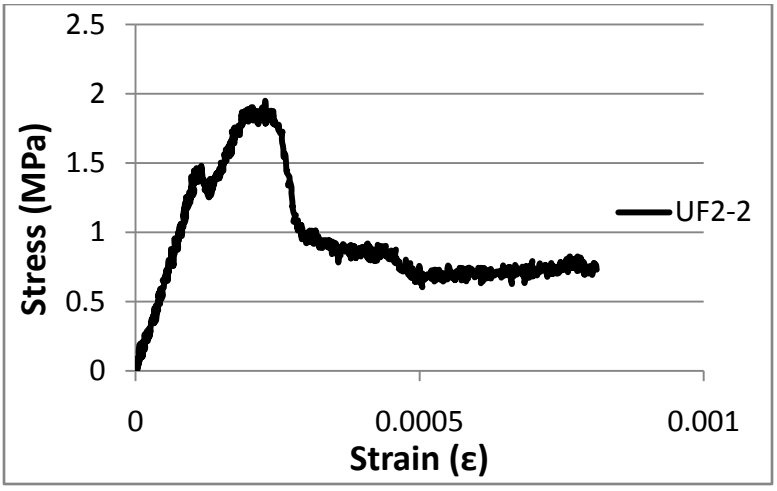

Fig. 38. Stress - strain curve for untreated fibers showing post crack and post yielding improvements

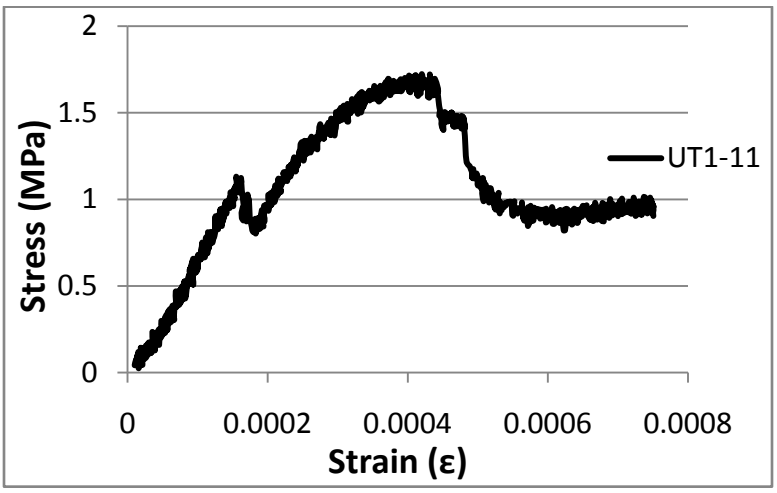

Fig. 39. Stress – strain curve for untreated CNTs showing improved post crack and post yielding behavior

Table 7 shows the average ultimate strain for each batch at 7, 14, and 28 days. At 7 days, it is observed that the addition of both CNTs and CNFs improves the ultimate strain capacity of cement paste. In general, the untreated nano-filaments outperformed the treated nano-filaments. The addition of untreated CNFs is able to increase the average strain capacity above the plain cement reference samples by 100% and 142%. The addition of untreated CNTs gave a broad

range of results. Untreated CNTs were able to increase the strain capacity by as little as 2% for UT1 to 179% for UT2. As the samples aged, the percent gains show a decreasing trend. At 14 days the untreated CNFs increases the strain capacity to 46% and 61%, while the untreated CNTs shows an increase between 30% for UT1, and 61% for UT2. At 28 days, UF1 has a strain capacity 73% higher than the reference, while UF2 was 47% better. For the ultimate strain capacities, both concentrations of untreated CNFs outperformed untreated CNTs. This is most likely attributed to the higher aspect ratios of the untreated CNFs (1000 for CNFs compared to 150 for CNTs) which makes untreated CNFs more effective as reinforcements due to larger interaction with the cement matrix. However, at 28 days, the same trend does not describe treated nano-filaments. At 28 days, treated CNTs ranged between a 22% increase for TT2 and a 16% decrease in strain capacity for TT1; whereas, treated CNFs ranged between 4% and 28%. Another reason for the untreated CNFs to outperform the untreated CNTs maybe because of the enhanced dispersion achieved when using the untreated CNFs.

Table 7
Ductility (ultimate strain) of the cement specimens after 7, 14, and 28 days.

	Day		
	7	14	28
Reference	4.30E-02	5.83E-02	5.34E-02
UF1	8.58E-02	8.51E-02	9.24E-02
TF1	7.44E-02	5.43E-02	6.81E-02
UF2	1.04E-01	9.36E-02	7.84E-02
TF2	7.12E-02	8.39E-02	5.53E-02
UT1	4.40E-02	7.59E-02	6.53E-02
TT1	8.30E-02	6.64E-02	4.46E-02
UT2	1.20E-01	9.37E-02	6.36E-02
TT2	7.55E-02	5.80E-02	6.52E-02

The average peak stress (i.e. average flexural strength) results are shown in Table 8. UF1 at 7 days has an increase of 79% increase in strength. At 14 days, UF1 increases 65%, and at 28 days, UF1 shows an increase of 60% above the plain cement. The 7 and 14 day test for the other three samples (UF2, UT1, and UT2), shows a decrease in strength between 29% and 69%. However, at 28 days, the strengths of UF2 and UT2 show an increase above the plain cement. At 28 days, UF2 increases 46%, and UT2 increases 37% above the reference sample. UT1 still shows a decrease in strength of 49%. These trends show that bonding between cement and nano-filaments are age-dependent, and hinder the performance at 7 and 14 days. However, at 28 days, the bond strength increases to the point where the strength is above the reference sample. This delay in strength can also be attributed to less concentration of C-S-H at early age. As for the treated nano-filaments, at 7 days, they all showed an increase in strength between 34% and 63%. However, at 14 and 28 days, the strengths decreased considerably. At 14 days, the strength dropped between 54% and 78%, and at 28 days, the strengths dropped between 53% and 84%. The microstructural mechanisms responsible for this increase/decrease in strength are discussed in detail in the following section.

Table 8
Average peak strength of the different batches (MPa).

	Day		
	7	14	28
Reference	6.60	7.55	8.79
UF1	11.82	12.43	14.02
TF1	10.08	1.62	1.91
UF2	2.24	2.89	12.81
TF2	8.81	2.97	1.44
UT1	4.71	2.35	4.54
TT1	10.75	3.02	4.15
UT2	2.27	3.48	12.00
TT2	9.78	3.08	2.38

The Young's modulus shows the same general trend as the strength. As shown in Table 9, the average modulus is lower than the reference sample. Both the 7 and 14 day tests show similar decreases. The stiffness of the untreated nano-filaments decreased between 5% and 39% for both test days. However, as with the peak stresses, the average Young's modulus at the 28 day test is able to outperform the plain cement. At 28 days, the stiffness increases by 1% for UF1, 25% for UF2, 3% for UT1, and 23% for UT2. This delayed increase in stiffness is most likely attributed to the same cause for the delayed strength increases; the bonding between nano-filaments and cement. However, for treated nano-filaments, the trend shows a weakening of the stiffness with respect to age. At 28 days, the stiffness decreased between 22% for TT1 and 66% for TF2. This clearly shows that treated nano-filaments in their present state, within cementitious materials, reduces the stiffness with respect to age.

Table 9
Average Young's modulus of the different batches (GPa).

	Day		
	7	14	28
Reference	15.09	13.08	15.00
UF1	14.21	12.40	15.18
TF1	13.49	6.81	8.03
UF2	10.31	10.17	18.74
TF2	12.07	9.45	5.14
UT1	13.69	10.92	15.41
TT1	13.08	11.26	11.77
UT2	9.20	9.04	18.50
TT2	12.99	9.71	7.17

The toughness is calculated within MATLAB by simply integrating the area under the stress vs. strain curve. From Table 10, the average toughness of UF1 shows an increase of 242%, 119%, and 170% for 7, 14, and 28 day tests, respectively. At 7 days, UF2 and UT2 increase by

4% and 20%, respectively. At 14 days, UF2, UT1, and UT2 all have a lower toughness ranging between 39% and 78% below the plain cement sample. At 28 days, UF2 increases to 112% and UT2 increases to 64% above the reference sample. At 7 days, TF1. TF2, TT1, and TT2 all increased the toughness by 154%, 118%, 196%, and 135%, respectively. However, at 14 and 28 days, the strengths all dropped significantly below the reference sample.

Table 10
Average fracture toughness of the different batches (MPa).

	Day		
	7	14	28
Reference	1.47E-01	2.54E-01	2.26E-01
UF1	5.02E-01	5.56E-01	6.11E-01
TF1	3.74E-01	5.56E-02	5.43E-02
UF2	1.53E-01	1.54E-01	4.79E-01
TF2	3.20E-01	9.29E-02	3.79E-02
UT1	9.65E-02	8.77E-02	1.75E-01
TT1	4.35E-01	7.10E-02	8.81E-02
UT2	1.76E-01	1.51E-01	3.71E-01
TT2	3.45E-01	8.49E-02	7.70E-02

Figs. 40-47 plot the average data presented in Tables 7-10. The data is presented to compare the reference sample to either CNFs, or CNTs. For the untreated nano-filaments, the data presented in Figs. 40-47 shows an increasing trend for the strength, stiffness, and toughness, accompanied with a decrease in ductility. These trends are most likely attributed to the delay in the interfacial bonding mechanism between nano-filaments and cement paste. However, for treated nano-filaments, the data decreases with respect to age. Only the toughness of both concentrations of treated CNFs showed an increase with respect to age. One hypothesis proposed to explain the drop in mechanical properties with respect to age for the treated nano-filaments could be due to the rapid formation of ettringite. Ettringite is formed through a reaction with

present calcium aluminates and sulfates. Ettringite forms expansive crystals throughout the cement, which is harmless when the cement is plastic and can expand. However, if ettringite forms after the cement has hardened, the expansion creates internal tensile stresses within the cement which leads to a weakened product. In the samples with functionalized nano-filaments, if excessive sulfate ions were left over from washing off the sulfuric acid, or if a sulfate functional group was created, these sulfate ions could have led to excessive ettringite formation.

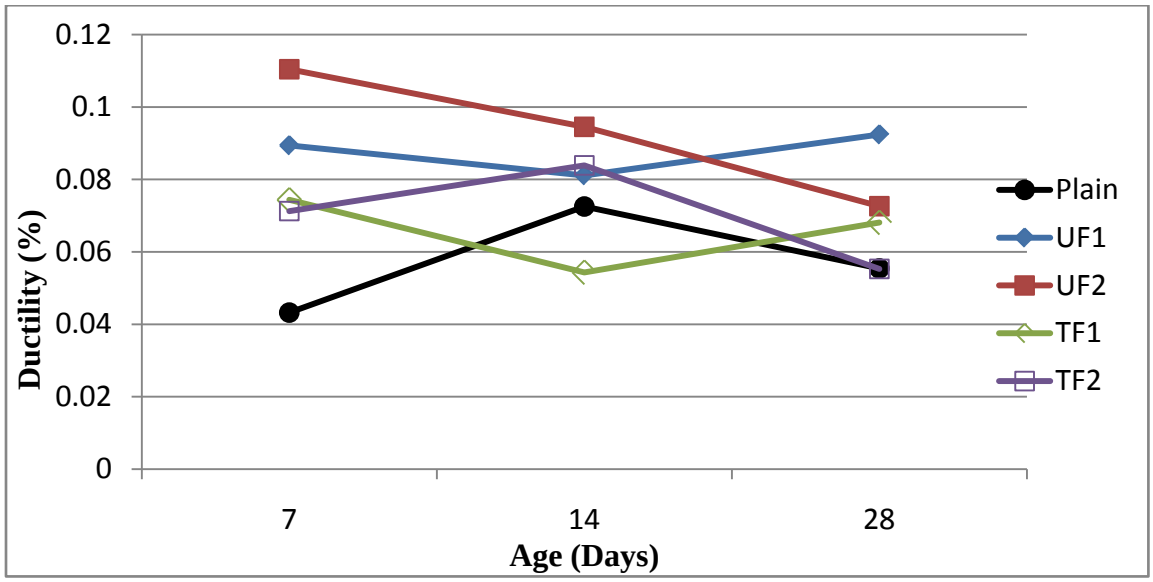

Fig. 40. Comparison between untreated and treated CNFs on the ductility of cement pate.

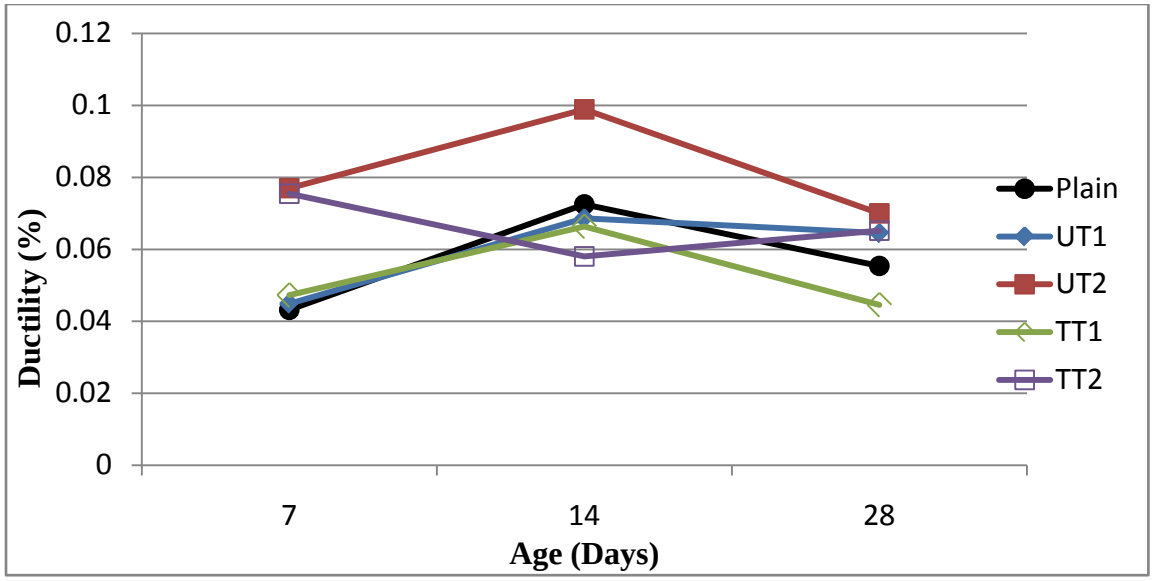

Fig. 41. Comparison between untreated and treated CTFs on the ductility of cement pate.

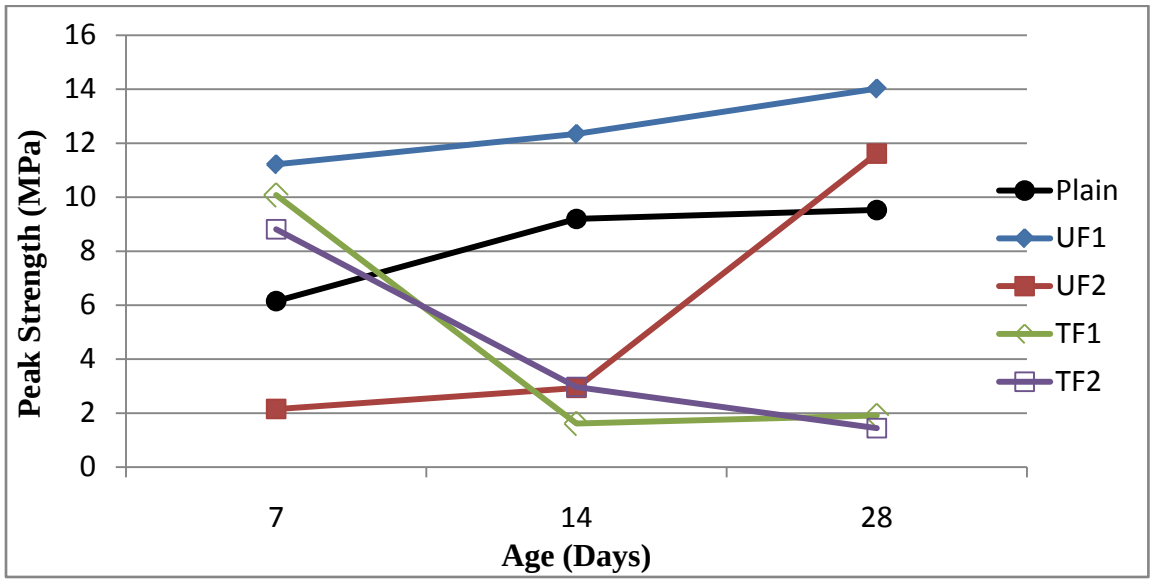

Fig. 42. Comparison between untreated and treated CNFs on the peak flexural strength of cement pate.

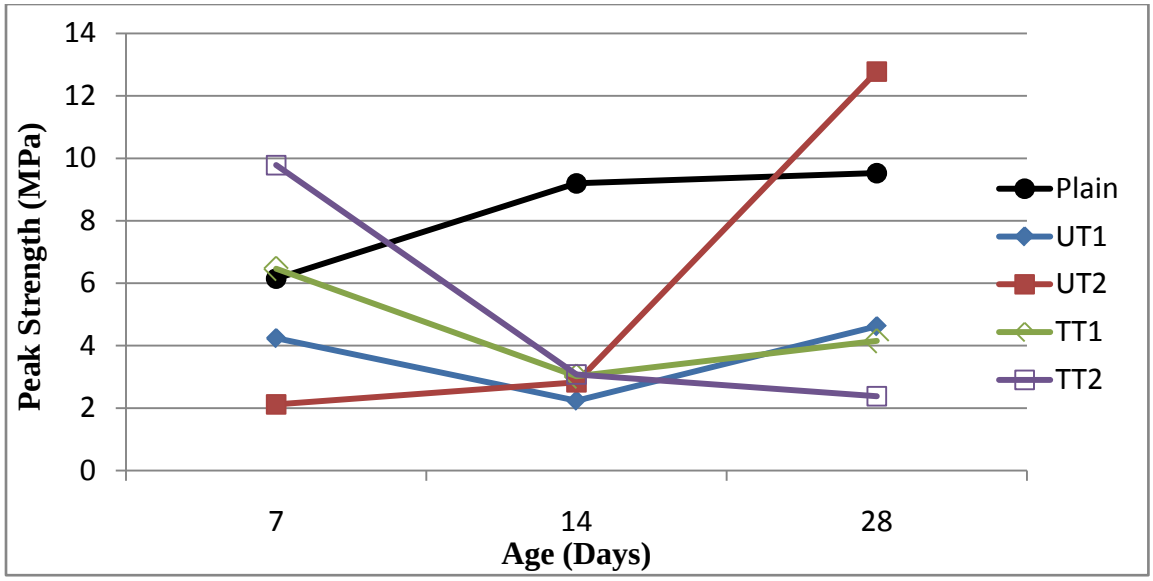

Fig. 43. Comparison between untreated and treated CNTs on the peak flexural strength of cement pate.

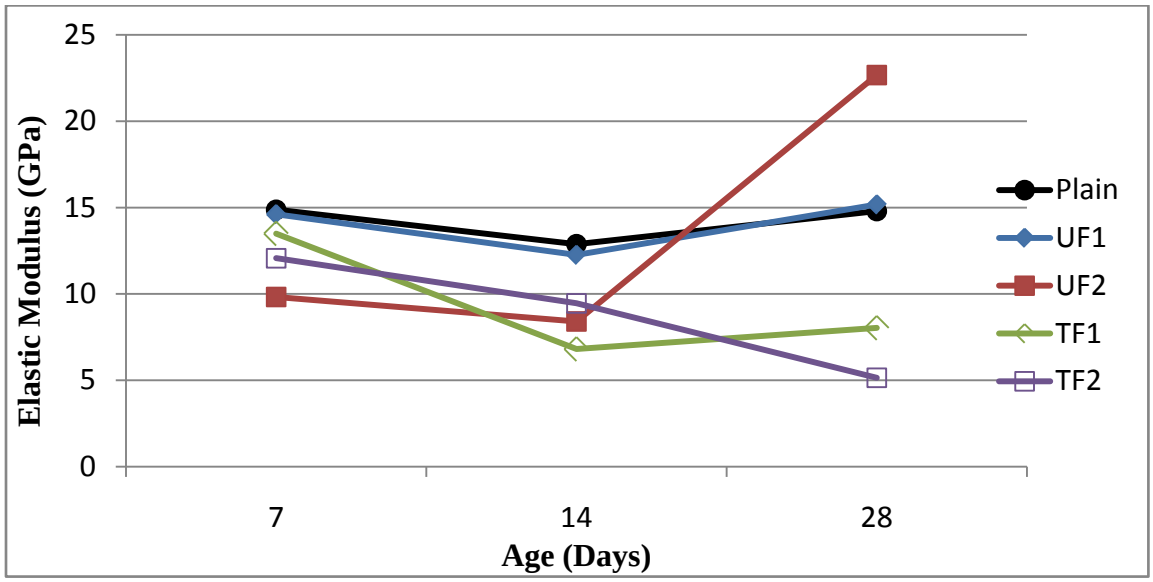

Fig. 44. Comparison between untreated and treated CNFs on the Young's modulus of cement pate.

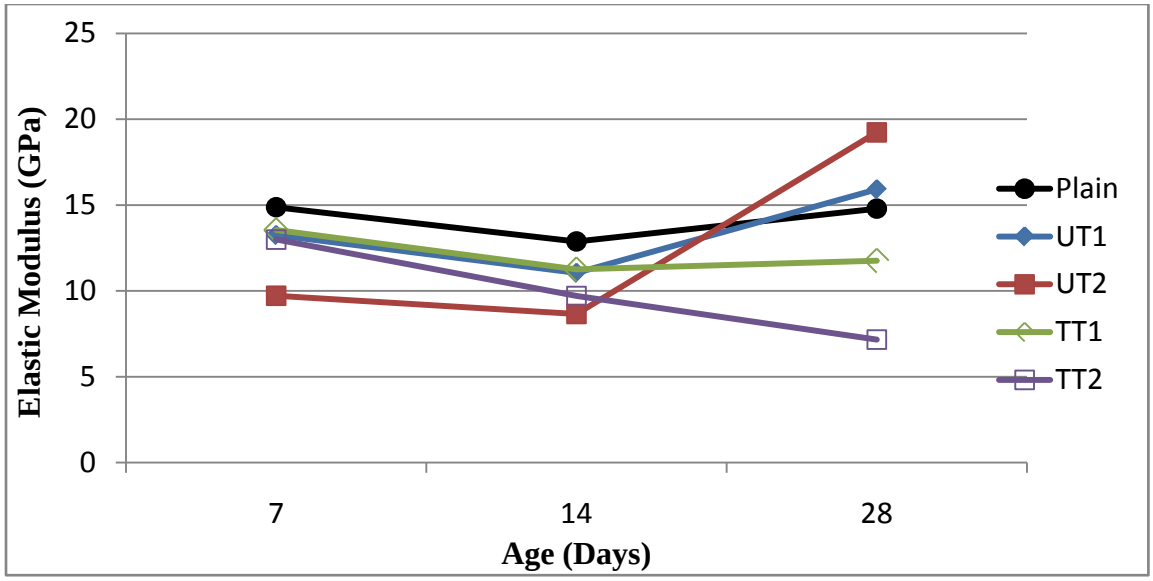

Fig. 45. Comparison between untreated and treated CNTs on the Young's modulus of cement pate.

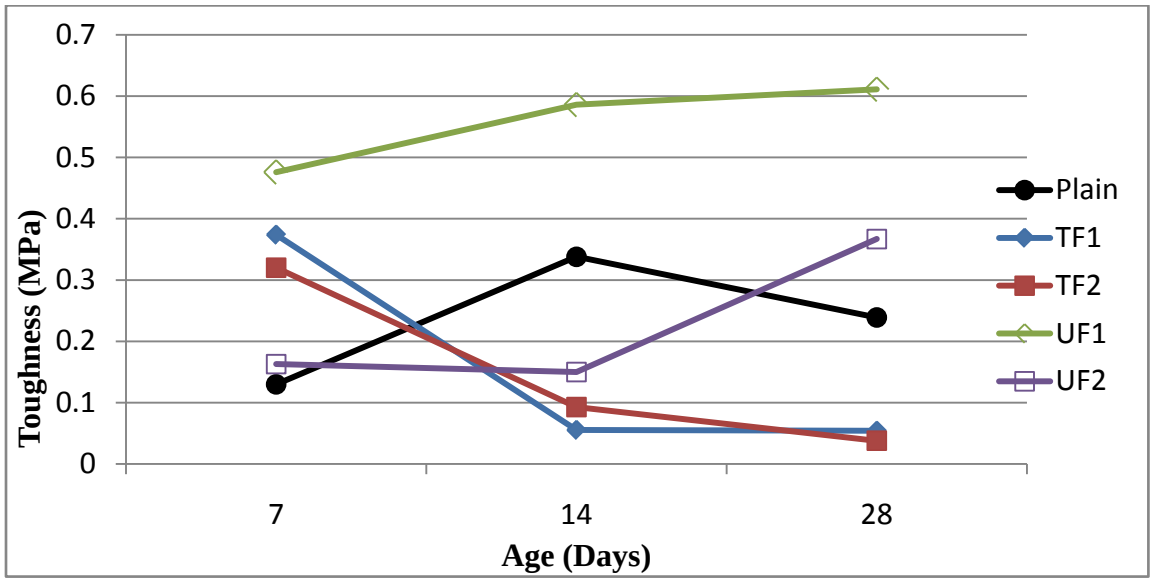

Fig. 46. Comparison between untreated and treated CNFs on the fracture toughness of cement pate.

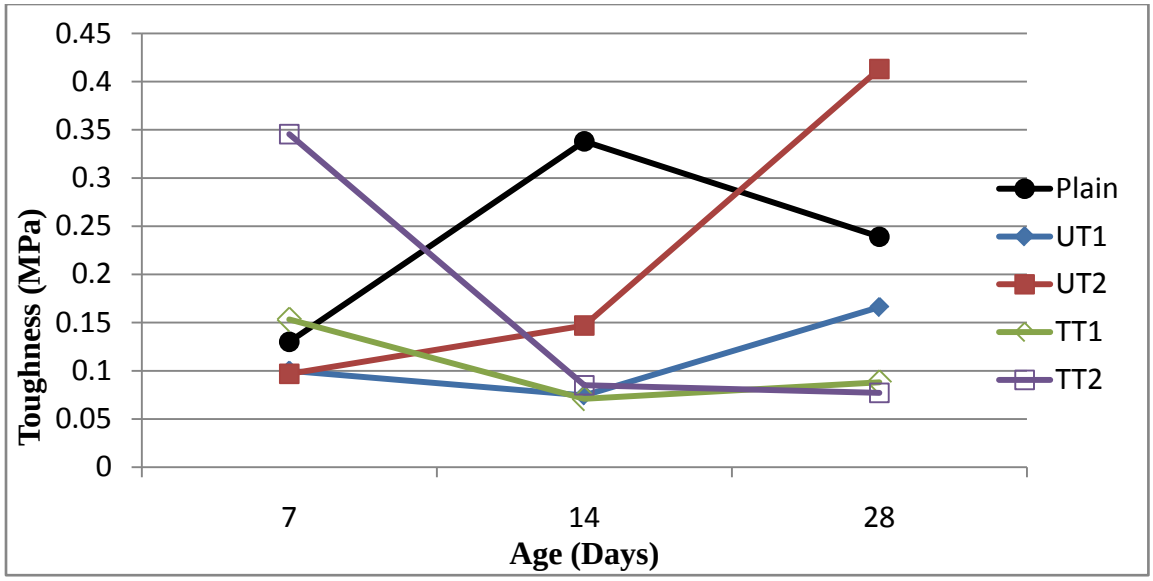

Fig. 47. Comparison between untreated and treated CNTs on the fracture toughness of cement pate.

Box plots of the five samples are shown in Figs. 48-50 for the 7, 14, and 28 day tests, respectively. On each box, the central line represents the median, and the edges of the box are the 25th and 75th percentiles. The box plot represents the middle half of the data within the distribution. This means that the bottom 25 percent and top 25 percent are not included within the box. The closer the spacing is between the 25th and 75th percentiles represent lower error between the test results. The arrows above the box plot indicate the batches in which the Student's t-test failed to reject the null hypothesis. In other words, an arrow above indicates that at an 80% confidence interval, there is a chance the nano-composite sample has similar properties to the plain cement sample. When looking at the statistical results, a clear trend shows up on the 14 and 28 day results for the ductility and fracture toughness. The Student's t-test showed that statistically, the addition of nano-filaments has little effect on the ductility and toughness of cement paste. However, the addition of nano-filaments can alter the stiffness and flexural strength of the cement. In some cases, the stiffness and strength can improve; however, in

general, the addition of nano-filaments hinders the performance of cement paste. Also, it can be seen when looking at Figs. 48-50 that there is no clear trend between the addition of either the CNTs or CNFs and the relative error within each batch.

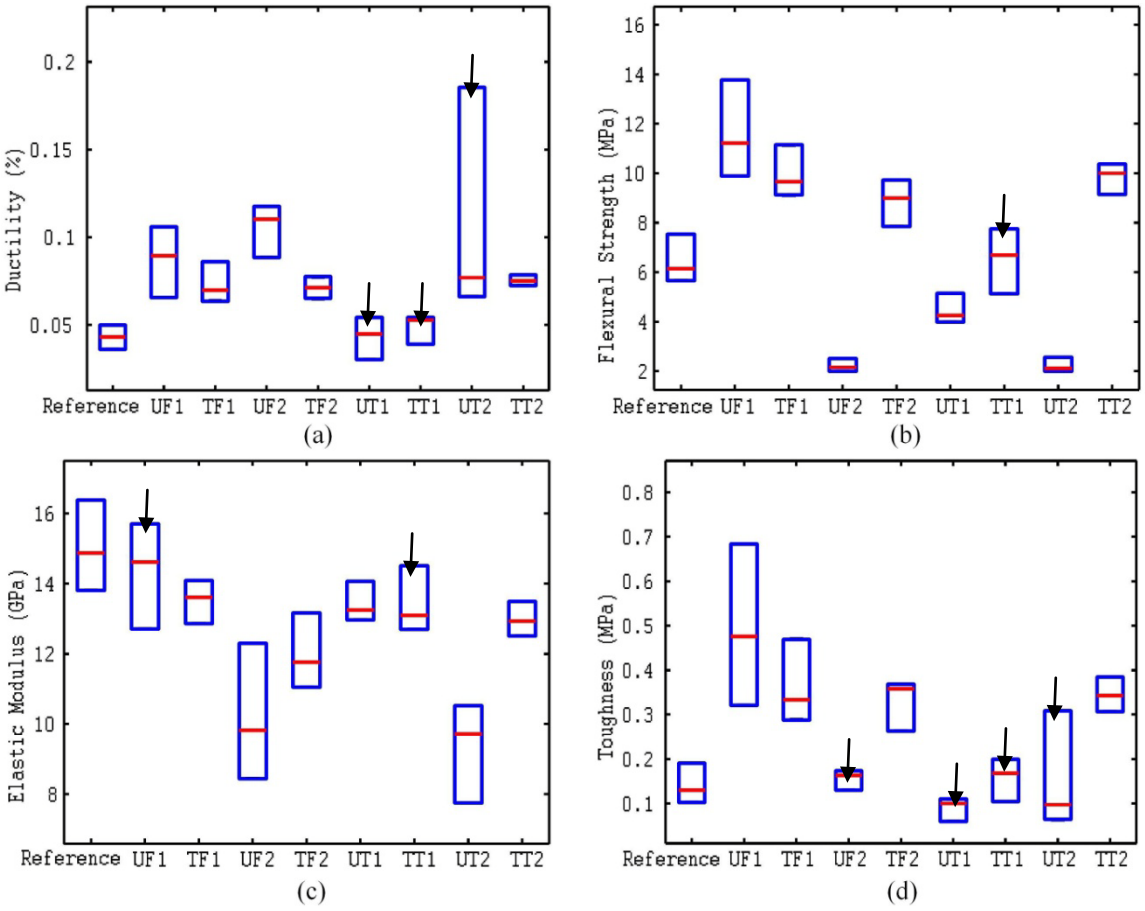

Fig. 48. Box plots of (a) ductility, (b) ultimate flexural strength, (c) Young's modulus, and (d) toughness for all data at 7 days. The arrows above the boxes indicate results that are statistically similar to the reference sample.

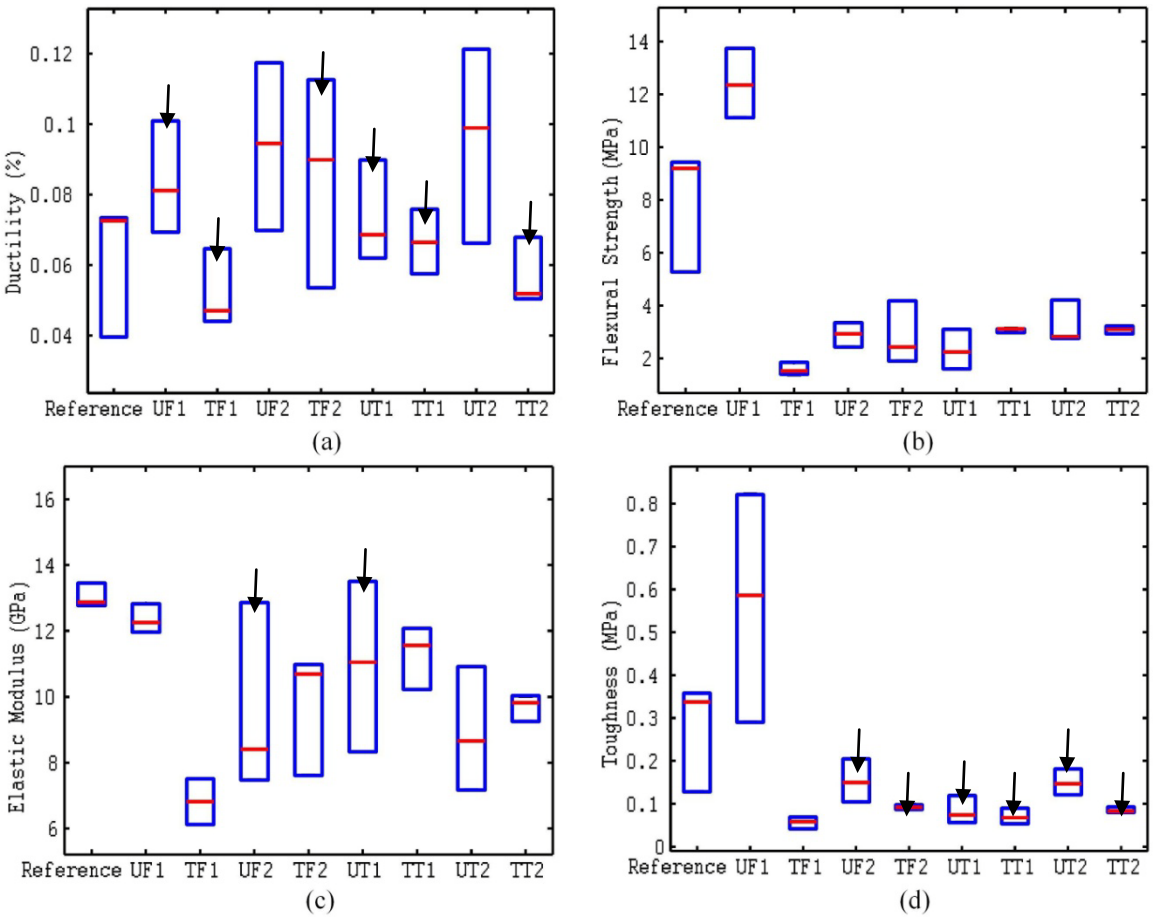

Fig. 49. Box plots of (a) ductility, (b) ultimate flexural strength, (c) Young's modulus, and (d) toughness for all data at 14 days. The arrows above the boxes indicate results that are statistically similar to the reference sample.

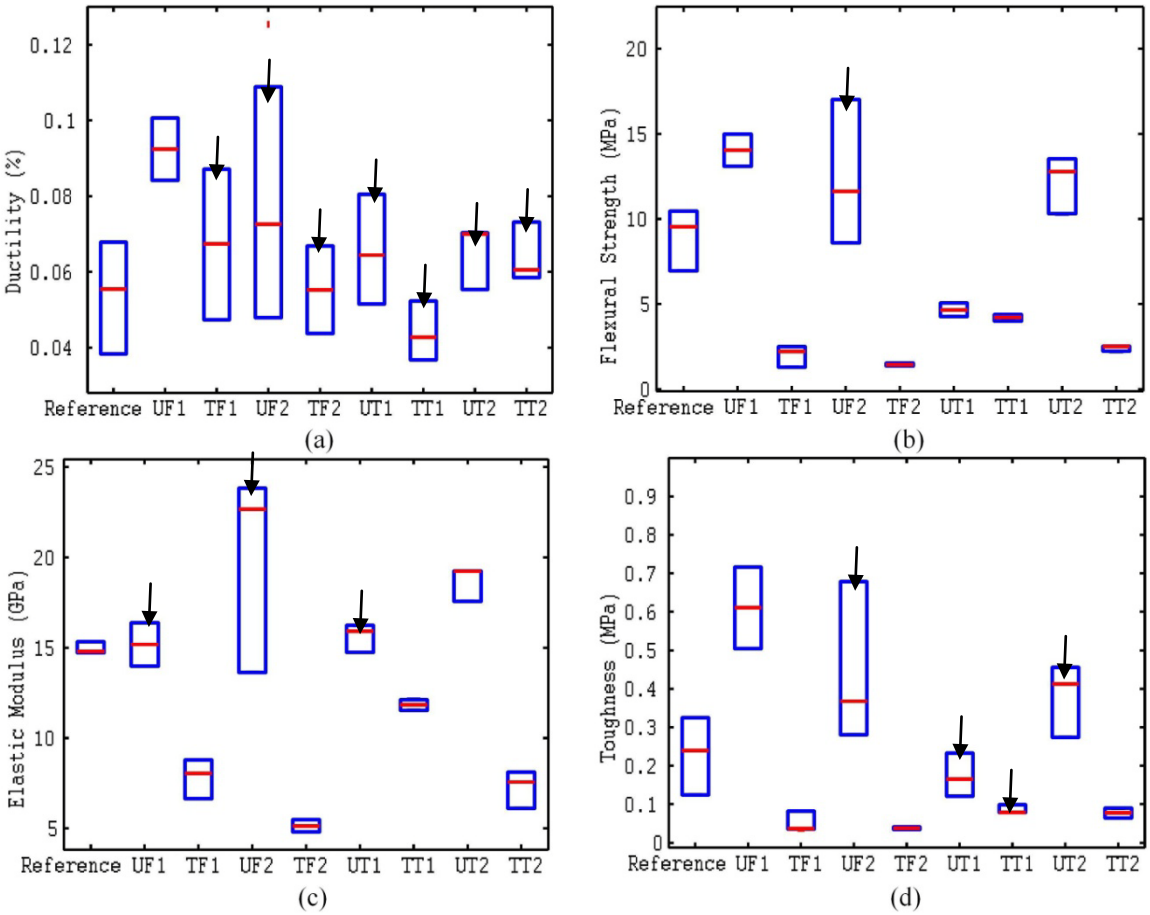

Fig. 50. Box plots of (a) ductility, (b) ultimate flexural strength, (c) Young's modulus, and (d) toughness for all data at 28 days. The arrows above the boxes indicate results that are statistically similar to the reference sample.

5.3 SEM Observation

An SEM was used to observe dispersion and bonding properties between the nano-filaments and the cement paste. The JEOL JSM-7500F, an ultra high resolution field emission scanning electron microscope (FE-SEM), was used to observe the fracture surface of the samples. After the samples had been tested, the fracture surface was cut into an approximately 1mm x 1mm x 0.5mm sample, and coated with a 3 nm-thick Platinum/Palladium layer to enhance surface conductivity. To reduce surface charging, all images used an acceleration voltage of 6kV. Fig.

51 shows the different phases of cement with CNFs embedded. Fig. 51a has a region of C-H and a small bundle of CNFs, and Fig. 51b shows small ettringite crystals along with a broken CNF. The amorphous background in both images is C-S-H. Fig. 52 is an image of CNTs bundled along the fracture surface of the cement.

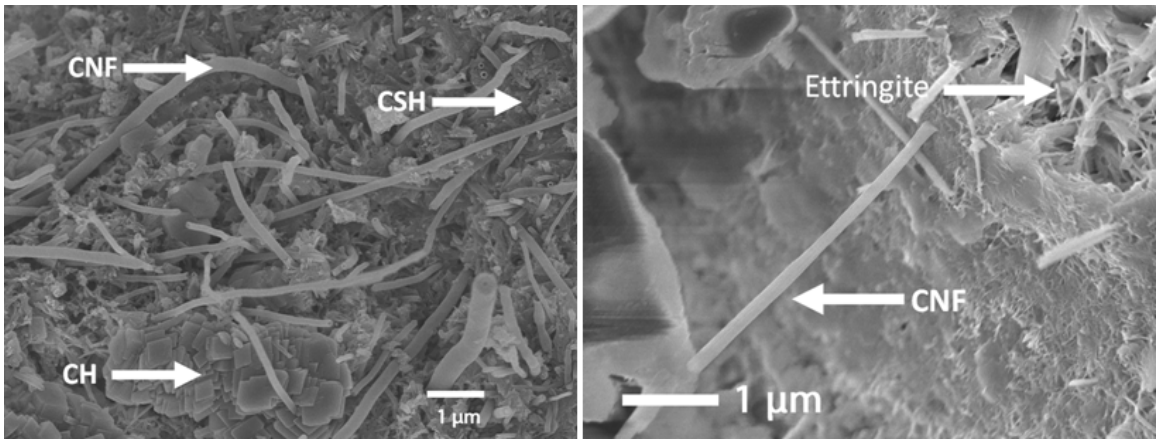

(a) (b)

Fig. 51. Image showing the different phases of cement (a) CSH and CH along with the CNFs, and (b) showing Ettringite which looks very similar to CNTs.

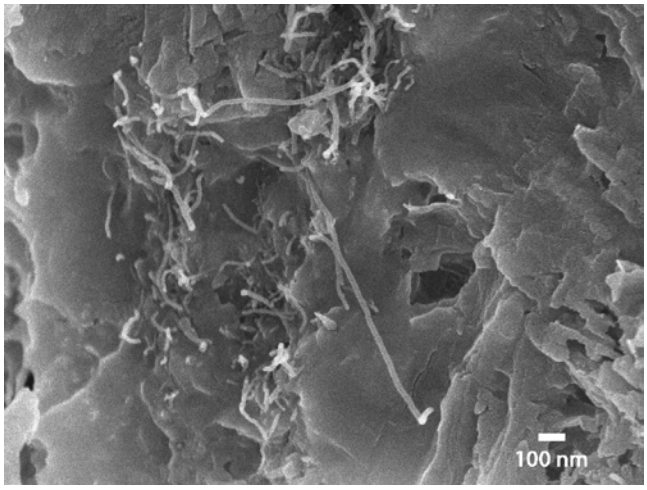

Fig. 52. SEM image of CNTs protruding out from the fracture surface of the cement.

5.3.1 Agglomeration

The SEM observations of the fractured surface on the hardened cement containing either CNTs or CNFs show poor dispersion within the cement matrix. In fact, large areas observed under the SEM showed no evidence of either CNTs or CNFs. Despite the best efforts to maintain uniform dispersion of nano-filaments within the aqueous solution, combining a well-dispersed aqueous mixture with cement resulted in a relatively poor dispersion. Fig. 53a shows the typical SEM image. In the image, a crack can be seen; however, there are no CNFs anywhere within the region. On the other hand, Fig. 53b shows an area with a high concentration of CNFs. Although what causes the poor dispersion is unknown, it may be that the size of the cement grains plays a crucial role in the dispersion of nano-filaments within the cement matrix as illustrated in Fig. 54 [48]. As the cement hydrates, areas that were previously hard cement grains absent of nano-filaments become hydrated without any CNTs or CNFs.

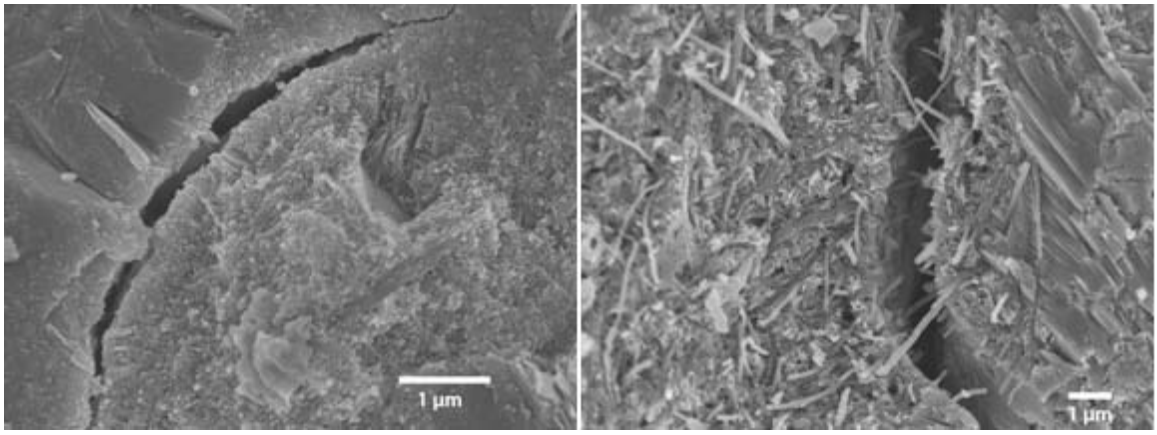

(a) (b)

Fig. 53. (a) SEM image of the fractured surface with no CNFs within the region; (b) CNF bundled within a small area.

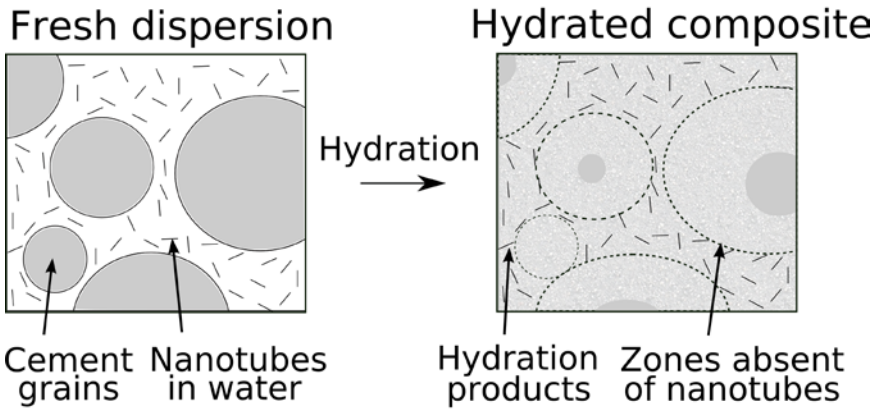

Fig. 54. Illustration of the effect of cement grains on dispersibility of CNTs/CNFs. The large grains create zones that are absent of nano-tubes/fibers even after hydration has progressed.

5.3.2 Crack Bridging and Fiber Pullout

Fig. 55a shows a CNF bridging a micro-crack, while the CNFs in Fig. 55b have been pulled out from the other wall. As of now, there is no way of controlling or optimizing the bond between nano-filaments and cement matrix. This is a topic that has yet to be researched, and ways to control the interfacial bond strength needs to be addressed. For untreated CNFs and CNTs, pull out was very common with the samples observed under the SEM. In the authors' opinion, the untreated nano-filaments have a smooth surface for which the cement paste cannot properly develop a strong bond. This is where surface functionalization can be very helpful. By adding covalent bonds to the surface of the nano-filaments, new molecules can then bond directly with the hydration products of the cementitious materials.

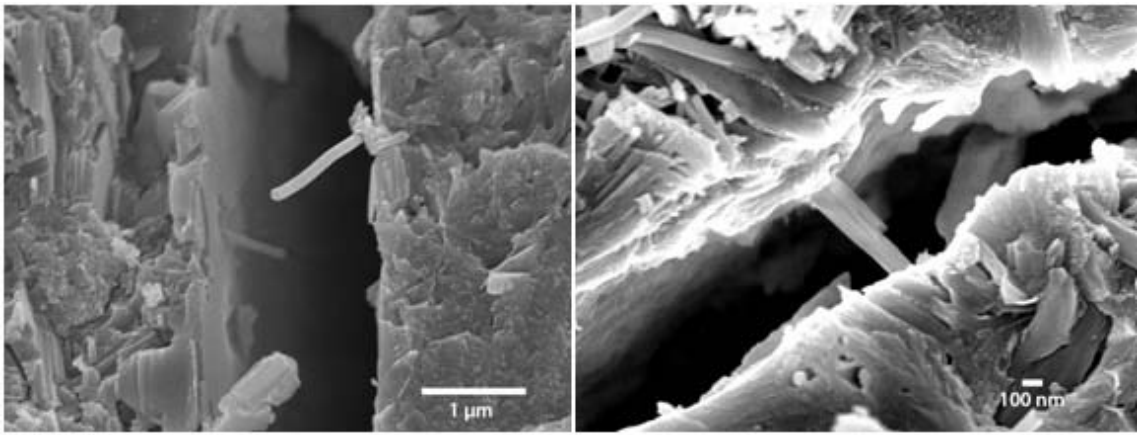

(a) (b)

Fig. 55. (a) SEM image of a micro-crack bridged by a CNF; (b) CNF pulled out from a micro-crack.

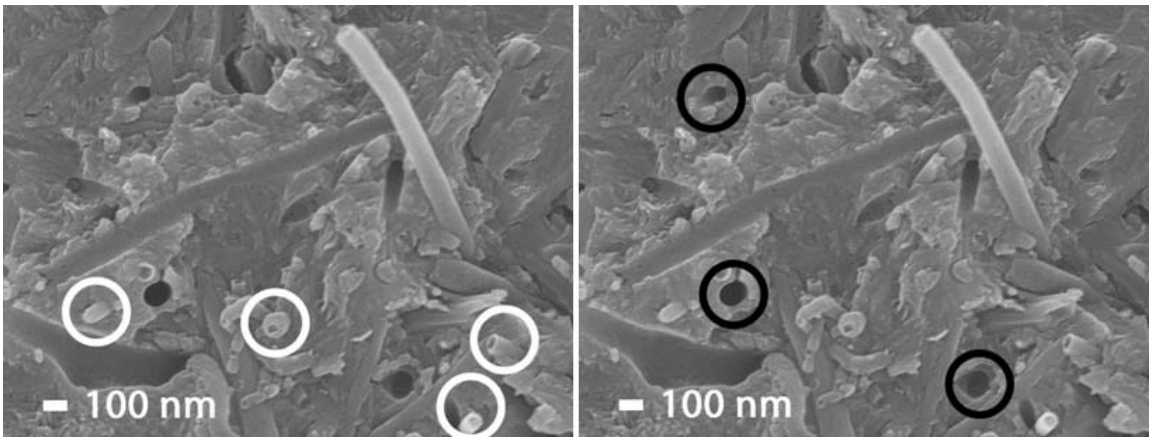

(a) (b)

Fig. 56. Evidence of both (a) fiber breakage indicated by the white circles, and (b) fiber pullout indicated by the black circles.

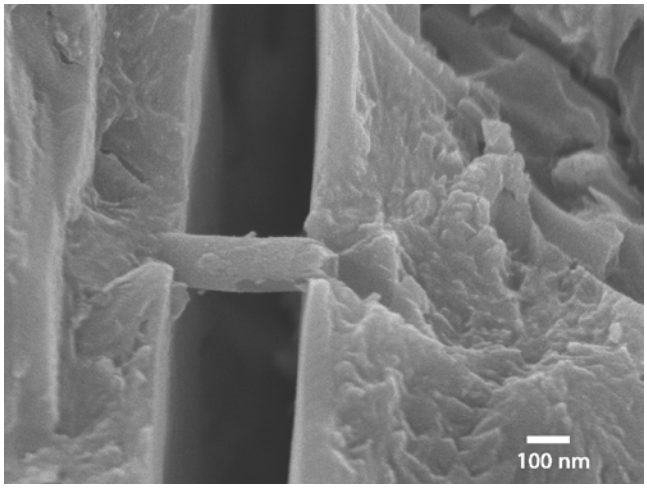

Fig. 57. Close up of a CNF on the fracture surface of cement. The CNF originally bridge the nano-crack before fracturing.

5.3.3 Surface Functionalization

One observation of this lack of surface bonding is shown in Fig. 58. Fig. 58a shows functionalized CNFs embedded within cement paste. It is evident from this image that the functionalized CNFs have a surface coated with cement paste. Fig. 58b is an image of untreated CNFs within cement. In this image, a clear distinction can be made between the CNF and the cement surrounding it. There is no evidence of cement clinging to the surface of the CNF. This means that the interfacial bond between cement and CNFs is weaker for the untreated CNFs when compared to the acid treated CNFs. The interfacial bond was created most likely through the covalent bonds between nano-filaments and cement. However, as previously noted, cement samples embedded with functionalized nano-filaments experienced weakened mechanical properties. Although it is not fully understood why this happened, one hypothesis is that the cement experienced rapid deterioration caused by the functionalized nano-filaments. This deterioration could be caused by the formation of expansive crystalline structures such as Ettringite. The reduction in strength caused by the addition of functionalized nano-filaments

needs to be further investigated. If functionalization increases the ability for the nano-filaments to bond, then its use in cement should improve the strength of cement.

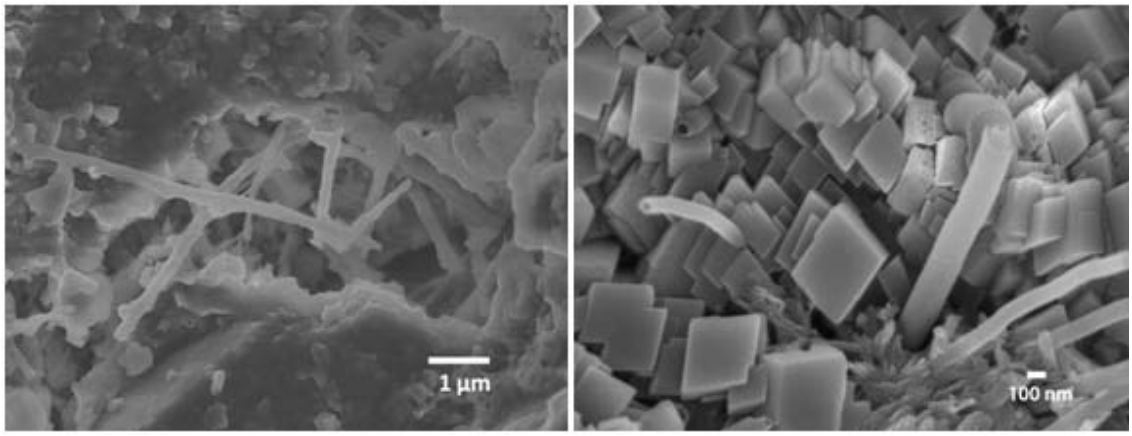

(a) (b)

Fig. 58. (a) SEM image of treated CNFs embedded within the cement paste; (b) Fractured end of a CNF protruding from the fractured surface of the cement.

6 CONCLUSION

6.1 Conclusion

In this study, the mechanical properties of cement paste reinforced with untreated and acid treated CNTs and CNFs have been investigated at concentrations of 0.1 wt% and 0.2 wt% by weight of cement. The specimens were tested through the use of a three point flexural test frame. Acid treated nanotubes were produced with the use of sulfuric and nitric acids in a reflux condenser. After the nano-filaments were washed of all the residual acid, the oxidation was calculated with the use of an XPS machine.

The dispersion of the nano-filaments was studied by mixing the nano-filaments with water and various amounts of surfactants. The solutions were then mixed with an ultrasonic mixer. After mixing, the CNTs and CNFs were observed under the TEM and optical microscope. In order to successfully disperse the nano-filaments without adversely affecting the hydration of the cement paste, an optimal amount of surfactant was chosen to be 0.5 wt% by weight of dry cement.

While studying the dispersion of nano-filaments within aqueous solutions, a major problem encountered was in the qualitative assessment of the dispersion. In this study, a novel method to quantify the degree of dispersion and agglomeration was developed. By using images of different dispersions, a MATLAB program was developed to calculate the dispersion and agglomeration percentage. The program was able to show an improvement of 5.44% and 6.52% in the dispersion and agglomeration, respectively, when CNFs were ultrasonically dispersed rather than hand shaken.

To make the cement samples, nano-filaments were first dispersed with water and a surfactant using an ultrasonic mixer, then combined with cement using a 0.4 water to cement ratio and poured into molds. The samples were allowed to cure for 7, 14, and 28 days and tested at

each age. For almost all cases, the addition of untreated CNFs and CNTs helped to increase the ultimate strain capacity (i.e. ductility) up to 150% higher than plain cement paste, which is crucial for structural applications where higher ductility and strain capacity to failure is needed. For the early ages, 7 and 14 days, negative effects are seen for the flexural strength, Young's modulus, and fracture toughness. However, at 28 days, these properties increase beyond the plain cement. SEM images verified poor dispersion within the cement paste matrix, the bridging effects which transfer the load across the nano/micro-cracks, and the fibers pullout due to weak bond.

The addition of treated CNTs and CNFs showed a drop in most mechanical properties. In general, at 7 days, the treated CNTs and CNFs had improvements up to 65% above plain cement for ultimate strain capacity and peak strength, while the Young's modulus decreased slightly. At 14 days, all mechanical properties of the treated CNT and CNF samples showed a decrease when compared to plain cement. At 28 days, the treated CNFs had large improvements in fracture toughness, while all other mechanical properties had decreased.

For the untreated nano-filaments, the delayed enhancements in strength, ductility, and toughness, accompanied with a reduction in stiffness, are likely due to a shift in the bonding between the nano-filaments and the cement matrix. At early ages, 7 and 14 days, more nano-filaments pulled out allowing for higher strain capacities. Whereas, at the 28 day test, the bonding between nano-filaments and cement matrix increased to the point where the nano-filaments are more susceptible to breaking rather than gradually being pulled out. Moreover, generally, it is seen that untreated CNFs give improved performance due to their higher aspect ratio as compared to CNTs. As for the treated nano-filaments, the age dependent reduction in performance is most likely due to time dependent formations of weaker chemical structures within the cement. This could be caused by the growth of ettringite or other cement byproducts,

and should be further investigated to understand what is causing this reduction so it can be avoided.

6.2 Limitations

In the presented research, many limitations are present. First and foremost, the size of the specimens had to be very small. The small cross-section produces higher error do to many factors. These errors can be from large air voids which has a greater strength reduction then if present in larger specimens. Also, the small cross-sections made post crack measurements extremely difficult. If the specimens were larger, crack propagation could be slower, making post-crack data collection more accurate. Another cause of error was due to the change in location of the initial crack location in relation to the center of the beam. If the specimens could be molded with a notch, or have a notch saw cut, then the location of the crack will always be mid-span. Another way to reduce errors produced while testing is to change to a four point bend test. The three point bend used in this research could have lead to additional error in the testing results from the lack of a constant moment (zero shear) region produced in a four point bend.

Second, it proved to be difficult to study the dispersion properly. Dispersion is very important in making sure there is adequate load transfer between the cement matrix and the nano-filaments. Merely looking at aqueous dispersions under the TEM does not produce reliable results for how the dispersion will be within the hydrated cement. A better approach should be devised to get a better understanding of how the dispersion changes from the aqueous solution to hydrated cement. In order to look at the dispersion within hydrated cement, a sample could be prepared with either an ion mill or even a focused ion beam to get a thickness small enough to be electron transparent under the TEM. Proper dispersion could not be seen under the SEM. The nano-filaments below the surface were not visible.

6.3 Future Research

To get a better understanding of how and why the nano-filament are able to reinforce cementitious materials, many areas still need to be researched. To better understand the dispersion of nano-filaments, and optimize the use of chemical surfactants, one area of research that needs to be studied is how to develop charts or tables that can be used to determine the amount of surfactant needed for different concentrations of nano-filaments. An example could be to determine the optimum amount of surfactant versus nano-filament aspect ratio, or surfactant versus specific area.

Another area to focus on for future research is in the optimization of the methods to quantify the degree of dispersion and agglomeration. In the presented research, the bounds on the integral were determined based on the analysis of an image, and then the bounds were changed based on trial and error. To properly quantify the dispersion and agglomeration, the bounds need to be based on scientific reasoning. For example, the bounds could be based on the relative error from the pixel length, error of the scale bars, error caused by processing the images, or many other variables. Moreover, the agglomeration calculations should be changed from being dependent on the mean of the particle size to being based on the diameter of the single particle.

Another area to focus research on in the future is to study methods available to quantify the dispersion within hardened cement paste. The cement will have to be thinned to the point of being electron transparent for the TEM with the use of an ion mill or focused ion beam. Once the samples are properly prepared, the change in dispersion between aqueous solution and hydrated cement can be compared. This will provide valuable insight into how the dispersion is affected by the hydration process of cement paste.

REFERENCES

[1] Altoubat S, Yazdanbakhsh A, and Rieder K-A. Shear behavior of macro-synthetic fiber-reinforced concrete beams without stirrups. Materials Journal 2009; 106(4): 381-89.

[2] Fischer G and Li VC. Effect of fiber reinforcement on the response of structural members. Engineering Fracture Mechanics 2007; 74(1-2): 258-72.

[3] Li VC and Maalej M. Toughening in cement based composites. Part II: fiber reinforced cementitious composites. Cement and Concrete Composites 1996; 18(4): 239-49.

[4] Mangat PS, Motamedi-Azari M, and Shakor Ramat BB. Steel fibre-cement matrix interfacial bond characteristics under flexure. International Journal of Cement Composites and Lightweight Concrete 1984; 6(1): 29-37.

[5] Ostertag CP, Yi CK, and Vondran G. Tensile strength enhancement in interground fiber cement composites. Cement and Concrete Composites 2001; 23(4-5): 419-25.

[6] Savastano JH, Warden PG, and Coutts RSP. Microstructure and mechanical properties of waste fibre-cement composites. Cement and Concrete Composites 2005; 27(5): 583-92.

[7] Wang C, Li K-Z, Li H-J, Jiao G-S, Lu J, and Hou D-S. Effect of carbon fiber dispersion on the mechanical properties of carbon fiber-reinforced cement-based composites. Materials Science and Engineering: A 2008; 487(1-2): 52-57.

[8] Coleman JN, Khan U, Blau WJ, and Gun'ko YK. Small but strong: a review of the mechanical properties of carbon nanotube-polymer composites. Carbon 2006; 44(9): 1624-52.

[9] Marrs B, Andrews R, and Pienkowski D. Multiwall carbon nanotubes enhance the fatigue performance of physiologically maintained methyl methacrylate-styrene copolymer. Carbon 2007; 45(10): 2098-104.

[10] Wang JG, Fang ZP, Gu AJ, Xu LH, and Liu F. Effect of amino-functionalization of multi-walled carbon nanotubes on the dispersion with epoxy resin matrix. Journal of Applied Polymer Science 2006; 100(1): 97-104.

[11] Bacsa RR, Laurent C, Peigney A, Bacsa WS, Vaugien T, and Rousset A. High specific surface area carbon nanotubes from catalytic chemical vapor deposition process. Chemical Physics Letters 2000; 323(5-6): 566-71.

[12] Tsivilis S, Chaniotakis E, Kakali G, and Batis G. An analysis of the properties of Portland limestone cements and concrete. Cement and Concrete Composites; 24(3-4): 371-78.

[13] Iijima S. Helical microtubules of graphitic carbon. Nature 1991; 354(6348): 56-58.

[14] Li C and Chou T-W. A structural mechanics approach for the analysis of carbon nanotubes. International Journal of Solids and Structures 2003; 40(10): 2487-99.

[15] Malloy T. Holding our breath for a test rule for carbon nanotubes. 2010; http://legalplanet.wordpress.com/2009/06/17/holding-our-breath-for-a-test-rule-for-carbon-nanotubes/.

[16] Carbon nanowire inside a carbon nanotube. 2010; http://www.aip.org/png/2003/186.htm.

[17] Mamalis AG, Vogtländer LOG, and Markopoulos A. Nanotechnology and nanostructured materials: trends in carbon nanotubes. Precision Engineering 2004; 28(1): 16-30.

[18] Yakobson BI and Smalley RE. Fullerene nanotubes: C-1000000 and beyond. American Scientist 1997; 85(4): 324-37.

[19] Thess A, Lee R, Nikolaev P, Dai HJ, Petit P, Robert J, et al. Crystalline ropes of metallic carbon nanotubes. Science 1996; 273(5274): 483-87.

[20] Zhou ZP, Lai CL, Zhang LF, Qian Y, Hou HQ, Reneker DH, et al. Development of carbon nanofibers from aligned electrospun polyacrylonitrile nanofiber bundles and characterization of their microstructural, electrical, and mechanical properties. Polymer 2009; 50(13): 2999-3006.

[21] Yu MF, Lourie O, Dyer MJ, Moloni K, Kelly TF, and Ruoff RS. Strength and breaking mechanism of multiwalled carbon nanotubes under tensile load. Science 2000; 287(5453): 637-40.

[22] Diamond structures. 2010; http://www.diamonds-are-forever.org.uk/diamond-structures.htm.

[23] Falling into the gap - Berkeley lab researchers take a critical first step toward graphene transistors. 2010; http://www.lbl.gov/Science-Articles/Archive/sabl/2007/Nov/gap.html.

[24] Makar JM and Beaudoin JJ. Carbon nanotubes and their application in the construction industry. In 1st International Symposium on Nanotechnology in Construction. Paisley, Scotland, June 22-25, 2003; 331-341.

[25] Makar JM, Margeson JC, and Luh J. Carbon nanotube/cement composite - early results and potential applications. in 3rd International Conference on Construction Materials: Performance, Innovation and Structural Implications. Vancouver, B.C., Aug. 22-24, 2005; 1-10.

[26] Sáez de Ibarra Y, Gaitero JJ, Erkizia E, and Campillo I. Aromic force microscopy and nanoindentation of cement pastes with nanotube dispersions. Physica Status Solidi A 2006; 203(6): 1076-81.

[27] Li GY, Wang PM, and Zhao X. Mechanical behavior and microstructure of cement composites incorporating surface-treated multi-walled carbon nanotubes. Carbon 2005; 43(6): 1239-45.

[28] Li GY, Wang PM, and Zhao X. Pressure-sensitive properties and microstructure of carbon nanotube reinforced cement composites. Cement and Concrete Composites 2007; 29(5): 377-82.

[29] Cwirzen A, Habermehl-Cwirzen K, and Penttala V. Surface decoration of carbon nanotubes and mechanical properties of cement/carbon nanotube composites. Advances in Cement Research 2008; 20(2): 65-73.

[30] Nasibulin AG, Shandakov SD, Nasibulina LI, Cwirzen A, Mudimela PR, Habermehl-Cwirzen K, et al. A novel cement-based hybrid material. New Journal of Physics 2009; 11: 11.

[31] Shah SP, Konsta-Gdoutos MS, and Metaxa ZS, Highly-dispersed carbon nanotubes-reinforced cement-based materials: United States Patent Application Publication, US 2009/0229494 A1.

[32] Konsta-Gdoutos MS, Metaxa ZS, and Shah SP. Multi-scale mechanical and fracture characteristics and early-age strain capacity of high performance carbon nanotube/cement nanocomposites. Cement and Concrete Composites; 32(2): 110-15.

[33] Chaipanich A, Nochaiya T, Wongkeo W, and Torkittikul P. Compressive strength and microstructure of carbon nanotubes-fly ash cement composites. Materials Science and Engineering: A 2010; 527(4-5): 1063-67.

[34] Sanchez F. Carbon nanofiber/cement composites: challenges and promises as structural materials. Int. J. Mater. Struct. Integrity 2009; 3(2-3): 217-226.

[35] Sanchez F and Ince C. Microstructure and macroscopic properties of hybrid carbon nanofiber/silica fume cement composites. Composites Science and Technology 2009; 69(7-8): 1310-18.

[36] Fu K, Huang W, Lin Y, Riddle LA, Carroll DL, and Sun Y-P. Defunctionalization of Functionalized Carbon Nanotubess. Nano Letters 2001; 1(8): 439-41.

[37] Hamon MA, Hui H, Bhowmik P, Itkis HME, and Haddon RC. Ester-functionalized soluble single-walled carbon nanotubes. Applied Physics A: Materials Science & Processing 2002; 74(3): 333.

[38] Wong SS, Joselevich E, Woolley AT, Cheung CL, and Lieber CM. Covalently functionalized nanotubes as nanometre-sized probes in chemistry and biology. Nature 1998; 394(6688): 52.

[39] Bahr JL and Tour JM. Covalent chemistry of single-wall carbon nanotubes. Journal of Materials Chemistry 2002; 12(7): 1952-58.

[40] Moore VC, Strano MS, Haroz EH, Hauge RH, Smalley RE, Schmidt J, et al. Individually suspended single-walled carbon nanotubes in various surfactants. Nano Letters 2003; 3(10): 1379-82.

[41] Chen W, Auad ML, Williams RJJ, and Nutt SR. Improving the dispersion and flexural strength of multiwalled carbon nanotubes-stiff epoxy composites through [beta]-hydroxyester surface functionalization coupled with the anionic homopolymerization of the epoxy matrix. European Polymer Journal 2006; 42(10): 2765-72.

[42] Kim JA, Seong DG, Kang TJ, and Youn JR. Effects of surface modification on rheological and mechanical properties of CNT/epoxy composites. Carbon 2006; 44(10): 1898-905.

[43] Li SQ, Wang F, Wang Y, Wang JW, Ma J, and Xiao J. Effect of acid and TETA modification on mechanical properties of MWCNTs/epoxy composites. Journal of Materials Science 2008; 43(8): 2653-58.

[44] Xie X-L, Mai Y-W, and Zhou X-P. Dispersion and alignment of carbon nanotubes in polymer matrix: a review. Materials Science and Engineering: R: Reports 2005; 49(4): 89-112.

[45] Grunlan C, Liu L, and Regev O. Weak polyelectrolyte control of carbon nanotube dispersion in water. Journal of Colloid and Interface Science 2008; 317(1): 346-49.

[46] Grunlan JC, Liu L, and Kim YS. Tunable single-walled carbon nanotube microstructure in the liquid and solid states using poly(acrylic acid). Nano Letters 2006; 6(5): 911-15.

[47] Islam MF, Rojas E, Bergey DM, Johnson AT, and Yodh AG. High weight fraction surfactant solubilization of single-wall carbon nanotubes in water. Nano Letters 2003; 3(2): 269-73.

[48] Yazdanbakhsh A, Grasley Z, Tyson B, and Abu Al-Rub R. Carbon nanofibers and nanotubes in cementitious materials: some issues on dispersion and interfacial bond. ACI Special Publication 2009; V. SP 267: 21-34.

[49] Zhang HW, Wang JB, and Guo X. Predicting the elastic properties of single-walled carbon nanotubes. Journal of the Mechanics and Physics of Solids 2005; 53(9): 1929-50.

[50] Ago H, Kugler T, Cacialli F, Salaneck WR, Shaffer MSP, Windle AH, et al. Work functions and surface functional groups of multiwall carbon nanotubes. The Journal of Physical Chemistry B 1999; 103(38): 8116-21.

[51] Datsyuk V, Kalyva M, Papagelis K, Parthenios J, Tasis D, Siokou A, et al. Chemical oxidation of multiwalled carbon nanotubes. Carbon 2008; 46(6): 833-40.

[52] Lakshminarayanan PV, Toghiani H, and Pittman Jr CU. Nitric acid oxidation of vapor grown carbon nanofibers. Carbon 2004; 42(12-13): 2433-42.

[53] Zhang G, Sun S, Yang D, Dodelet J-P, and Sacher E. The surface analytical characterization of carbon fibers functionalized by H2SO4/HNO3 treatment. Carbon 2008; 46(2): 196-205.

[54] Dyke CA and Tour JM. Covalent functionalization of single-walled carbon nanotubes for materials applications. The Journal of Physical Chemistry A 2004; 108(51): 11151-59.

[55] Mickelson ET, Huffman CB, Rinzler AG, Smalley RE, Hauge RH, and Margrave JL. Fluorination of single-wall carbon nanotubes. Chemical Physics Letters 1998; 296(1-2): 188-94.

[56] Hudson JL, Casavant MJ, and Tour JM. Water-soluble, exfoliated, nonroping single-wall carbon nanotubes. Journal of the American Chemical Society 2004; 126(36): 11158-59.

[57] Wang Y, Iqbal Z, and Mitra S. Rapidly functionalized, water-dispersed carbon nanotubes at high concentration. Journal of the American Chemical Society 2006; 128(1): 95-99.

[58] Bandyopadhyaya R, Nativ-Roth E, Regev O, and Yerushalmi-Rozen R. Stabilization of individual carbon nanotubes in aqueous solutions. Nano Letters 2001; 2(1): 25-28.

[59] Eckel DF, Balogh MP, Fasulo PD, and Rodgers WR. Assessing organo-clay dispersion in polymer nanocomposites. Journal of Applied Polymer Science 2004; 93(3): 1110-17.

[60] Xie S, Harkin-Jones E, Shen Y, Hornsby P, McAfee M, McNally T, et al. Quantitative characterization of clay dispersion in polypropylene-clay nanocomposites by combined transmission electron microscopy and optical microscopy. Materials Letters 2010; 64(2): 185-88.

[61] Luo ZP and Koo JH. Quantifying the dispersion of mixture microstructures. Journal of Microscopy-Oxford 2007; 225(2): 118-25.

[62] Luo ZP and Koo JH. Quantification of the layer dispersion degree in polymer layered silicate nanocomposites by transmission electron microscopy. Polymer 2008; 49(7): 1841-52.

[63] Luo ZP and Koo JH. Quantitative study of the dispersion degree in carbon nanofiber/polymer and carbon nanotube/polymer nanocomposites. Materials Letters 2008; 62(20): 3493-96.

[64] Bakshi SR, Batista RG, and Agarwal A. Quantification of carbon nanotube distribution and property correlation in nanocomposites. Composites Part A: Applied Science and Manufacturing 2009; 40(8): 1311-18.

[65] The MathWorks. 2010; http://www.mathworks.com.

[66] Vibra-Cell liquid processing. 2010; http://www.sonics.biz/lp-vibra.htm.

[67] NI LabVIEW. 2010; http://www.ni.com/labview.

APPENDIX A

Plain Cement

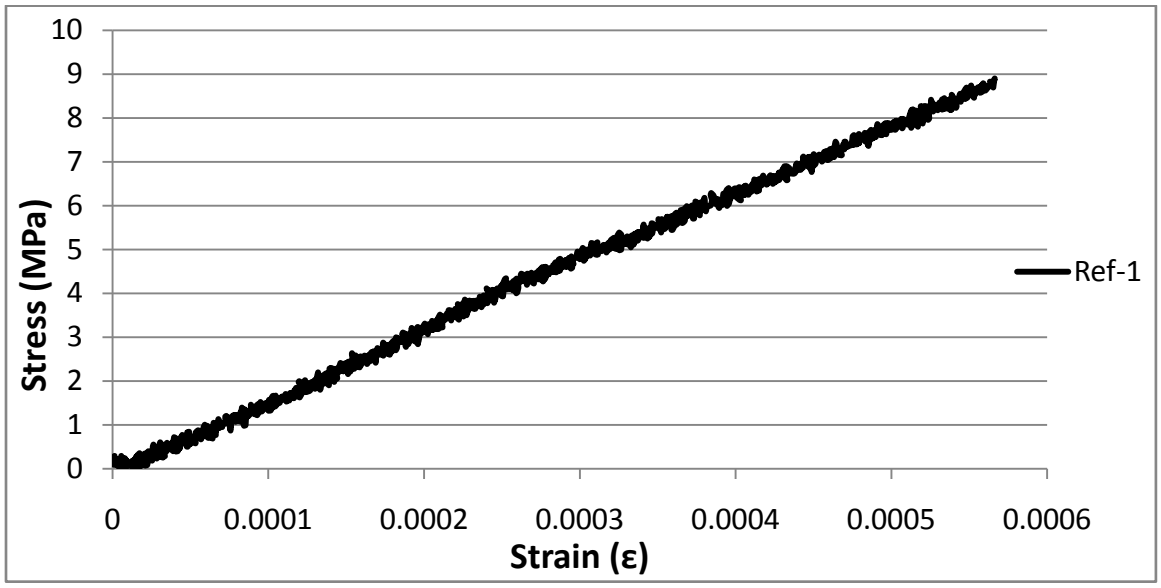

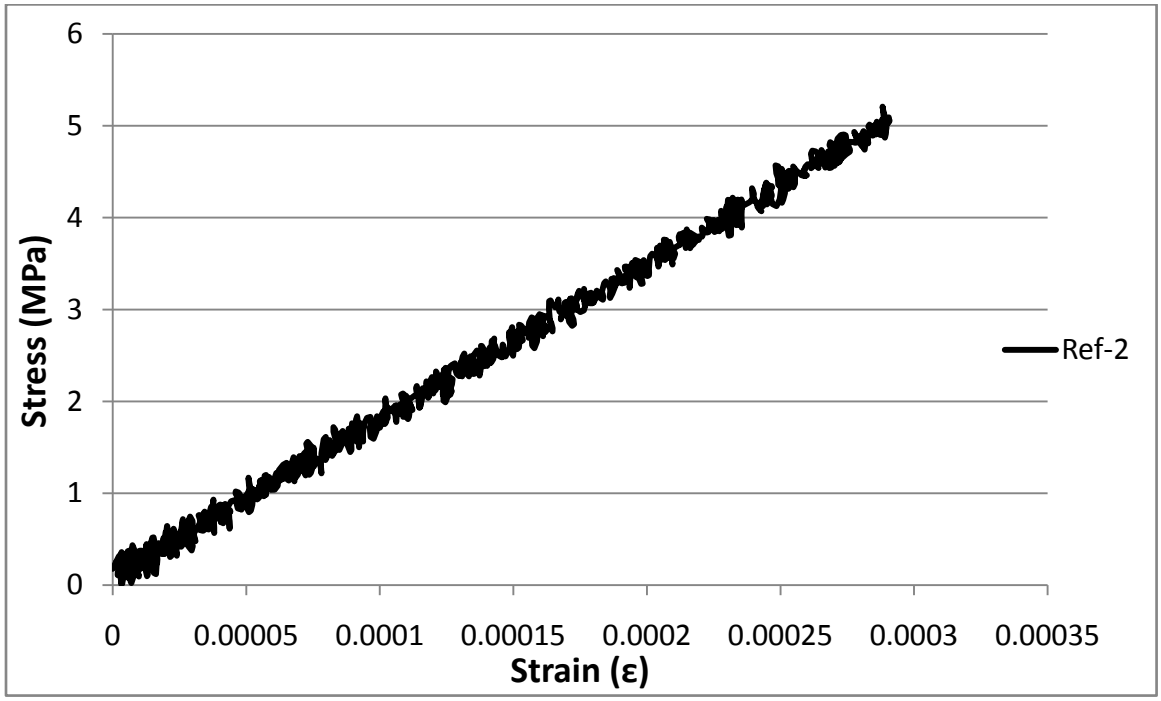

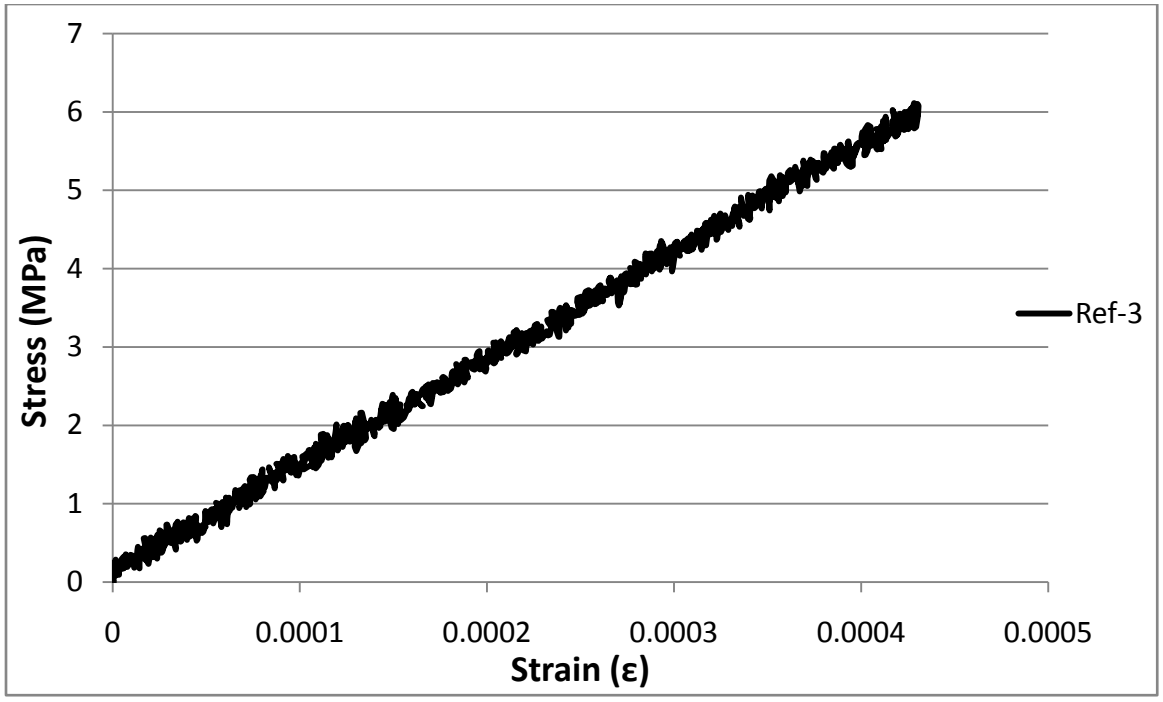
7
6
5
4
3
2
1
0
Stress (MPa)
0
0.0001
0.0002
0.0003
0.0004
0.0005
Strain (ε)
Ref-3

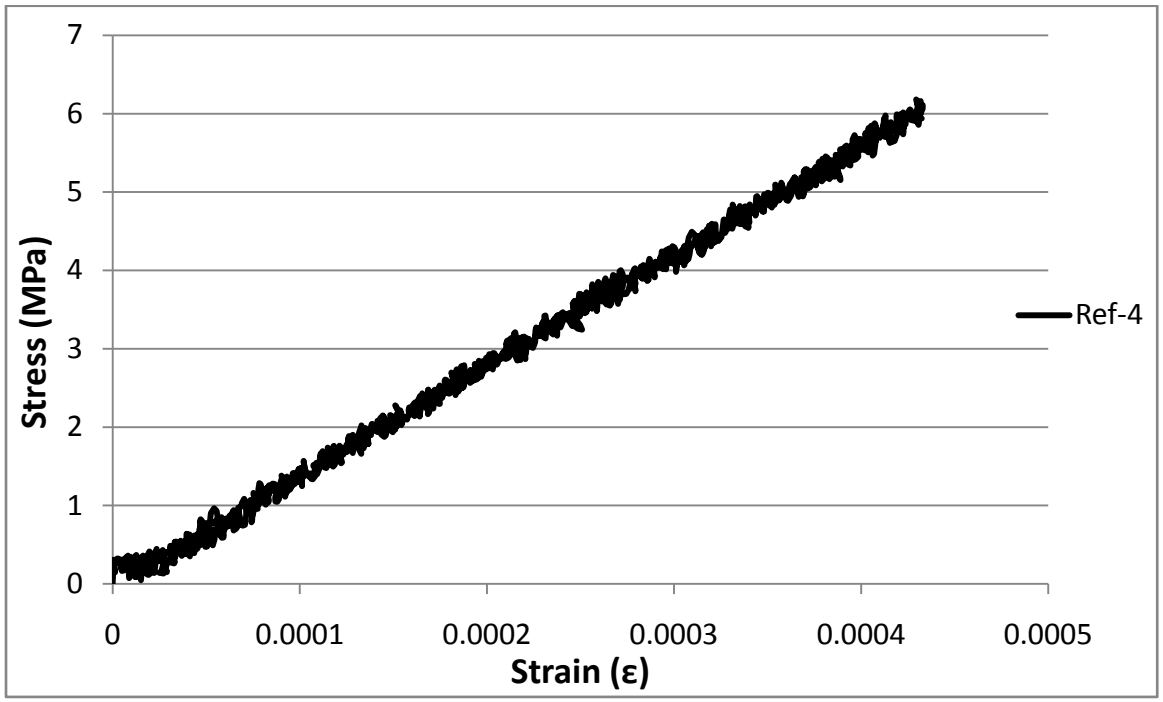
7
6
5
4
3
2
1
0
Stress (MPa)
0
0.0001
0.0002
0.0003
0.0004
0.0005
Strain (ε)
Ref-4

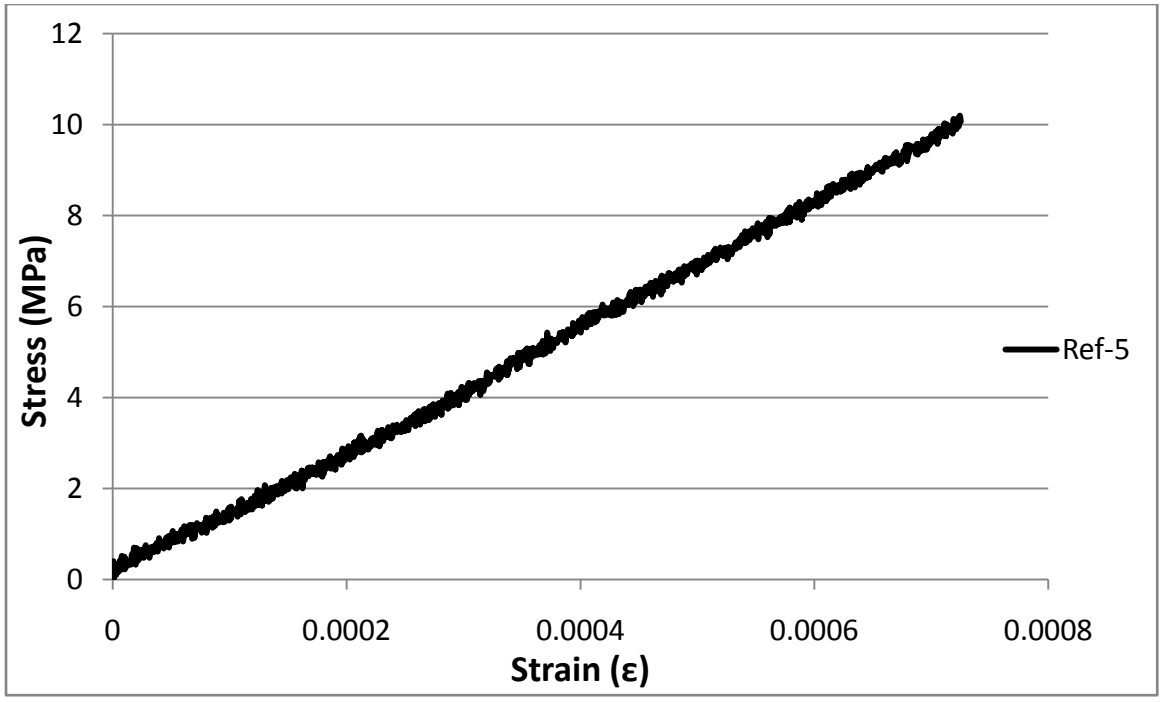
12
10
8
6
4
2
0
Stress (MPa)
0
0.0002
0.0004
0.0006
0.0008
Strain (ε)
Ref-5

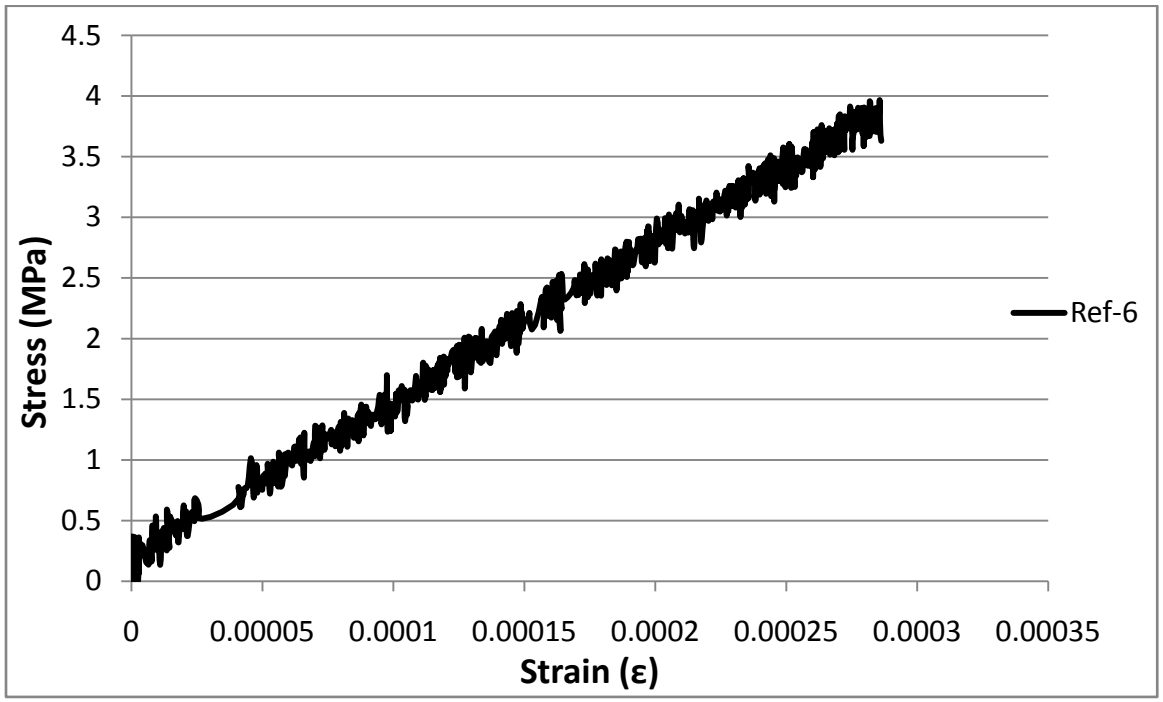
4.5
4
3.5
3
2.5
2
1.5
1
0.5
0
Stress (MPa)
0
0.00005
0.0001
0.00015
0.0002
0.00025
0.0003
0.00035
Strain (ε)
Ref-6

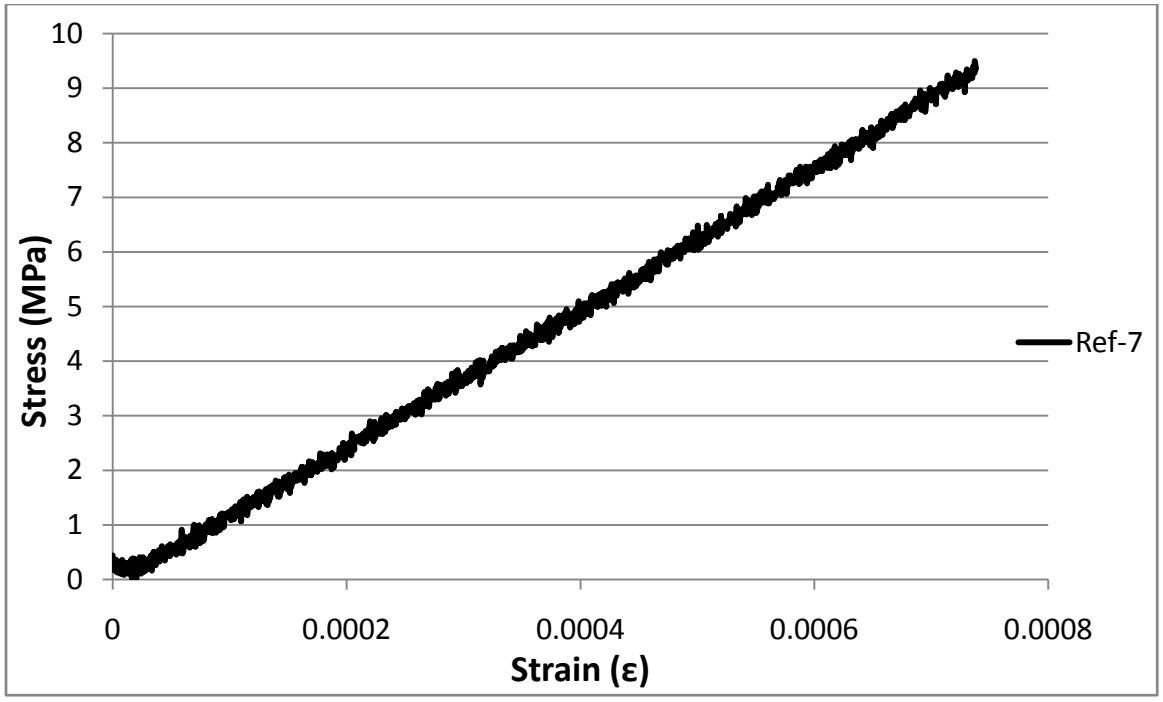
10
9
8
7
6
5
4
3
2
1
0
Stress (MPa)
0
0.0002
0.0004
0.0006
0.0008
Strain (ε)
Ref-7

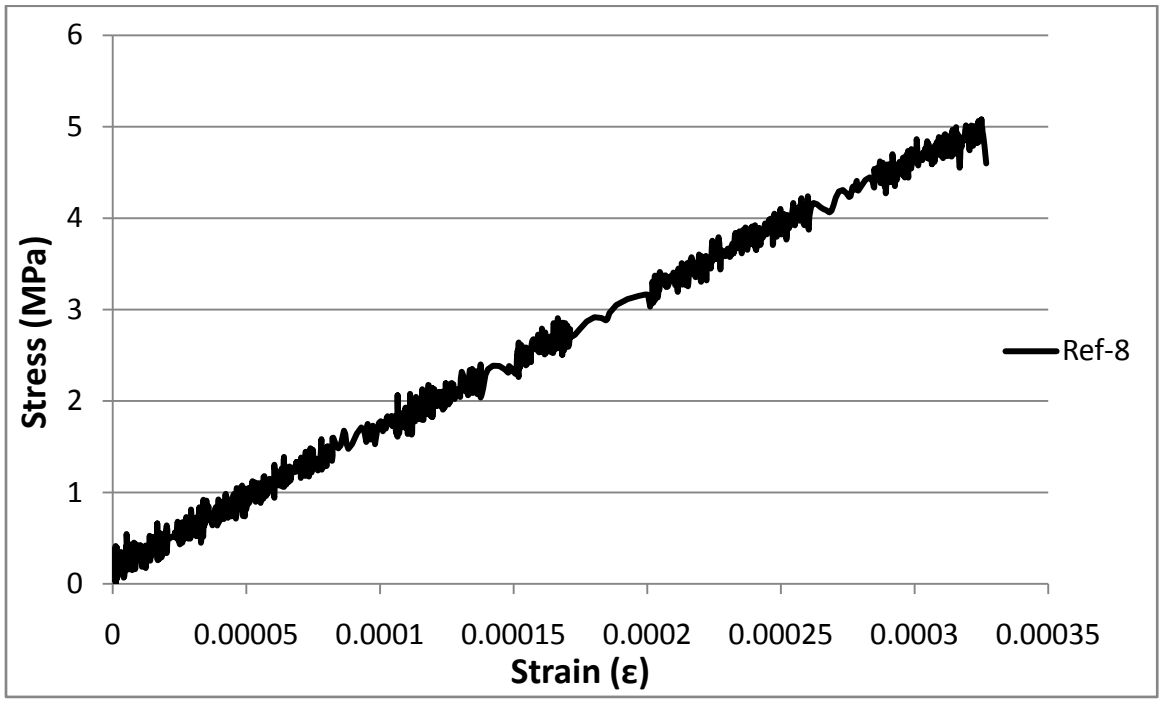
6
5
4
3
2
1
0
Stress (MPa)
0
0.00005
0.0001
0.00015
0.0002
0.00025
0.0003
0.00035
Strain (ε)
Ref-8

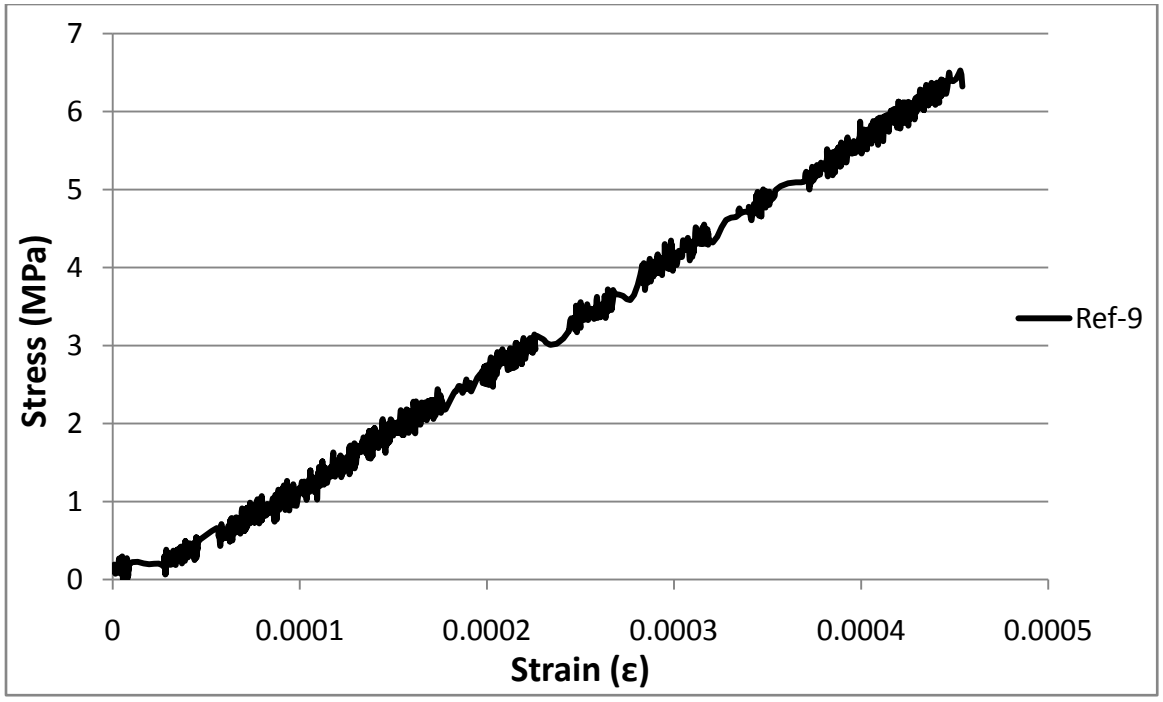
7
6
5
4
3
2
1
0
Stress (MPa)
0
0.0001
0.0002
0.0003
0.0004
0.0005
Strain (ε)
Ref-9

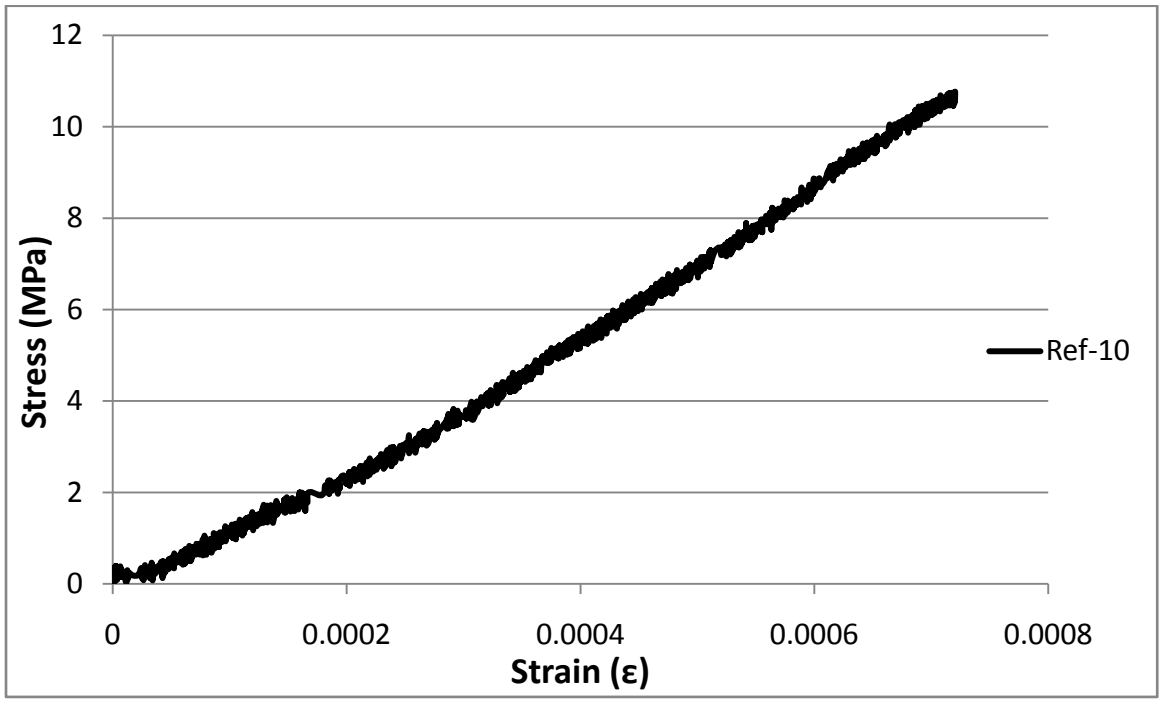
12
10
8
6
4
2
0
Stress (MPa)
0
0.0002
0.0004
0.0006
0.0008
Strain (ε)
Ref-10

Untreated Fibers at 0.1%

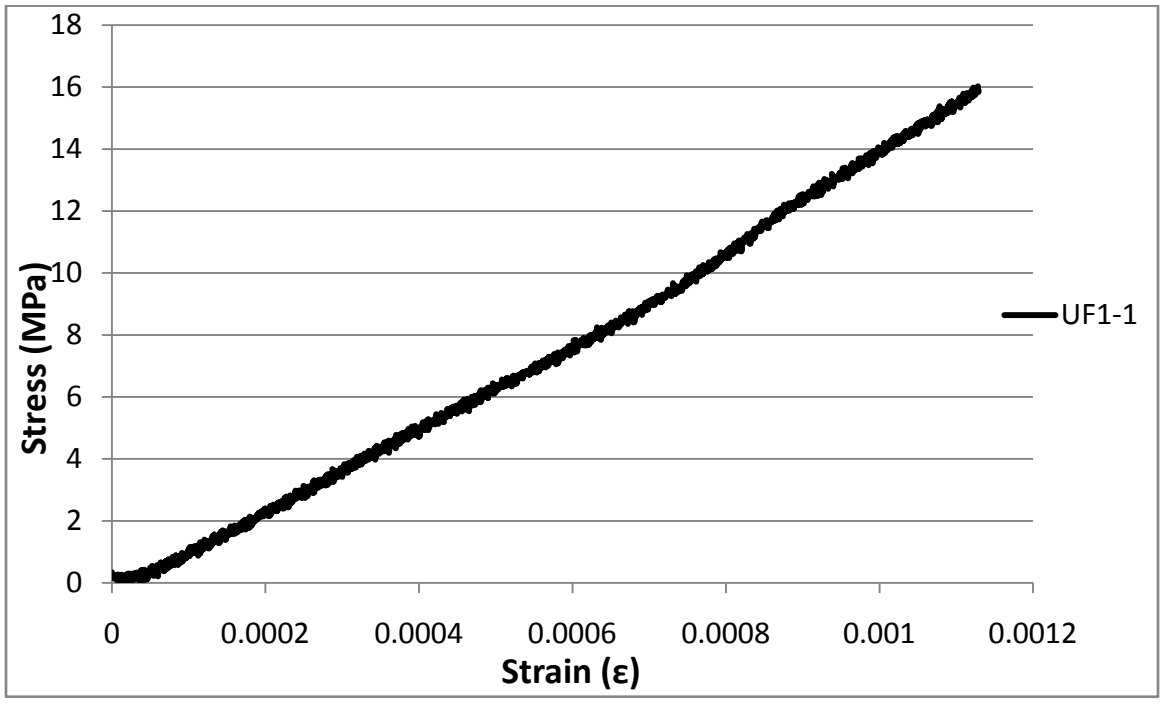

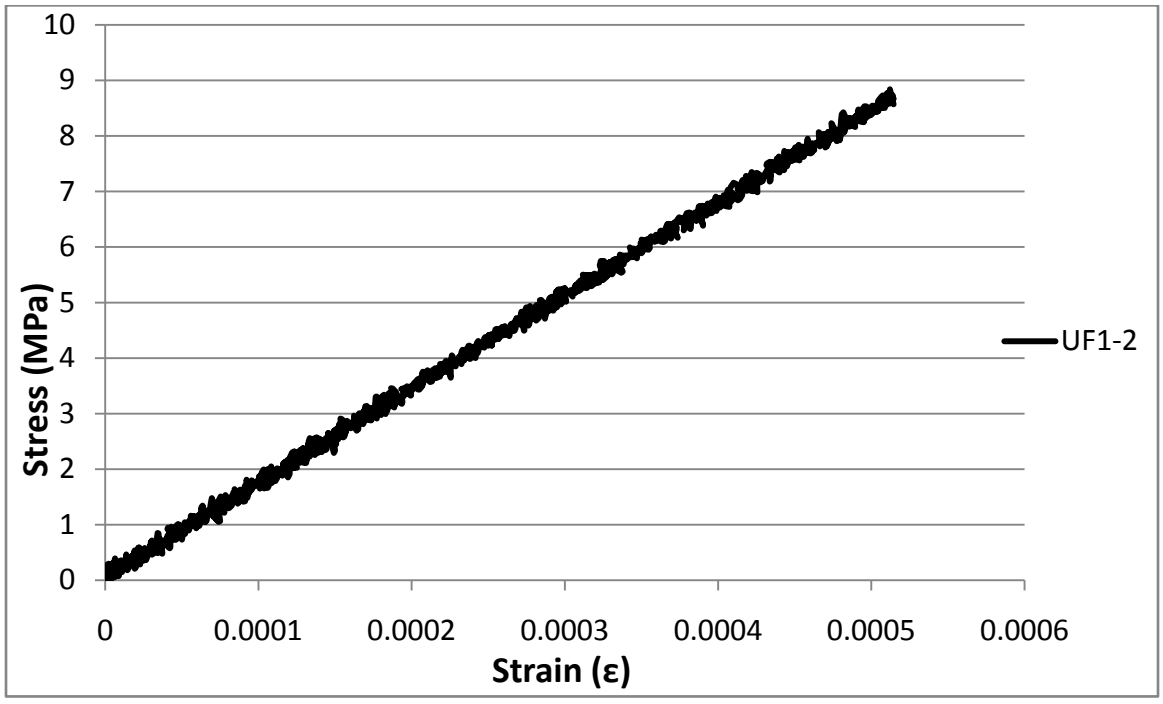

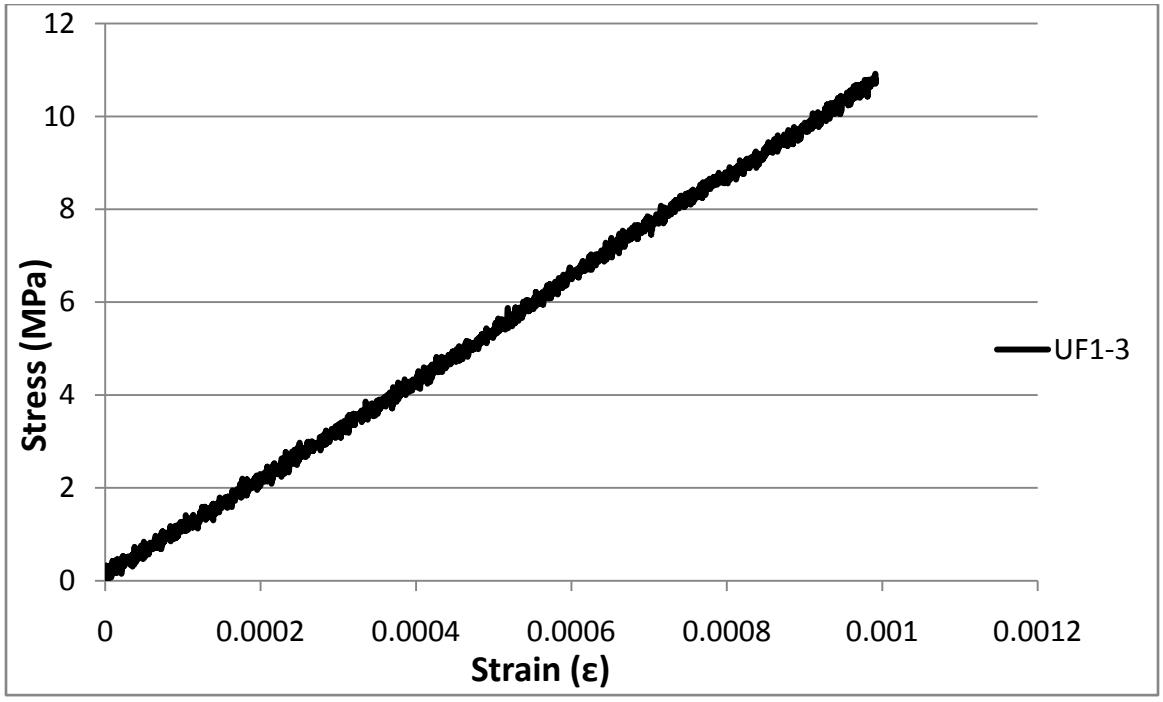
12
10
8
6
4
2
0
Stress (MPa)
0
0.0002
0.0004
0.0006
0.0008
0.001
0.0012
Strain (ε)
UF1-3

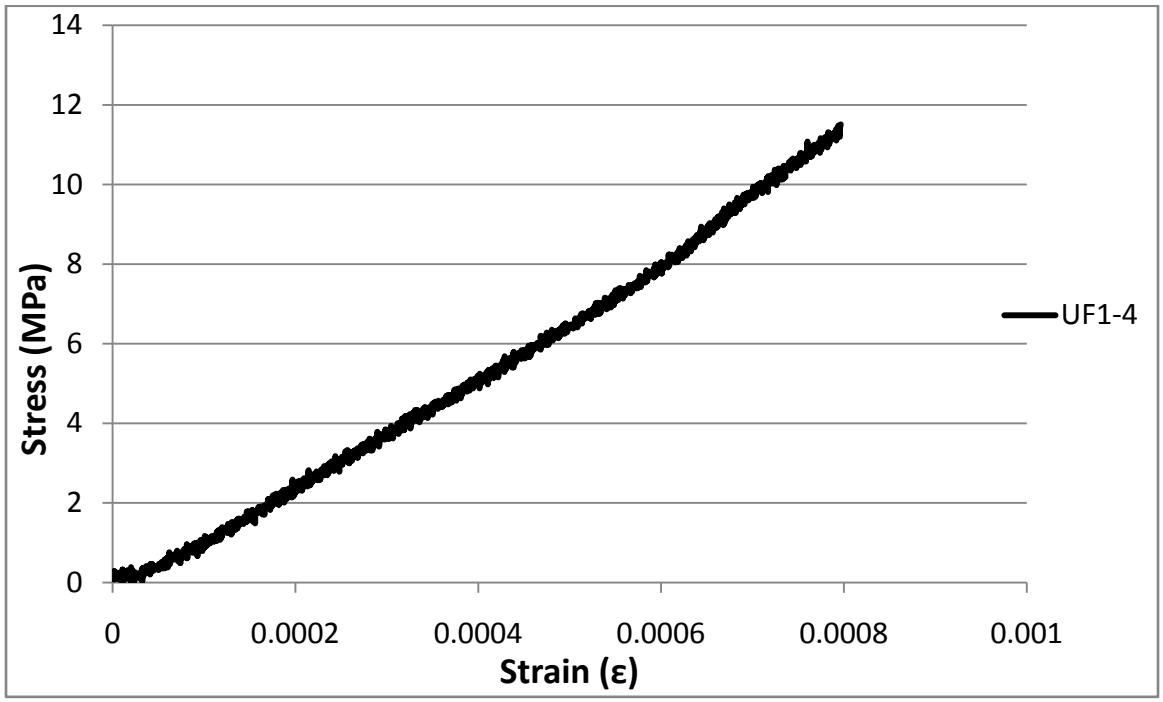
14
12
10
8
6
4
2
0
Stress (MPa)
0
0.0002
0.0004
0.0006
0.0008
0.001
Strain (ε)
UF1-4

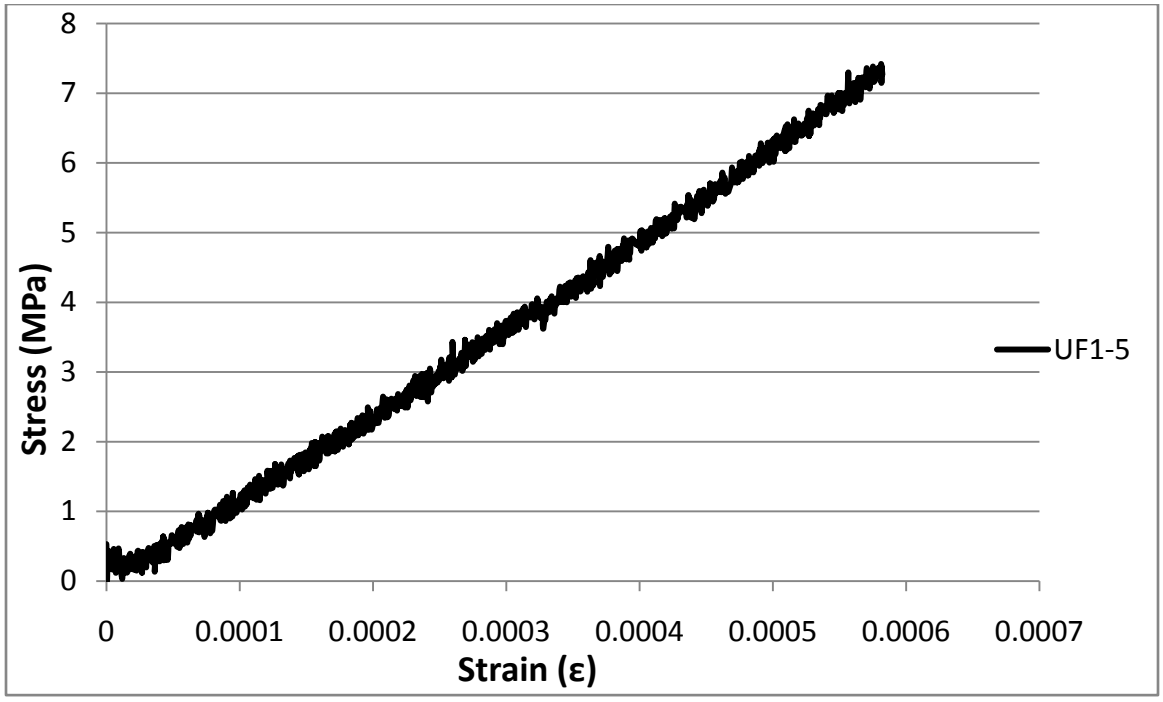
8
7
6
5
4
3
2
1
0
Stress (MPa)
0
0.0001
0.0002
0.0003
0.0004
0.0005
0.0006
0.0007
Strain (ε)
UF1-5

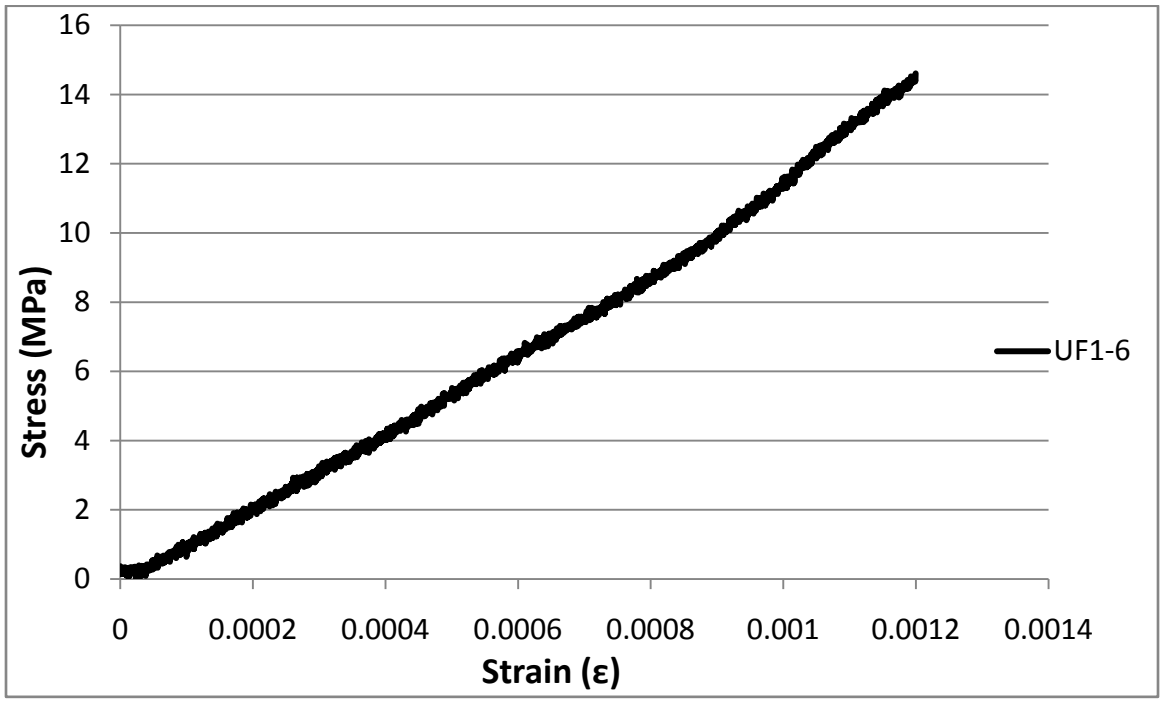
16
14
12
10
8
6
4
2
0
Stress (MPa)
0
0.0002
0.0004
0.0006
0.0008
0.001
0.0012
0.0014
Strain (ε)
UF1-6

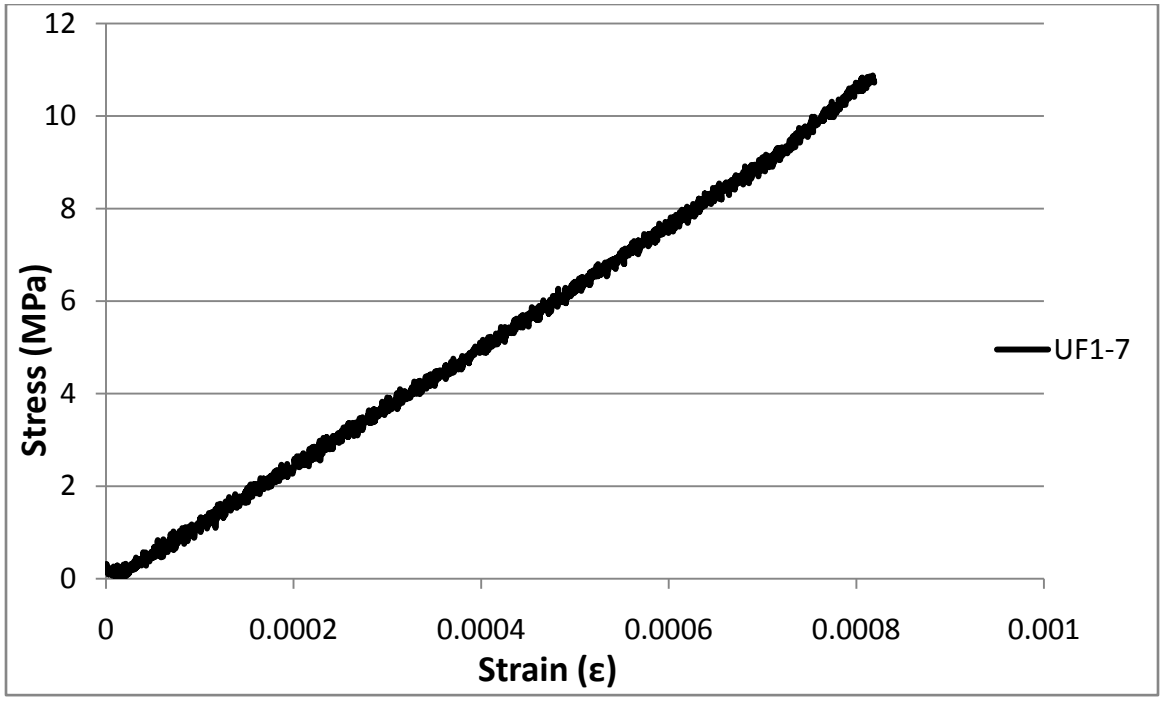
12
10
8
6
4
2
0
Stress (MPa)
0
0.0002
0.0004
0.0006
0.0008
0.001
Strain (ε)
UF1-7

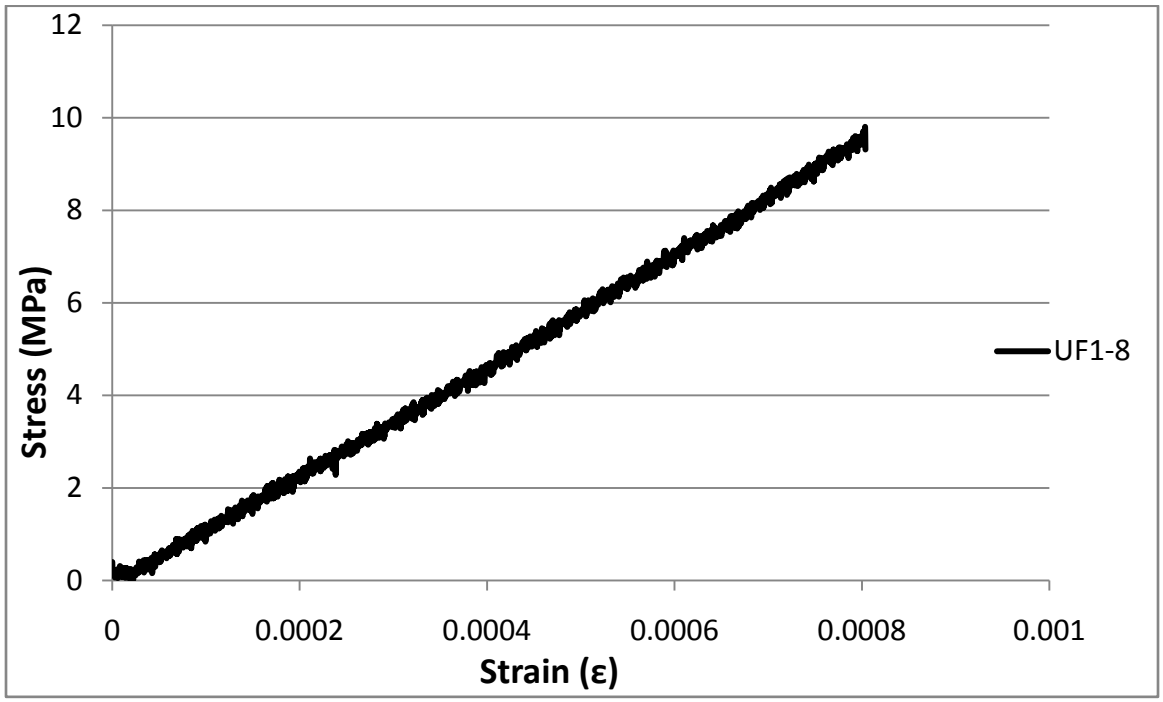
12
10
8
6
4
2
0
Stress (MPa)
0
0.0002
0.0004
0.0006
0.0008
0.001
Strain (ε)
UF1-8

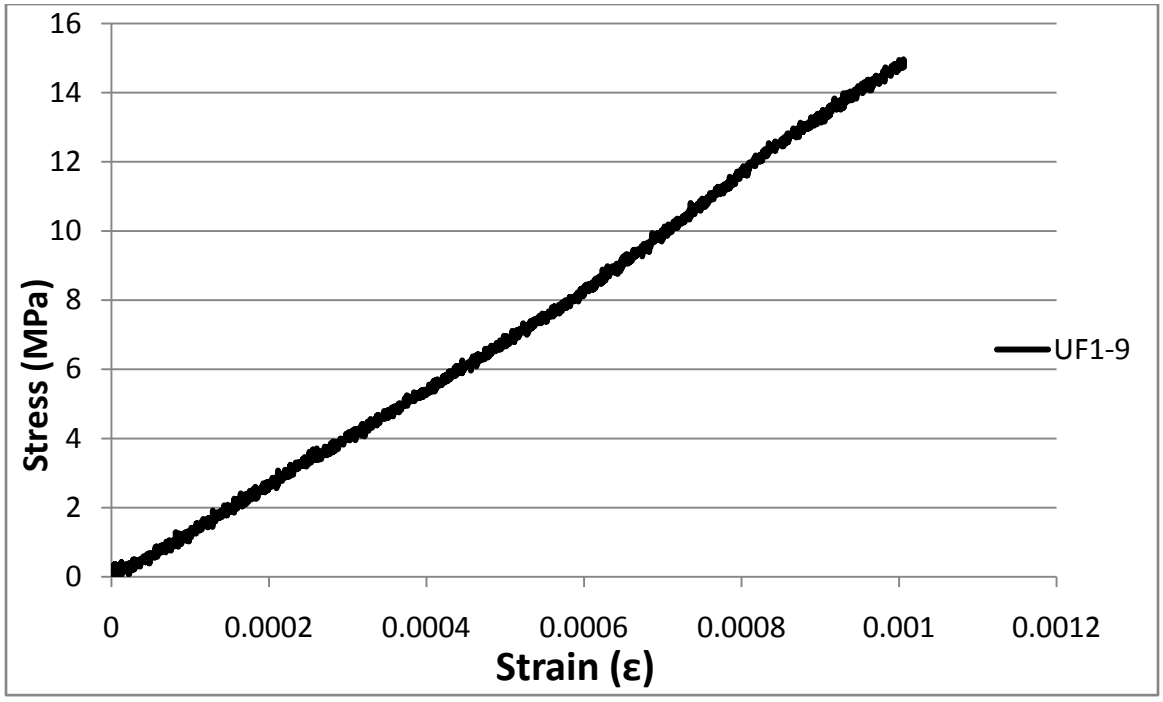
16
14
12
10
8
6
4
2
0
Stress (MPa)
0
0.0002
0.0004
0.0006
0.0008
0.001
0.0012
Strain (ε)
UF1-9

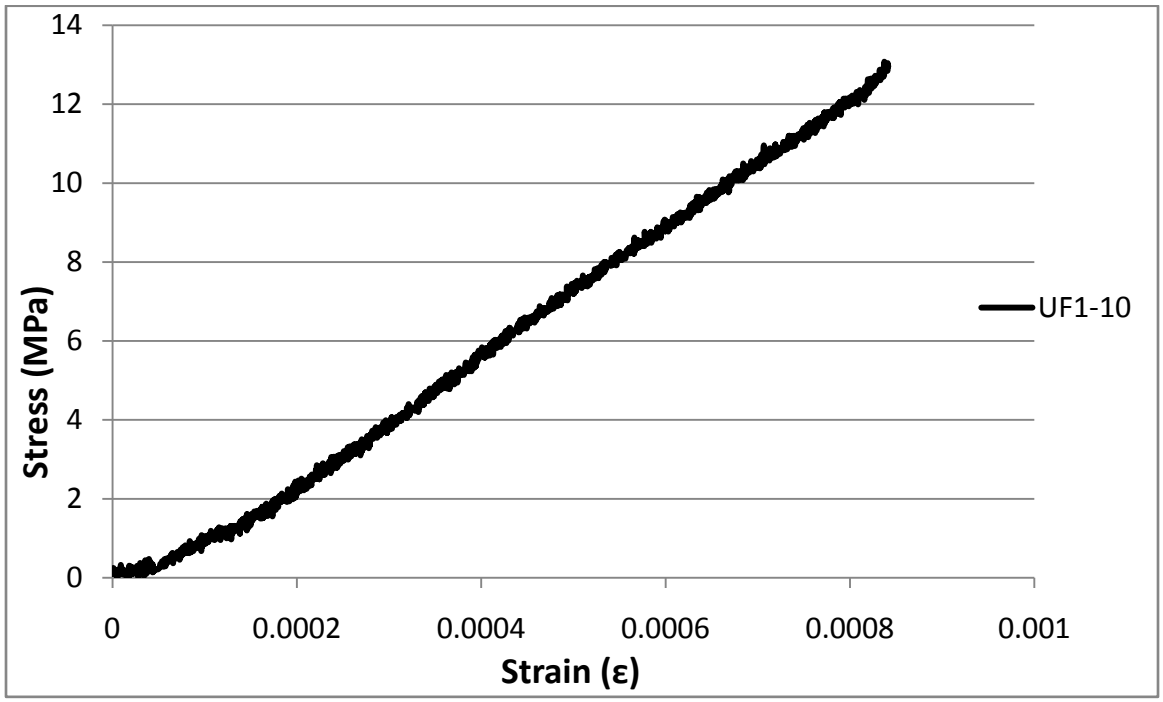
14
12
10
8
6
4
2
0
Stress (MPa)
0
0.0002
0.0004
0.0006
0.0008
0.001
Strain (ε)
UF1-10

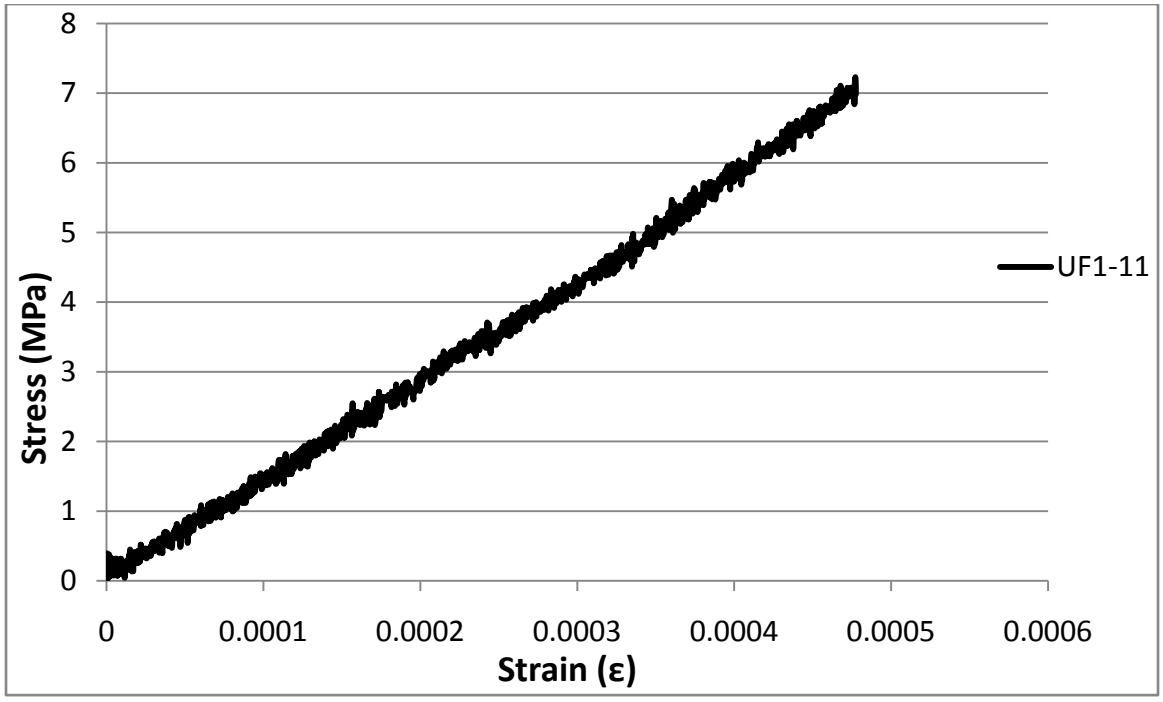
8
7
6
5
4
3
2
1
0
Stress (MPa)
0
0.0001
0.0002
0.0003
0.0004
0.0005
0.0006
Strain (ε)
UF1-11

Untreated Fibers at 0.2%

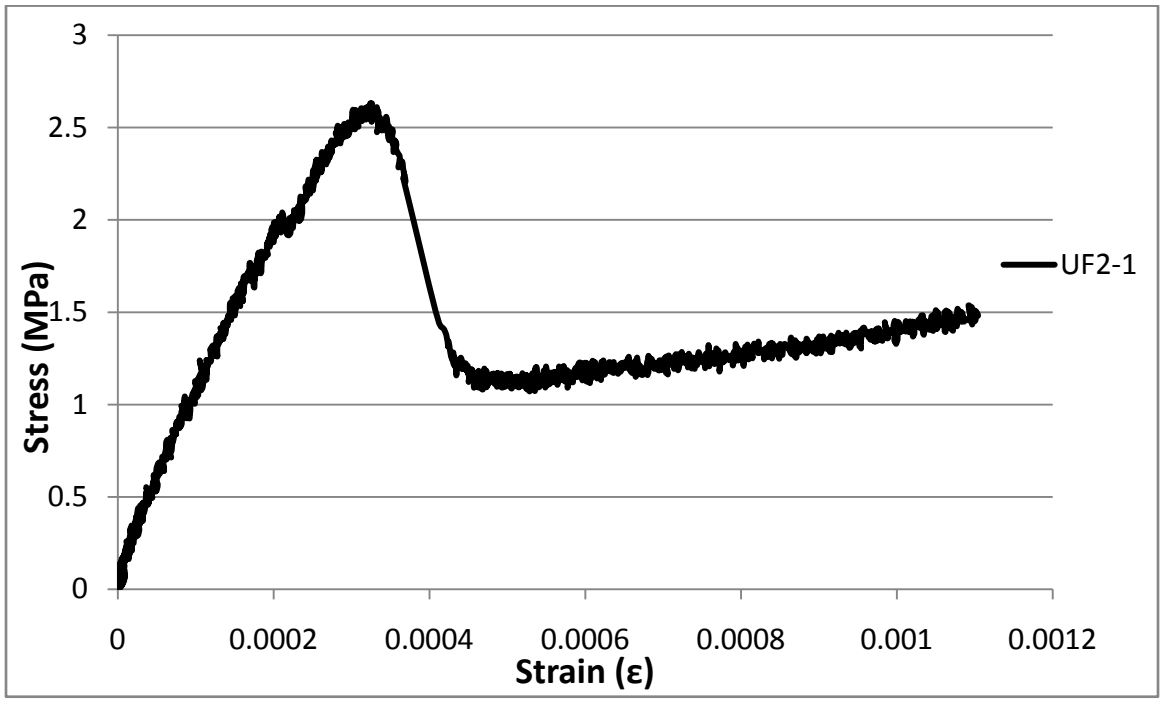

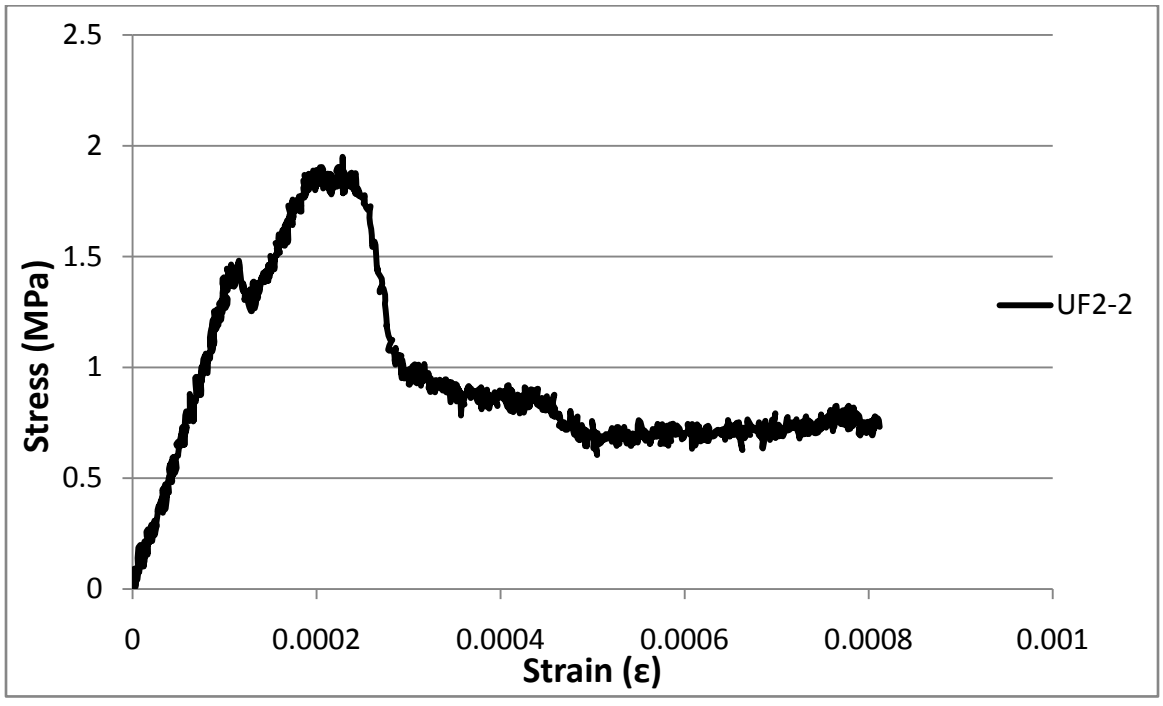

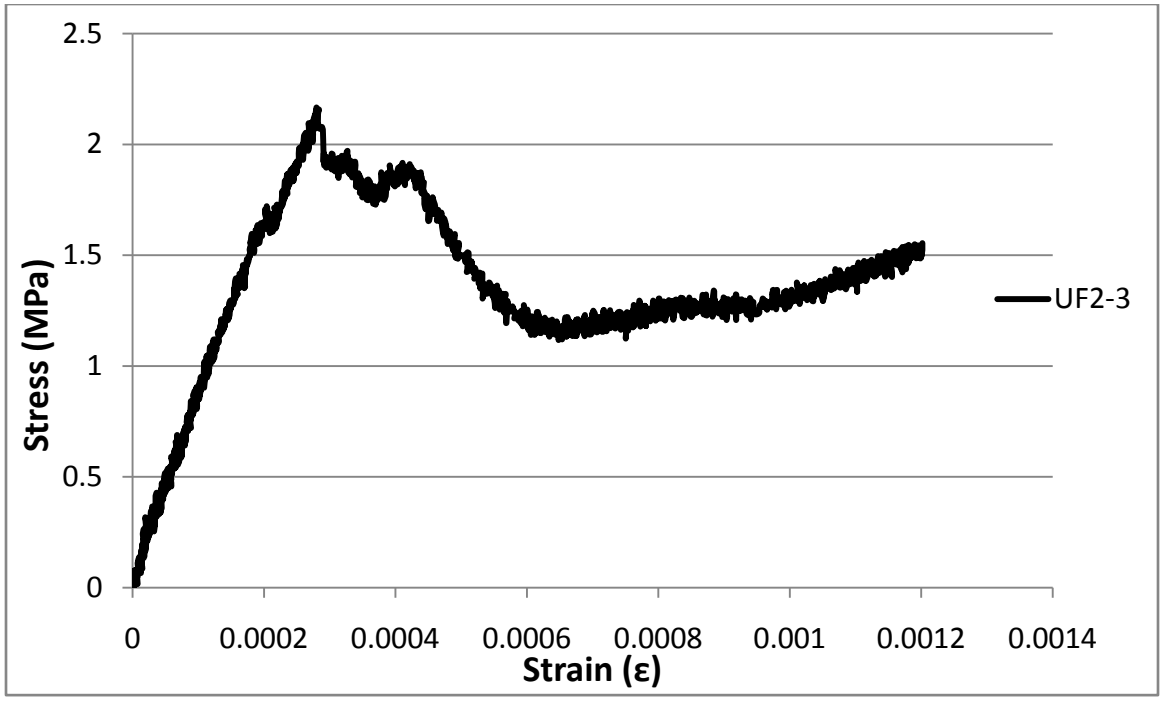
2.5
2
1.5
1
0.5
0
Stress (MPa)
0
0.0002
0.0004
0.0006
0.0008
0.001
0.0012
0.0014
Strain (ε)
UF2-3

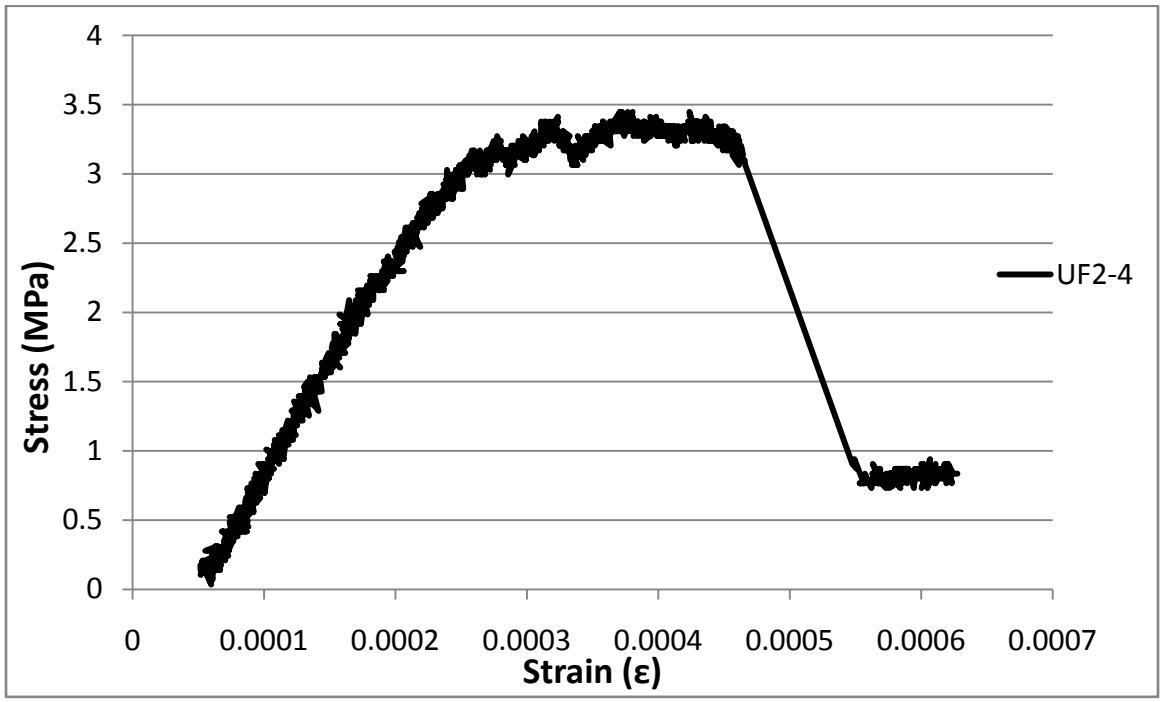
4
3.5
3
2.5
2
1.5
1
0.5
0
Stress (MPa)
0
0.0001
0.0002
0.0003
0.0004
0.0005
0.0006
0.0007
Strain (ε)
UF2-4

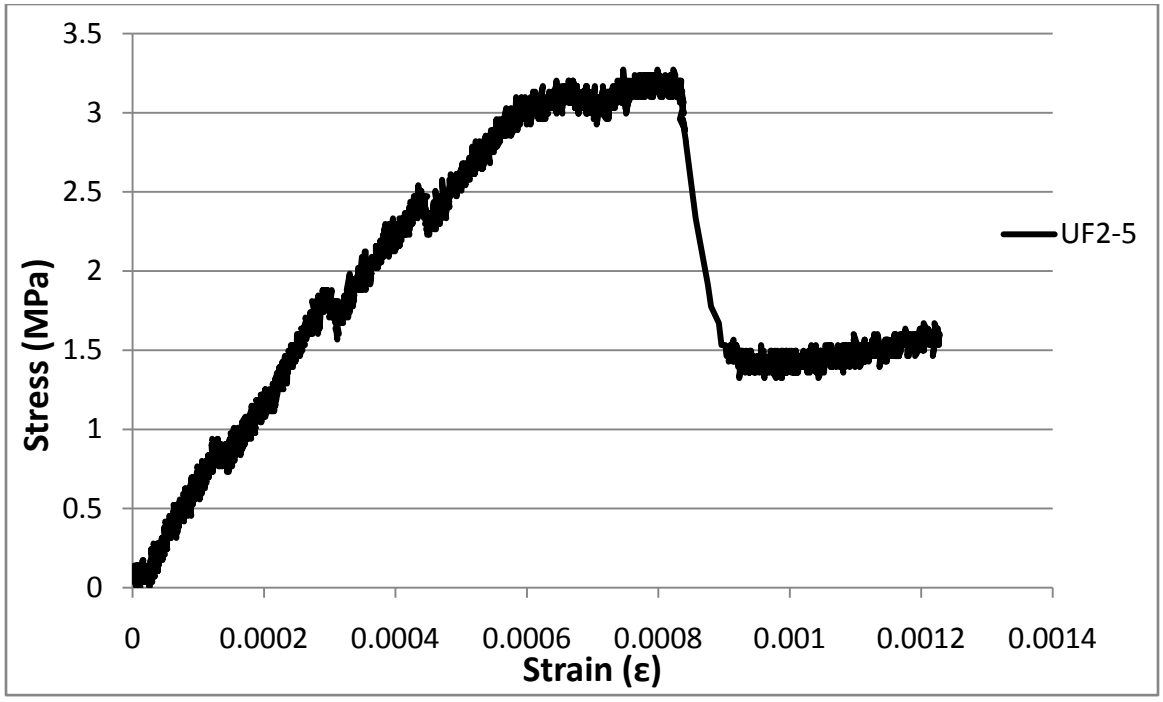
3.5
3
2.5
2
1.5
1
0.5
0
Stress (MPa)
0
0.0002
0.0004
0.0006
0.0008
0.001
0.0012
0.0014
Strain (ε)
UF2-5

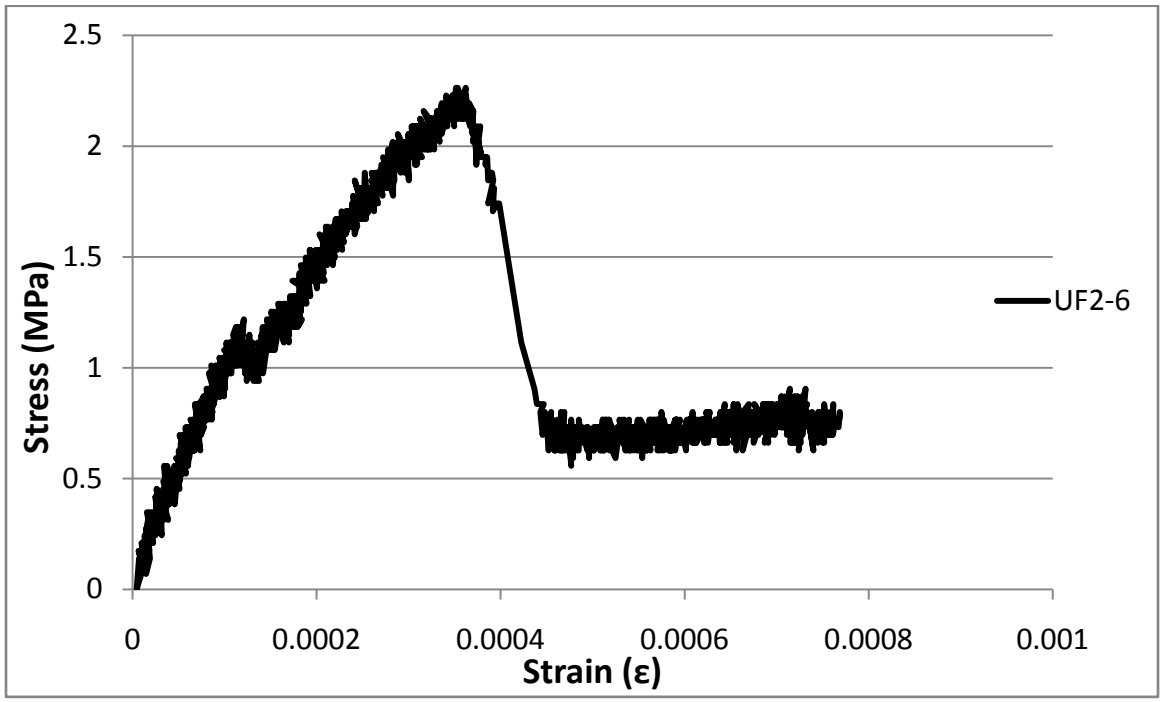
2.5
2
1.5
1
0.5
0
Stress (MPa)
0
0.0002
0.0004
0.0006
0.0008
0.001
Strain (ε)
UF2-6

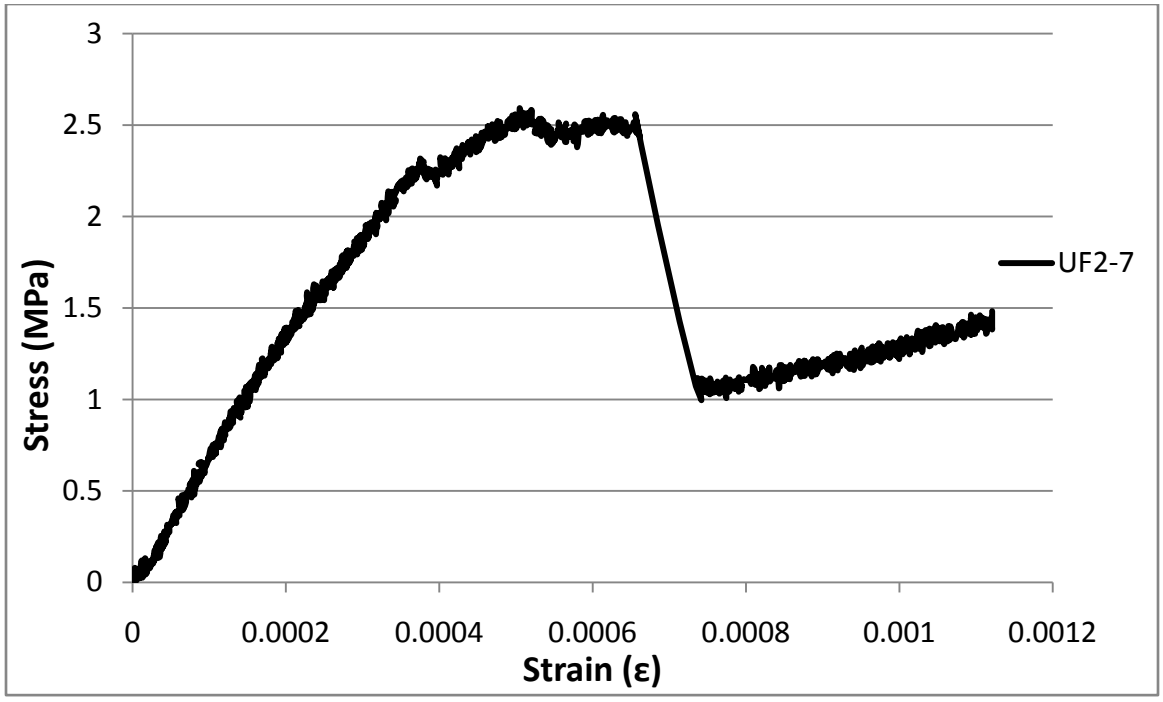
3
2.5
2
1.5
1
0.5
0
Stress (MPa)
0
0.0002
0.0004
0.0006
0.0008
0.001
0.0012
Strain (ε)
UF2-7

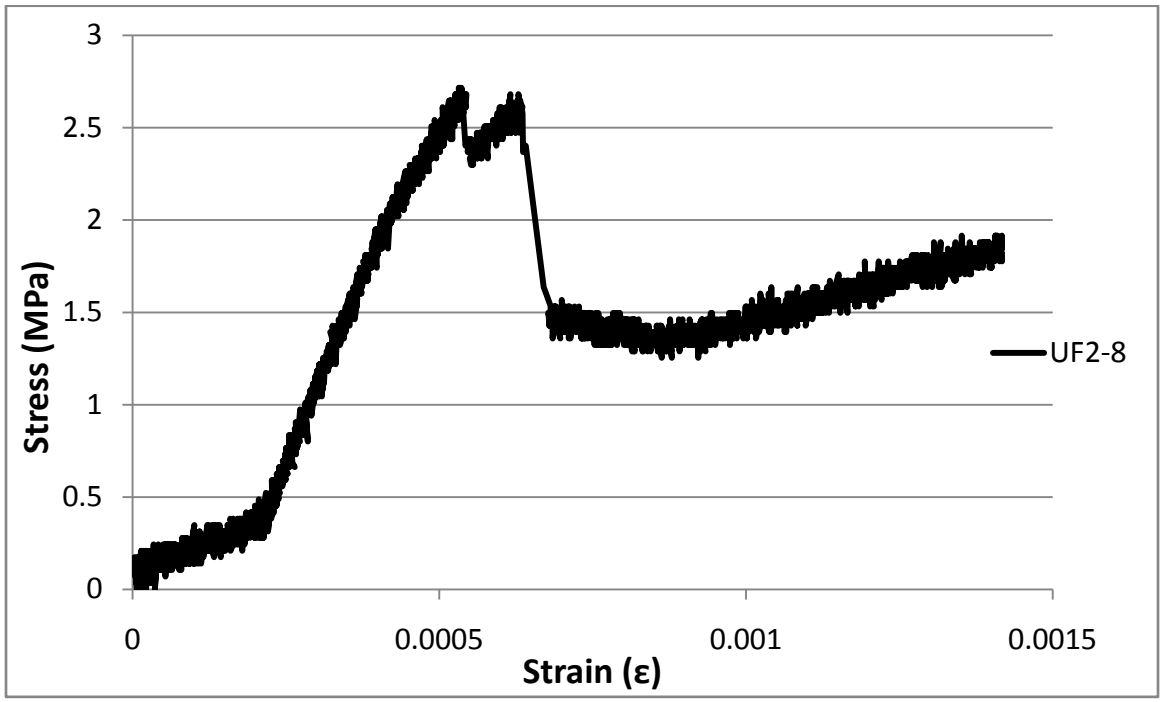
3
2.5
2
1.5
1
0.5
0
Stress (MPa)
0
0.0005
0.001
0.0015
Strain (ε)
UF2-8

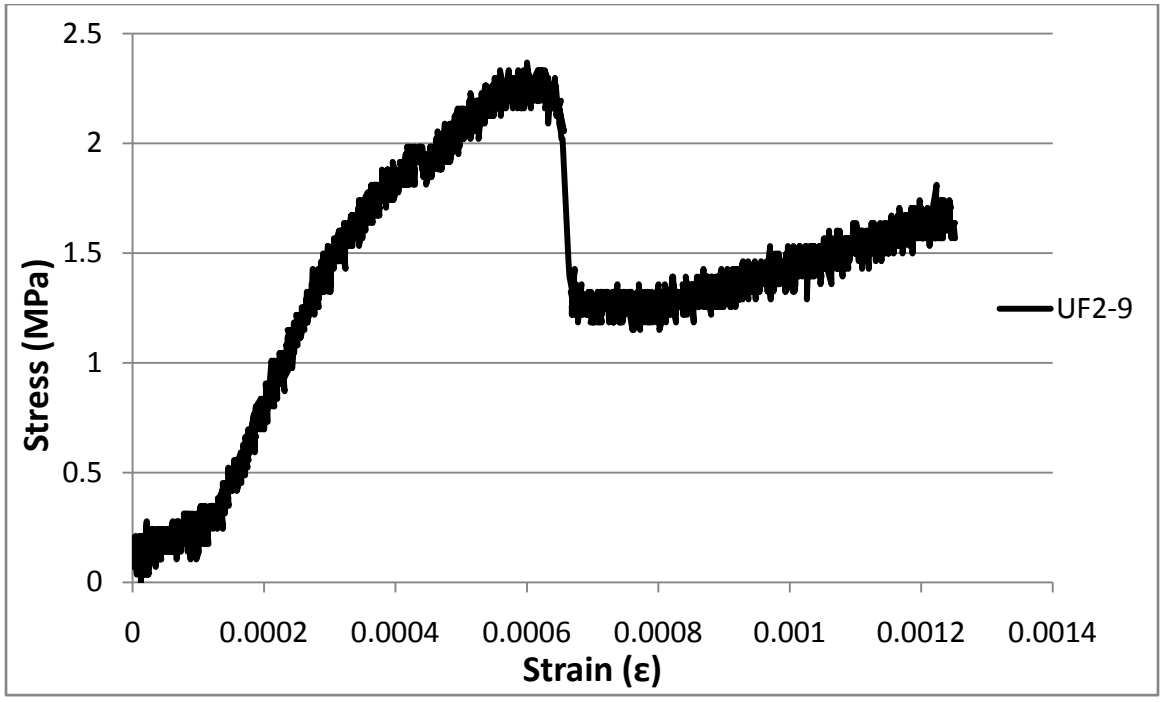
2.5
2
1.5
1
0.5
0
Stress (MPa)
0
0.0002
0.0004
0.0006
0.0008
0.001
0.0012
0.0014
Strain (ε)
UF2-9

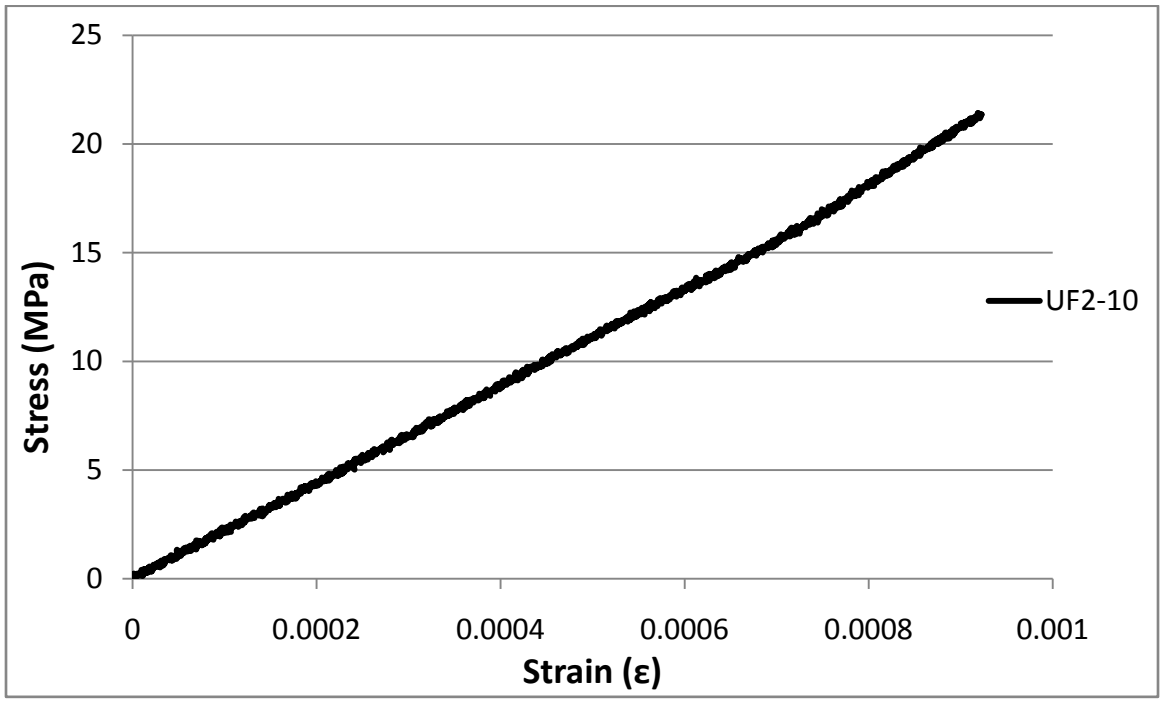
25
20
15
10
5
0
Stress (MPa)
0
0.0002
0.0004
0.0006
0.0008
0.001
Strain (ε)
UF2-10

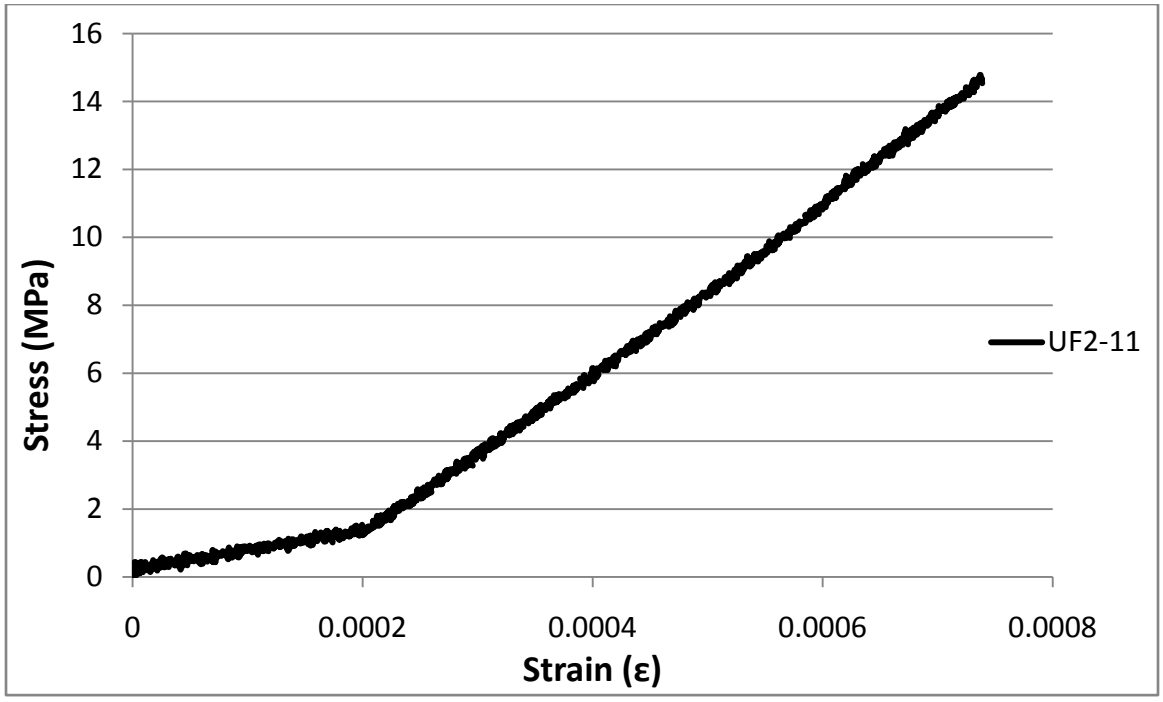
16
14
12
10
8
6
4
2
0
Stress (MPa)
0
0.0002
0.0004
0.0006
0.0008
Strain (ε)
UF2-11

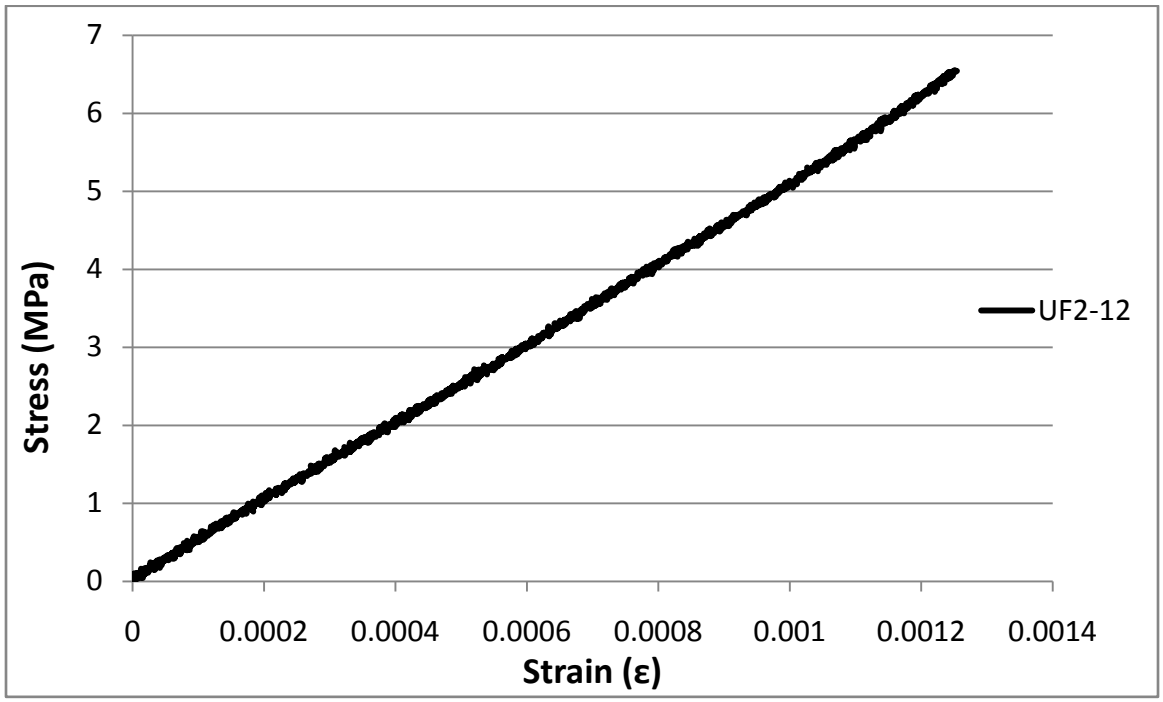
7
6
5
4
3
2
1
0
Stress (MPa)
0
0.0002
0.0004
0.0006
0.0008
0.001
0.0012
0.0014
Strain (ε)
UF2-12

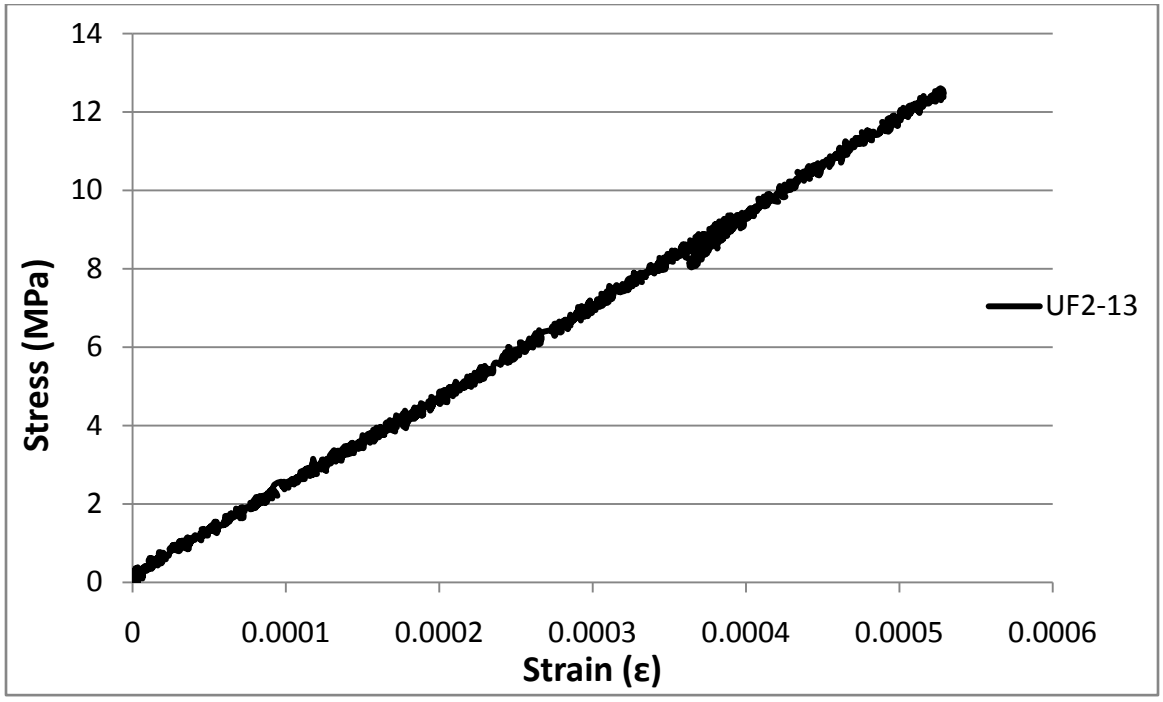
14
12
10
8
6
4
2
0
Stress (MPa)
0
0.0001
0.0002
0.0003
0.0004
0.0005
0.0006
Strain (ε)
UF2-13

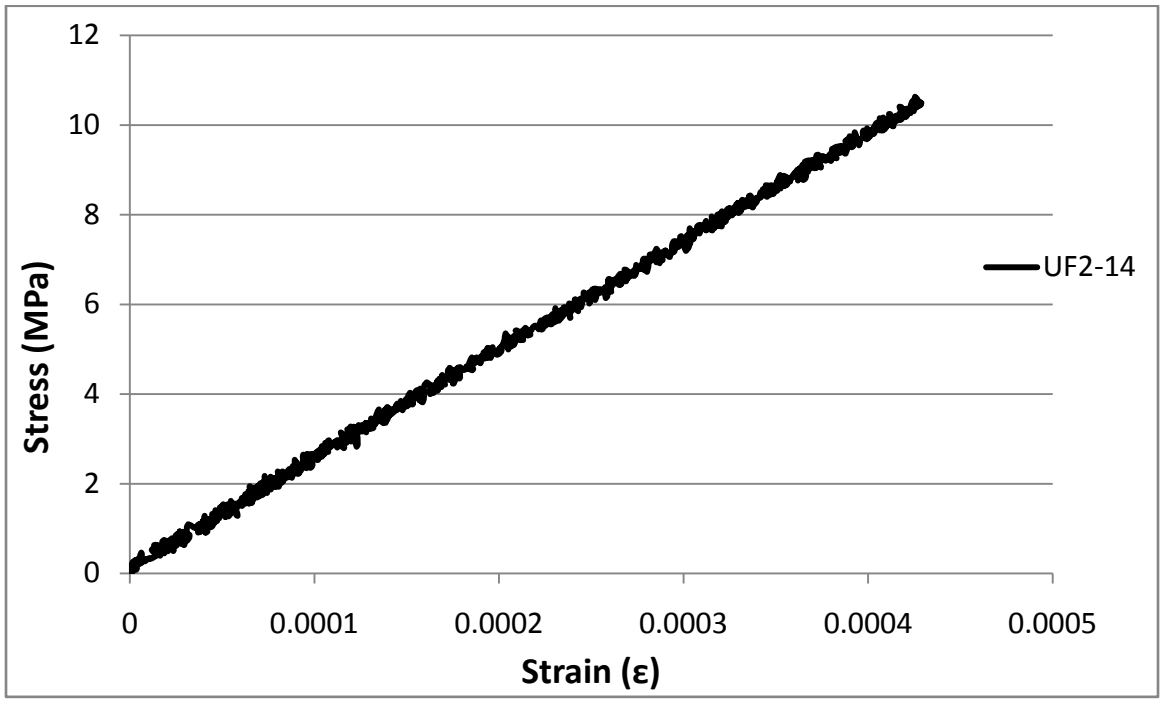
12
10
8
6
4
2
0
Stress (MPa)
0
0.0001
0.0002
0.0003
0.0004
0.0005
Strain (ε)
UF2-14

Untreated Tubes at 0.1%

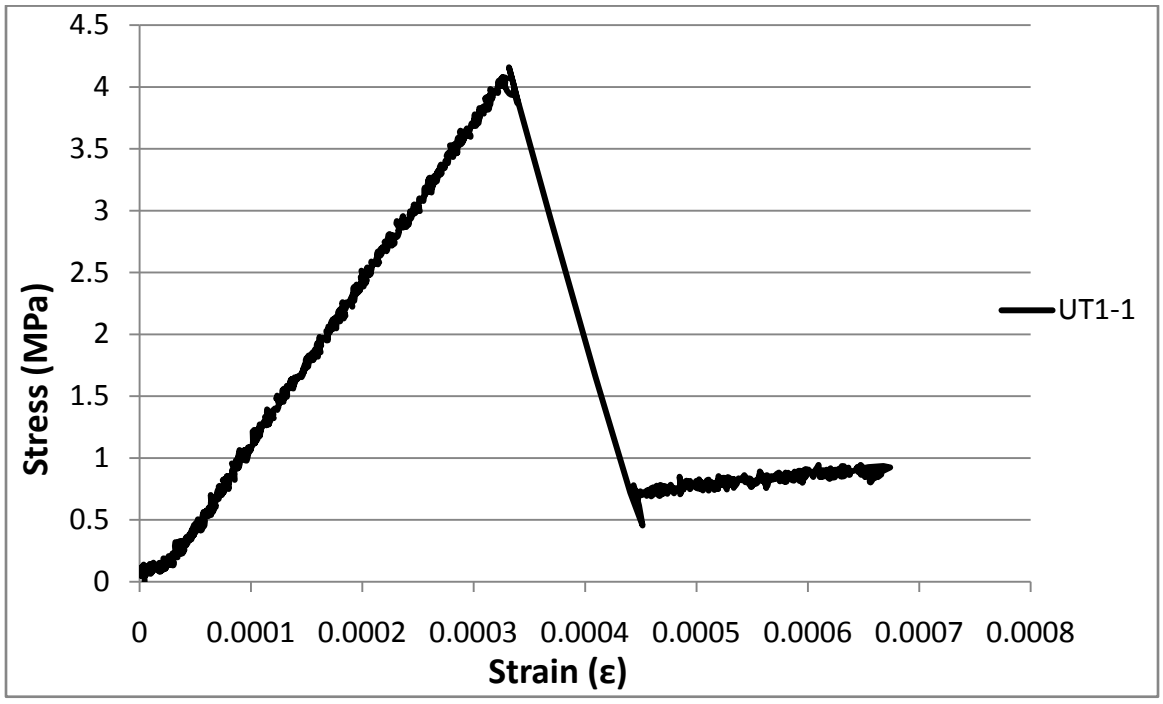

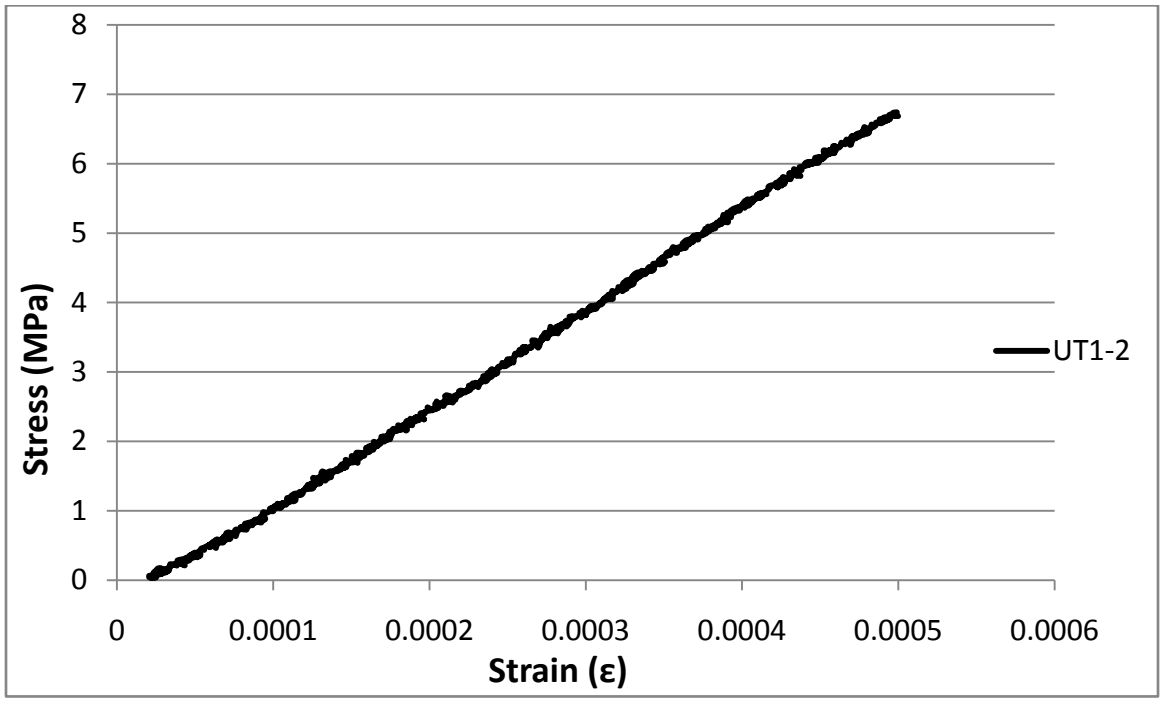

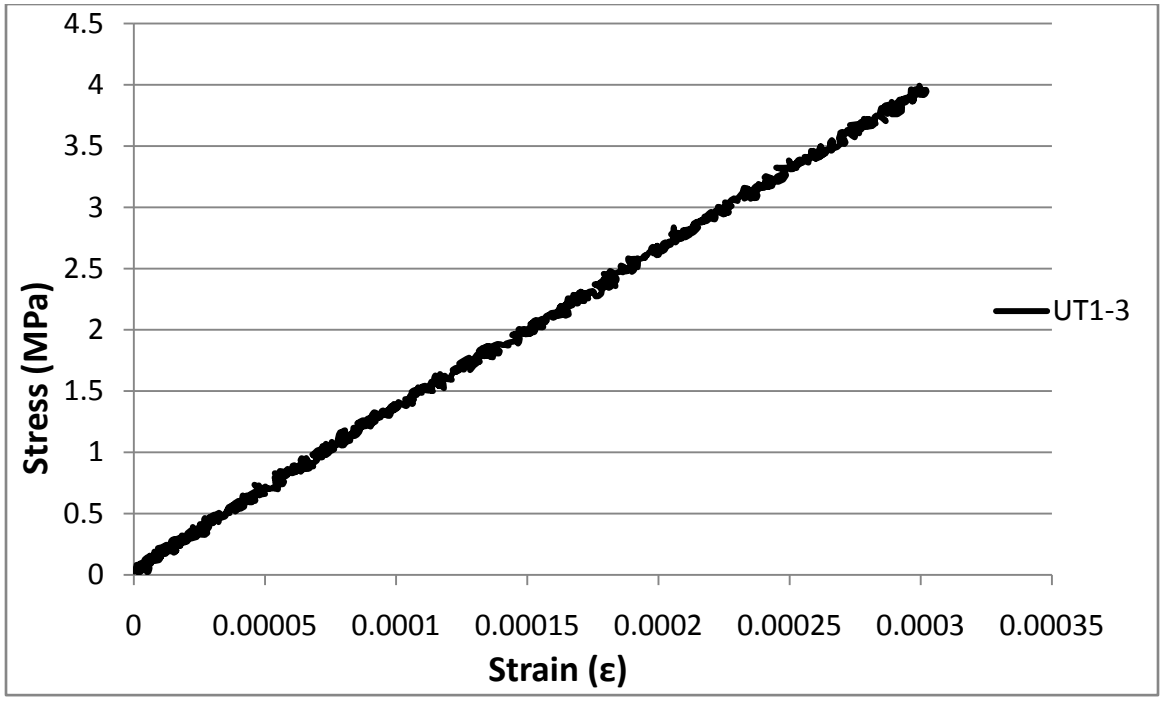
4.5
4
3.5
3
2.5
2
1.5
1
0.5
0
Stress (MPa)
0
0.00005
0.0001
0.00015
0.0002
0.00025
0.0003
0.00035
Strain (ε)
UT1-3

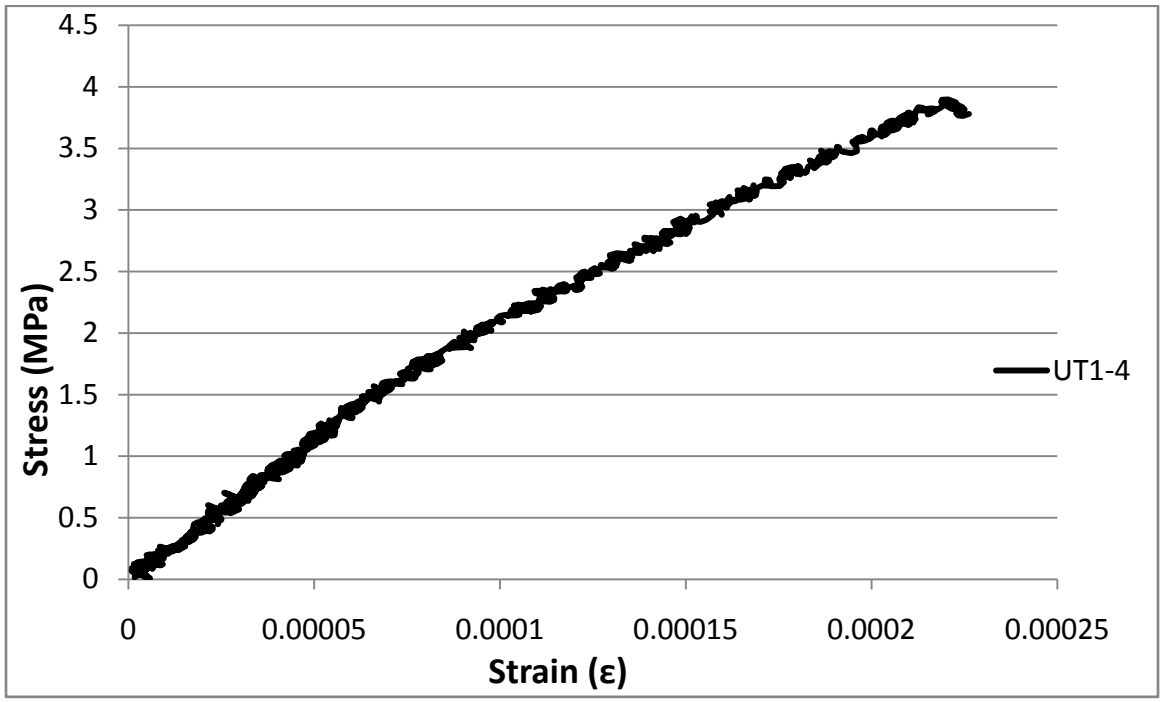
4.5
4
3.5
3
2.5
2
1.5
1
0.5
0
Stress (MPa)
0
0.00005
0.0001
0.00015
0.0002
0.00025
Strain (ε)
UT1-4

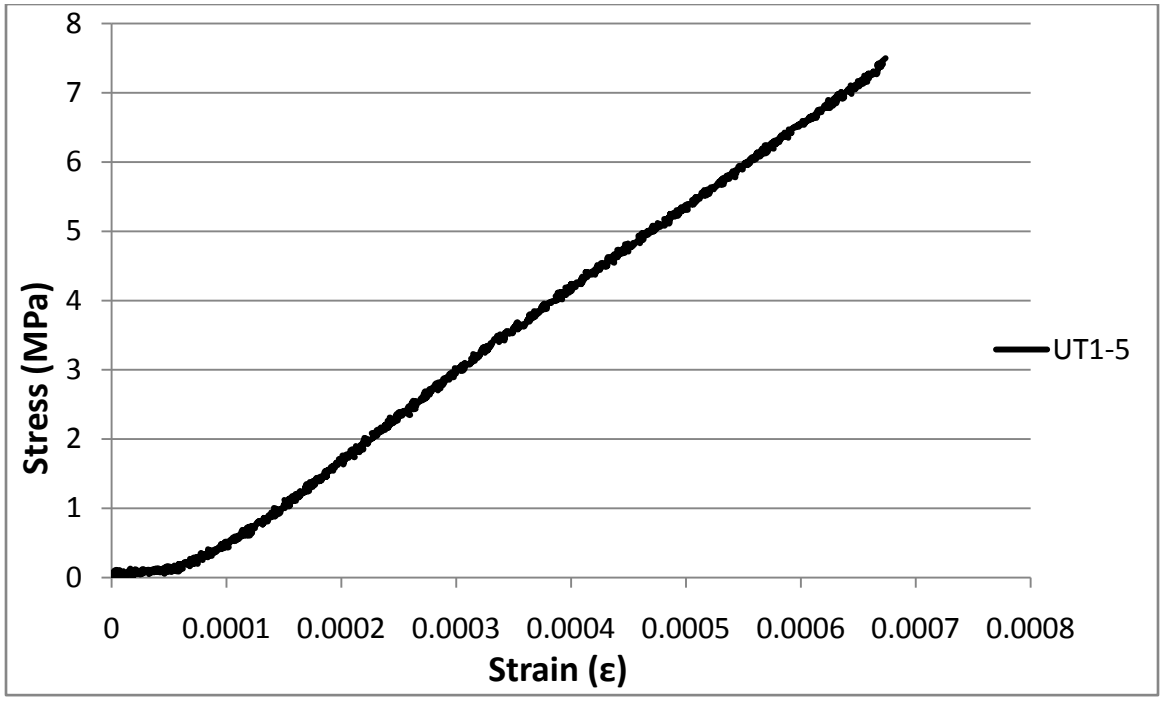
8
7
6
5
4
3
2
1
0
Stress (MPa)
0
0.0001
0.0002
0.0003
0.0004
0.0005
0.0006
0.0007
0.0008
Strain (ε)
UT1-5

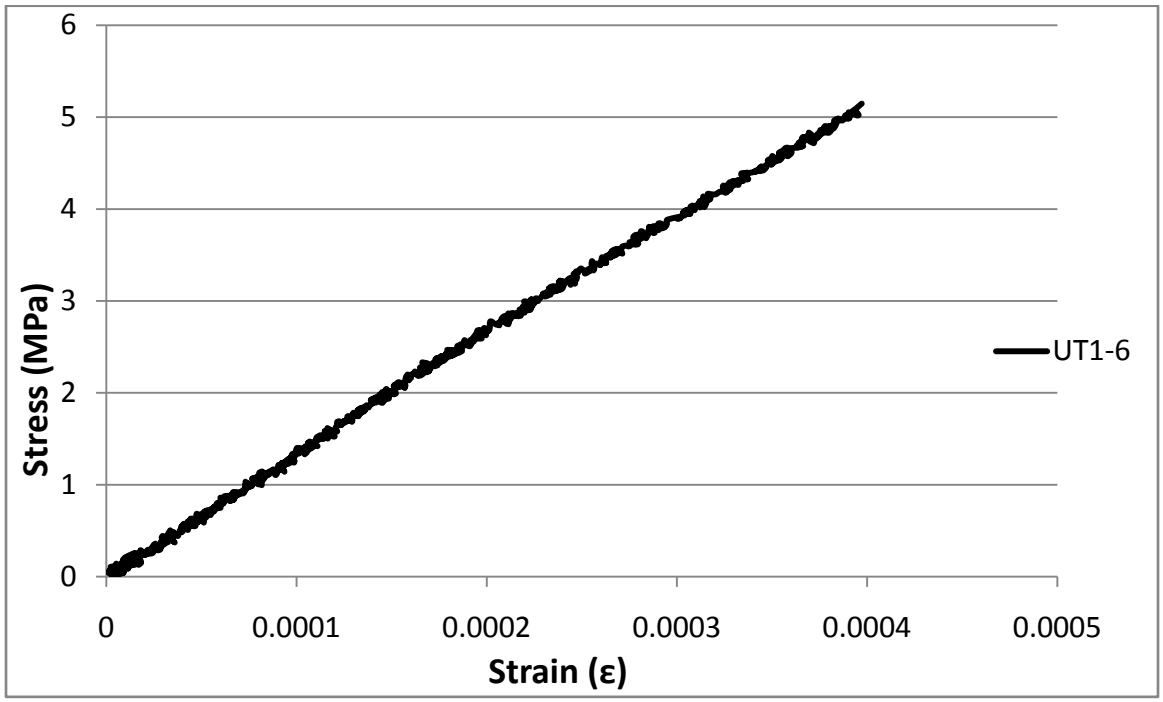
6
5
4
3
2
1
0
Stress (MPa)
0
0.0001
0.0002
0.0003
0.0004
0.0005
Strain (ε)
UT1-6

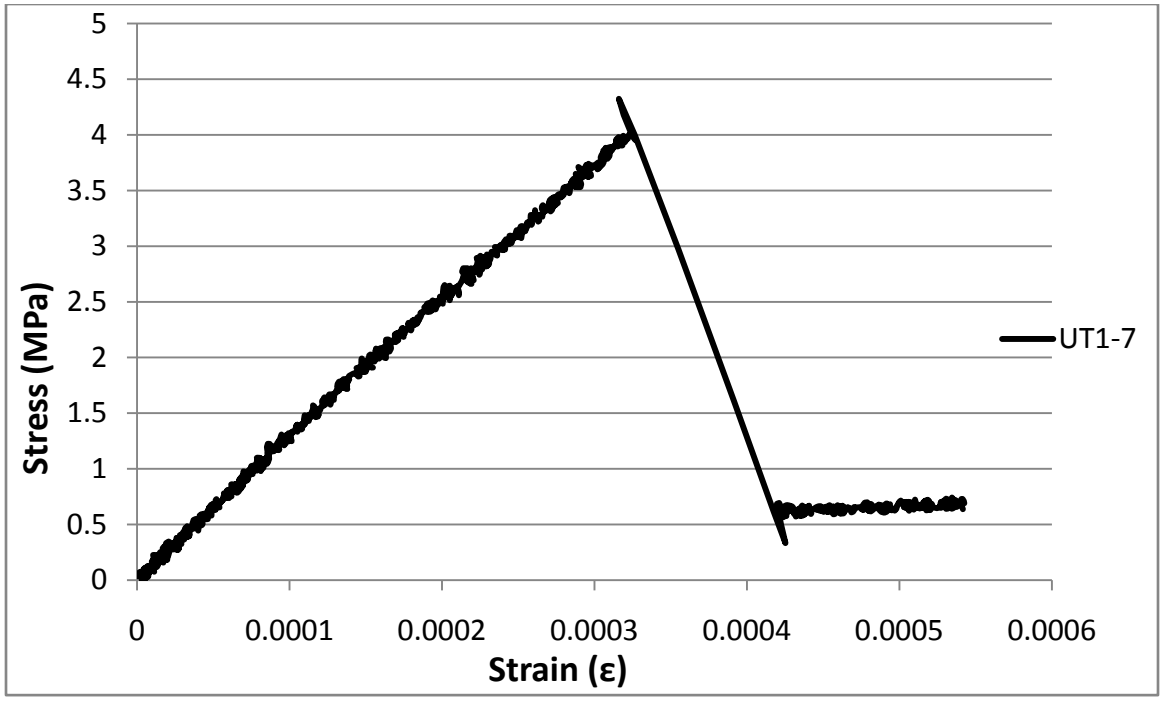
5
4.5
4
3.5
3
2.5
2
1.5
1
0.5
0
Stress (MPa)
0
0.0001
0.0002
0.0003
0.0004
0.0005
0.0006
Strain (ε)
UT1-7

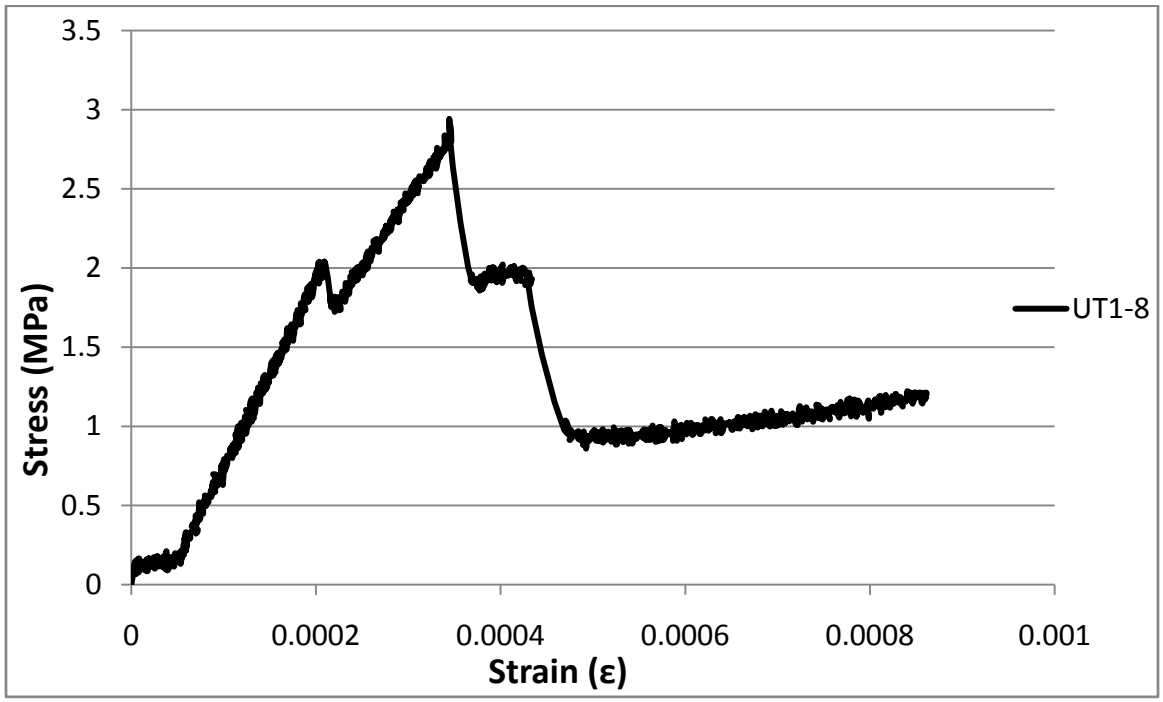
3.5
3
2.5
2
1.5
1
0.5
0
Stress (MPa)
0
0.0002
0.0004
0.0006
0.0008
0.001
Strain (ε)
UT1-8

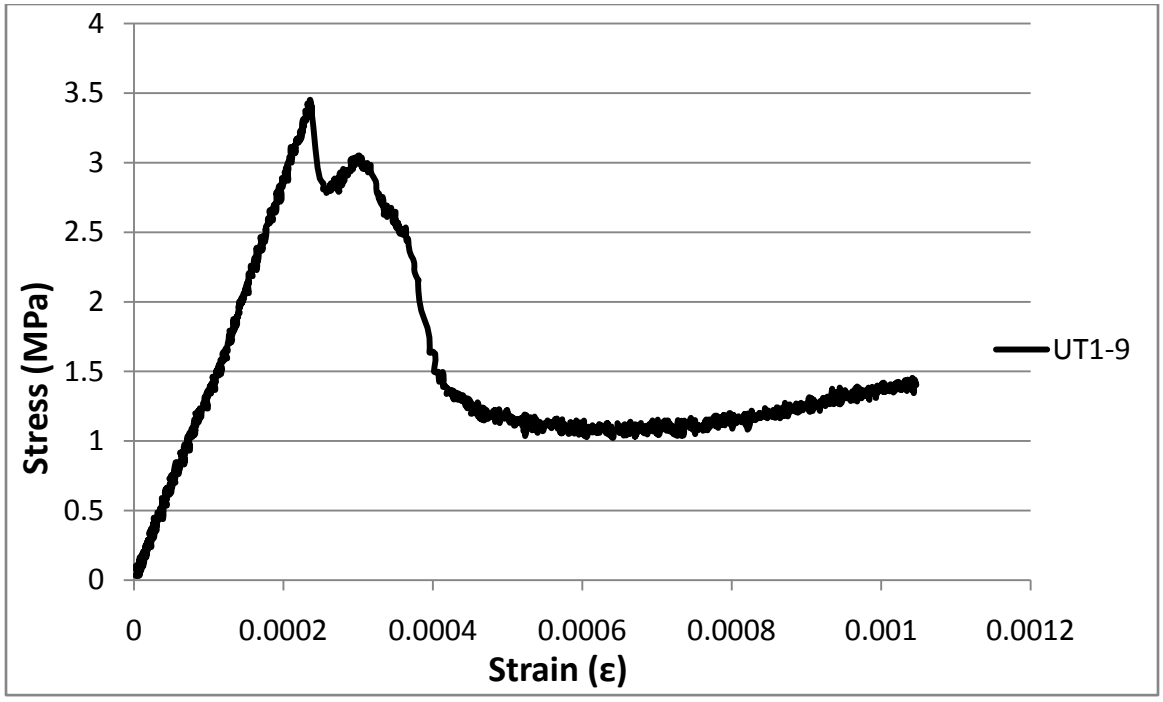
4
3.5
3
2.5
2
1.5
1
0.5
0
Stress (MPa)
0
0.0002
0.0004
0.0006
0.0008
0.001
0.0012
Strain (ε)
UT1-9

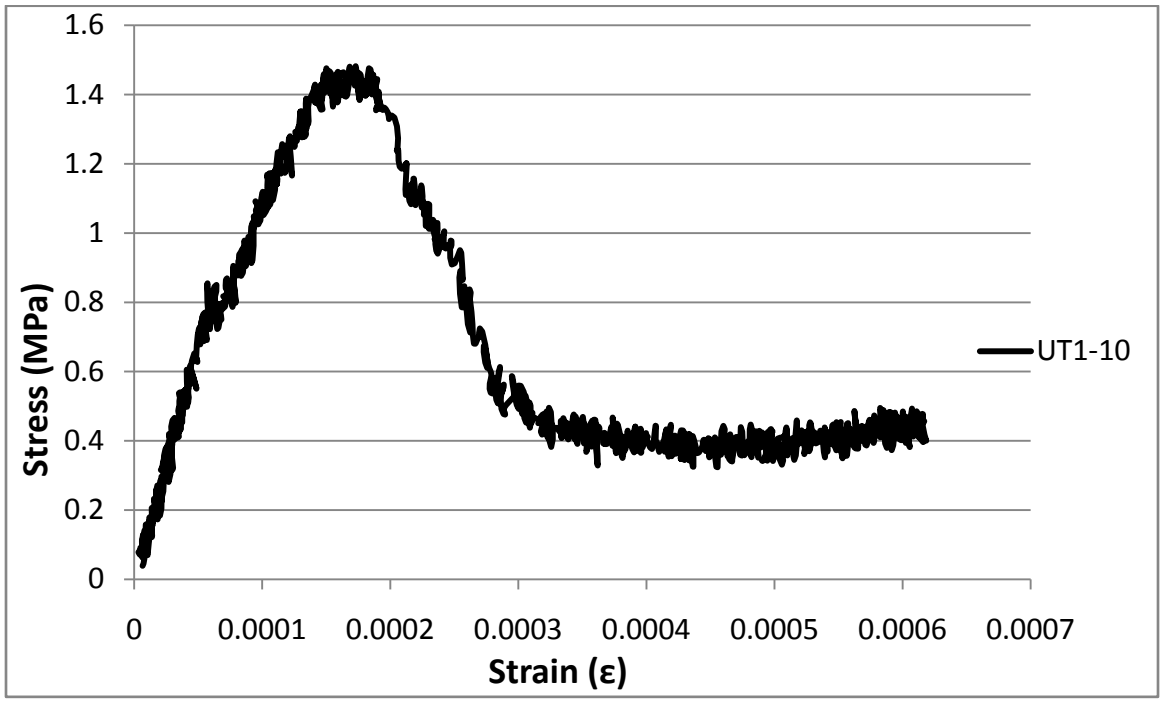
1.6
1.4
1.2
1
0.8
0.6
0.4
0.2
0
Stress (MPa)
0
0.0001
0.0002
0.0003
0.0004
0.0005
0.0006
0.0007
Strain (ε)
UT1-10

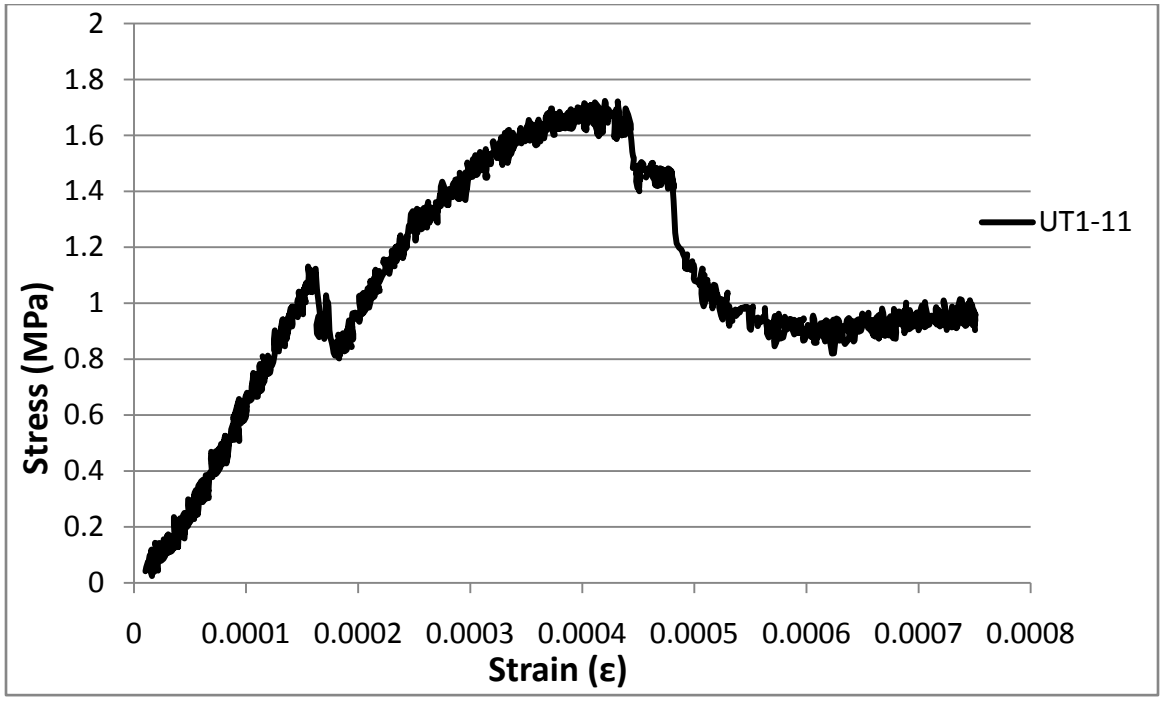
2
1.8
1.6
1.4
1.2
1
0.8
0.6
0.4
0.2
0
Stress (MPa)
0
0.0001
0.0002
0.0003
0.0004
0.0005
0.0006
0.0007
0.0008
Strain (ε)
UT1-11

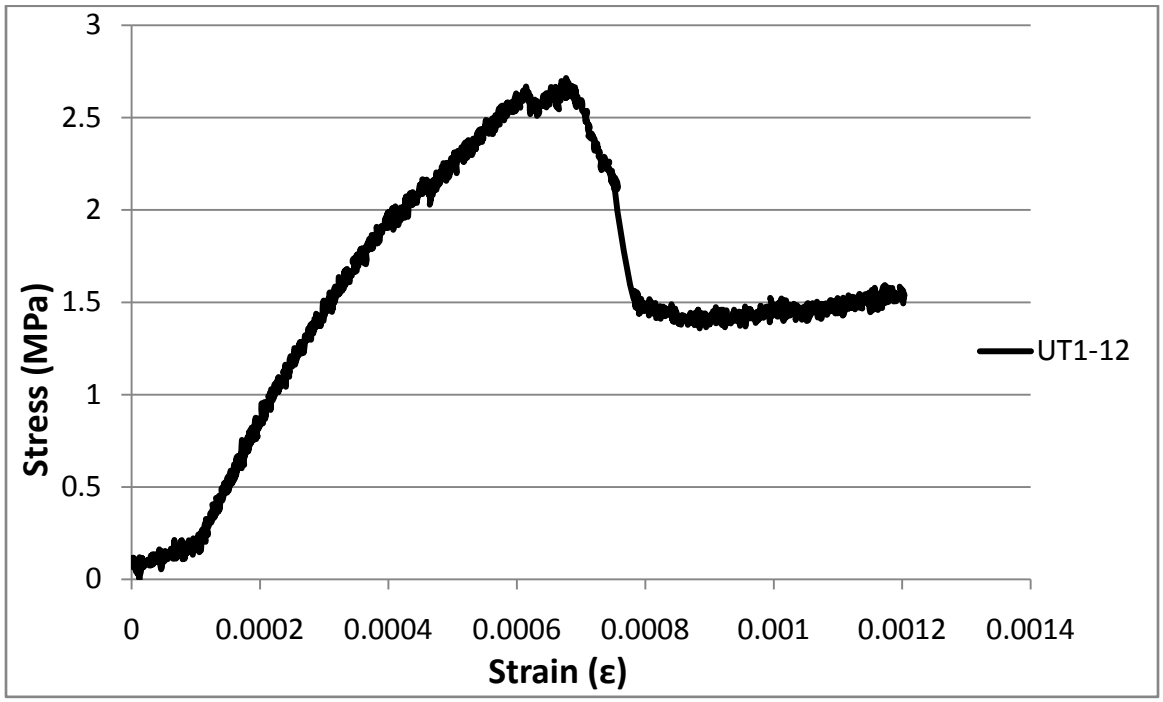
3
2.5
2
1.5
1
0.5
0
Stress (MPa)
0
0.0002
0.0004
0.0006
0.0008
0.001
0.0012
0.0014
Strain (ε)
UT1-12

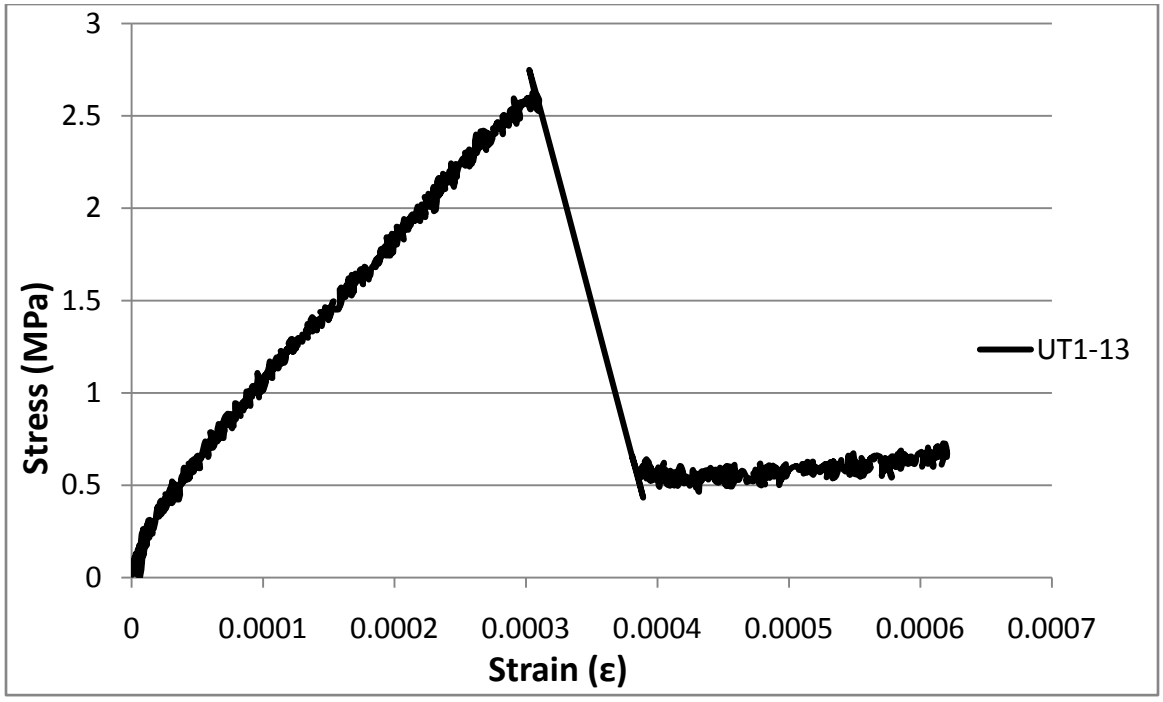
3
2.5
2
1.5
1
0.5
0
Stress (MPa)
0
0.0001
0.0002
0.0003
0.0004
0.0005
0.0006
0.0007
Strain (ε)
UT1-13

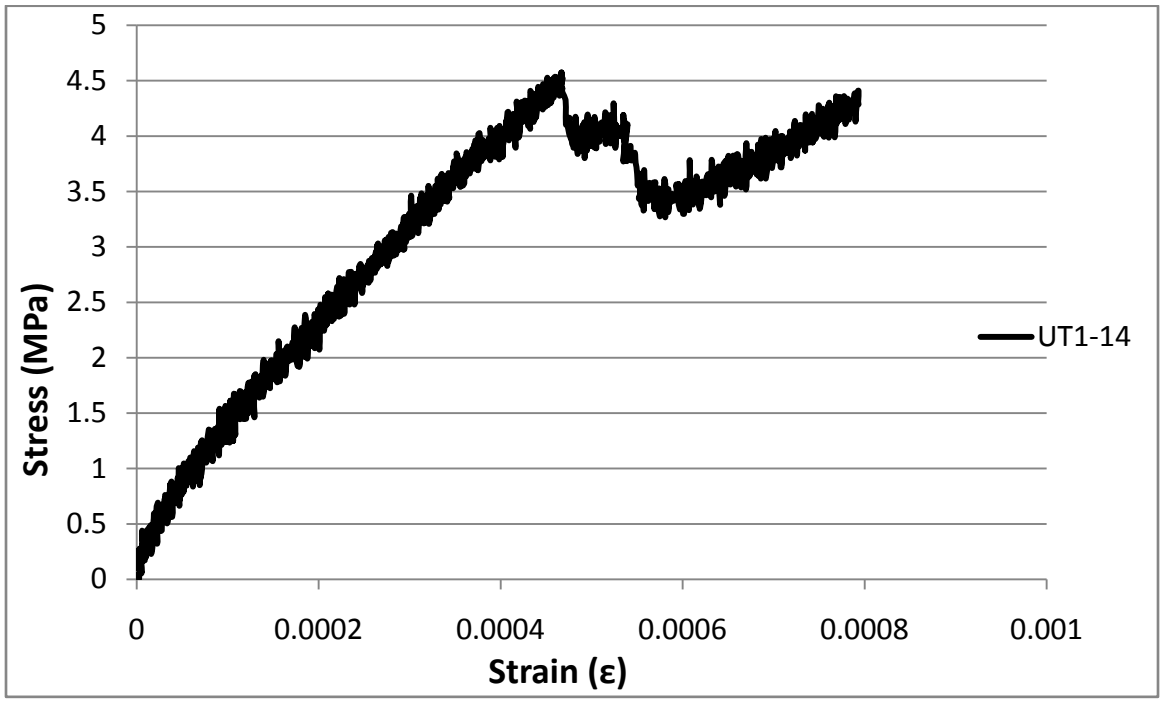
5
4.5
4
3.5
3
2.5
2
1.5
1
0.5
0
Stress (MPa)
0
0.0002
0.0004
0.0006
0.0008
0.001
Strain (ε)
UT1-14

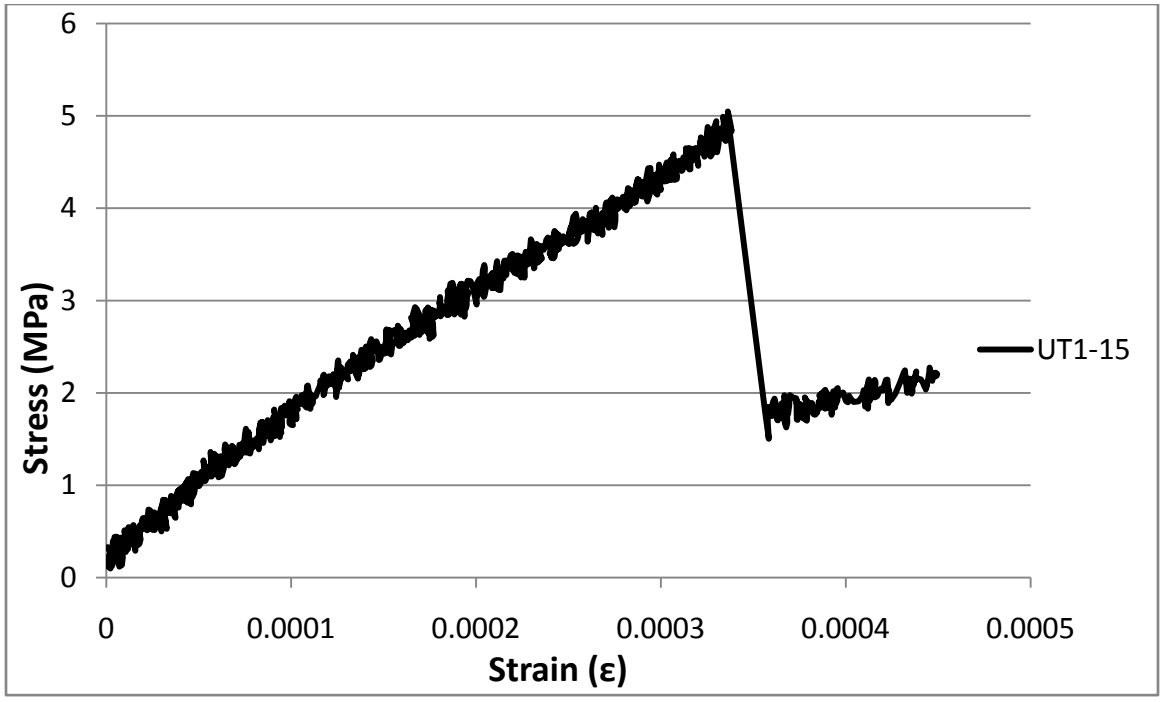
6
5
4
3
2
1
0
Stress (MPa)
0
0.0001
0.0002
0.0003
0.0004
0.0005
Strain (ε)
UT1-15

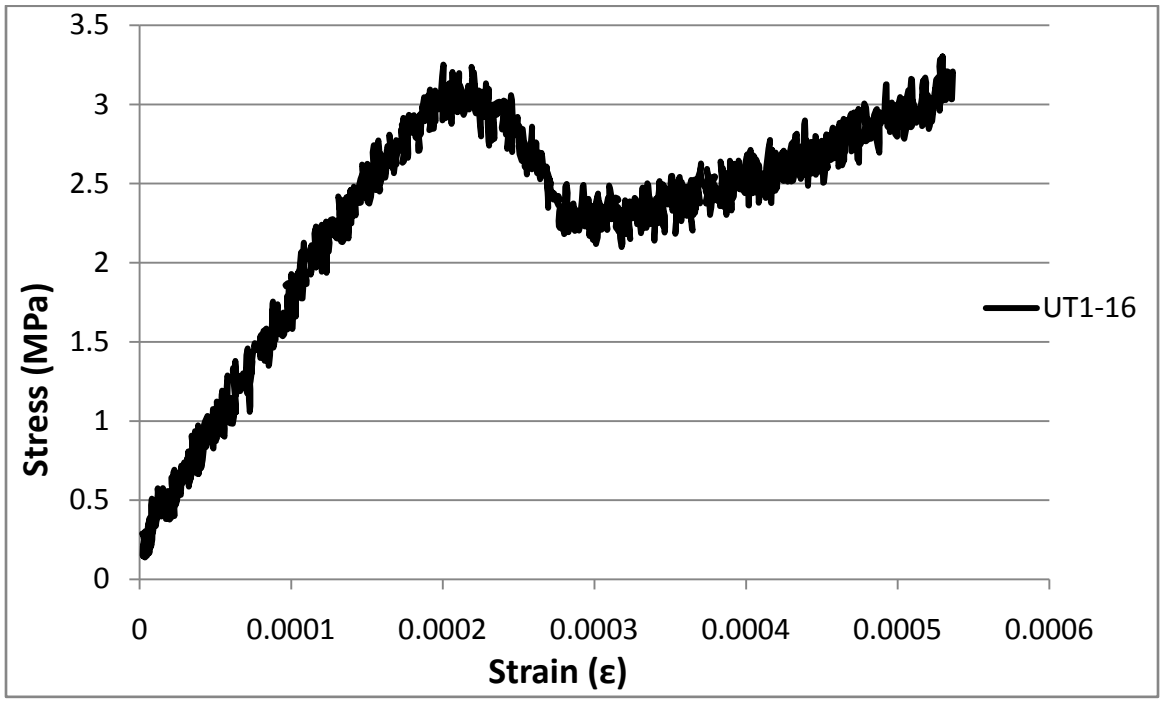
3.5
3
2.5
2
1.5
1
0.5
0
Stress (MPa)
0
0.0001
0.0002
0.0003
0.0004
0.0005
0.0006
Strain (ε)
UT1-16

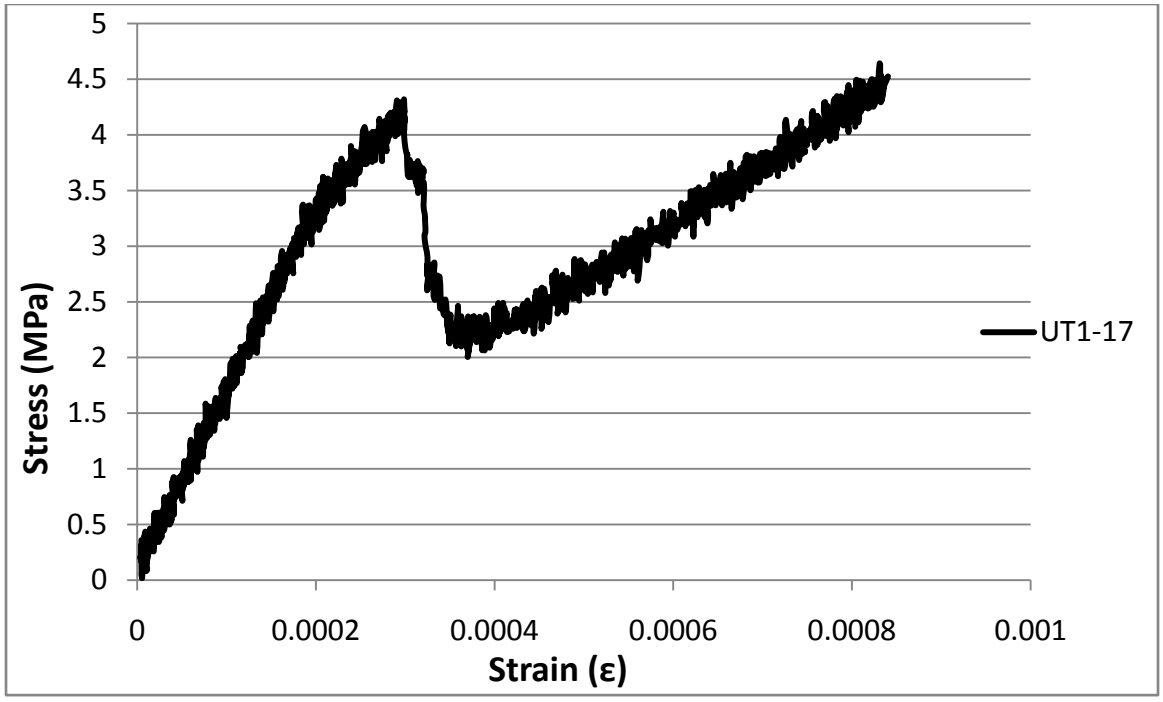
5
4.5
4
3.5
3
2.5
2
1.5
1
0.5
0
Stress (MPa)
0
0.0002
0.0004
0.0006
0.0008
0.001
Strain (ε)
UT1-17

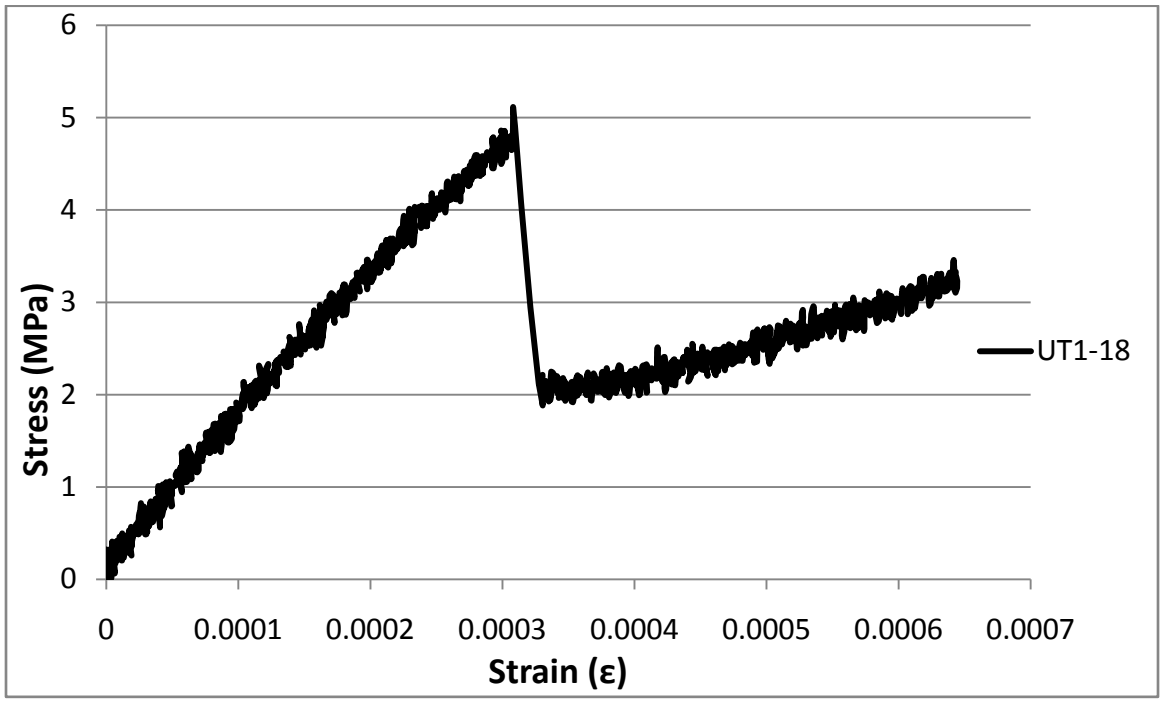
6
5
4
3
2
1
0
Stress (MPa)
0
0.0001
0.0002
0.0003
0.0004
0.0005
0.0006
0.0007
Strain (ε)
UT1-18

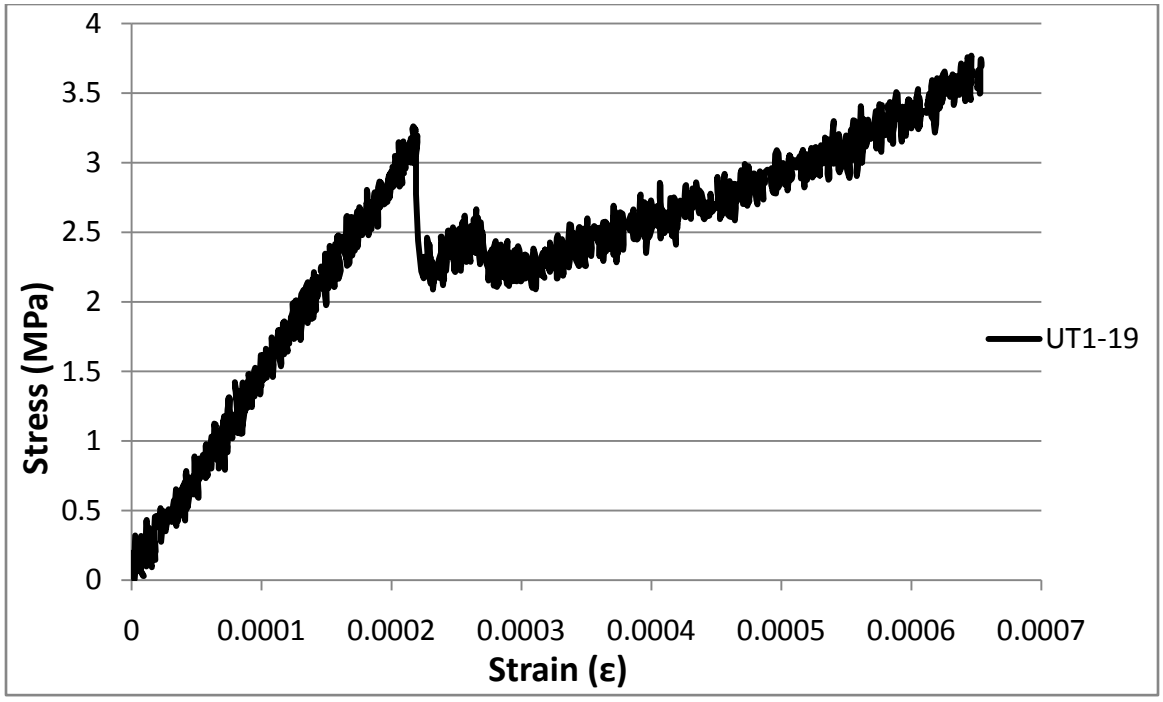
4
3.5
3
2.5
2
1.5
1
0.5
0
Stress (MPa)
0
0.0001
0.0002
0.0003
0.0004
0.0005
0.0006
0.0007
Strain (ε)
UT1-19

Untreated Tubes at 0.2%

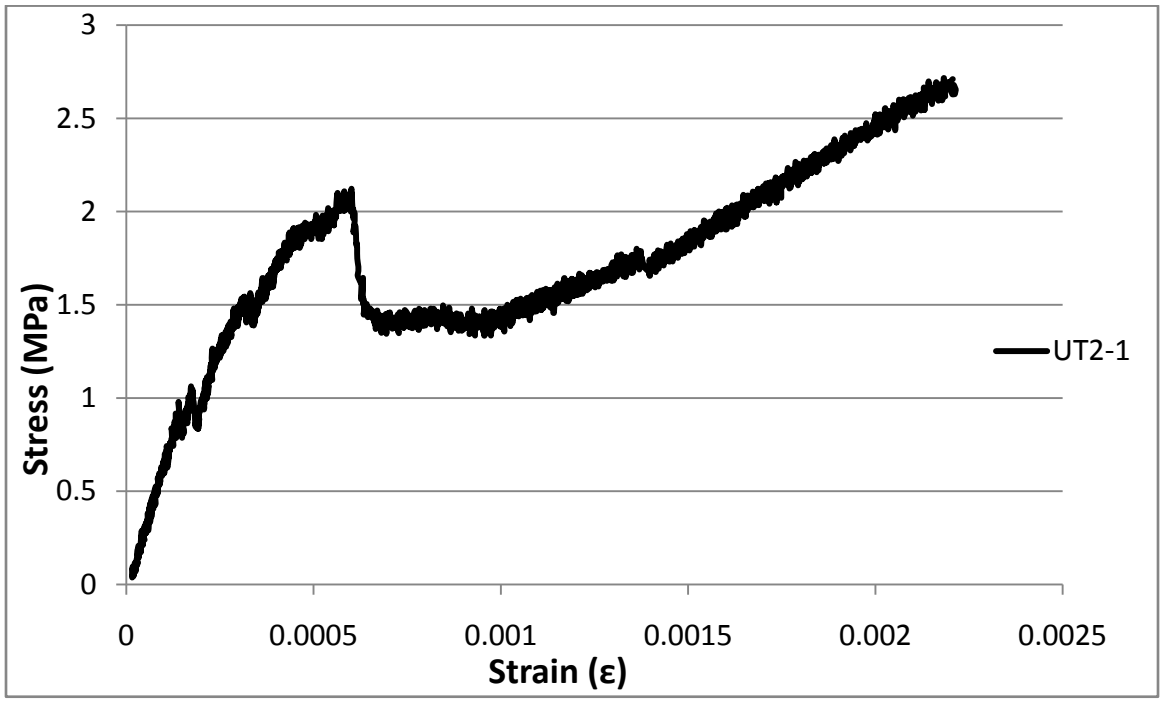

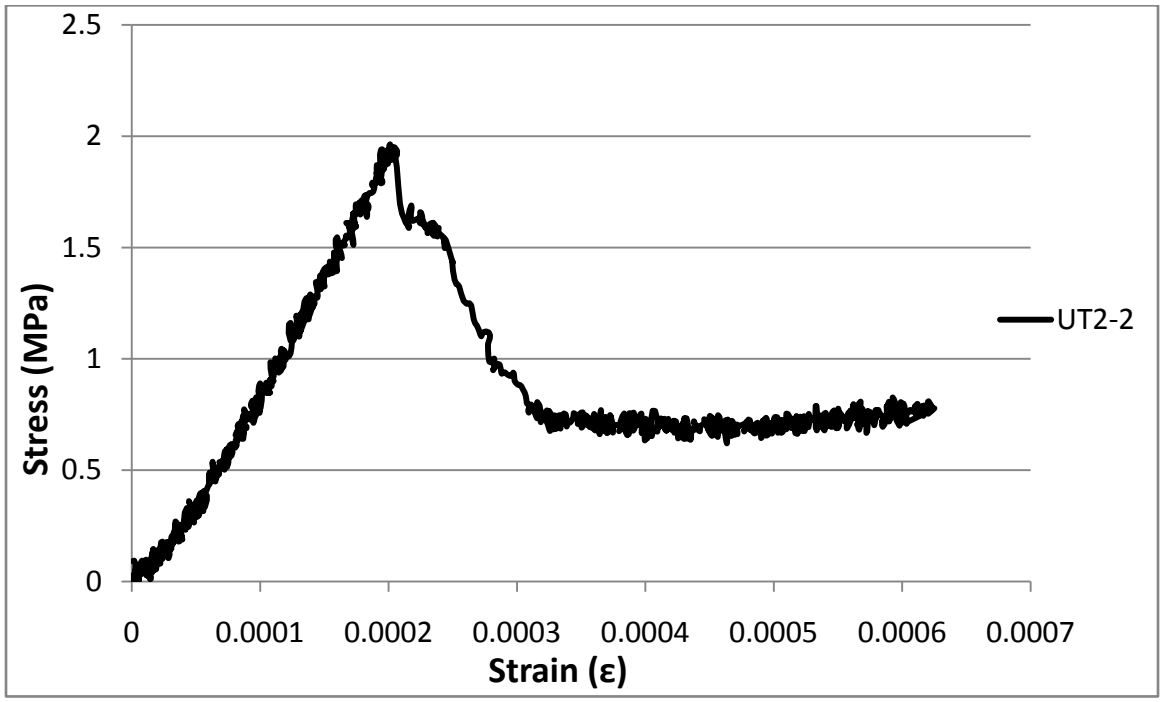

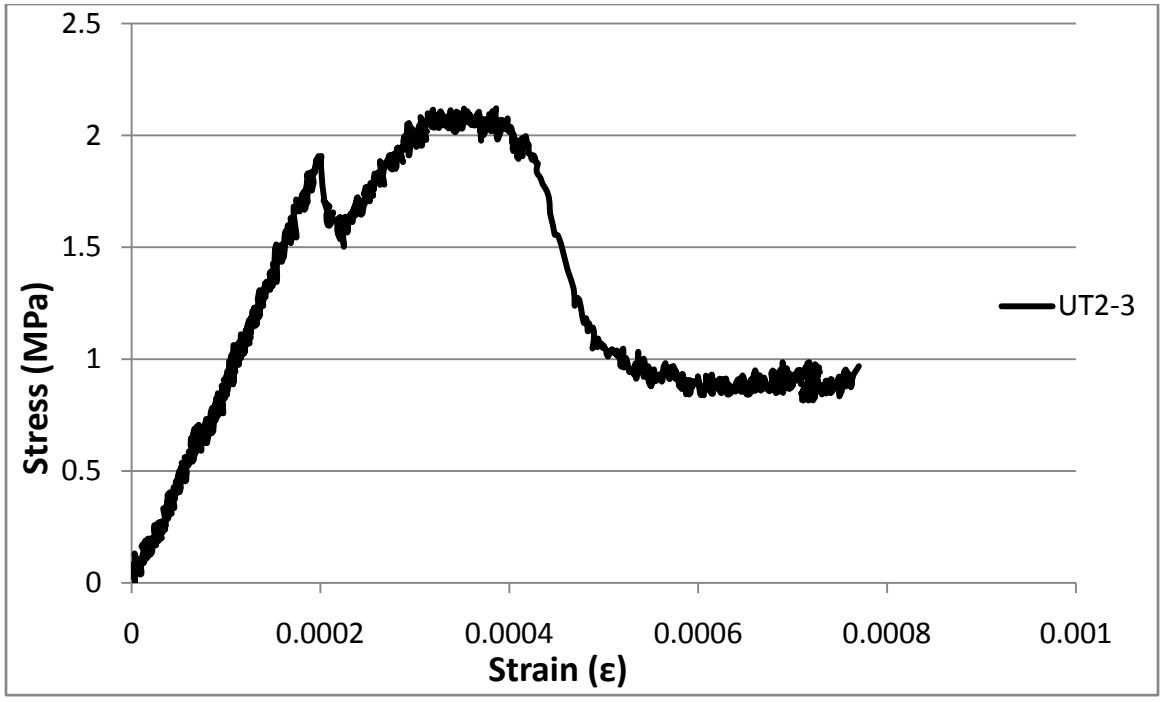
2.5
2
1.5
1
0.5
0
Stress (MPa)
0
0.0002
0.0004
0.0006
0.0008
0.001
Strain (ε)
UT2-3

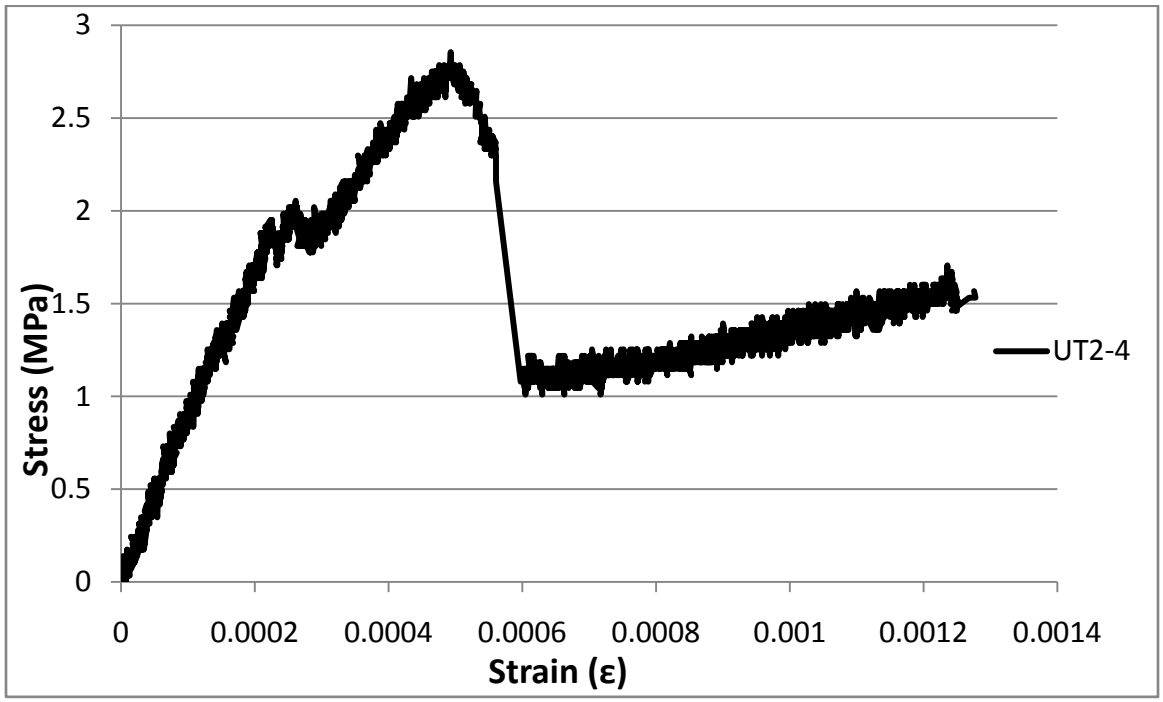
3
2.5
2
1.5
1
0.5
0
Stress (MPa)
0
0.0002
0.0004
0.0006
0.0008
0.001
0.0012
0.0014
Strain (ε)
UT2-4

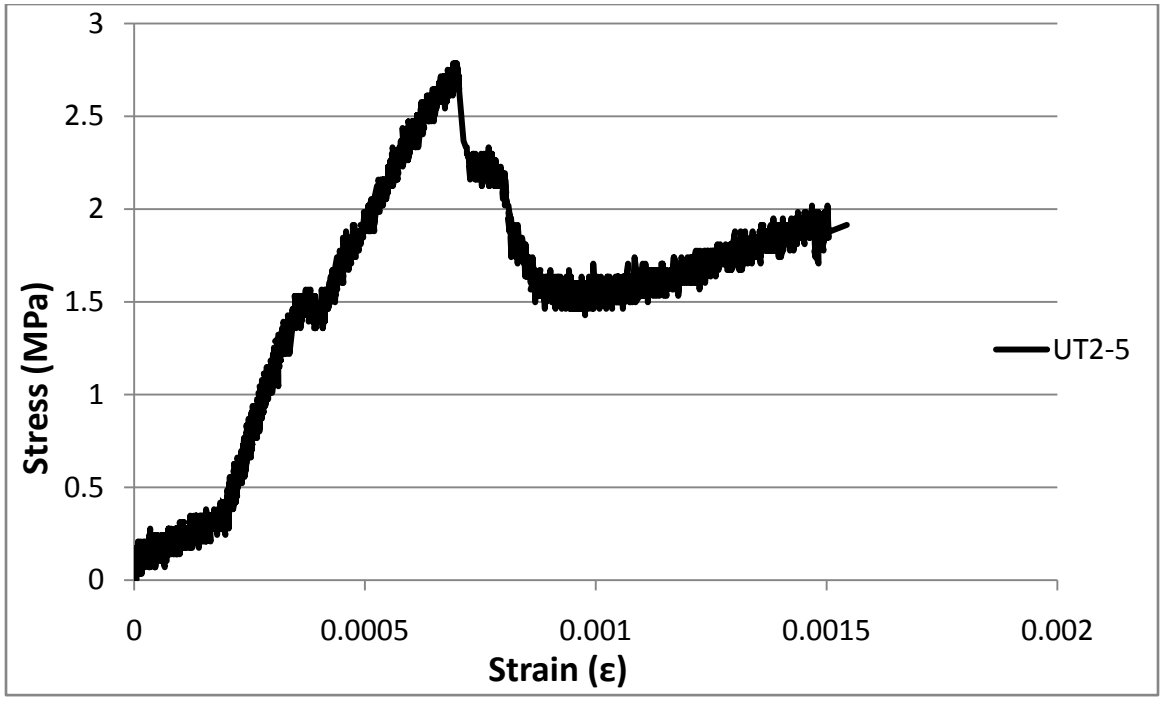
3
2.5
2
1.5
1
0.5
0
Stress (MPa)
0
0.0005
0.001
0.0015
0.002
Strain (ε)
UT2-5

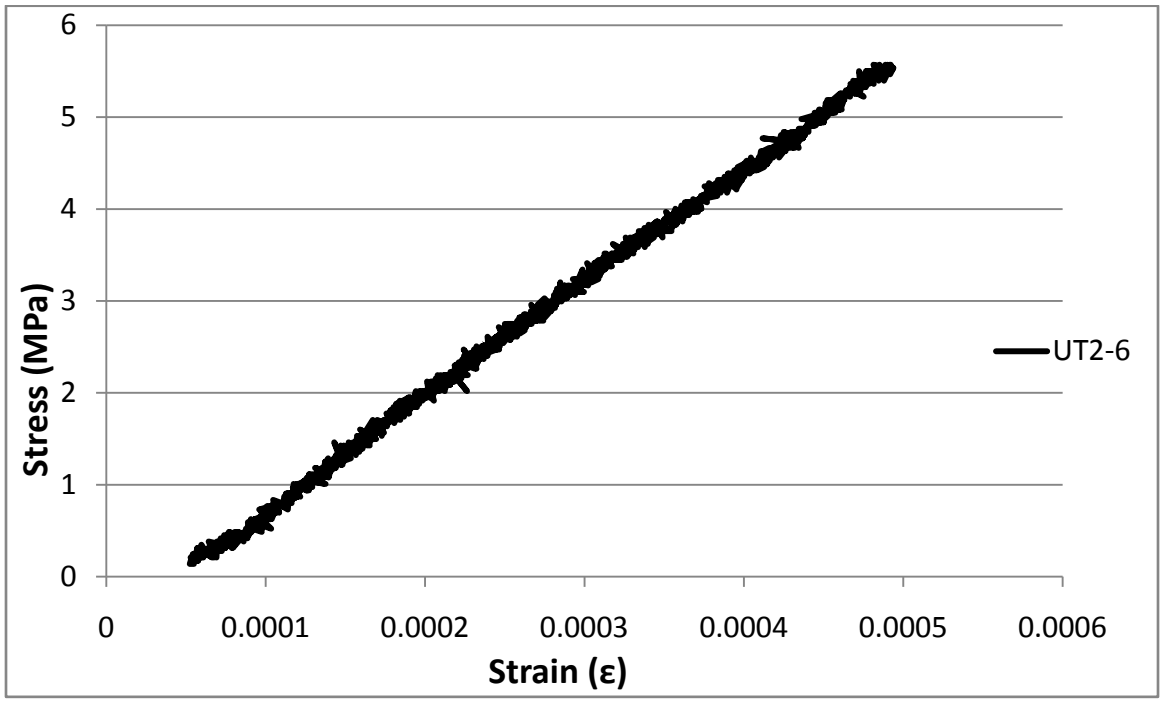
6
5
4
3
2
1
0
Stress (MPa)
0
0.0001
0.0002
0.0003
0.0004
0.0005
0.0006
Strain (ε)
UT2-6

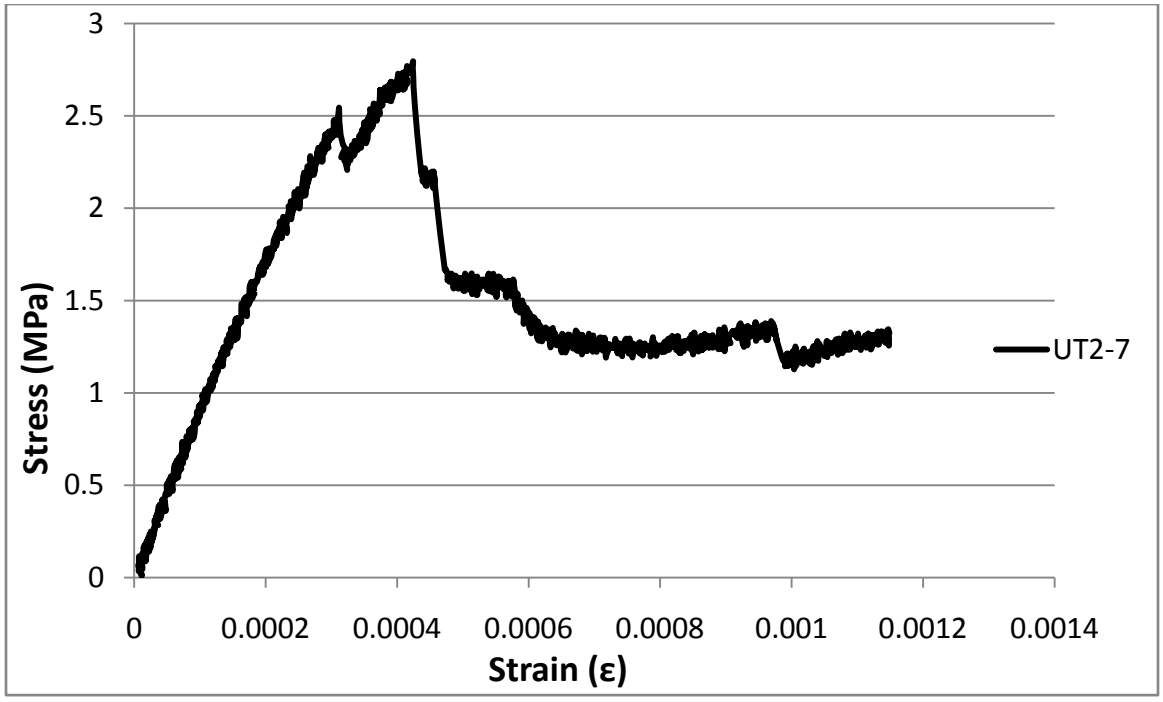
3
2.5
2
1.5
1
0.5
0
Stress (MPa)
0
0.0002
0.0004
0.0006
0.0008
0.001
0.0012
0.0014
Strain (ε)
UT2-7

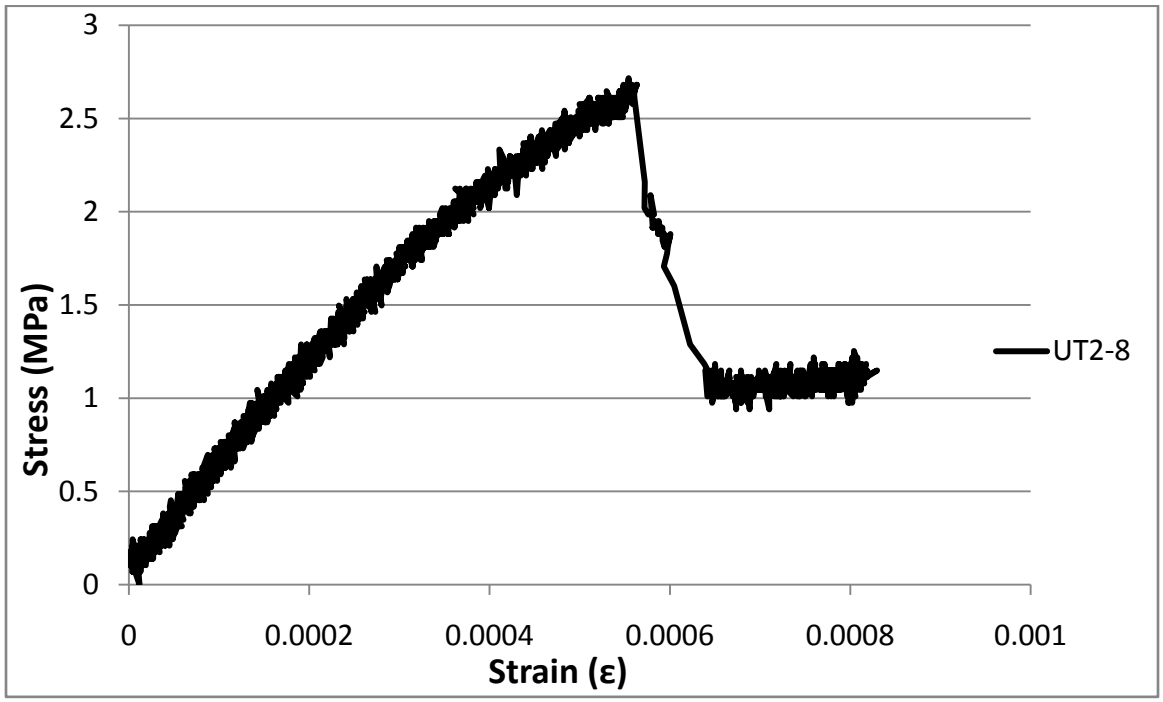
3
2.5
2
1.5
1
0.5
0
Stress (MPa)
0
0.0002
0.0004
0.0006
0.0008
0.001
Strain (ε)
UT2-8

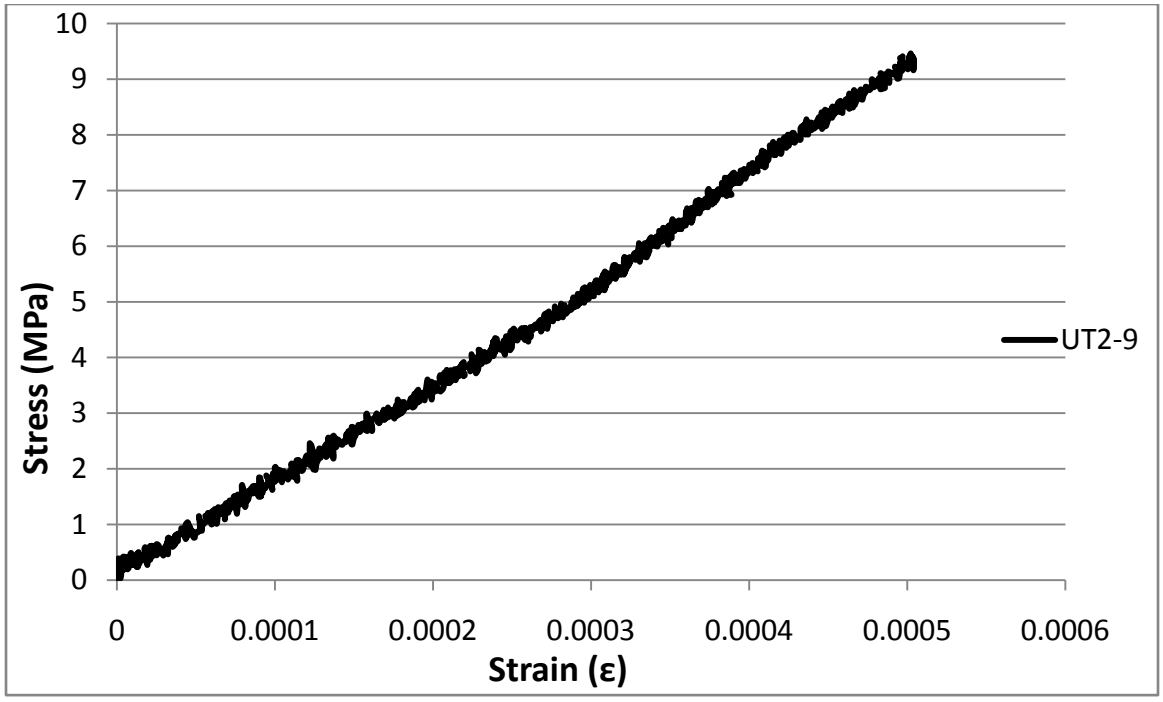
10
9
8
7
6
5
4
3
2
1
0
Stress (MPa)
0
0.0001
0.0002
0.0003
0.0004
0.0005
0.0006
Strain (ε)
UT2-9

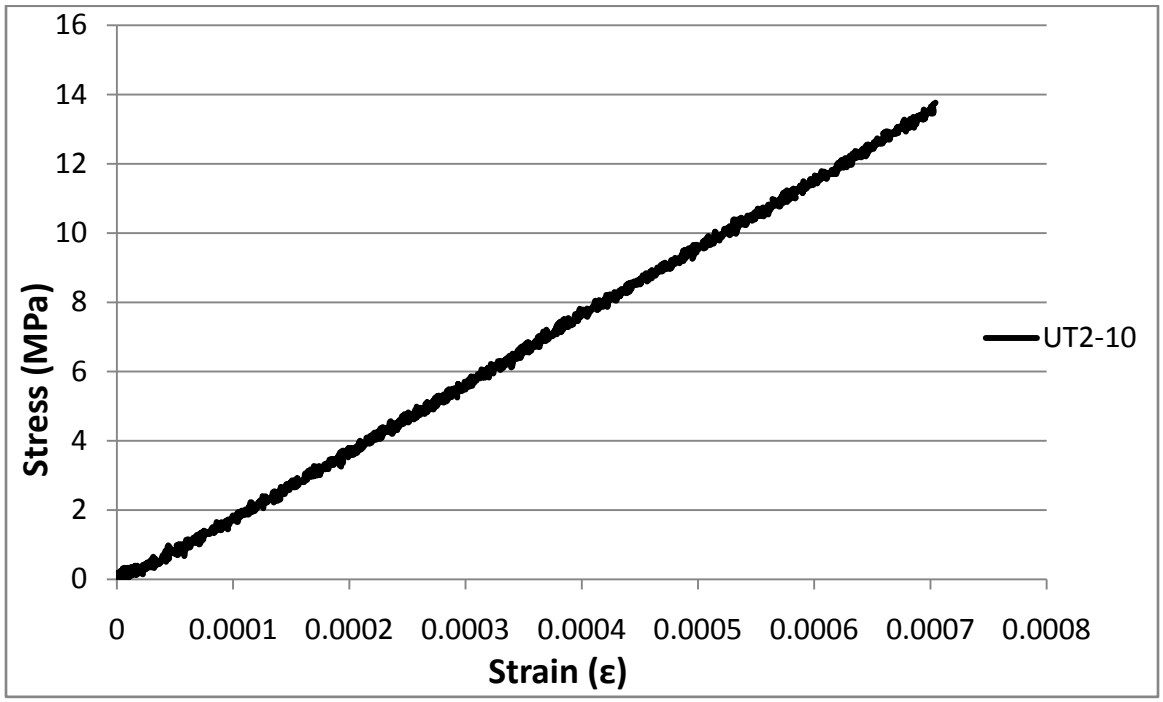
16
14
12
10
8
6
4
2
0
Stress (MPa)
0
0.0001
0.0002
0.0003
0.0004
0.0005
0.0006
0.0007
0.0008
Strain (ε)
UT2-10

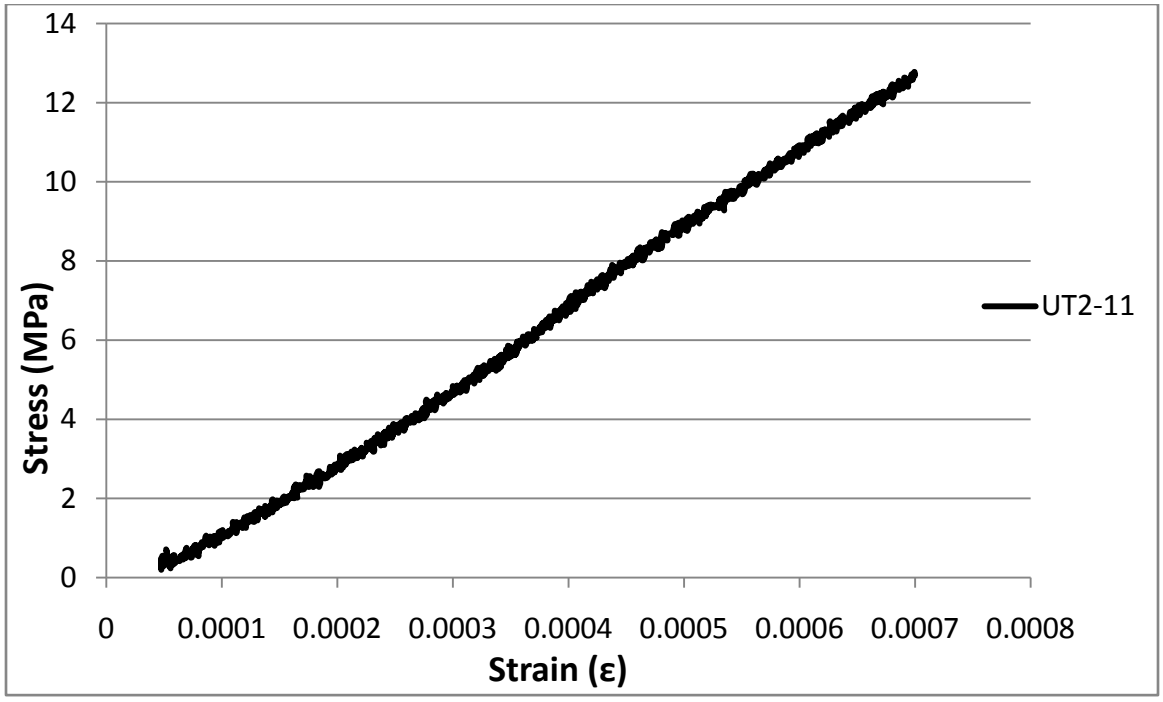
14
12
10
8
6
4
2
0
Stress (MPa)
0
0.0001
0.0002
0.0003
0.0004
0.0005
0.0006
0.0007
0.0008
Strain (ε)
UT2-11

Treated Fibers at 0.1%

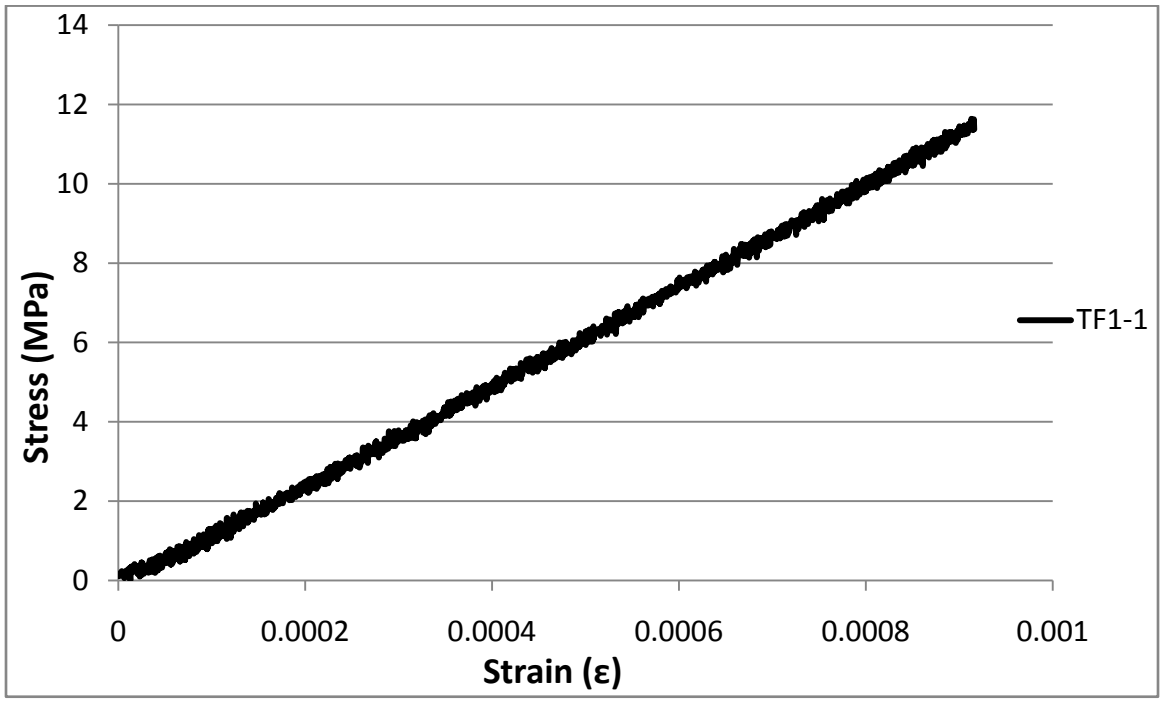

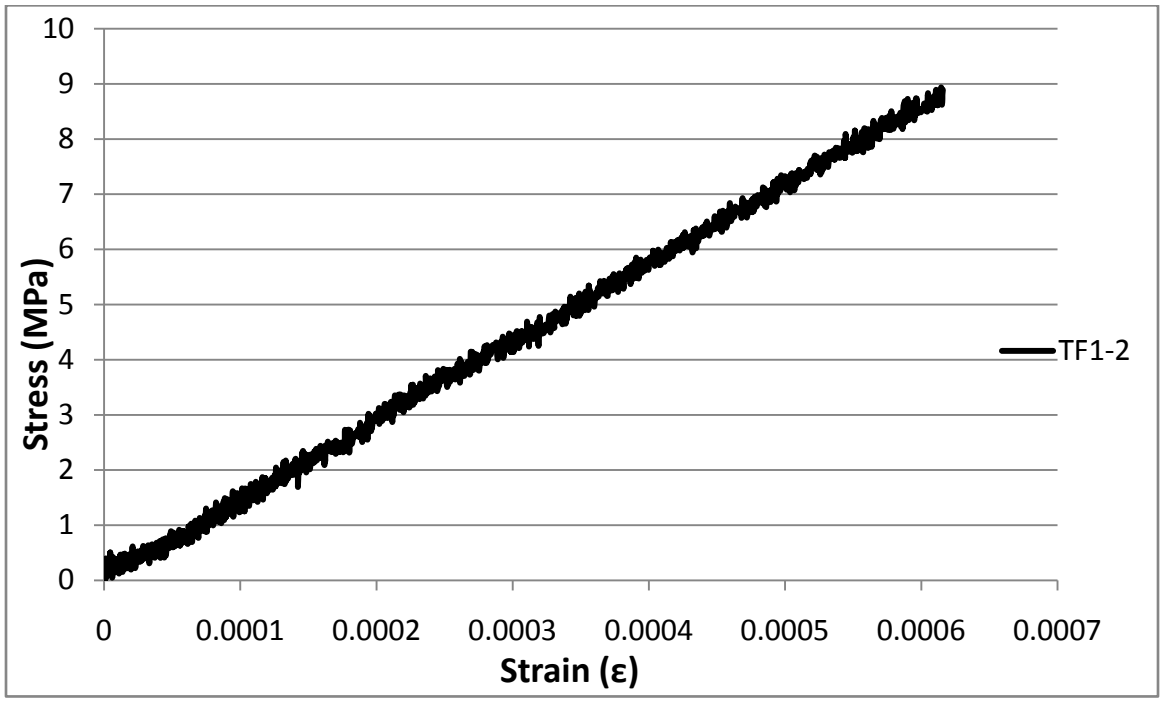

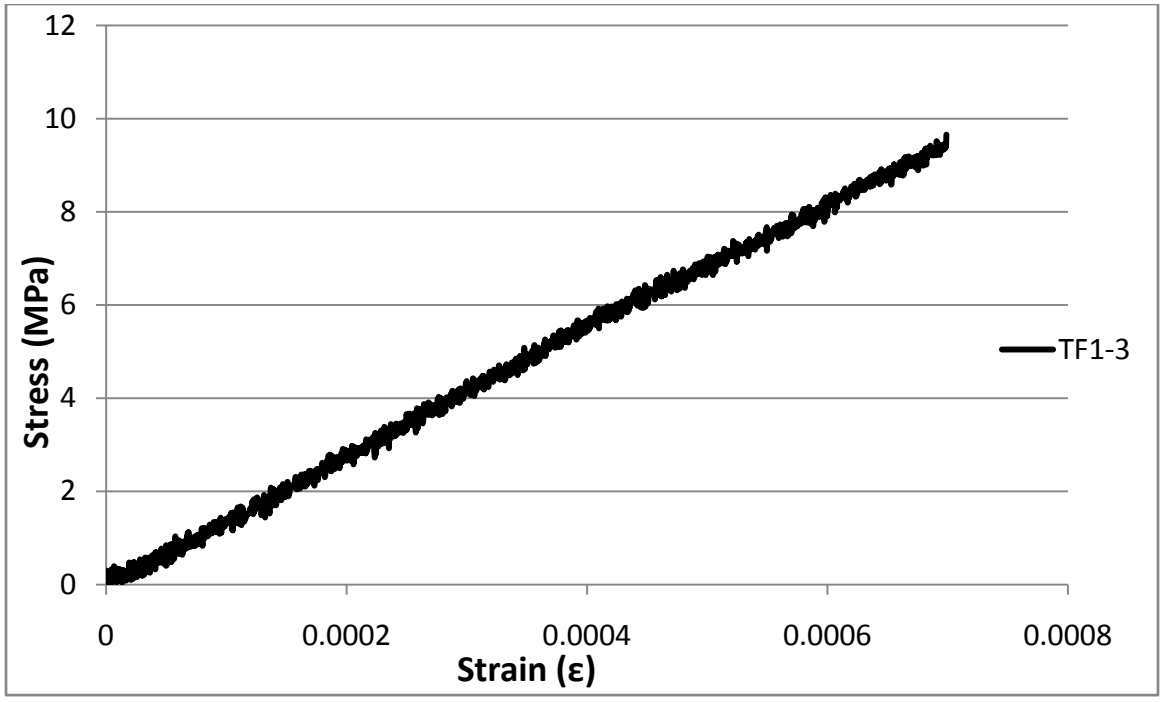
12
10
8
6
4
2
0
Stress (MPa)
0
0.0002
0.0004
0.0006
0.0008
Strain (ε)
TF1-3

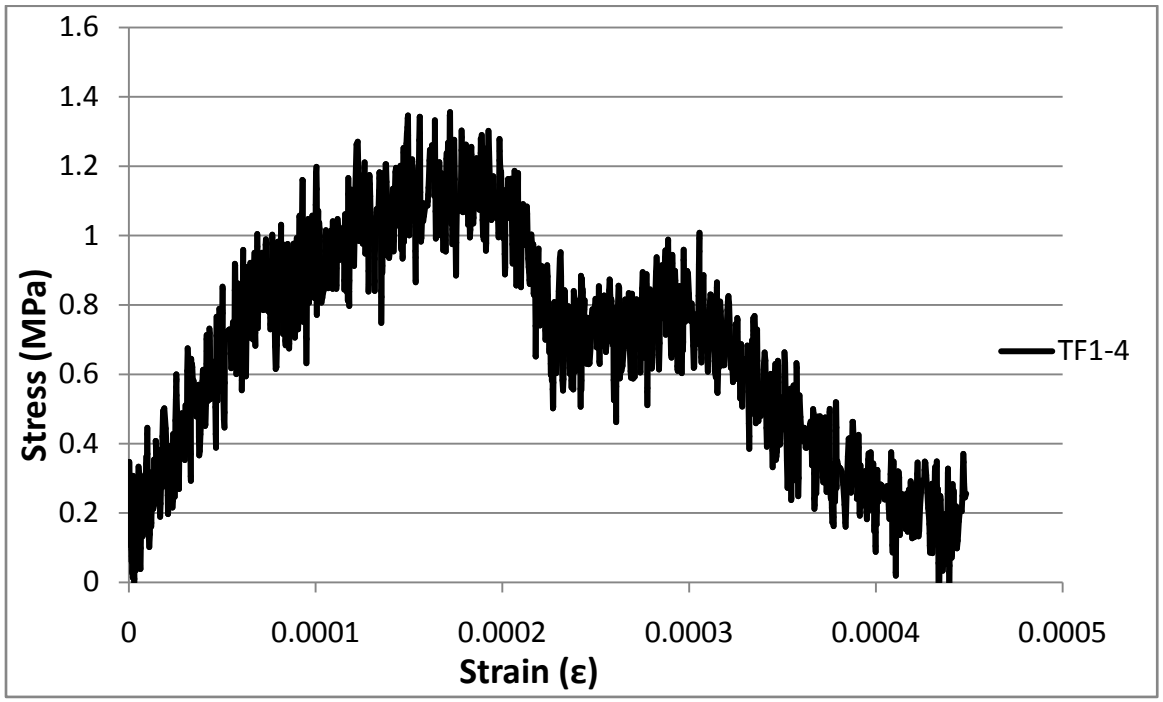
1.6
1.4
1.2
1
0.8
0.6
0.4
0.2
0
Stress (MPa)
0
0.0001
0.0002
0.0003
0.0004
0.0005
Strain (ε)
TF1-4

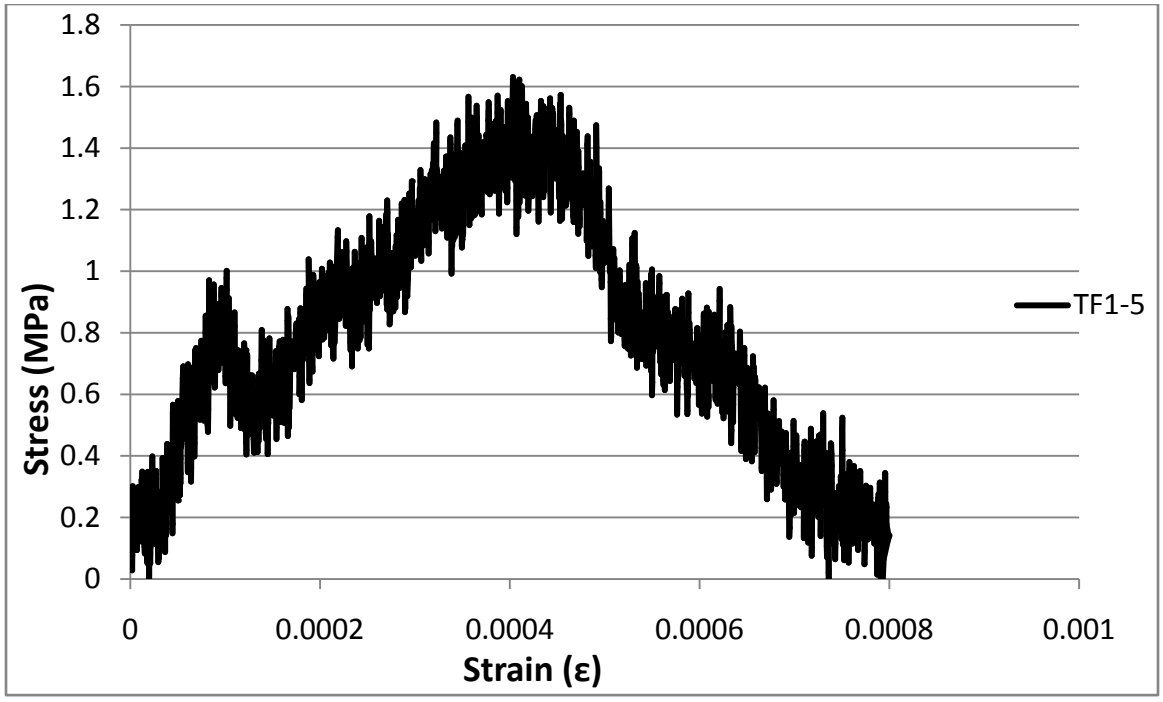
1.8
1.6
1.4
1.2
1
0.8
0.6
0.4
0.2
0
Stress (MPa)
0
0.0002
0.0004
0.0006
0.0008
0.001
Strain (ε)
TF1-5

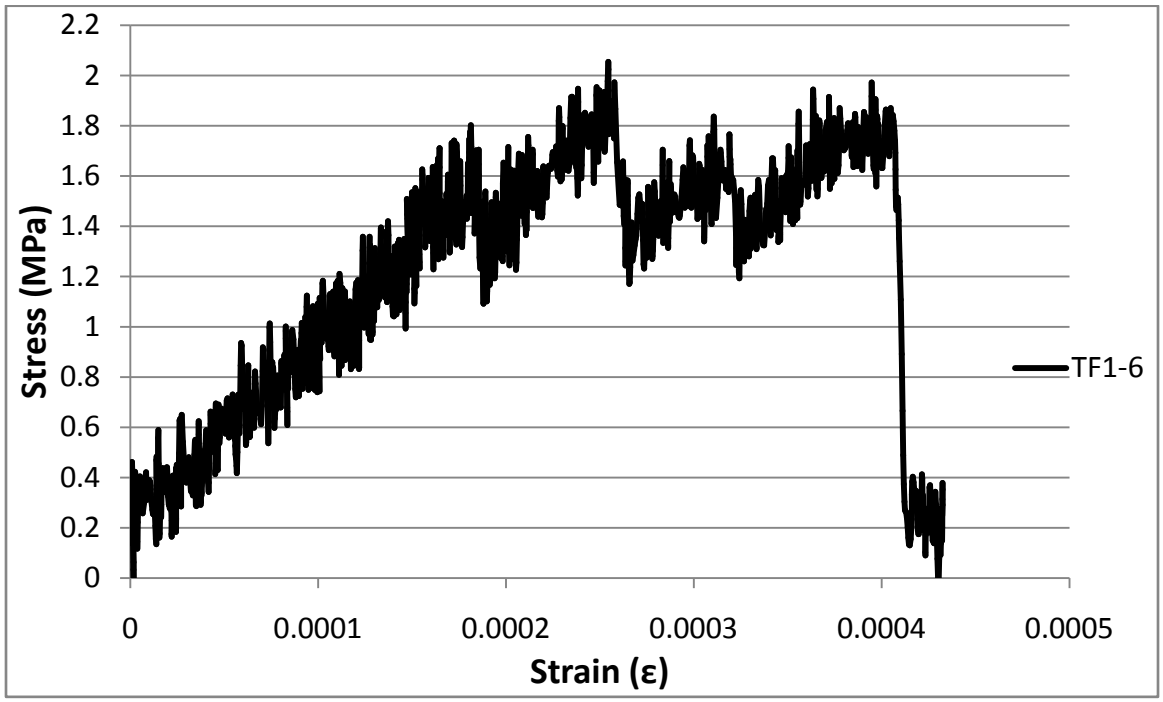
2.2
2
1.8
1.6
1.4
1.2
1
0.8
0.6
0.4
0.2
0
Stress (MPa)
0
0.0001
0.0002
0.0003
0.0004
0.0005
Strain (ε)
TF1-6

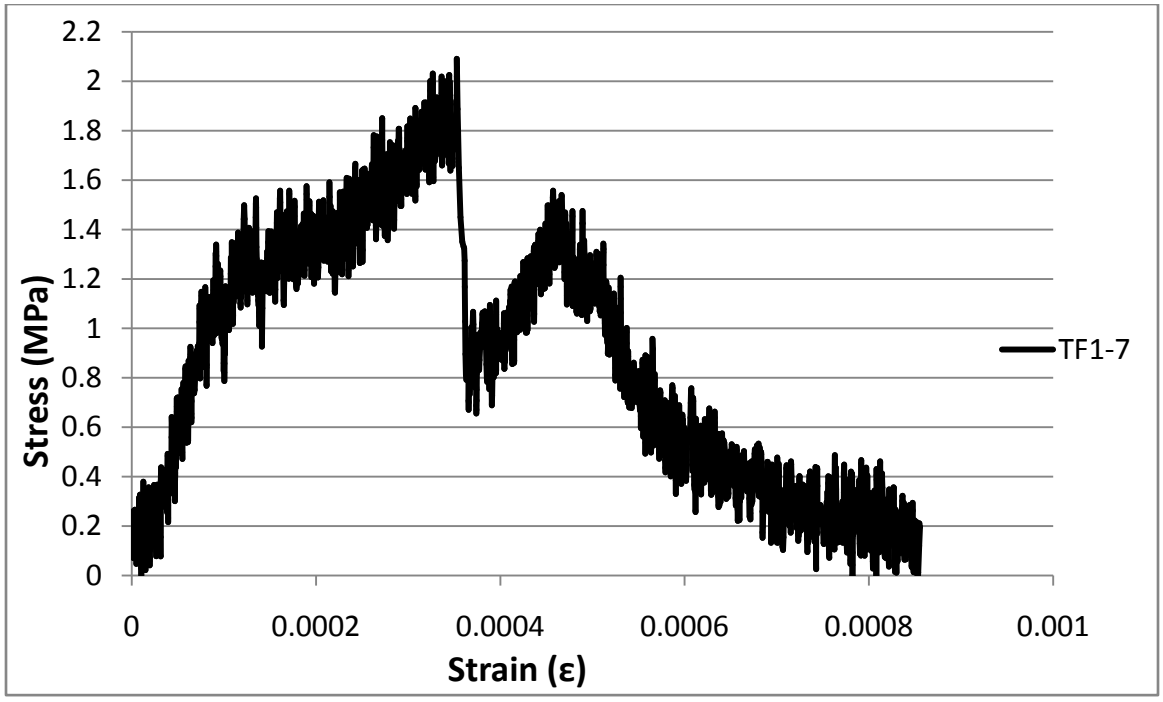
2.2
2
1.8
1.6
1.4
1.2
1
0.8
0.6
0.4
0.2
0
Stress (MPa)
0
0.0002
0.0004
0.0006
0.0008
0.001
Strain (ε)
TF1-7

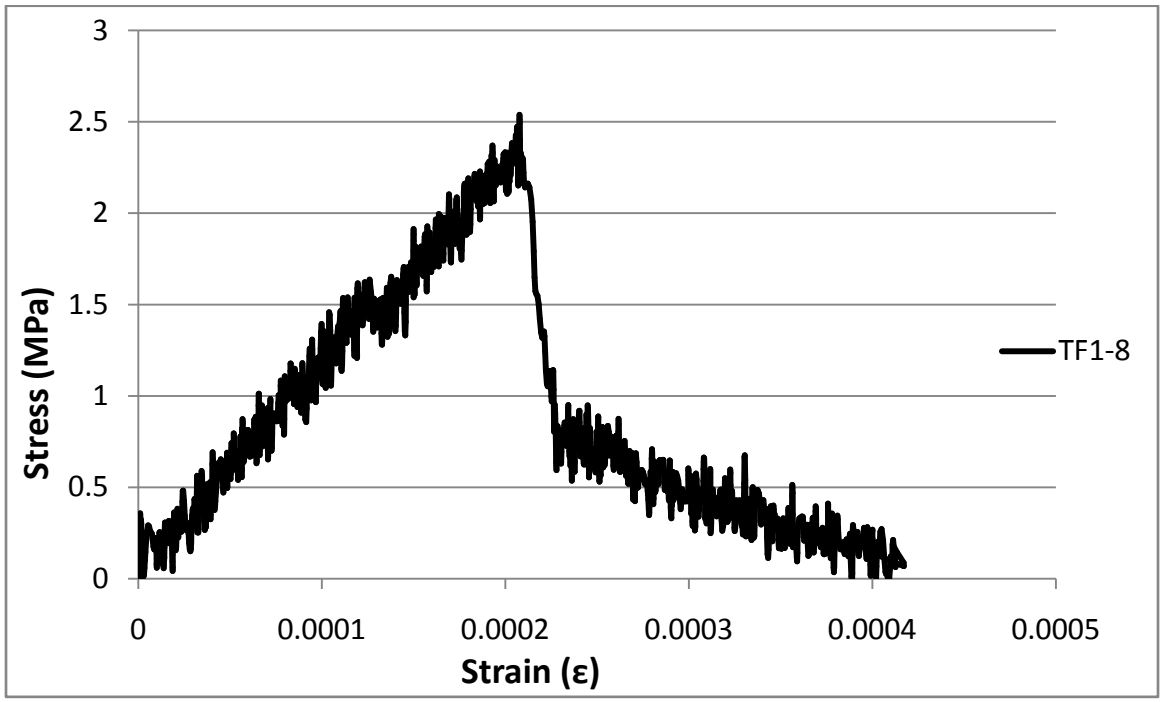
3
2.5
2
1.5
1
0.5
0
Stress (MPa)
0
0.0001
0.0002
0.0003
0.0004
0.0005
Strain (ε)
TF1-8

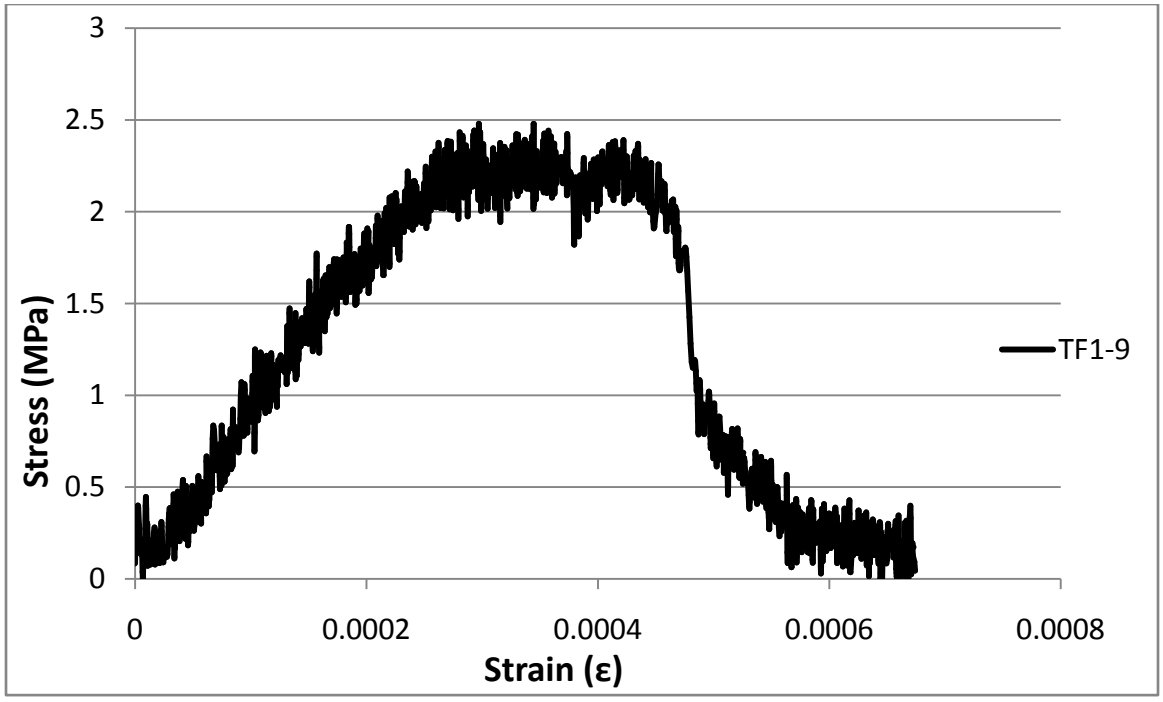
3
2.5
2
1.5
1
0.5
0
Stress (MPa)
0
0.0002
0.0004
0.0006
0.0008
Strain (ε)
TF1-9

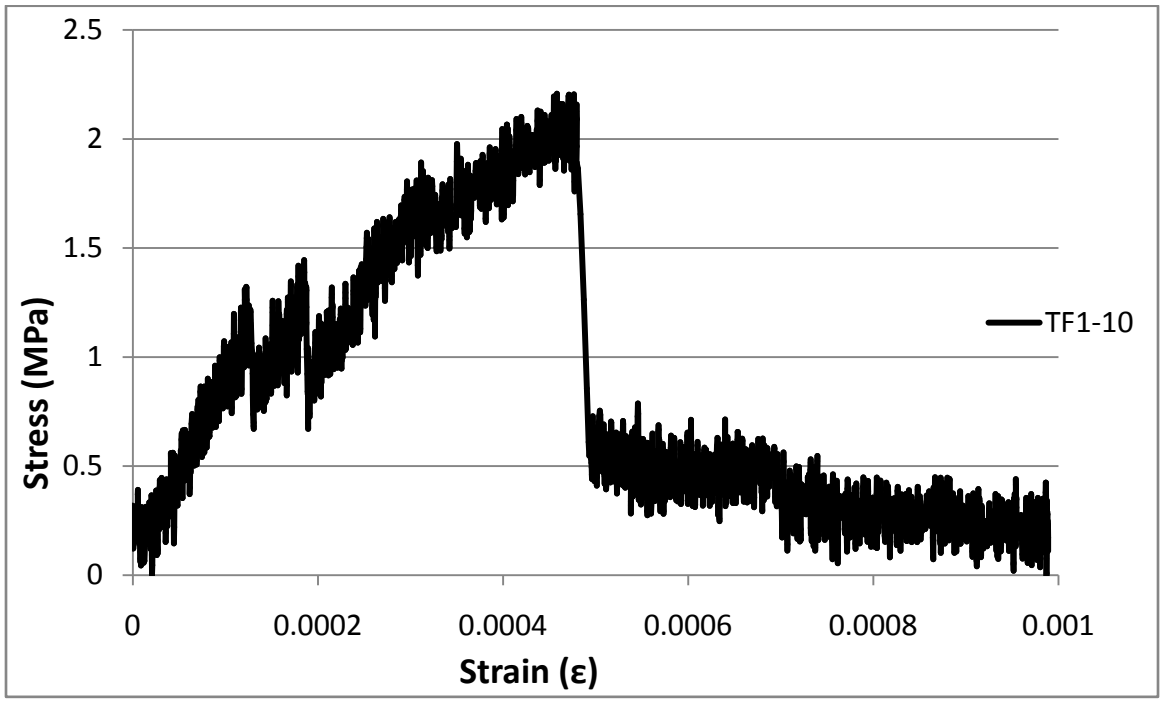
2.5
2
1.5
1
0.5
0
Stress (MPa)
0
0.0002
0.0004
0.0006
0.0008
0.001
Strain (ε)
TF1-10

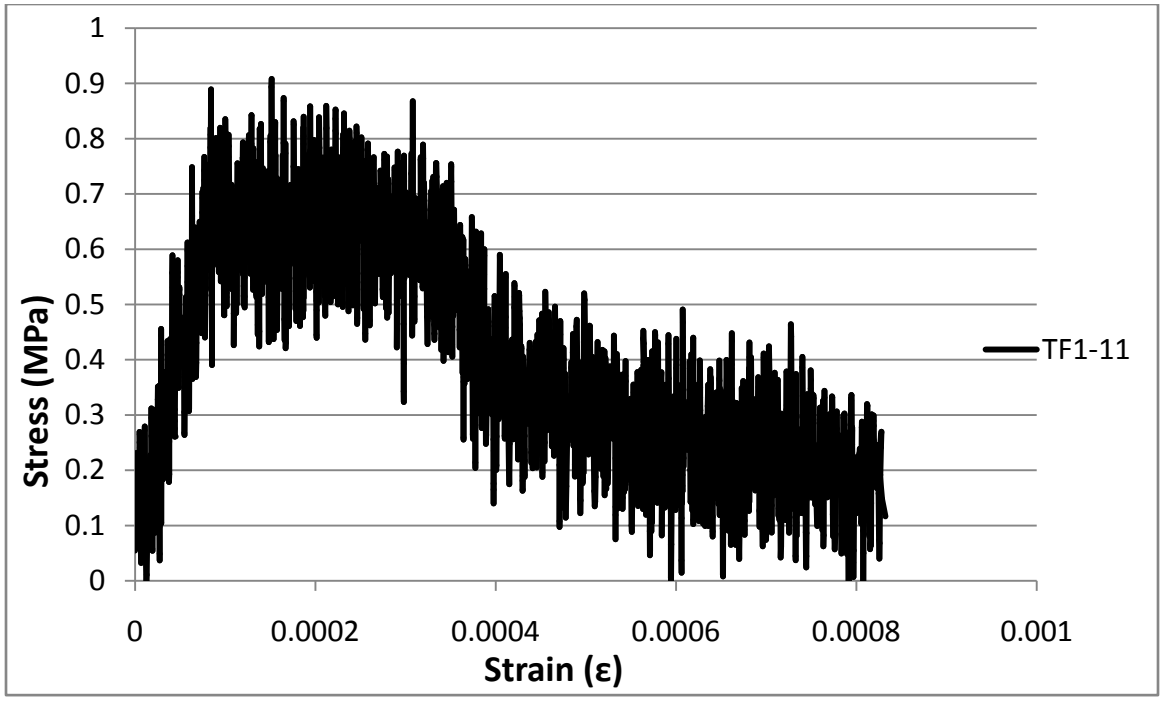
1
0.9
0.8
0.7
0.6
0.5
0.4
0.3
0.2
0.1
0
Stress (MPa)
0
0.0002
0.0004
0.0006
0.0008
0.001
Strain (ε)
TF1-11

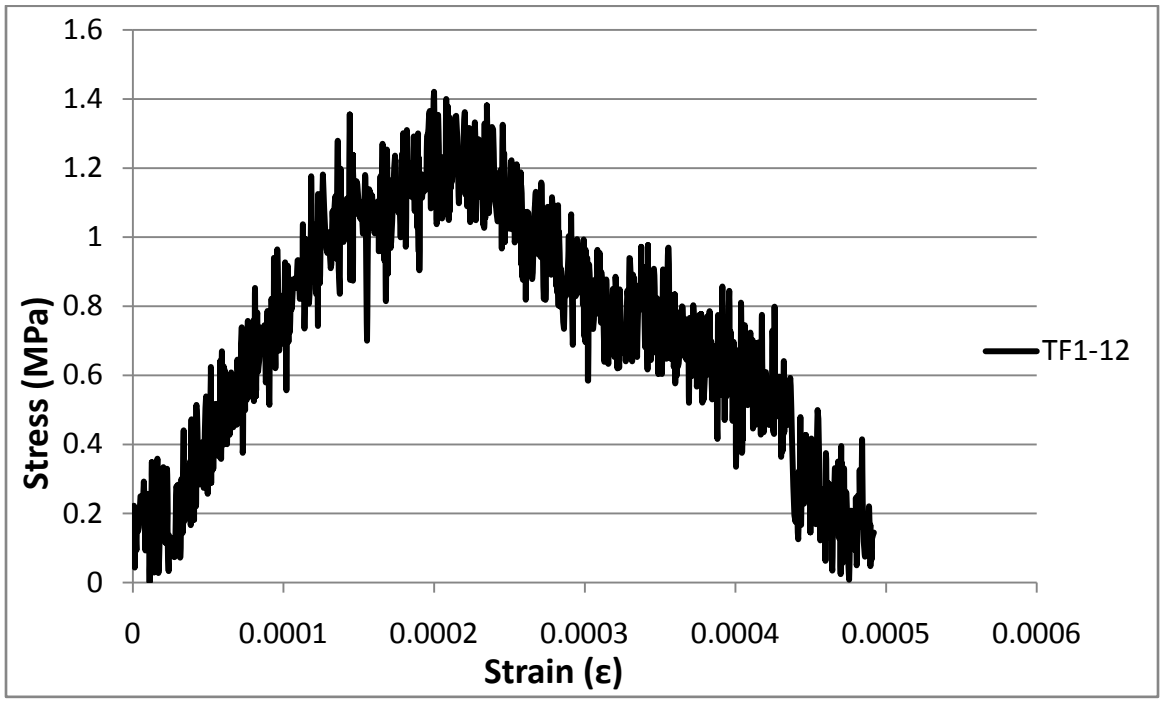
1.6
1.4
1.2
1
0.8
0.6
0.4
0.2
0
Stress (MPa)
0
0.0001
0.0002
0.0003
0.0004
0.0005
0.0006
Strain (ε)
TF1-12

Treated Fibers at 0.2%

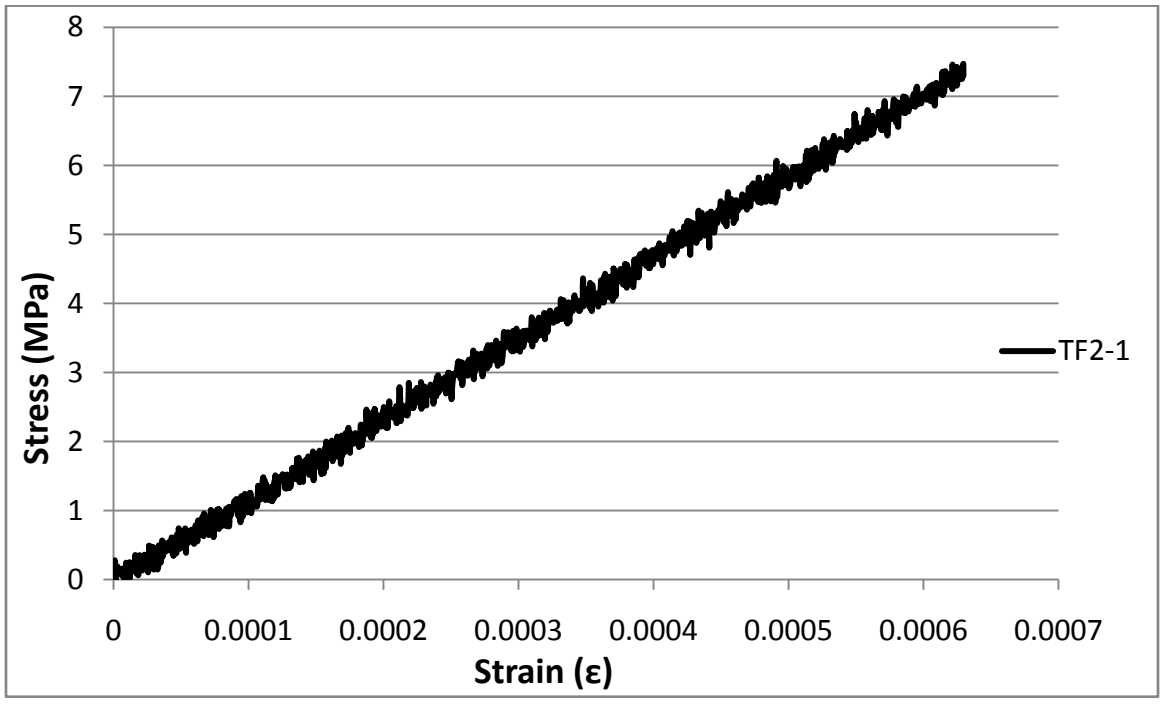

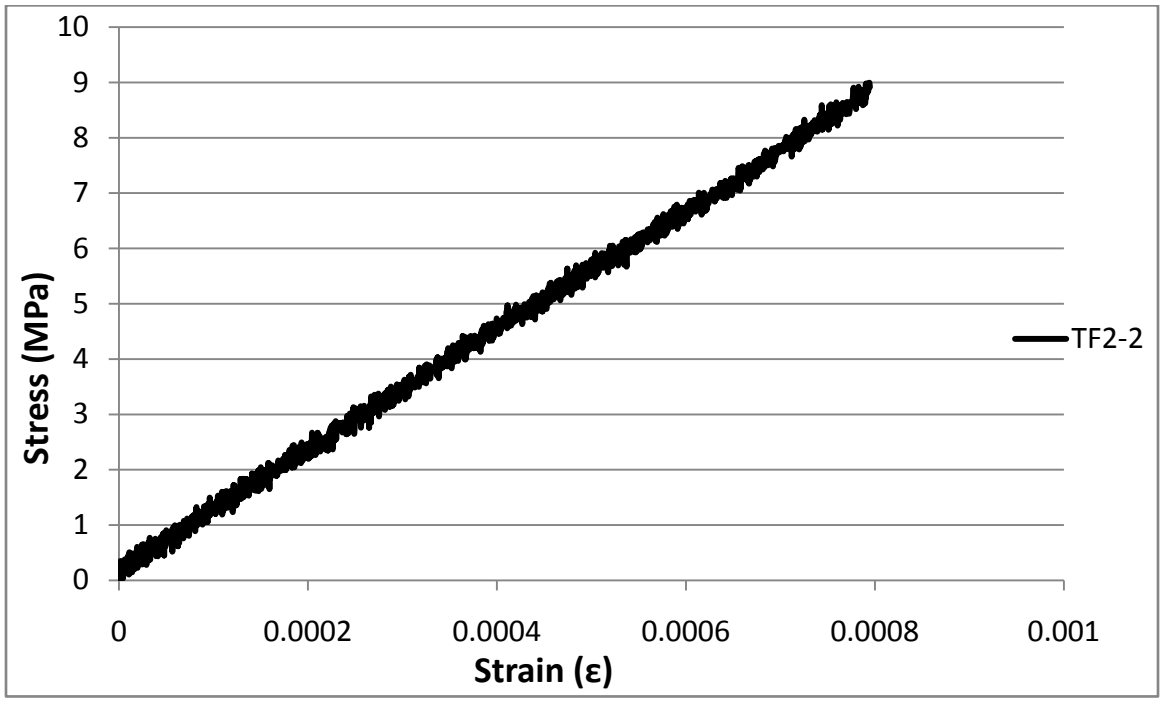

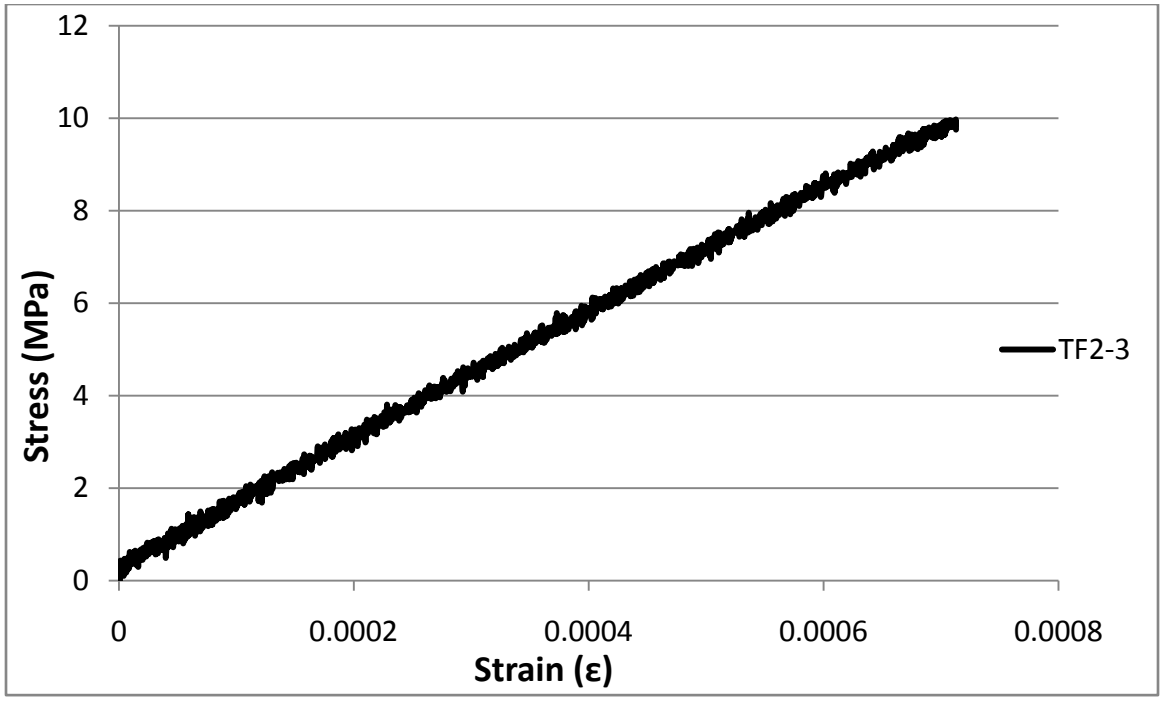
12
10
8
6
4
2
0
Stress (MPa)
0
0.0002
0.0004
0.0006
0.0008
Strain (ε)
TF2-3

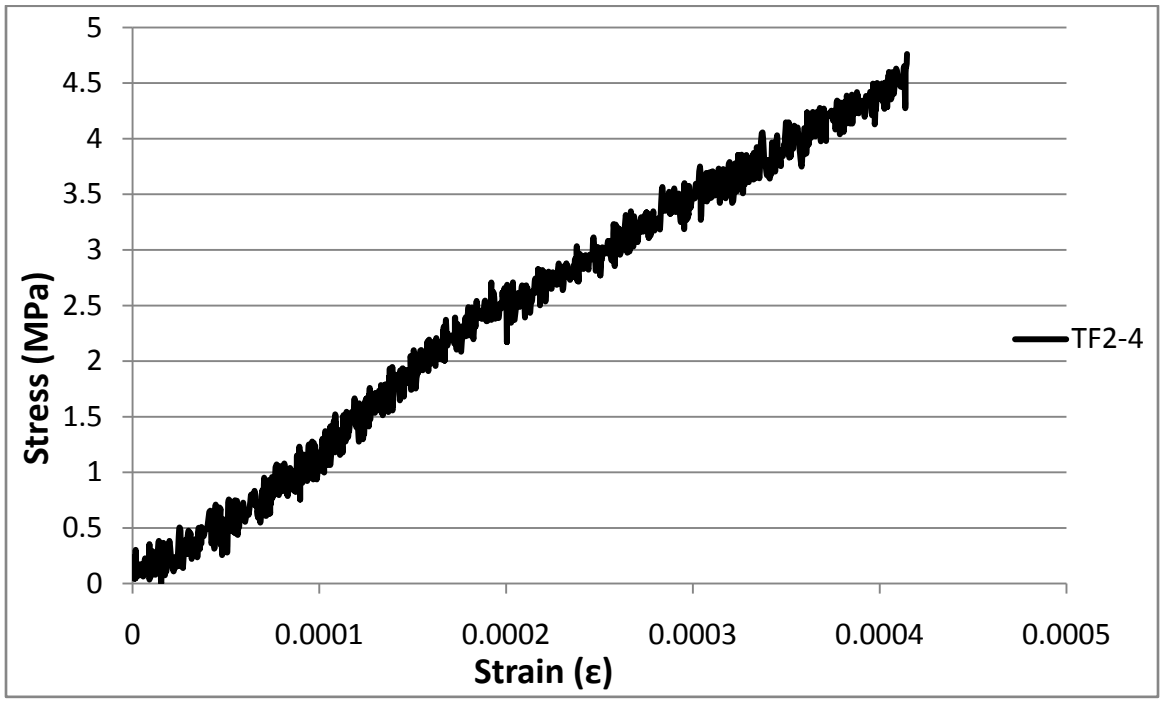
5
4.5
4
3.5
3
2.5
2
1.5
1
0.5
0
Stress (MPa)
0
0.0001
0.0002
0.0003
0.0004
0.0005
Strain (ε)
TF2-4

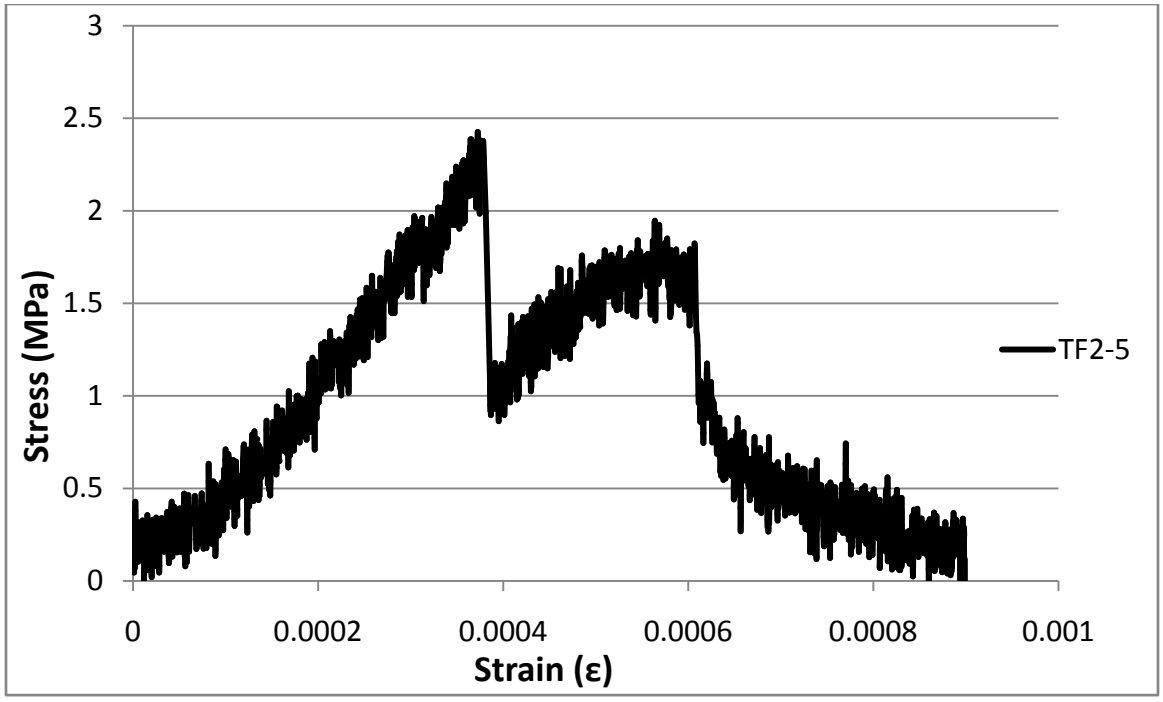
3
2.5
2
1.5
1
0.5
0
Stress (MPa)
0
0.0002
0.0004
0.0006
0.0008
0.001
Strain (ε)
TF2-5

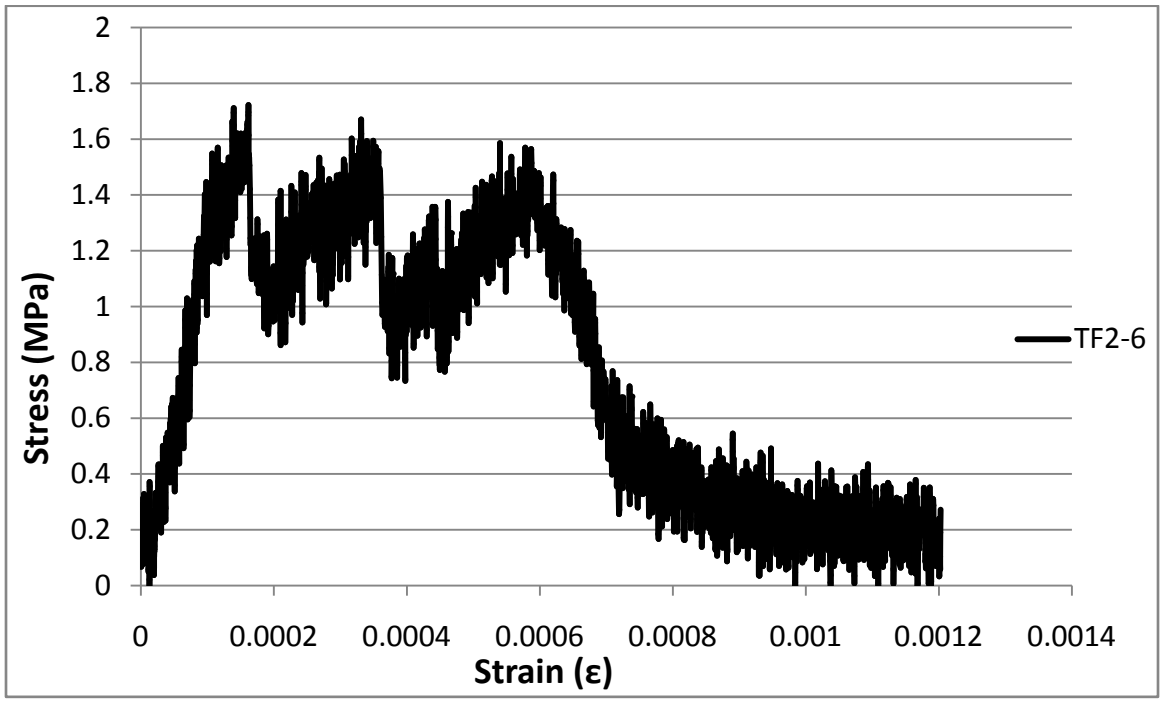
2
1.8
1.6
1.4
1.2
1
0.8
0.6
0.4
0.2
0
Stress (MPa)
0
0.0002
0.0004
0.0006
0.0008
0.001
0.0012
0.0014
Strain (ε)
TF2-6

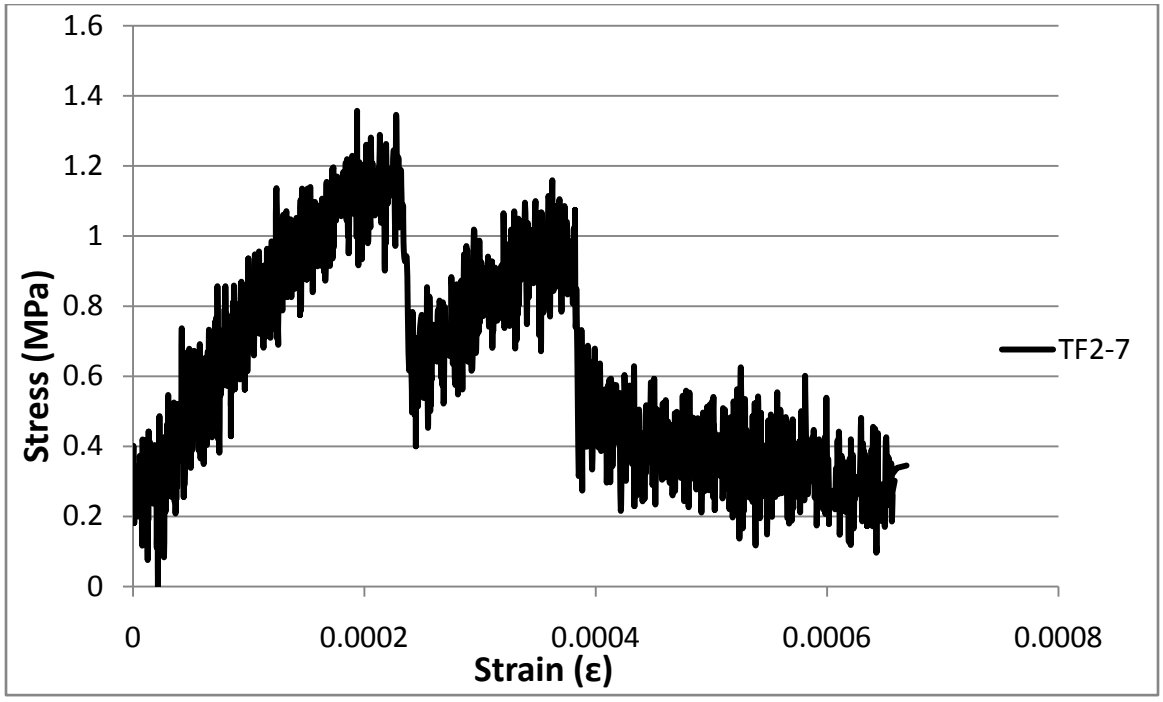
1.6
1.4
1.2
1
0.8
0.6
0.4
0.2
0
Stress (MPa)
0
0.0002
0.0004
0.0006
0.0008
Strain (ε)
TF2-7

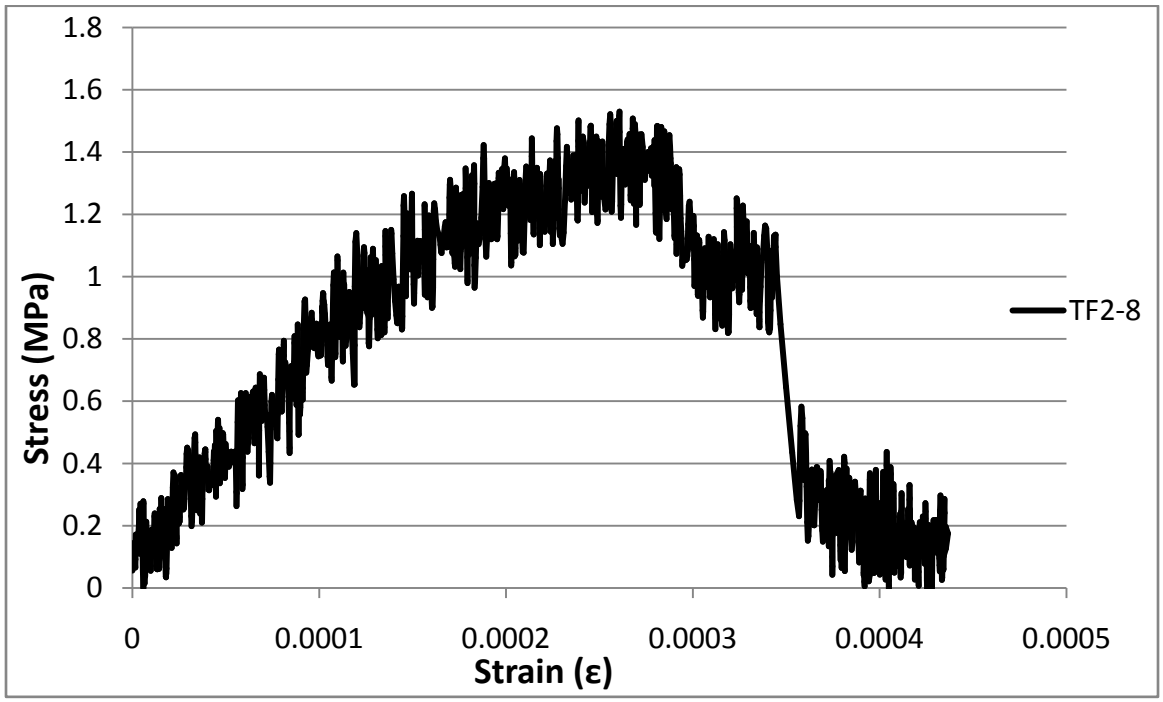
1.8
1.6
1.4
1.2
1
0.8
0.6
0.4
0.2
0
Stress (MPa)
0
0.0001
0.0002
0.0003
0.0004
0.0005
Strain (ε)
TF2-8

Treated Tubes at 0.1%

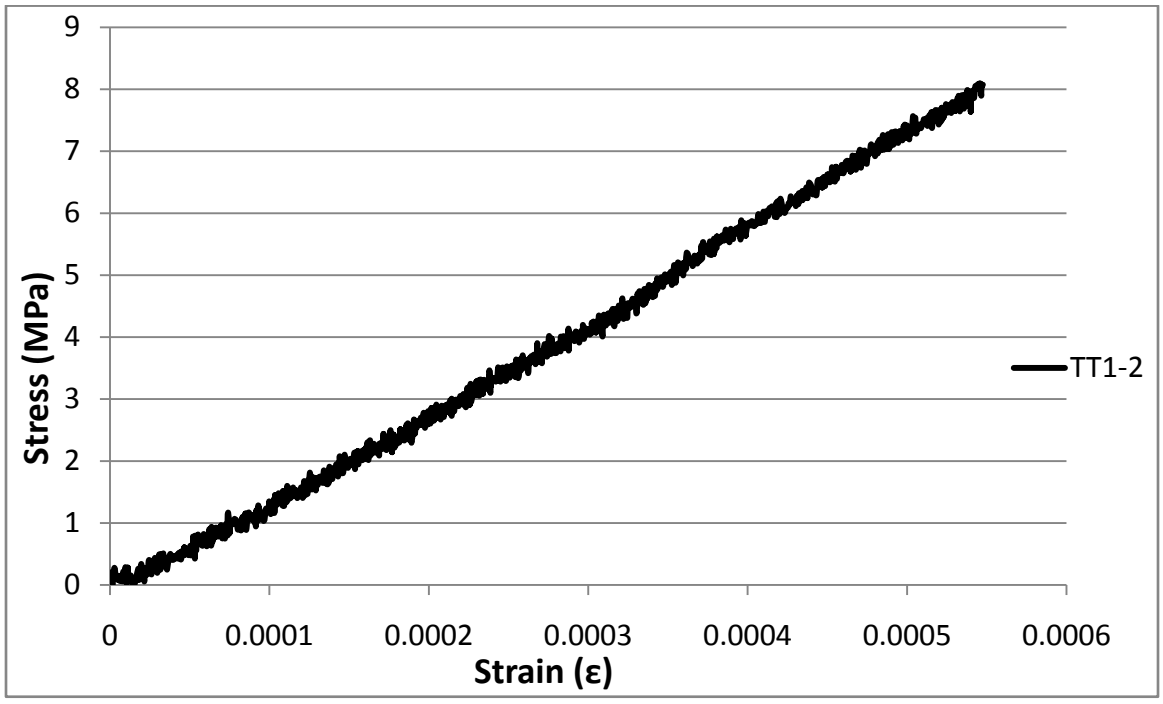

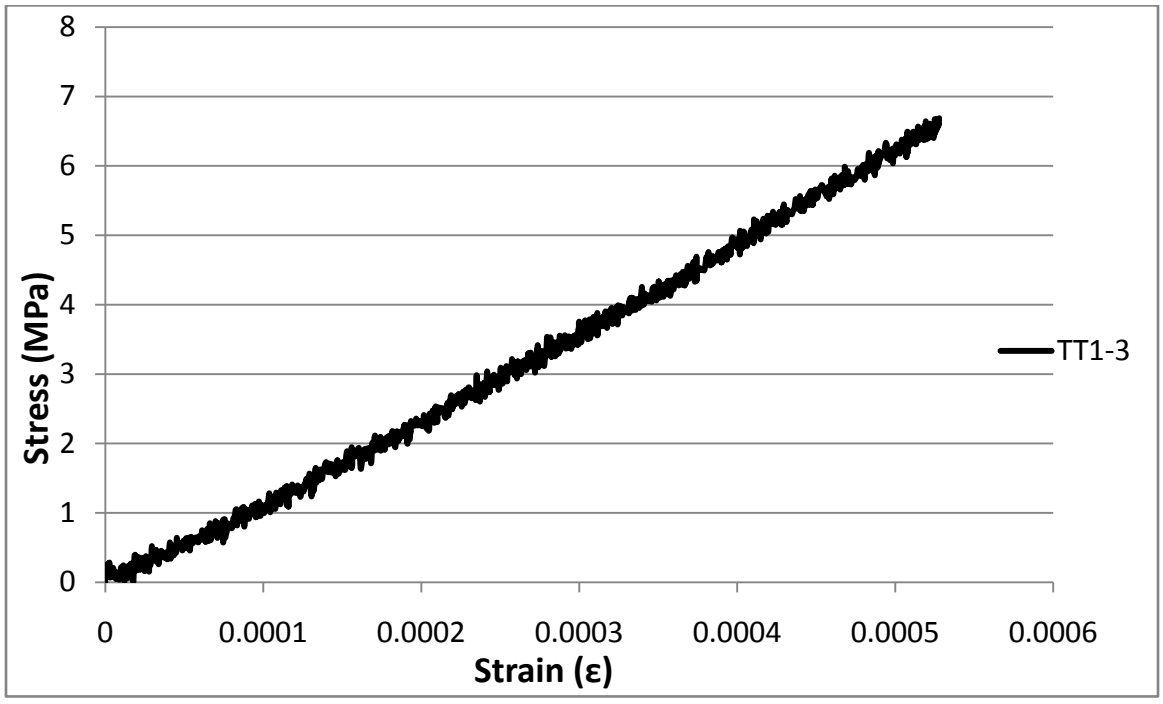

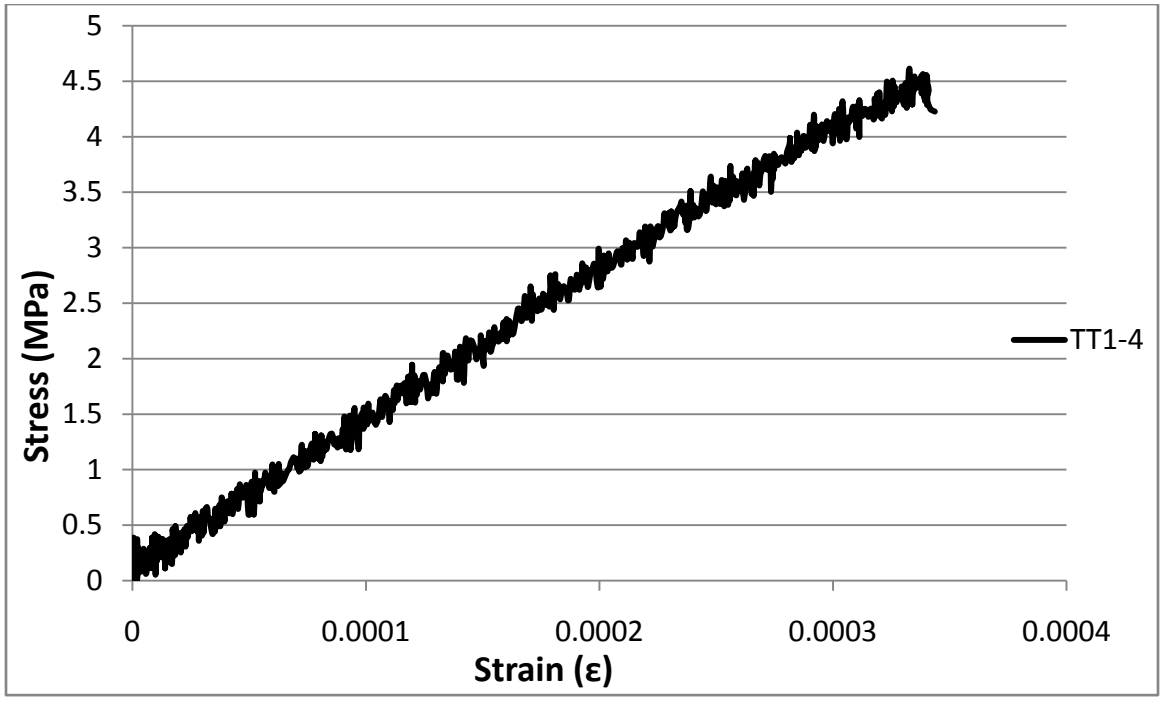
5
4.5
4
3.5
3
2.5
2
1.5
1
0.5
0
Stress (MPa)
0
0.0001
0.0002
0.0003
0.0004
Strain (ε)
TT1-4

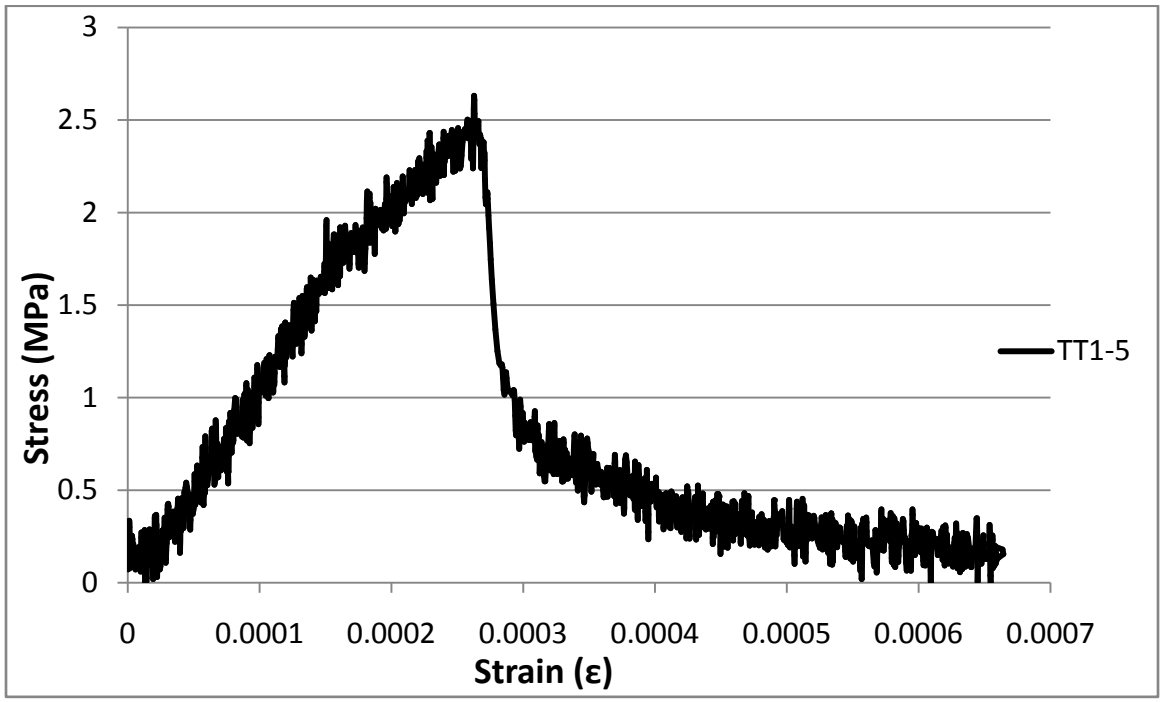
3
2.5
2
1.5
1
0.5
0
Stress (MPa)
0
0.0001
0.0002
0.0003
0.0004
0.0005
0.0006
0.0007
Strain (ε)
TT1-5

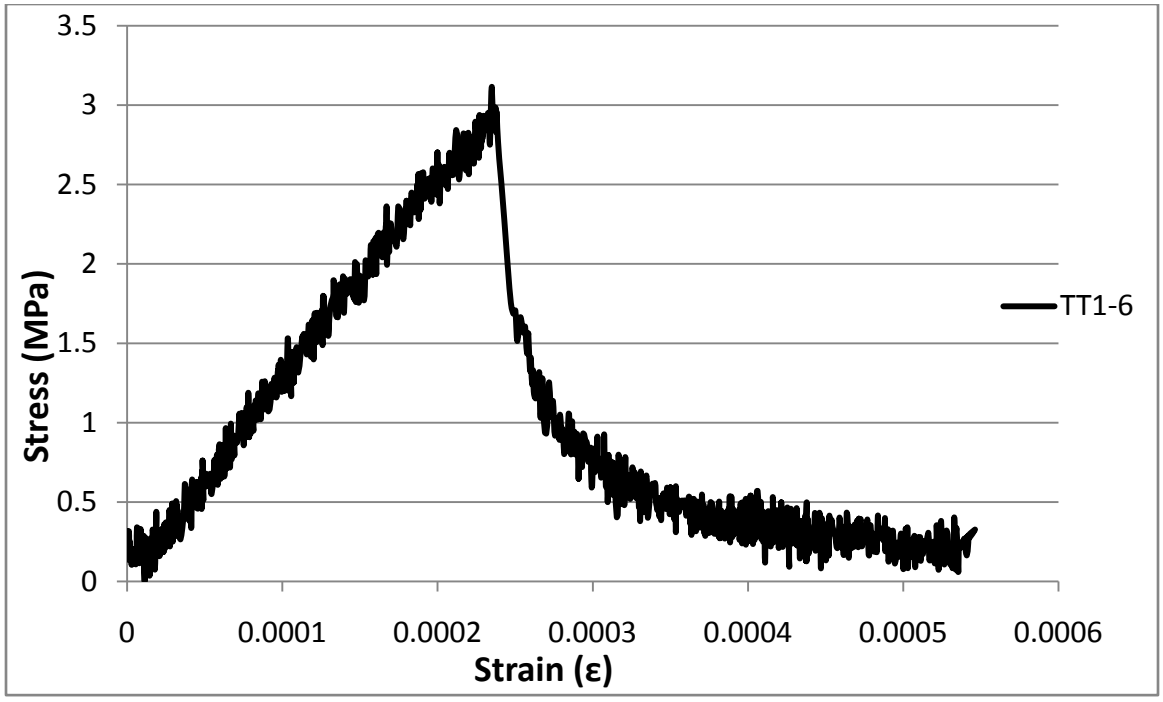
3.5
3
2.5
2
1.5
1
0.5
0
Stress (MPa)
0
0.0001
0.0002
0.0003
0.0004
0.0005
0.0006
Strain (ε)
TT1-6

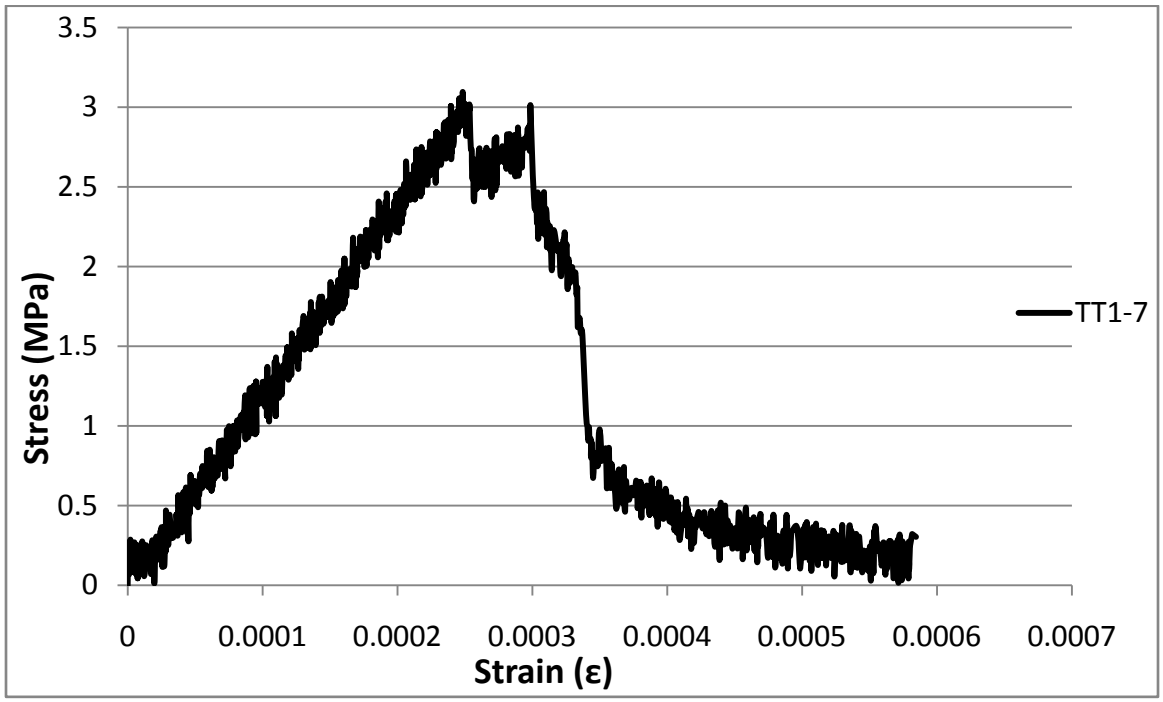
3.5
3
2.5
2
1.5
1
0.5
0
Stress (MPa)
0
0.0001
0.0002
0.0003
0.0004
0.0005
0.0006
0.0007
Strain (ε)
TT1-7

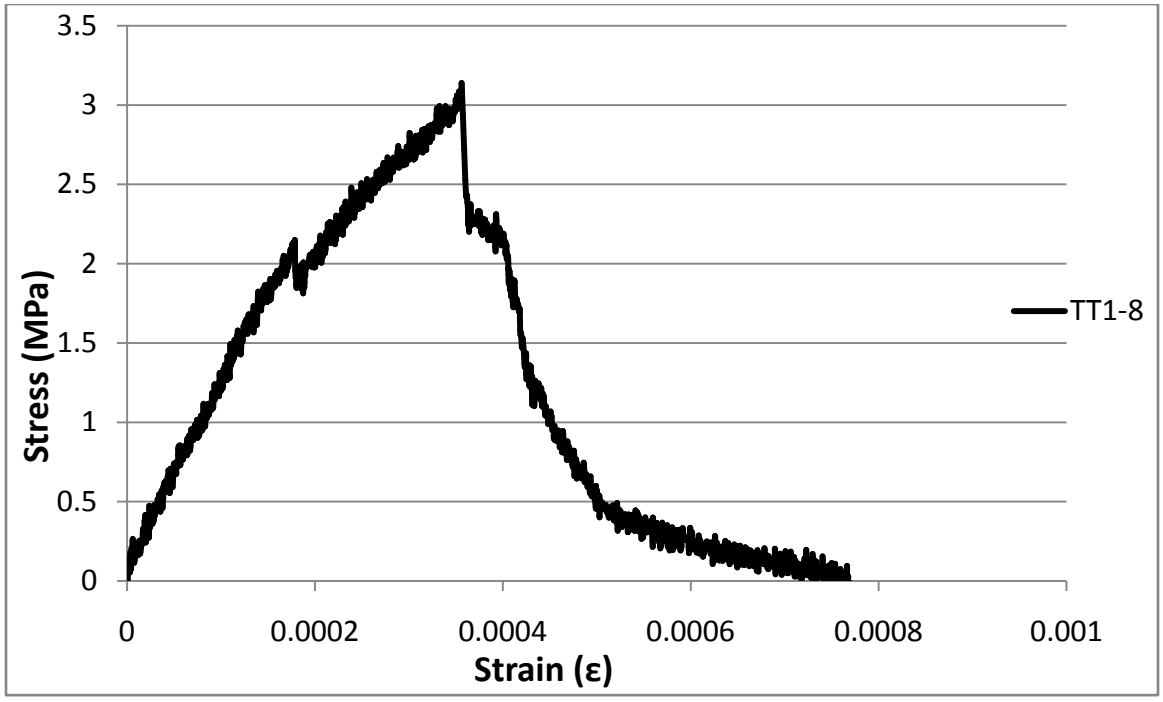
3.5
3
2.5
2
1.5
1
0.5
0
Stress (MPa)
0
0.0002
0.0004
0.0006
0.0008
0.001
Strain (ε)
TT1-8

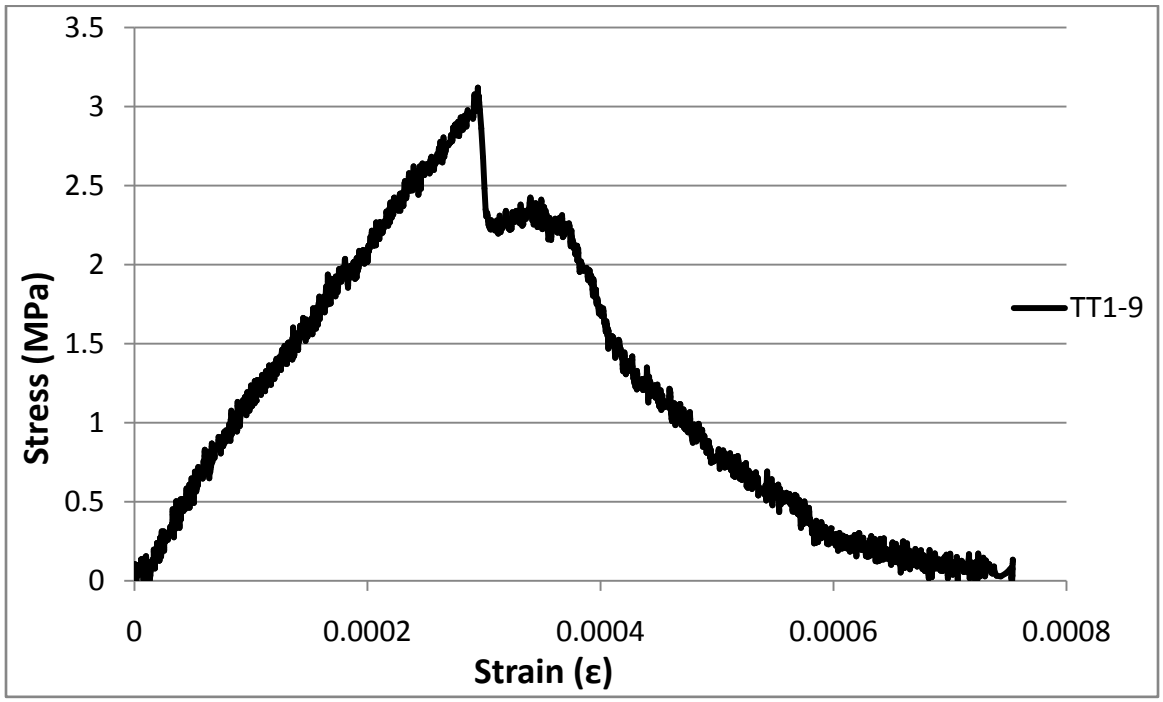
3.5
3
2.5
2
1.5
1
0.5
0
Stress (MPa)
0
0.0002
0.0004
0.0006
0.0008
Strain (ε)
TT1-9

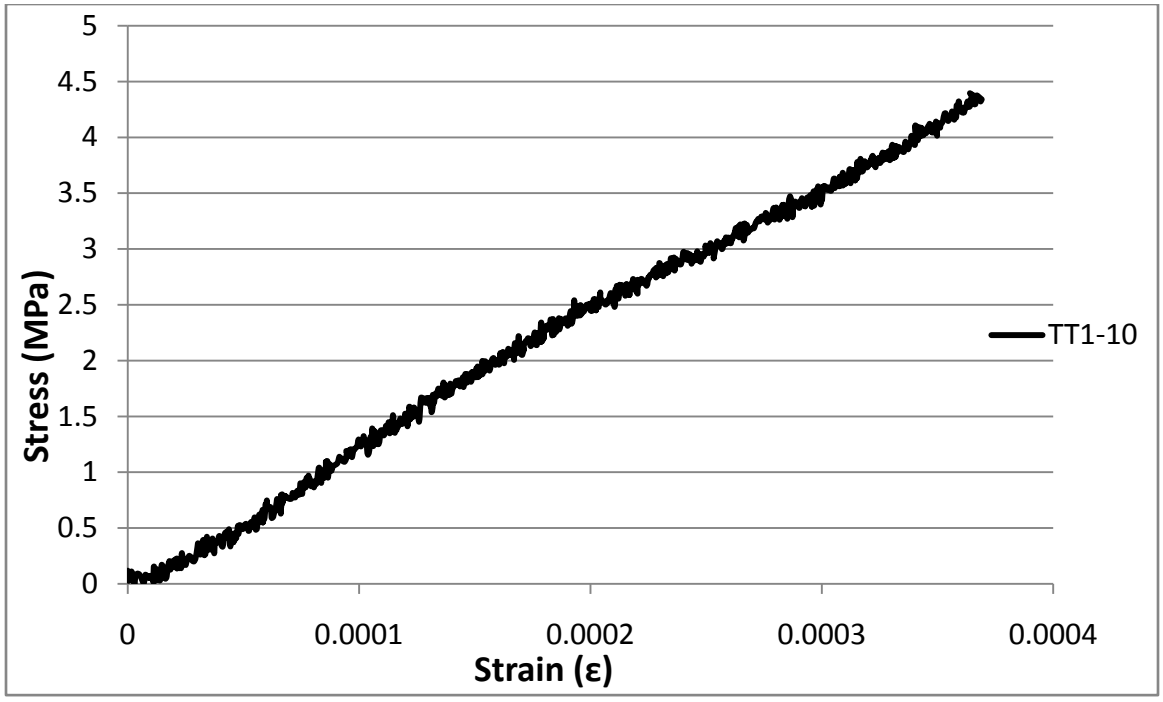
5
4.5
4
3.5
3
2.5
2
1.5
1
0.5
0
Stress (MPa)
0
0.0001
0.0002
0.0003
0.0004
Strain (ε)
TT1-10

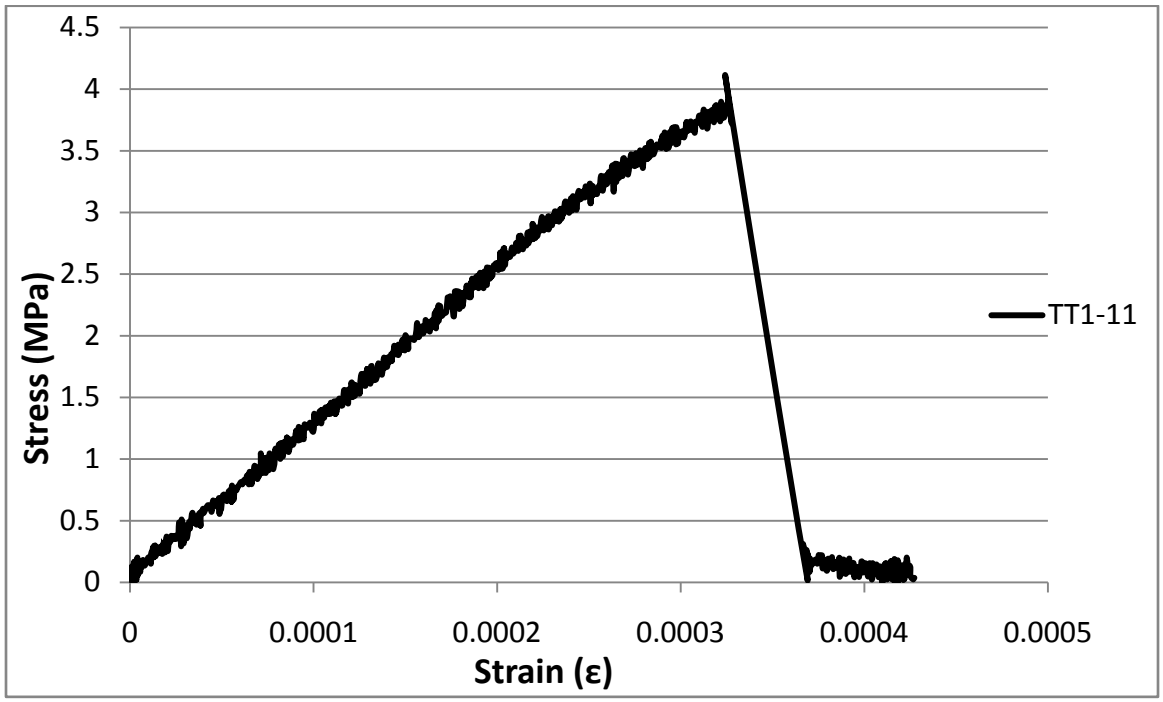
4.5
4
3.5
3
2.5
2
1.5
1
0.5
0
Stress (MPa)
0
0.0001
0.0002
0.0003
0.0004
0.0005
Strain (ε)
TT1-11

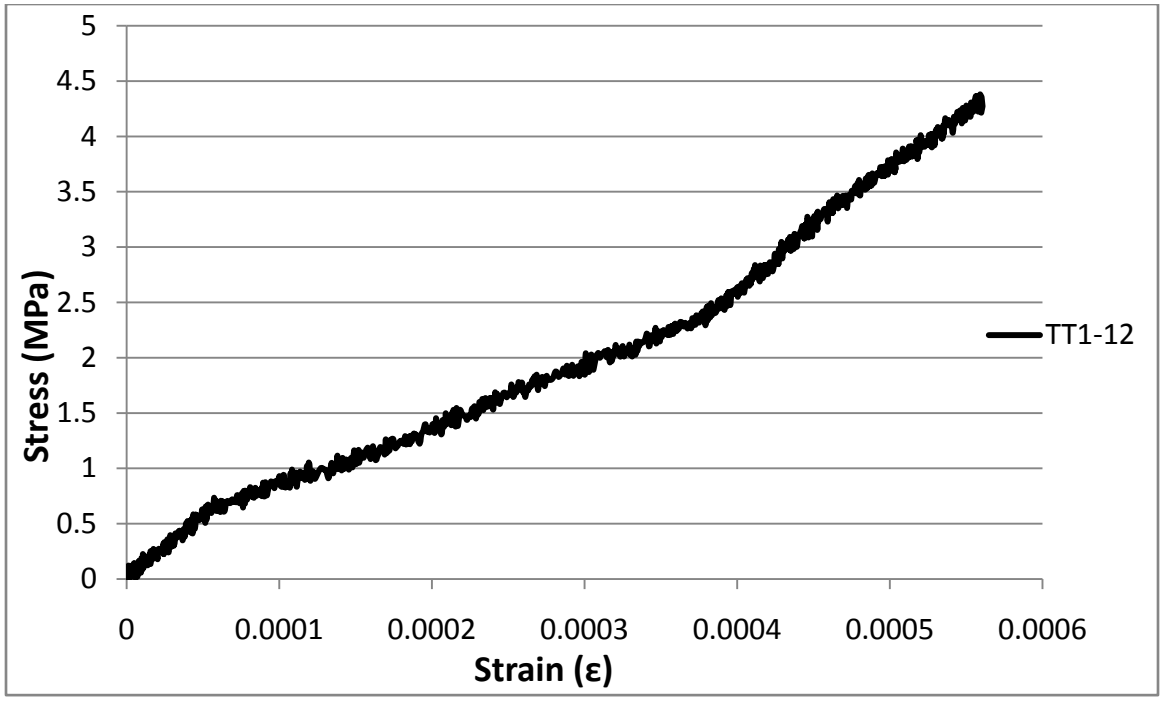
5
4.5
4
3.5
3
2.5
2
1.5
1
0.5
0
Stress (MPa)
0
0.0001
0.0002
0.0003
0.0004
0.0005
0.0006
Strain (ε)
TT1-12

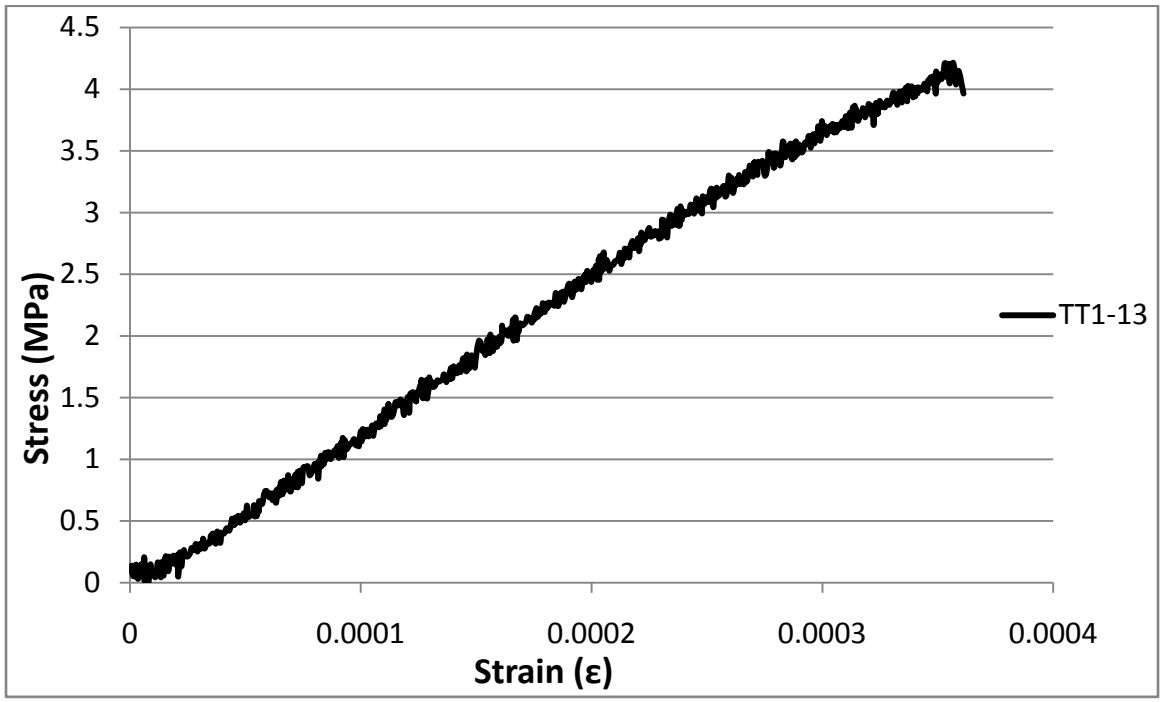
4.5
4
3.5
3
2.5
2
1.5
1
0.5
0
Stress (MPa)
0
0.0001
0.0002
0.0003
0.0004
Strain (ε)
TT1-13

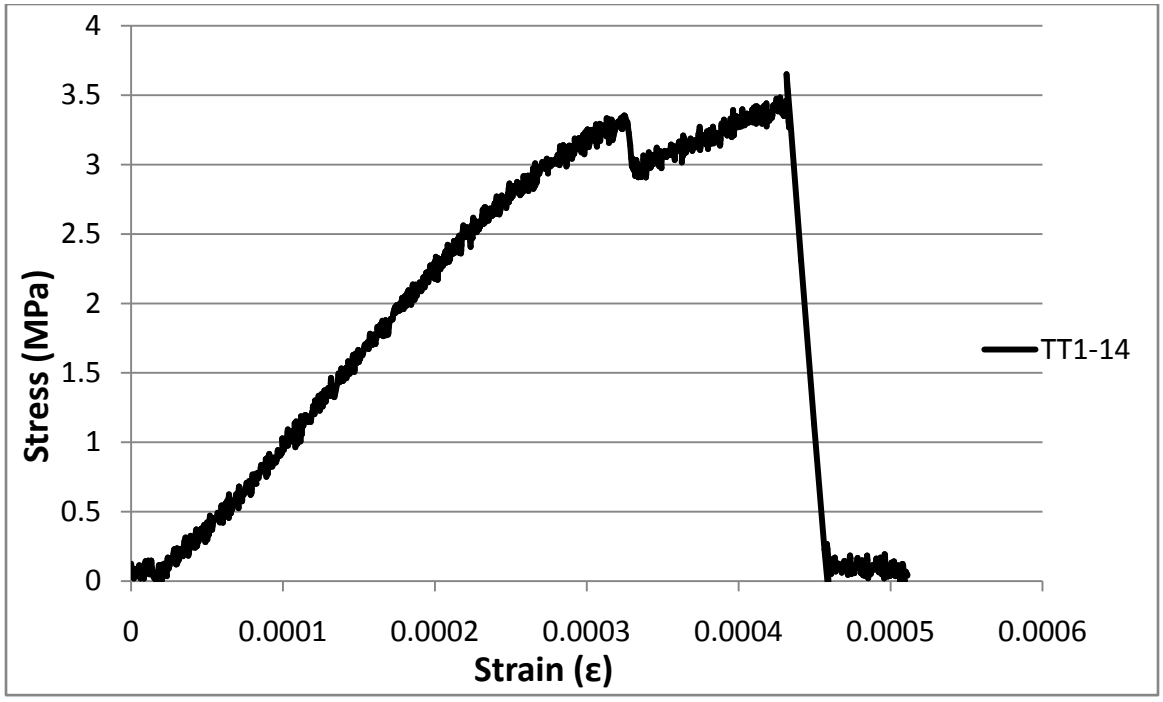
4
3.5
3
2.5
2
1.5
1
0.5
0
Stress (MPa)
0
0.0001
0.0002
0.0003
0.0004
0.0005
0.0006
Strain (ε)
TT1-14

Treated Tubes at 0.2%

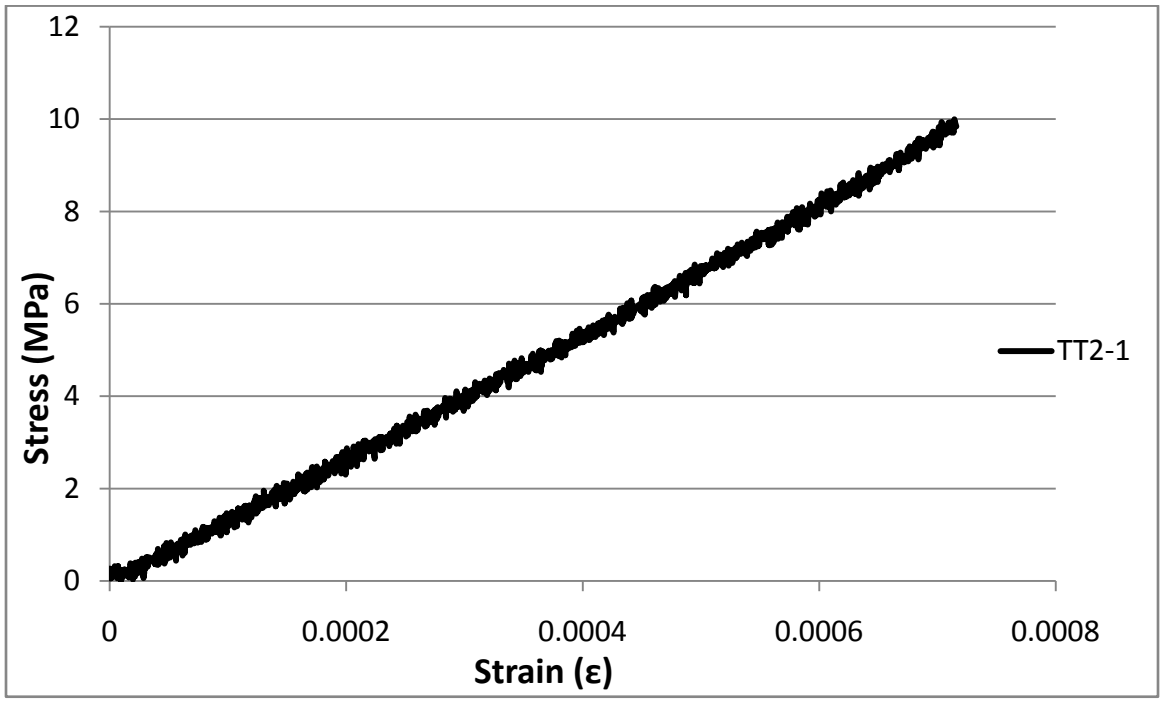

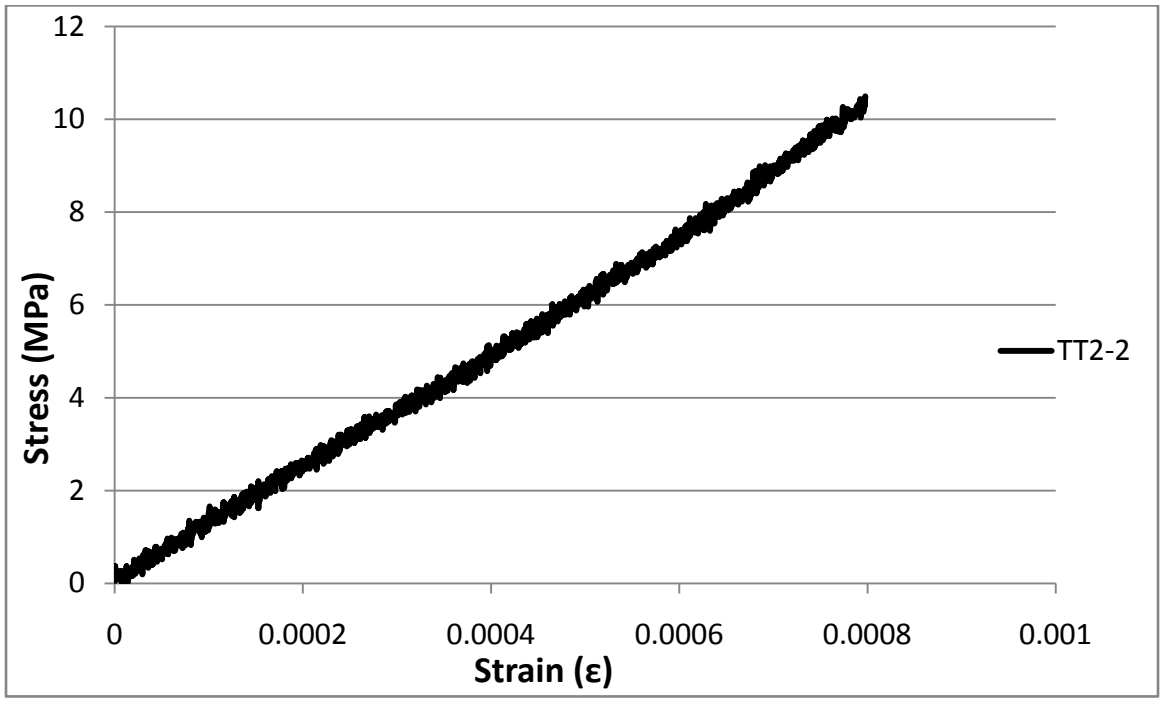

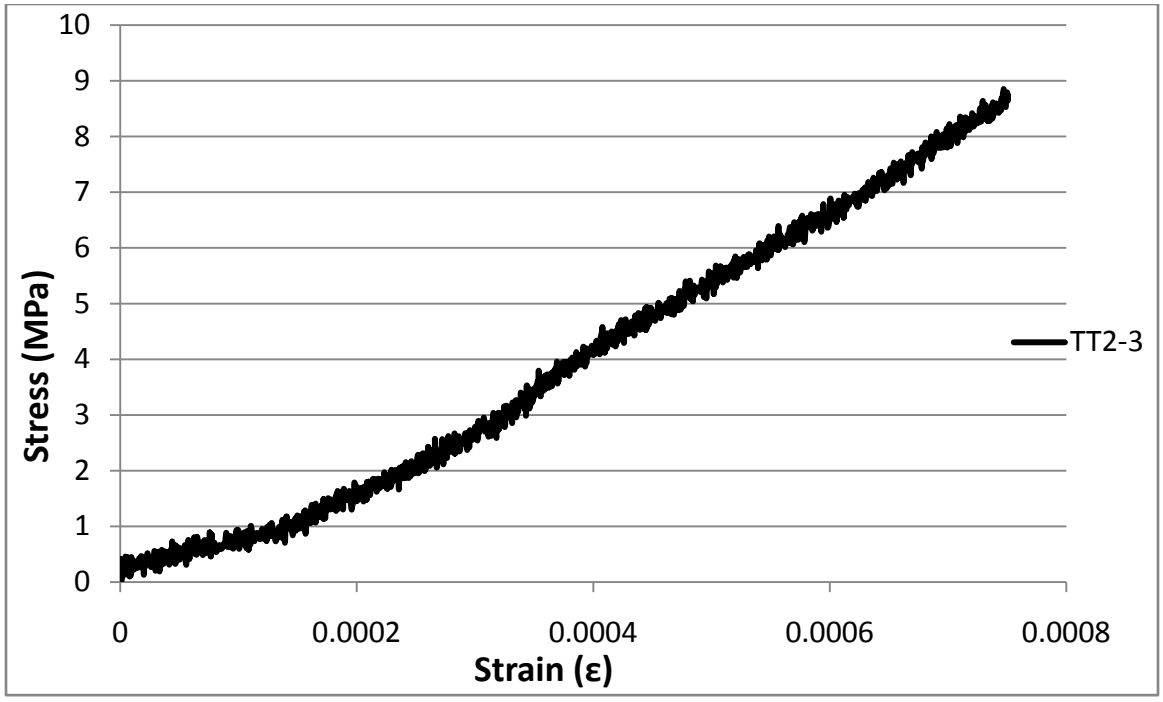
10
9
8
7
6
5
4
3
2
1
0
Stress (MPa)
0
0.0002
0.0004
0.0006
0.0008
Strain (ε)
TT2-3

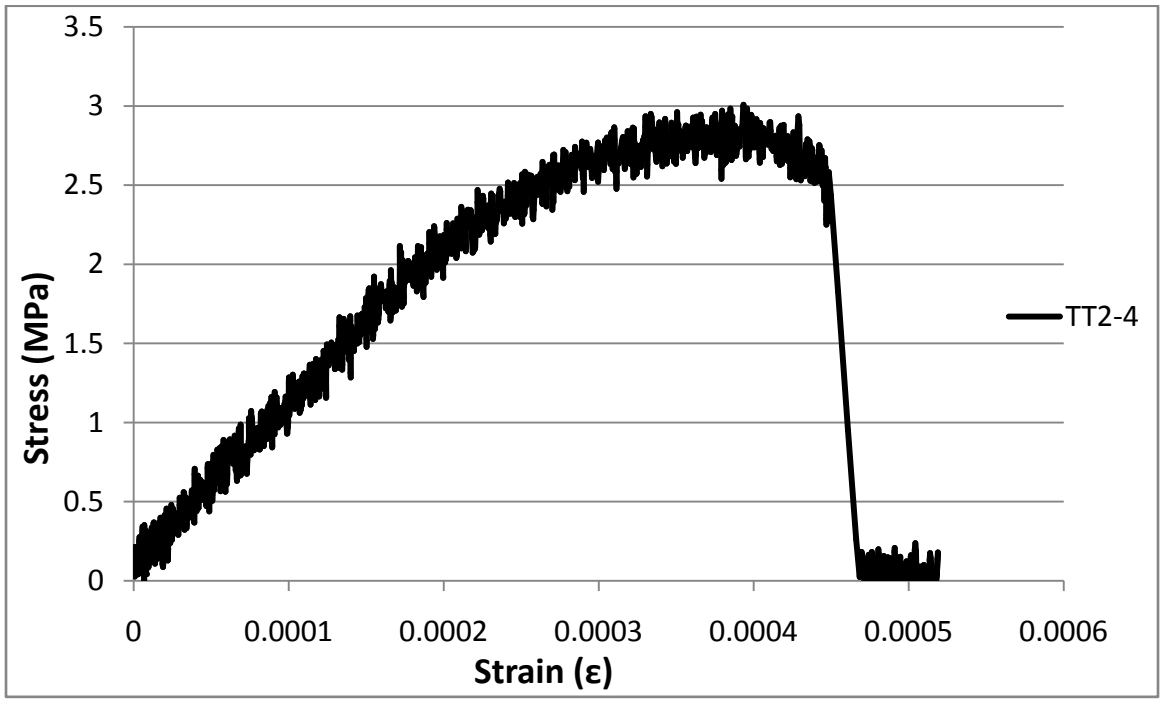
3.5
3
2.5
2
1.5
1
0.5
0
Stress (MPa)
0
0.0001
0.0002
0.0003
0.0004
0.0005
0.0006
Strain (ε)
TT2-4

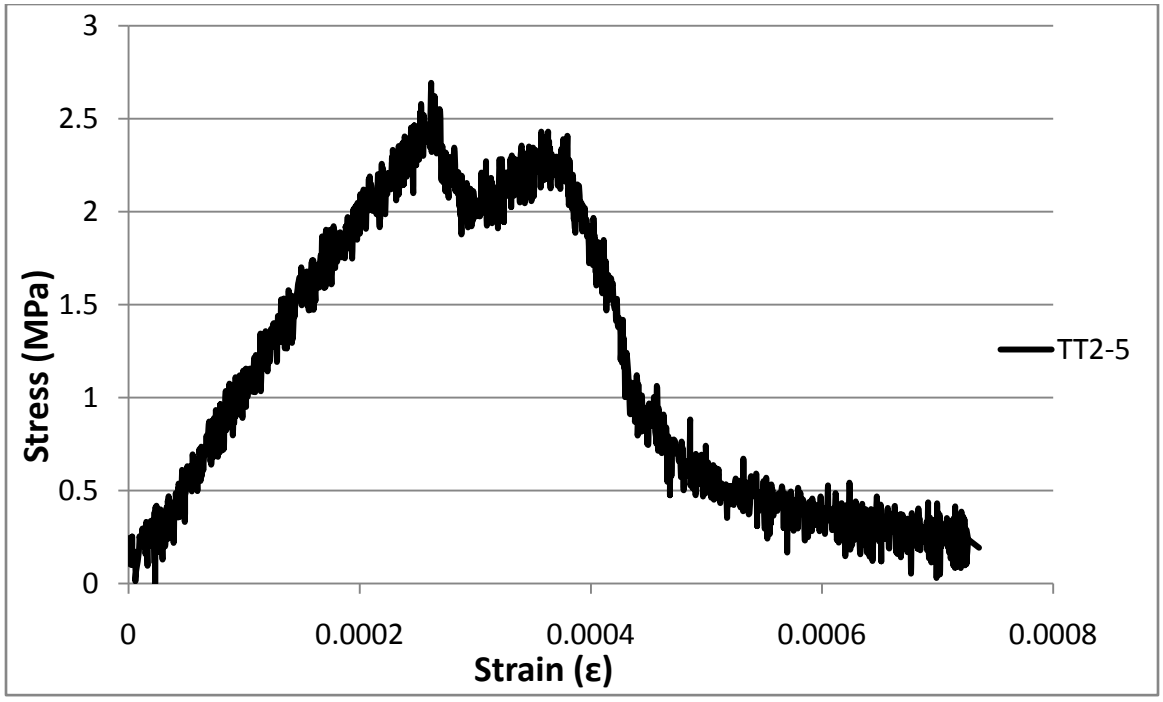
3
2.5
2
1.5
1
0.5
0
Stress (MPa)
0
0.0002
0.0004
0.0006
0.0008
Strain (ε)
TT2-5

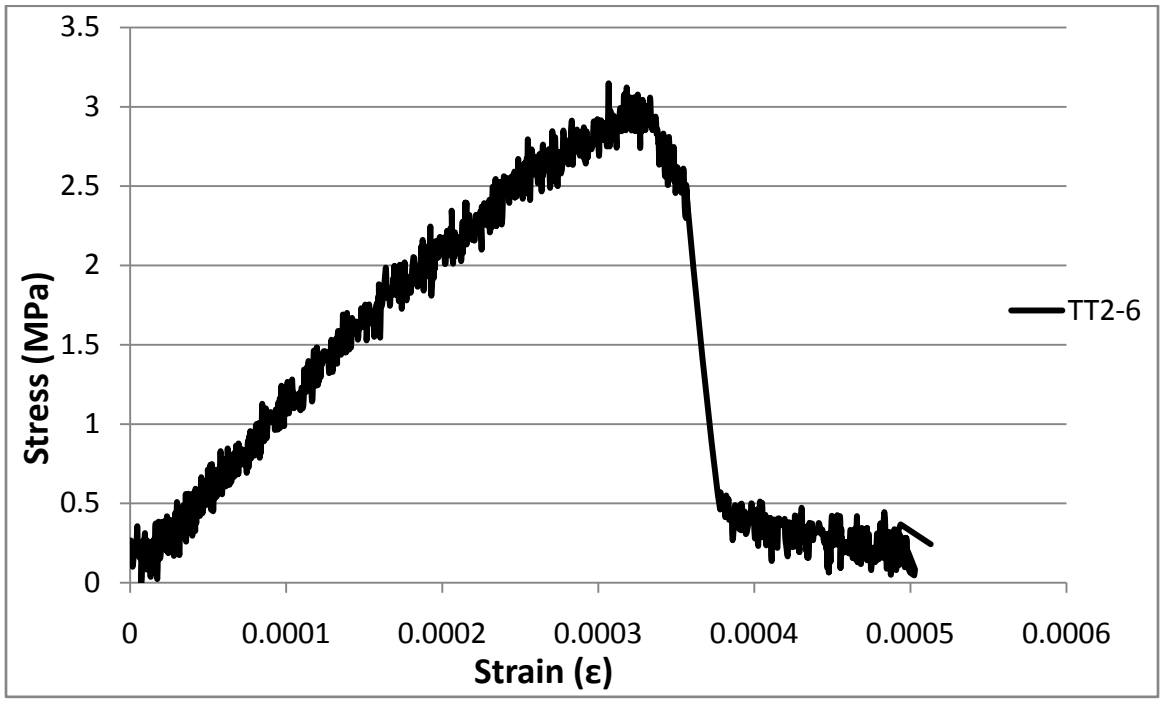
3.5
3
2.5
2
1.5
1
0.5
0
Stress (MPa)
0
0.0001
0.0002
0.0003
0.0004
0.0005
0.0006
Strain (ε)
TT2-6

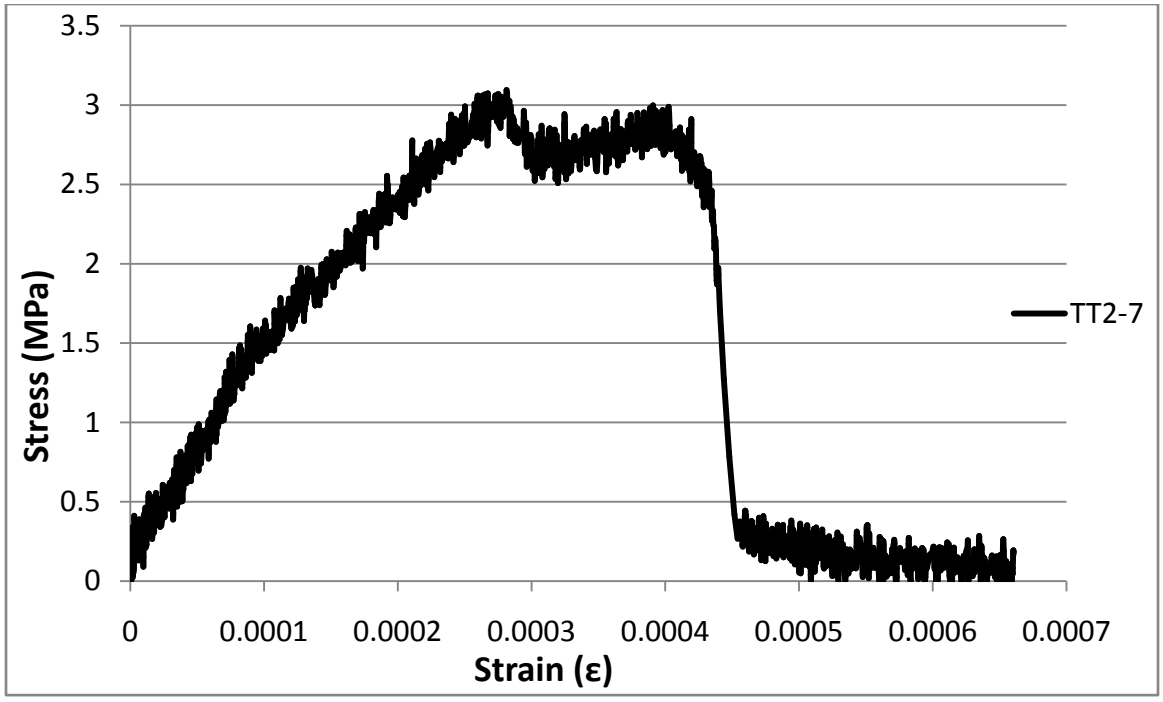
3.5
3
2.5
2
1.5
1
0.5
0
Stress (MPa)
0
0.0001
0.0002
0.0003
0.0004
0.0005
0.0006
0.0007
Strain (ε)
TT2-7

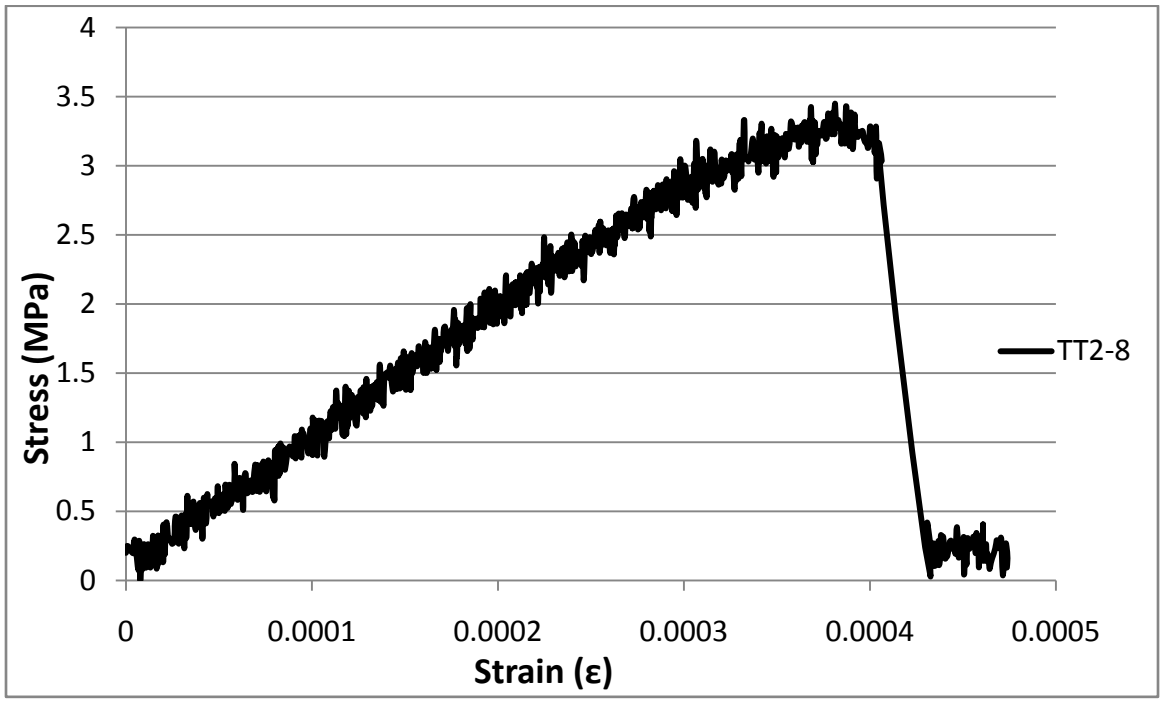
4
3.5
3
2.5
2
1.5
1
0.5
0
Stress (MPa)
0
0.0001
0.0002
0.0003
0.0004
0.0005
Strain (ε)
TT2-8

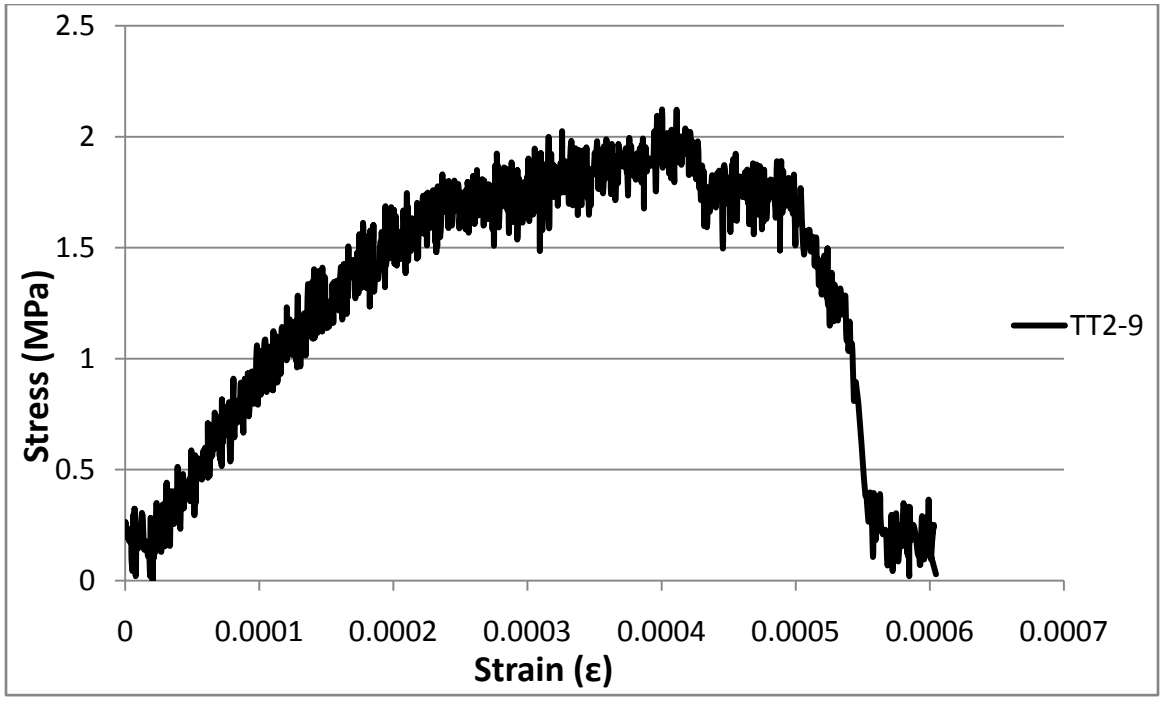
2.5
2
1.5
1
0.5
0
Stress (MPa)
0
0.0001
0.0002
0.0003
0.0004
0.0005
0.0006
0.0007
Strain (ε)
TT2-9

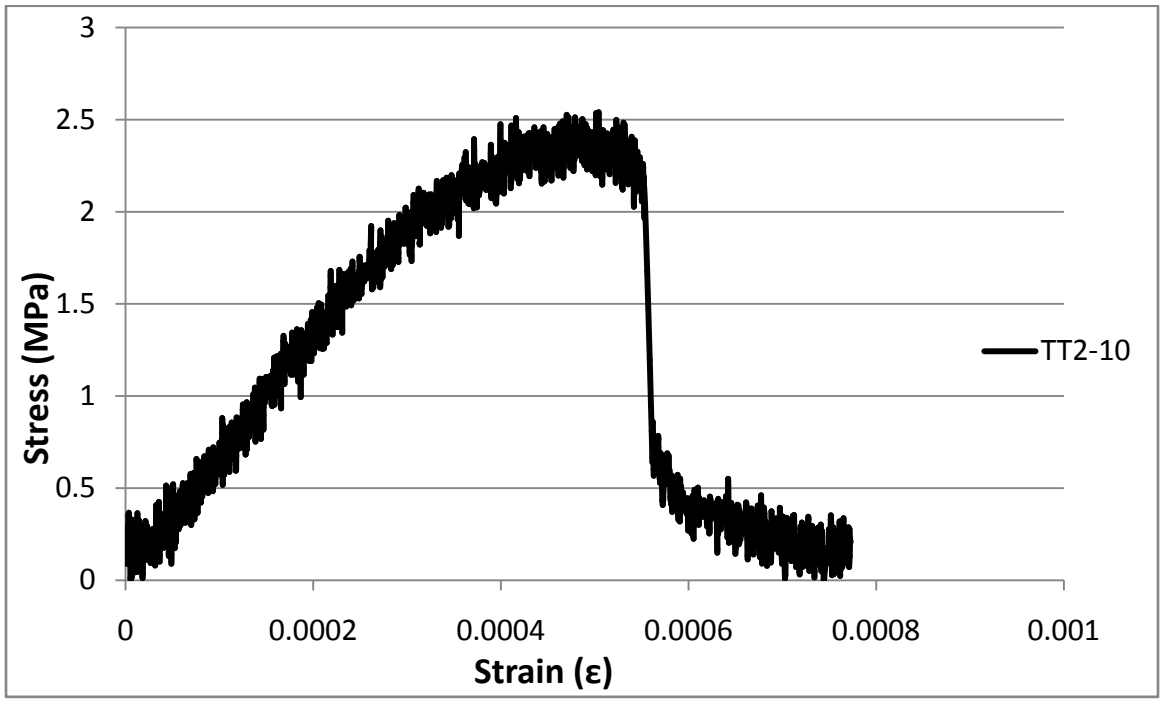
3
2.5
2
1.5
1
0.5
0
Stress (MPa)
0
0.0002
0.0004
0.0006
0.0008
0.001
Strain (ε)
TT2-10

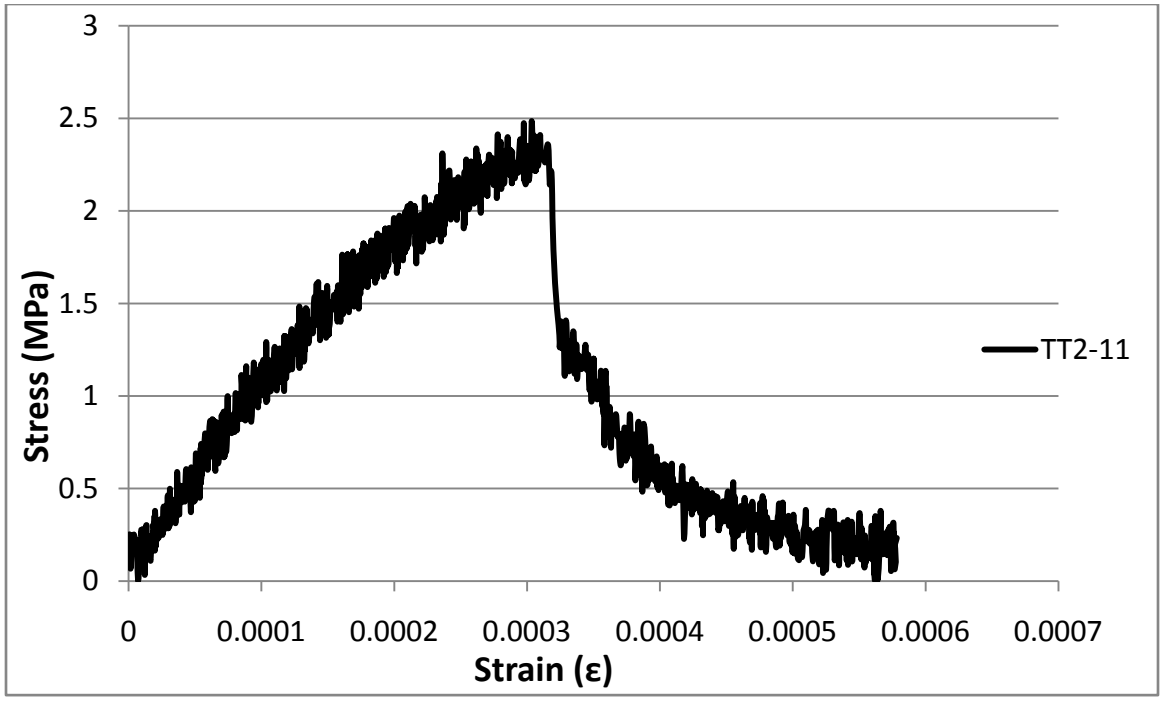
3
2.5
2
1.5
1
0.5
0
Stress (MPa)
0
0.0001
0.0002
0.0003
0.0004
0.0005
0.0006
0.0007
Strain (ε)
TT2-11

VITA

Name: Bryan Michael Tyson

Address: Construction, Geotechnical, and Structural Division
3136 TAMU
College Station, TX 77843

Email Address: bmt9554@tamu.edu

Education: M.S., Civil Engineering,
Texas A&M University, 2010

B.S., Civil Engineering,
Texas A&M University, 2008